



universität
wien

DISSERTATION

Supramolekulare Chemie Organischer Azide

angestrebter akademischer Grad

Doktor der Naturwissenschaften (Dr. rer.nat.)

Verfasser:	Mag. Peter Walla
Matrikel-Nummer:	0214489
Dissertationsgebiet (lt. Studienblatt):	419 Chemie
Betreuer:	O. Univ.-Prof. Dr. Udo H. Brinker

Wien, am 17. Dezember 2008



universität
wien

DISSERTATION

Supramolecular Chemistry of Organic Azides

Author:	Mag. Peter Walla
Matriculation number:	0214489
Dissertation field	419 Chemistry
Supervising tutor:	O. Univ.-Prof. Dr. Udo H. Brinker

Vienna, December 17, 2008

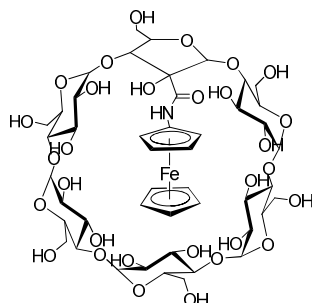
Dedicated to my wife Gabriela and my son Peter

Abstrakt (Deutsch)

Die vorgelegte Arbeit umfasst sowohl physikalische als auch synthetisch-organische Aspekte der Chemie. Spektroskopische und theoretische Methoden wurden angewandt, um die Konformationsanalyse und Thermodynamik der supramolekularen Komplexe zu verstehen.

Wie aus den induzierten Zirkulardichroismus - (ICD) und 2D ROESY Studien ermittelt wurde, ist die Ko-konformation von Ferrocenylazid (FcN_3) im Hohlraum des β -Cyclodextrins (β -CyD) von Lösungsmittel und Temperatur abhängig. Thermodynamische Untersuchungen, basierend auf der ICD Titration in Ethylenglykol, zeigten, dass durch die Monosubstitution des Ferrocens mit der Azidogruppe die Affinität zum β -CyD um den Faktor 2.5 erniedrigt wird. Während das Ferrocen (FcH) nur eine mäßige Assoziation zum β -CyD in DMSO aufweist, dissoziiert der $\text{FcN}_3@ \beta$ -CyD Komplex in diesem Lösungsmittel praktisch vollständig.

Laut der Kristallstrukturanalyse, besitzt das Ferrocen eine equatoriale Ausrichtung in der Kavität des permethylierten β -CyD (TRIMEB), wohingegen eine axiale Lage im nativen β -CyD begünstigt ist. Im Gegensatz dazu nimmt das FcN_3 Molekül in seinem Einschlusskomplex mit TRIMEB eine bimodale Orientierung ein. Mittels NMR Experimente in D_2O konnte gezeigt werden, dass Zugabe von TRIMEB die chemische Äquivalenz der Ferrocenprotonen aufhebt. Trotz des schnellen Austauschprozesses wird die Rotation der Azidogruppe gehindert. Die Zersetzung eines $\text{FcN}_3@(\alpha\text{-CyD})_2$ Komplexes lieferte ein Produkt mit komplexer Struktur:



Entgegen der erwarteten C-H Einschiebung des Ferrocenyl Nitrens fand dabei eine ungewöhnliche Pyranose – Furanose Umwandlung statt.

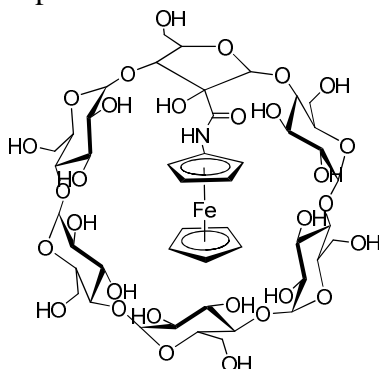
Röntgenstrukturanalysen des 2-Adamantan Azid - β -CyD Komplexes zeigten, dass das Gastmolekül eine bimodale Ausrichtung einnimmt. In D_2O lagert sich das 1-Adamantanazid mit „apikaler“ Orientierung in den Hohlraum des β -CyD ein, wie sich aus der 2D ROESY Messung herausstellte. Die 1- und 2-Adamantanazide bilden stabile Komplexe mit β -CyD, deren sehr große Assoziationskonstanten mit ICD Titrationen bestimmt wurden. In wässrigem Ethanol weist 1-Adamantanazid eine kooperative Bindung zum α -CyD unter Bildung eines 1:2 Inklusionskomplexes auf. Die in den Kavitäten der CyD eingeschlossenen Adamantylnitrene, welche photolytisch aus den entsprechenden Aziden generiert wurden, reagierten erstaunlicherweise nicht mit dem CyD-Gerüst.

Abstract (English)

This work involves physical as well as organic synthetic aspects of chemistry. Spectroscopic and theoretical chemistry methods were utilized to shed light into conformational analysis and thermodynamics of supramolecular complexes.

As inferred from Induced Circular Dichroism (ICD) and 2D DOESY studies, the co-conformation of ferrocenyl azide (FcN_3) in the cavity of β -Cyclodextrin (β -CyD) is tuned by solvent and temperature. Studies on thermodynamics based on ICD titration conducted in ethylene glycol showed, that upon substituting the ferrocene by the azide group, the affinity towards the β -CyD decreased by a factor of 2.5. Whereas the ferrocene (FcH) exhibits moderate binding to β -CyD in DMSO, the $\text{FcN}_3@ \beta$ -CyD complex is practically dissociated in this solvent.

The crystal structure analysis of the $\text{FcH}@ \text{TRIMEB}$ (2,3,6-per-*O*-methyl- β -CyD) complex revealed an equatorial inclusion of ferrocene in the cavity, which is in contrast to the axial inclusion observed in native β -CyD. In the solid state, FcN_3 adopts a bimodal disposition inside the TRIMEB cavity. The ^1H NMR spectra recorded in heavy water showed that the presence of TRIMEB caused chemical nonequivalence of the FcN_3 protons. Despite the fast exchange process, the rotation of the azide group was hindered. Upon the decomposition of the $\text{FcN}_3@(\alpha\text{-CyD})_2$ complex, a product with a complex structure was isolated:



Instead of the expected nitrene insertion into the C-H bonds of α -CyD, an unusual glucopyranose – furanose conversion took place.

X-ray analysis has shown that 2-adamantane azide adopts a bimodal disposition inside β -CyD. In deuterium oxide, 1-adamantane azide takes an apical orientation within the cavity of β -CyD, as inferred from the 2D ROESY measurement. The 1- and 2-adamantane azides form stable complexes with β -CyD, as demonstrated by large binding constants determined by ICD titration. 1-Adamantane azide binds cooperatively to α -CyD forming a stable 1:2 inclusion complex. The adamantyl nitrenes, generated by photolysis of 1- and 2-adamantane azides included in the cavity of α - and β -CyDs, surprisingly did not modify the CyD scaffold.

Parts of this work have been published or presented at conferences:

Publications

- 1) “Solvent- and Temperature-Tuned Orientation of Ferrocenyl Azide Inside β -Cyclodextrin” Walla, P., Arion, V. B., Brinker, U. H. *J. Org. Chem.* **2006**, *71*, 3274 – 3277 (see p. 22).
- 2) “Solvent and Temperature-Dependent Co-Conformation of Ferrocenyl Azide inside β -Cyclodextrin: Induced Circular Dichroism, Quantum Mechanical, and NMR Studies” Walla, P., Brecker, L., Brinker, U. H. *manuscript in preparation* (see p. 41).
- 3) “Structure-Chemistry Relationship in Ferrocenyl Azide-Cyclodextrin Complexes” Walla, P., Brecker, L., Arion, V. B., Brinker, U. H. *manuscript in preparation* (see p. 86).
- 4) “Study of the Structure and Photochemical Decomposition of the Adamantane Azides Included in α - and β -Cyclodextrins” Walla, P., Kokkotas, N., Krois, D., Arion, V. B., Brinker, U. H. *manuscript in preparation* (see p. 137).
- 5) “Unusual 1:2 Stoichiometry of Phenyl Azide – Calix[4]arene Clathrate: Crystal Structure and Thermal Analysis Studies” Wagner, G.; Walla, P.; Arion, V. B.; Brinker, U. H. *manuscript in preparation* (not included in this thesis).

Presentations at conferences

- 1) “Supramolecular Nitrene Chemistry: Photolysis of the Ferrocenyl Azide@ β -Cyclodextrin Complex” Walla, P., Brinker, U. H. Poster Presentation. International Conference on Supramolecular Science and Technology (ICSS & T), 5. – 9. 9. 2004, Prague, Czech Republic.
- 2) “Supramolecular Nitrene Chemistry: Photolysis of the Ferrocenyl Azide@ β -Cyclodextrin Complex” Walla, P., Brinker, U. H. Poster Presentation. 2nd European Students Conference on Physical Organic and Polymer Chemistry (PHOPOC II), 15. – 17. 9. 2004, Vienna, Austria.
- 3) “Unusual Reaction of Ferrocenyl Nitrene Constrained within α -Cyclodextrin” Walla, P., Arion, V. B., Brecker, L., Brinker, U. H. Lecture Presentation. 3rd European Students Conference on Physical, Organic, and Polymer Chemistry (PHOPOC III), 18. – 20. 9. 2006, Vienna, Austria.
- 4) “Supramolecular Nitrene Chemistry” Walla, P., Brinker, U. H. Lecture Presentation. 12th Austrian Chemical Days, 10. – 13. 9. 2007, Klagenfurt, Austria.

Acknowledgment

The experimental work and the compilation of this PhD Thesis was performed between the years 2003 and 2008. During this period, many people have helped me to solve “daily research problems”. Herewith, I would like to express my cordial gratefulness to them.

First and foremost, I would like to thank Prof. Udo H. Brinker, that he introduced me to the field of supramolecular chemistry and to the chemistry of neutral reactive intermediates. I very much appreciate the liberty he provided to pursue my own scientific ideas.

I thank my colleagues Michael Abraham, Alexander Bepokoev, Wolfgang Knoll, Jean-Luc Mieusset, Mirjana Pacar, Karin Simon, Kuan-Jen (Stephan) Su, Gerald Wagner and Marcel Wieland for creating an enjoyable working atmosphere and helpful discussions.

I am very thankful to:

- Alexey Gromov for discussions about laboratory techniques and strategies in organic synthesis
- Michael Zinke for the discussions concerning practical aspects of HPLC
- Stephan Bruckner for discussions about mathematical methods of finding a global minima
- Ion Chiorescu for help and many discussions about molecular modeling
- Alexander Roller for recording plenty of X-ray single crystal measurements and discussions about practical aspects of X-ray single crystal analysis
- Susanne Felsing for recording numerous NMR spectra
- Peter Unteregger for recording MS spectra and repairs of the circular dichroism instrument
- Heidi Schwartz for recording ESI-MS spectra
- Alexander Leitner for recording HPLC-ESI-MS spectra
- Walter Balba for manufacturing tailor-made glassware
- Dr. Peter Kasak for supporting discussions concerning the research strategy and general support

From the professional staff, I am indebted to:

- Profs. Harald Lehner and Otmar Hofer for the discussions concerning Circular Dichroism
- Dr. Lothar Brecker for the recording of NMR measurements and for fruitful discussions concerning problems associated with NMR spectroscopy
- Dr. Hanspeter Kählig for recording NMR spectra
- Profs. Karl Peter Wolschann and Alfred Karpfen for help with molecular modeling
- Prof. Michael Widhalm for help with practical problems associated with the techniques in an organic laboratory
- Prof. Walter Weissensteiner for discussions about stereochemistry of enantiomeric conformers

- Prof. Werner Mikenda for help with measurements of IR spectra and discussions concerning kinetics of the organic reactions monitored by IR spectroscopy
- Prof. Daniel Krois for help with Circular Dichroism and HPLC measurements
- Prof. Vladimir B. Arion for performing many X-ray single crystal analyses and for discussions concerning crystal structures
- Prof. Eberhard Lorbeer for discussions about gas chromatography
- Prof. David C. Doetschman from Department of Chemistry, State University of New York at Binghamton, Binghamton, N.Y., USA, for measuring EPR spectra

I express my gratitude also to my parents, family and friends for having supported me over the years.

I especially appreciate the patience of my son and my wife, since the finishing of this PhD Thesis required a lot of time.

This work was financially supported by the Fonds zur Förderung der wissenschaftlichen Forschung in Österreich (Project P12533-CHE).

Table of Contents

1.	Introduction	1
1.1	Background and Goals of the Dissertation	1
1.2	Chemistry of the Azido Group	3
1.2.1	Geometry	3
1.2.2	Electronic Structure and Spectra of Azides	4
1.2.3	Azides as Nitrene Precursors	9
1.2.3.1	Typical Nitrene Reactions	9
1.3	Cyclodextrins	12
1.3.1	Physical and Chemical Properties	12
1.3.2	Cyclodextrin Inclusion Complexes (CyD ICs)	14
1.3.3	Methods of Preparation of Cyclodextrin Inclusion Complexes	15
1.3.4	Methods for Structure Determination of Cyclodextrin Inclusion Complexes	16
1.3.4.1	Structures in Solution	16
1.3.4.1.1	NMR Methods	16
1.3.4.1.2	Induced Circular Dichroism	17
1.3.4.2	Structures in the Solid State	19
2.	Solvent- and Temperature-Tuned Orientation of Ferrocenyl Azide Inside β - Cyclodextrin	22
2.1	Abstract	22
2.2	Introduction	22
2.3	Results and Discussion	24
2.4	Conclusion	28
2.5	Experimental Section	28
3.	Solvent and Temperature Dependent Co-Conformation of Ferrocenyl Azide inside β -Cyclodextrin: Induced Circular Dichroism, Quantum Mechanical, and NMR Studies	41
3.1	Abstract	41
3.2	Introduction	41
3.3	Results	44
3.3.1	Stoichiometry of $\text{FcN}_3@ \beta\text{-CyD}$ Inclusion Complex	44
3.3.2	Association Constants (K_a) Determinations	45
3.3.3	Solution Co-conformation Studies	46
3.3.3.1	Structural Features of FcH and FcN_3 Guest Molecules	47
3.3.3.2	Calculation of UV-VIS Spectra of FcH and FcN_3 Guest Molecules	48
3.3.3.3	ICD Studies of FcH and FcN_3 Included in the Cavity of $\beta\text{-CyD}$	51
3.3.3.4	Study of the Solution Co-conformation by 2D ROESY Spectroscopy	56
3.4	Discussion	57
3.5	Conclusion	63
3.6	Experimental Section	64
4.	Structure–Chemistry Relationship in Ferrocenyl Azide–Cyclodextrin Complexes	86
4.1	Abstract	86
4.2	Introduction	86

4.3	Results and Discussion	87
4.4	Conclusion	94
4.5	Experimental Section	95
5.	Study of the Structure and Photochemical Decomposition of the Adamantane Azides Included in α - and β -Cyclodextrin	137
5.1	Abstract	137
5.2	Introduction	137
5.3	Results	138
5.3.1	Chemistry of the Adamantane Azides – Cyclodextrin Complexes	138
5.3.2	Single Crystal Structure of 2-Adamantane azide@ β -Cyclodextrin Complex	140
5.3.3	Theoretical Study of the Adamantane Azides	140
5.3.4	Determination of Association Constants Based on ICD.....	142
5.3.5	2D ROESY Spectra of Adamantane Azide – Cyclodextrin Complexes.....	147
5.4	Discussion	148
5.4.1	Chemistry of the Adamantane Azide – Cyclodextrin Complexes .	148
5.4.2	Single Crystal Structure of the 2-Adamantane Azide@ β -Cyclodextrin Complex	149
5.4.3	Theoretical Study of Adamantane Azides	149
5.4.4	Determination of Association Constants Based on ICD.....	150
5.4.5	2D ROESY Spectra of the Adamantane Azide – Cyclodextrin Complexes.....	151
5.5	Conclusion	152
5.6	Experimental Section	153
6.	Summary	167

1. Introduction

1.1 Background and Goals of the Dissertation

For a long time, reactive intermediates have been generated by conventional methods, for example in solution. Under these conditions, reactive intermediates react indiscriminately and their bimolecular reactions may proceed unrestricted. A principal question has to be asked, whether the reaction pathway of the ensued intermediate may be altered upon embedding it into a confined space? In recent years, a new research area has been established and reactive species have been investigated thoroughly within constrained systems. For example, Raymond et al. demonstrated the stabilization of $[\text{Me}_2\text{C}(\text{OH})\text{PEt}]^+$ and $[\text{CpRu}(\text{cod})]^+$ carbocations by the naphthalene-based tetrahedral $[\text{Ga}_x\text{LY}]^z$ host,¹ Cram and Warmuth have used hemicarcerands to spectroscopically characterise the highly unstable intermediates cyclobutadiene,² *o*-benzyne,³ and cycloheptatetraene,⁴ fluorophenoxycarbene⁵ and phenyl nitrene⁶ by preventing them from dimerization or reaction with bulk-phase species. Fujita and co-workers observed the formation of an otherwise nonisolable cyclic silanol trimer within the cavity of their M_6L_4 supramolecular host.⁷ Rebek et al. were able to inhibit homolytic bond cleavage of benzoyl peroxide by encapsulation, even at elevated temperatures for prolonged periods of time.⁸ Brinker et al. utilized cyclodextrins for altering reaction pathways of carbenes.⁹

As may be inferred from the title of this thesis, organic azides have been embedded into supramolecular host molecules. In this study, three organic azides have been investigated: ferrocenyl azide (FcN_3), 1-adamantane azide and 2-adamantane azide. Cyclodextrins were applied as host molecules. The thermal or photochemical decomposition of the azides studied in solution is well known. Thus the product distributions of the decompositions conducted within the cavity of cyclodextrins may be compared conveniently.

¹ (a) Ziegler, M., Brumaghim, J. L., Raymond, K. N. *Angew. Chem. Int. Ed.* **2000**, *39*, 4119. (b) Fiedler, D., Bergman, R. G., Raymond, K. N. *Angew. Chem. Int. Ed.* **2006**, *45*, 745.

² Cram, D. J., Tanner, M. E., Thomas, R. *Angew. Chem. Int. Ed.* **1991**, *30*, 1024.

³ Warmuth, R. *Angew. Chem. Int. Ed.* **1997**, *36*, 1347.

⁴ Warmuth, R., Marvel, M. A. *Angew. Chem. Int. Ed.* **2000**, *39*, 1117.

⁵ Liu, X., Chu, G., Moss, R. A., Sauers, R. R., Warmuth, R. *Angew. Chem. Int. Ed.* **2005**, *44*, 1994.

⁶ (a) Warmuth, R., Makowiec, S. *J. Am. Chem. Soc.* **2005**, *127*, 1084. (b) *idem.*, *ibid.* **2007**, *129*, 1233.

⁷ (a) Yoshizawa, M., Kusukawa, T., Fujita, M., Yamaguchi, K. *J. Am. Chem. Soc.* **2000**, *122*, 6311. (b) Yoshizawa, M., Kusukawa, T., Fujita, M., Sakamoto, S., Yamaguchi, K. *ibid.* **2001**, *123*, 10454.

⁸ Körner, S., Tucci, F. C., Rudkevich, D. M., Heinz, T., Rebek, J. Jr., *Chem. Eur. J.* **2000**, *6*, 187.

⁹ (a) Brinker, U. H.; Buchkremer, R.; Kolodziejczyk, M.; Kupfer, R.; Rosenberg, M.; Poliks, M. D.; Orlando, M.; Gross, M. L. *Angew. Chem., Int. Ed.* **1993**, *32*, 1344. (b) Rosenberg, M. G.; Kam, S. M.; Brinker, U. H. *Tetrahedron Lett.* **1996**, *37*, 3235. (c) Krois, D.; Bobek, M. M.; Werner, A.; Kählig, H.; Brinker, U. H. *Org. Lett.* **2000**, *2*, 315. (d) Rosenberg, M. G.; Brinker, U. H. *J. Org. Chem.* **2001**, *66*, 1517. (e) Knoll, W.; Bobek, M. M.; Giester, G.; Brinker, U. H. *Tetrahedron Lett.* **2001**, *42*, 9161. (f) Rosenberg, M. G.; Brinker, U. H. *J. Org. Chem.* **2003**, *68*, 4819. (g) Krois, D.; Brecker, L.; Werner, A.; Brinker, U. H. *Adv. Synth. Catal.* **2004**, *346*, 1367. (h) Rosenberg, M. G.; Brinker, U. H. In *Adv. Phys. Org. Chem.*; Richard, J. P., Ed.; Academic: New York, **2005**; Vol. 40, pp 1-47. (i) Rosenberg, M. G.; Brinker, U. H. *Eur. J. Org. Chem.* **2006**, 5423.

Azides have been applied frequently in the field of photoaffinity labeling,^{10, 11} but the exact structure of the products formed upon the build-in of the organic nitrene into the active site is often not known. Therefore, in this thesis the focus will be on the structure of the macromolecules, formed in the reaction of the nitrenes with the host molecule.

The structure of these products is closely related to the starting geometry of the supramolecular assembly. Thus, the determination of the structure of the supramolecular azide complexes with the host molecule is an other pursuit. Moreover, the knowledge of the mutual orientation of guest to host may help to:

- understand molecular recognition phenomena in enzyme-substrate interaction or catalysis, and may help to shed more light into structure-activity relationships in supramolecular chemistry
- understand the mechanism of reactions mediated by host macrocycles
- develop functional supramolecular materials, such as those for catalytic or analytical purposes

Consequently, the thermodynamic affinity of the guest towards the host molecule is of principal concern in this thesis.

¹⁰ (a) Lwowski, W. *Annals of the New York Academy of Sciences* **1980**, 346, 491. (b) Vodovozova, E. L. *Biochemistry (Moscow)*, **2007**, 72, 1.

¹¹ Bräse, S.; Gil, C.; Knepper, K.; Zimmermann, V. *Angew. Chem., Int. Ed.* **2005**, 44, 5188.

1.2 Chemistry of the Azido Group

1.2.1 Geometry

The structure of numerous azides, azide anions and azide radicals have been determined by the neutron, electron and X-ray scattering techniques, and with the help of UV and microwave spectroscopies. In general, the $N_a-N_b-N_c$ unit is linear and the angle α ($R-N_a-N_b$) lies within the range of $105-130^\circ$ (Figure 1).

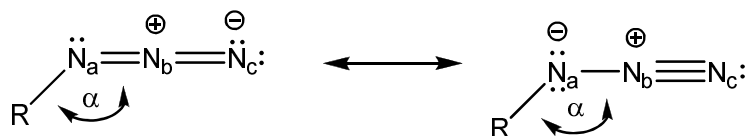
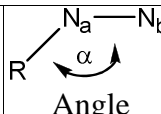


Figure 1. Resonance canonical structures of covalent azides. Adopted from ref. 12.¹³

One can write two canonical structures (Figure 1). Equal contributions of the resonance forms lead to the bond order 1.5 and 2.5 for bonds N_a-N_b and N_b-N_c , respectively. Table 1 summarizes some structural parameters of the azide group.

¹² Patai, S., Ed., *The Chemistry of the Azido Group*; Wiley: London, 1971.

¹³ I tried my best to notify all copyright holders to obtain their permission to reproduce their figures and tables in this thesis. Please contact me, if still a copyright infringement is found.

Azides	N_b-N_c Å	N_a-N_b Å	$R-N_a$ Å		Method
N_3 (azide radical)	1.1815	1.1815	-	-	UV spectroscopy ¹⁴
N_3 (in $Ba(N_3)_2$) ^a	1.166 ± 0.002	1.166 ± 0.002	-	-	Neutron diffraction ¹⁵
HN_3	1.133 ± 0.002	1.237 ± 0.002	0.975 ± 0.015	114° 8' $\pm 30'$	Microwave spectroscopy ¹⁶
CH_3N_3	1.12 ± 0.01	1.24 ± 0.01	1.47 ± 0.02	120 $\pm 2^\circ$	Electron diffraction ¹⁷
C_3N_{12} (cyanuric triazide)	1.11	1.26	1.38	114°	X-ray diffraction ¹⁸
PhN_3	1.142	1.237	1.422	118.44°	B3LYP / 6-31G(d) ¹⁹
PhN_3	1.133	1.240	1.432	115.54°	X-ray diffraction ¹⁹

^a N-N distances scattered around 1.17 ± 0.01 were reported for NaN_3 , LiN_3 and $Sr(N_3)_2$. Pringle, G. E.; Noakes, D. E. *Acta Cryst.* **1968**, *24B*, 262.

Table 1. Overview of some structural parameters of the azide group.

1.2.2 Electronic Structure and Spectra of Azides

The solution spectrum of HN_3 comprises two absorption bands in the near UV spectrum: a weak band at 260 nm ($\epsilon \sim 40 \text{ M}^{-1}\text{cm}^{-1}$) and a somewhat stronger band at about 200 nm ($\epsilon \sim 500 \text{ M}^{-1}\text{cm}^{-1}$).²⁰ Closson and Gray interpreted this spectrum in terms of molecular orbital theory.²⁰ The atomic *p*-orbitals of HN_3 are shown diagrammatically in Figure 2.

¹⁴ Douglas, A. E., Jones, W. J. *Can. J. Phys.* **1965**, *43*, 2216.

¹⁵ Choi, C. S., *Acta Cryst.* **1969**, *25B*, 2638.

¹⁶ Winnerwisser, M., Cook, R. L. *J. Chem. Phys.* **1964**, *41*, 999.

¹⁷ Livingston, R. L., Rao, C. N. R. *J. Phys. Chem.* **1960**, *64*, 756.

¹⁸ Knaggs, I. E., *Proc. Roy. Soc. (London)* **1935**, *150A*, 576.

¹⁹ "Unusual 1:2 Stoichiometry of a Phenyl Azide – Calix[4]arene Complex: Crystal Structure and Thermal Analysis Studies" Wagner, G., Arion, V. B., Walla, P., Brinker, U. H. *manuscript in preparation*.

²⁰ Closson, W. D., Gray, H. B. *J. Am. Chem. Soc.* **1963**, *85*, 290.

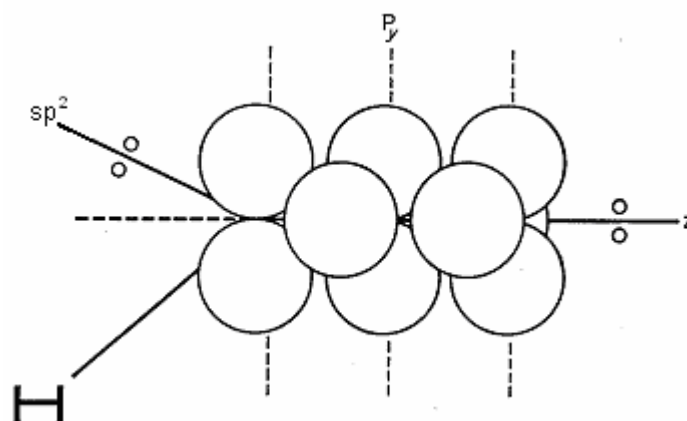
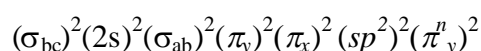


Figure 2. Atomic p -orbitals of HN_3 . Adopted from ref. 12.¹³

The first nitrogen, bonded to hydrogen is sp^2 -hybridized, the second and third are sp -hybridized; non-bonding pairs of electrons are indicated in the diagram by dots. The five p -orbitals of the nitrogens give rise to five delocalized molecular orbitals π_y , π_y^n , π_y^* , π_x , π_x^* , which in the ground state of HN_3 are occupied in order of increasing energy as follows (symbol “a”, “b” and “c” designate nitrogen atoms according to Figure 1):



Closson and Gray attribute the absorption band at 260 nm to the transition of an electron from the highest occupied π_y^n -orbital to the lowest unoccupied π_x^* -orbital (Figure 3).

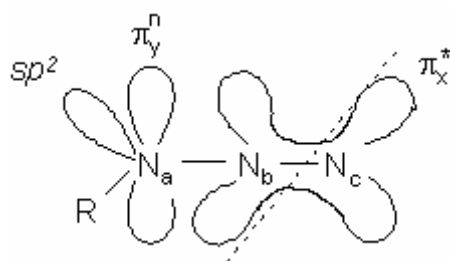


Figure 3. Representation of the orbitals involved in the longest wavelength absorption band ($\pi_y^n \rightarrow \pi_x^*$ transition type) in azoimide ($R = H$) and in simple alkyl azides. The n -superscript of the π_y^n orbital designates actually the non-bonding p_y atomic orbital of N_a depicted in Figure 2. Adopted from ref. 12.¹³

This transition leads to the excited electronic configuration $\dots (sp)^2(\pi_y^n)^1(\pi_x^*)^1$. The band at 200 nm is assigned to the transition $sp_2 \rightarrow \pi_y^*$ and produces the excited configuration $\dots (\pi_x)^2(sp^2)^1(\pi_y^n)^2(\pi_y^*)^1$. Both transitions are symmetry forbidden, hence the low extinction.

The spectra of alkyl azides have the same structure as the spectrum of HN_3 .^{20,21,22,23,24,25} A weak band at 287 nm (band I, $\epsilon \sim 25 \text{ M}^{-1}\text{cm}^{-1}$) is assigned to the

²¹ Sheinker, J. N. *Dokl. Akad. Nauk. SSSR*, **1951**, 77, 1043.

²² Lieber, E., Rao, C. N., Chao, T. S., Wahl, W. H. *J. Scient. Ind. Res.* **1957**, 16B, 95.

²³ Lieber, E., Thomas, A. E. *Appl. Spectrosc.* **1961**, 15, 144.

²⁴ Grammaticacis, P. *Compt. Rend.* **1957**, 144, 1517.

$\pi_y^n \rightarrow \pi_x^*$ transition (Figure 3), a stronger band at 216 nm (band II, $\epsilon \sim 500 \text{ M}^{-1}\text{cm}^{-1}$) to the transition $sp^2 \rightarrow \pi_y^*$. With an electron-releasing group attached to N_a the non-bonding π_y^n orbital is mainly localized on this atom i.e. it becomes more negative than N_c . Thus in alkyl azides both transitions involve a flow of charge from N_a to the other nitrogen atoms. Transition I is perpendicular in the sense that the π_y^n and π_x^* orbitals are perpendicular to each other; this accounts for its low intensity. The higher intensity of band II may be ascribed to the partial s character of the sp^2 hybridized orbital. Thus, we may designate the transition I as an $n \rightarrow \pi^*$ type, since the excitation involves a transfer of an electron from a non-bonding π to an antibonding π^* orbital. Moreover, band II can also be considered as an $n \rightarrow \pi^*$ transition as it involves the lone pair stemming from the sp^2 orbital. The position and extinction of these bands are independent of the structure of the alkyl group and are also remarkably insensitive to solvent changes (Table 2).²⁰

²⁵ Reynolds, G. A. Allen, J. A., Tinker, J. F. *J. Org. Chem.* **1959**, 24, 1205.

R	Solvent	λ_m (nm)	ϵ	Reference
Ethyl	Ethanol	286	26	21
n-Butyl	iso-Octane	286	24	20
t-Butyl	iso-Octane	288	-	20
s-Heptyl	Heptane	289	23	26
Cyclohexyl	iso-Octane	287	25	20
2-Phenethyl	Heptane	289	25	26
2-Chloroethyl	iso-Octane	283	34	20
2-Hydroxyethyl	iso-Octane	283	-	20
2-Acetoxyethyl	iso-Octane	284	25	20
Acetyl	Ethanol	288	25	21
Ethoxycarbonyl	iso-Octane	280	25	20
Methoxycarbonyl	Ethanol	260	40	21
H	iso-Octane	264	-	20
	Water	260	43	20

Table 2. The low energy absorption band in several alkyl and acyl azides RN_3 . Adopted from ref. 12.¹³

In the acyl azides, conjugation with the carbonyl group causes a small blue shift of the low energy band and a slight enhancement of its extinction (Table 2).

While the absorption spectrum of the alkyl azides is that of the isolated azido group, the spectra of aromatic azides are essentially those of the parent hydrocarbon, only a weak additional band due to the azido group appears as a shoulder on the long wavelength side of the hydrocarbon spectrum (Figure 4).²⁷

²⁶ Levene, P. A., Rothen, A. *J. Chem. Phys.* **1937**, 5, 985.

²⁷ Reiser, A., Bowes, G., Horne, R. J. *Trans. Faraday Soc.* **1966**, 62, 3162.

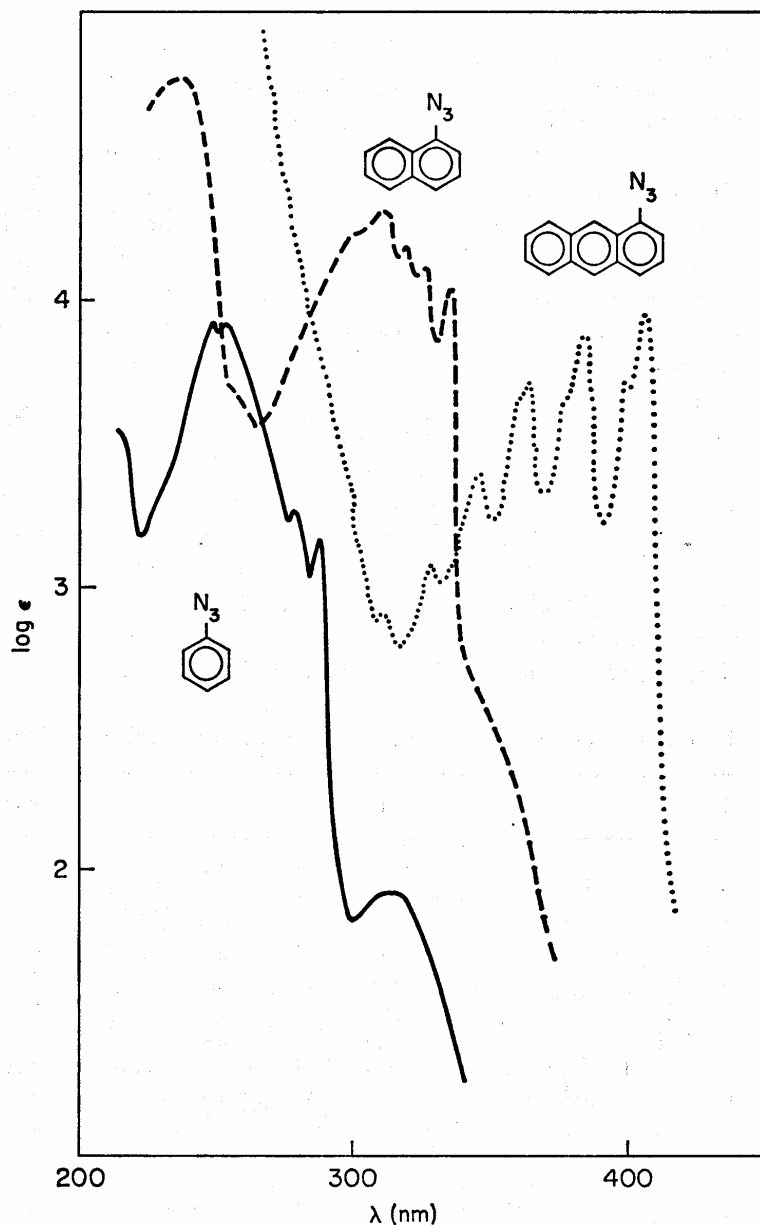


Figure 4. Absorption spectra of aromatic azides. Adopted from ref. 12.¹³

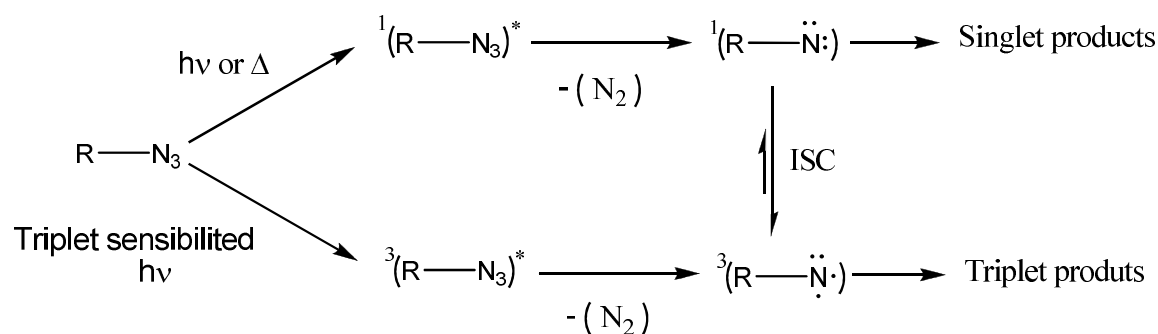
The coupling of the azido group with the aromatic system corresponds to a charge flow from nitrogen towards the aromatic ring. This lowers the energy of the non-bonding π_y^* -orbital below the level of the sp^2 orbital; consequently the azido band is assigned to the transition of lowest energy, namely $sp^2 \rightarrow \pi_y^*$, where the π_y^* -orbital extends now over the whole of the aromatic system.

The azido group affects the spectrum of the hydrocarbon itself in two ways: it causes a red shift of the 1L_a -band and a smaller red shift of the other bands (the size of the aromatic system is increased); it also reduces the symmetry of the molecule, thus enhancing the extinction of the symmetry forbidden transition 1L_b at the expense of the associated 1B -transition (intensity borrowing²⁸).

²⁸ Murrell, J. N. *The Theory of the Electronic Spectra of Organic Molecules*, Methuen, London, 1963.

1.2.3 Azides as Nitrene Precursors

Among others, azides seem to be the most practical and popular precursors for the generation of nitrenes.¹² The nitrene, an electron-deficient monovalent organic reactive intermediate, may be generated from the azide either thermally or photochemically (Scheme 1).



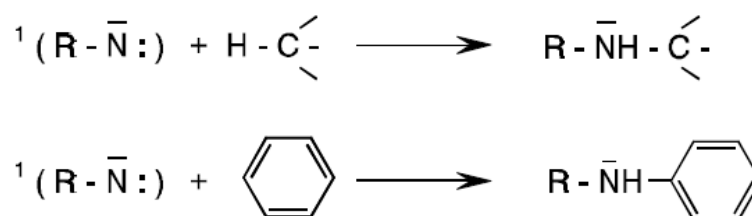
Scheme 1. Nitrene generation from azides.

The nitrogen atom of a nitrene has a sextet of electrons in its outer shell, and depending on the conditions, the species may exist either in the triplet diradical state or the electrophilic singlet state (Scheme 1). The singlet nitrene undergoes ISC (InterSystem Crossing) to its ground state triplet.

1.2.3.1 Typical Nitrene Reactions

For nitrenes, existing both in singlet and triplet states, there are different reaction pathways available:

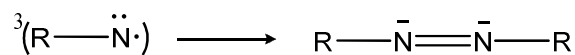
- If only the singlet nitrene is present, electrophilic attack on the binding electrons of a covalent single or multiple bond may take place. In analogy to the Doering-Prinzbach mechanism,²⁹ a **C-H insertion** of the nitrene takes place. This way a secondary amine is formed (Scheme 2).



Scheme 2. C-H Insertion of a singlet nitrene.

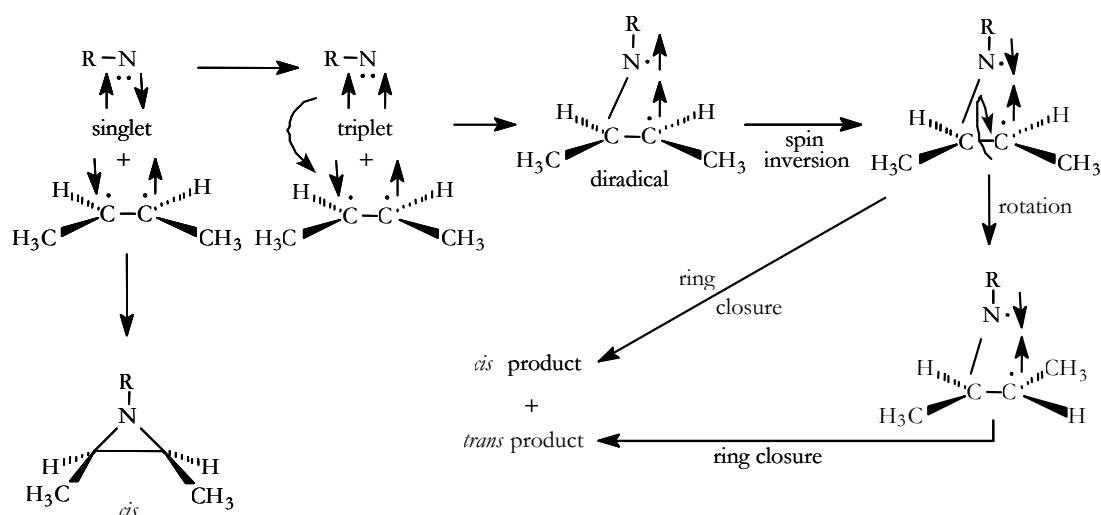
²⁹ Doering, W. v. E.; Prinzbach, H. *Tetrahedron* **1959**, 6, 24.

- The **Recombination** of two nitrenes is spin-allowed for both singlet and triplet nitrene. The first process is energetically more demanding and therefore the azo compound formation is attributed to the triplet nitrene reaction (Scheme 3).



Scheme 3. Azo compound formation by recombination of nitrenes.

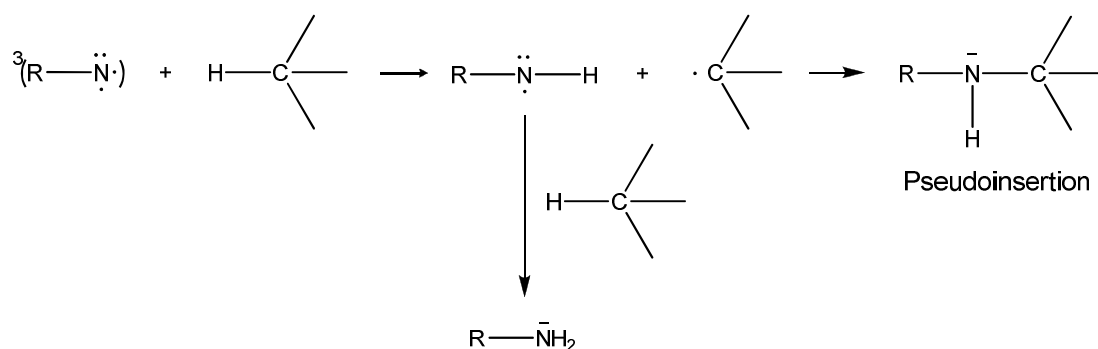
- The **Addition to Alkenes** may be the reaction of singlet as well as triplet nitrenes. The addition of the electrophilic singlet nitrene proceeds by a synchronous concerted mechanism and thus stereoselectively (Scheme 4).



Scheme 4. Stereochemistry of singlet and triplet nitrenes.

The triplet nitrene addition is not stereoselective and proceeds via a radical non-concerted stepwise mechanism.

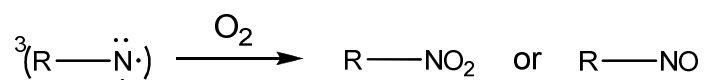
- The most common triplet nitrene reaction is a radical attack leading to **Hydrogen Abstraction** (Scheme 5).



Scheme 5. Hydrogen Abstraction by a triplet nitrene.

The recombination of the radical couple according to the Benson-DeMore mechanism³⁰ is called “Pseudoinsertion” (Scheme 5).

- The triplet nitrenes react with oxygen under the production of nitro or nitroso compounds (Scheme 6).



Scheme 6. Reaction of a triplet nitrene with oxygen.

³⁰ DeMore, W. B.; Benson, S. W. *Advan. Photochem.* **1964**, 2, 219.

1.3 Cyclodextrins

1.3.1 Physical and Chemical Properties

Cyclodextrins are macrocyclic oligosacchrides consisting of α -1,4-linked glucopyranose subunits. They appear like toroidal macro rings with a cavity in the center (Figure 5).³⁶

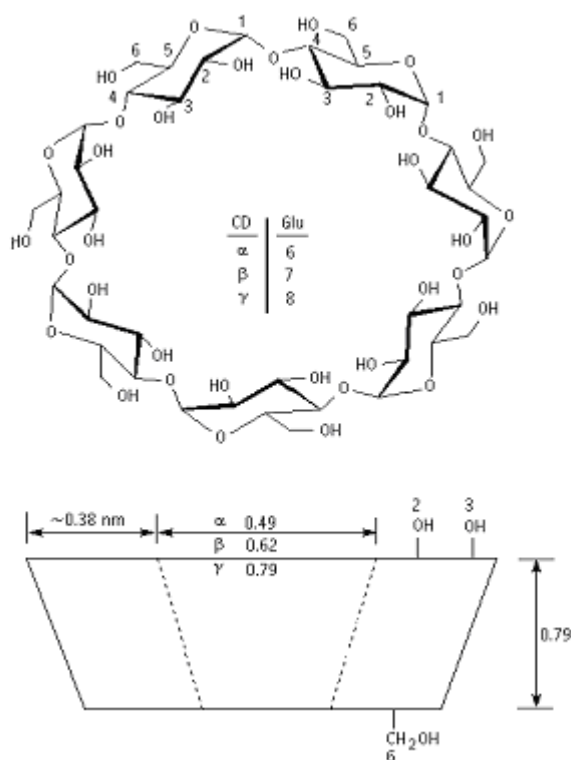


Figure 5. Structure of β -CyD (top) and approximate dimensions of α -, β -, and γ -CyDs (bottom). Adopted from ref. 31.¹³

Crystal structure analyses of cyclodextrins have revealed that all glucose residues in the ring possess the thermodynamically favored 4C_1 chair conformation with all substitutions in the equatorial position. The external surface of a cyclodextrin contains secondary hydroxyl groups situated on the upper rim of the ring, whereas primary hydroxyl groups are located on the bottom rim (Figure 5). The inner surface of the hydrophobic cavity is lined by hydrogen atoms and ether-like oxygens.³² The overall appearance of a cyclodextrin molecule resembles a truncated cone with the wide “open” and narrow “closed” apertures. The cavity diameters (maximum values based on the Van-der-Waals radii) are 5.3, 6.5, and 8.3 Å for α -CyD, β -CyD, and γ -CyD respectively. Table 3 summarizes the most important structural features of α -, β -, and γ -cyclodextrin.

³¹ Jindřich, J. <http://jindrich.org/CD/sbcdcon2.gif>.

³² Nagai, T. in “*Proceedings of the First International Symposium on Cyclodextrins*”, Szejtli, J. Ed., Reidel: Dordrecht, **1981**, p. 15.

	α	β	γ
Number of glucose units	6	7	8
Molecular weight (g/mol)	972	1135	1297
Solubility in water at 25 °C (g/100 mL)	14.5	1.85	23.2
$[\alpha]_D$ at 25 °C	150 ± 0.5	162.5 ± 0.5	177.4 ± 0.5
Cavity diameter, Å	4.7 - 5.3	6.0 - 6.5	7.5 - 8.3
Height of torus, Å	7.9 ± 0.1	7.9 ± 0.1	7.9 ± 0.1
Approx. volume of cavity, Å ³	174	262	427
Crystal water, wt %	10.2	13.2 - 14.5	8.13 - 17.7
Hydrolysis by <i>A. oryzae</i> α -amylase	negligible	slow	rapid

Table 3. Structural and physical properties of α -, β -, and γ -cyclodextrin.^{33, 34}

Due to the presence of hydroxyl groups, cyclodextrins are soluble in polar solvents.³⁵ Therefore, studies on cyclodextrins have been mostly conducted in aqueous media. Among the three native most common cyclodextrins, β -CyD has the lowest solubility in water (Table 3). This is ascribed to the intramolecular hydrogen bond formation between the C2-OH group of one glucopyranoside unit with the C3-OH group of the adjacent glucopyranose. A complete secondary belt is formed by these hydrogen bonds thus enhancing the rigidity of the β -CyD molecule. In α -CyD, the hydrogen bond belt is incomplete, because one glucopyranose unit is in a distorted position. The largest γ -CyD has a more flexible structure and is the most soluble of the three cyclodextrins.

³³ Szejtli, J. *Cyclodextrin Technology*, Kluwer: Dordrecht, 1988, p. 450.

³⁴ Luong, J. H. T.; Nguyen, A. L. *J. Chromatogr. A*, **1997**, 792, 431.

³⁵ Siegel, B.; Breslow, R. *J. Am. Chem. Soc.* **1975**, 97, 6869.

1.3.2 Cyclodextrin Inclusion Complexes (CyD ICs)

In contrast to the hydrophilic exterior, the inner surface of cyclodextrins is hydrophobic. In an aqueous solution, the cavity of a cyclodextrin is filled with energetically unstable water molecules (polar - non-polar interaction), which are readily displaced by appropriate “guest molecules”.³⁶ For the driving force of the inclusion process, two main components are involved: the repulsive forces between the included water molecules and the non-polar cyclodextrin cavity on one side, and between the bulk water and the non-polar guest molecule, on the other side. The various published studies on cyclodextrins indicate that the main interaction forces responsible for the complex formation are: van-der-Waals interactions,³⁷ hydrophobic interactions,^{38,39} strain energy of the macrocyclic ring,⁴⁰ dipolar interactions,⁴¹ and in some cases hydrogen bonding.⁴² Covalent bonding is inoperative in the cyclodextrin inclusion complexes – a phenomenon characteristic for supramolecular chemistry on the whole. In this way, aqueous solutions of cyclodextrins can form complexes with various solid, liquid, and even gaseous guest molecules,⁴³ for example with dyes,^{44,45,46,47} drugs,⁴⁸ small anions,⁴⁹ carboxylic acids,⁵⁰ and alcohols.⁵¹ Cyclodextrins can also form inclusion compounds in the solid state.⁵²

Usually, complexes with 1:1 guest : host stoichiometries are formed, but 1:2 stoichiometries are frequently experienced as well.^{46,47,53} Ratio 2:1 and 2:2 have also been found^{54,55,56} and even more complicated ones.⁵⁷

Much of the work on cyclodextrin inclusion complexes has been focused on the determination of association constants. By forming an inclusion complex, a cyclodextrin may change some of the physical and chemical properties of the guest molecule. For example, spectrophotometric determinations^{44,47} are based on the difference in absorptivity of the free and complexed guest. In conductometric studies,^{58,59} the difference in mobility of the free and complexed ionic substrate is

³⁶ Cramer, F. *Chem. Ber.* **1951**, *84*, 851.

³⁷ Bergereon, R. J.; Pillor, D. M.; Gibeily, G.; Roberts, W. P. *Bioorg. Chem.* **1978**, *7*, 263.

³⁸ Harata, H. *Bull. Chem. Soc. Jpn.* **1976**, *49*, 2066.

³⁹ Tabushi, T.; Kiyosuke, Y.; Sugimoto, T.; Yamamura, K. *J. Am. Chem. Soc.* **1978**, *100*, 916.

⁴⁰ Manor, P. C.; Saenger, W. *J. Am. Chem. Soc.* **1974**, *96*, 3630.

⁴¹ Gelb, R. I.; Schwartz, L. M.; Cardelino, B.; Fuhrman, H. S.; Johnson, R. F.; Laufer, D. A. *J. Am. Chem. Soc.* **1981**, *103*, 1750.

⁴² Ref. 32, p. 141.

⁴³ Szejtli, J. *J. Incl. Phenom.* **1983**, *1*, 104.

⁴⁴ Cramer, F.; Saenger, W.; Spartz, H. C. H. *J. Am. Chem. Soc.* **1967**, *89*, 14.

⁴⁵ Matsui, Y.; Mochida, K. *Bull. Chem. Soc. Jpn.* **1978**, *51*, 673.

⁴⁶ Buss, V.; Reichardt, Ch. *J. Chem. Soc., Chem. Commun.* 1992, 1636.

⁴⁷ Tawarah, K. M.; Khouri, S. J. *Dyes and Pigments* **2000**, *45*, 229.

⁴⁸ Mwakibete, H.; Bloor, D. M.; Wyn-Jones, E. J. *J. Inclusion Phenom. Mol. Recognit. Chem.* **1991**, *10*, 497.

⁴⁹ Rohbach, R. P.; Rodriguez, L. J.; Eyring, E. M. *J. Phys. Chem.* **1977**, *81*, 944.

⁵⁰ Gelb, R. I.; Schwartz, L. M. *J. Inclusion Phenom. Mol. Recognit. Chem.* **1989**, *7*, 465.

⁵¹ Buvani, A.; Szejtli, J.; Barcza, L. *J. Inclusion Phenom.* **1983**, *1*, 151.

⁵² Cramer, F.; Hettler, H. *Naturw.* **1967**, *54*, 625.

⁵³ Schiller, R. L.; Coates, J. H.; Lincoln, S. F. *J. Chem. Soc., Faraday Trans. 1.* **1984**, *80*, 1257.

⁵⁴ Connors, K.; Pendergast, D. *J. Am. Chem. Soc.* **1984**, *106*, 7607.

⁵⁵ Hirai, H.; Toshima, N.; Uenoyama, S. *Bull. Chem. Soc. Jpn.* **1985**, *58*, 1156.

⁵⁶ Park, J. W.; Song, H. *J. Phys. Chem.* **1989**, *93*, 6454.

⁵⁷ Hamai, S. *J. Phys. Chem.* **1989**, *93*, 2074.

⁵⁸ Wojcik, J. F.; Rohrbach, R. P. *J. Phys. Chem.* **1975**, *79*, 2251.

changed. Upon inclusion of an achiral guest into the chiral cyclodextrin cavity, it may become optically active and exhibit induced Cotton effects.⁶⁰ Sometimes the maximum of the UV absorption band is shifted by several nm and fluorescence is strongly enhanced, since the fluorescing molecule is transferred from the polar aqueous media into a non-polar surrounding.⁶¹ In NMR spectra, the chemical shifts of the anisotropically shielded atoms may be significantly altered.⁶²

In many cases cyclodextrins mimic artificial enzymes,^{63,64} accelerating various organic reactions and modifying reaction pathways.^{65,66}

Thermal analysis has also been used in the study of inclusion compounds.^{67,68} In some cases no melting peaks of the guests were detected, after the inclusion of the guest into the cavity of cyclodextrin. In thermal decomposition studies it was observed that the decomposition of the complexed guest occurs above the decomposition temperature of the uncomplexed molecule.^{69,70} The general stabilization of guest molecules gives rise to the wide application of cyclodextrin inclusion complexes.

1.3.3 Methods of Preparation of Cyclodextrin Inclusion Complexes

Several methods for the preparation of cyclodextrin complexes were reviewed.⁷¹ These are: the coprecipitation, the slurry, the paste and the dry mixing methods.

The coprecipitation method is most commonly used in small scale laboratory applications. The guest molecule is added to an aqueous solution of cyclodextrin and if the solubility of the complex formed is exceeded, the complex will precipitate and can be isolated by filtration or centrifugation. However, the large amount of solvent necessary makes this method industrially unattractive. In general, when the guest molecule is soluble in water (e.g. due to the presence of polar functional groups such as hydroxy or carboxy groups), it may be added directly into an aqueous solution of CyDs. Insoluble guests may at first be dissolved in alcohols and consequently mixed with an aqueous solution of CyDs. The isolated complexes, however, also contain the included alcohols.^{9g, 72} Solvent-free ICs may be prepared by replacing alcohols by e.g. diethyl ether. The use of Et₂O facilitates phase transfer because Et₂O and H₂O are partially miscible. Under these conditions, a competitively formed CyD IC with Et₂O can be formed. Bubbling argon⁷³ or nitrogen⁷⁴ through the CyD solution appears to be able to remove the ether.

⁵⁹ Tawarah, K. M.; Wazwaz, A. A. *J. Chem. Soc. Faraday Trans.* **1993**, 89, 1729.

⁶⁰ Harata, K.; Uedaira, H. *Bull. Chem. Soc. Jpn.* **1975**, 48, 375.

⁶¹ Tung, C. H.; Zhen, Z.; Xu, H. *J. Photochem.* **1986**, 32, 311.

⁶² Demarco, P. V.; Thakkar, A. L. *J. Chem. Soc., Chem. Commun.* **1970**, 2.

⁶³ Griffiths, D. W.; Bender, M. L.; *Adv. Catal.* **1973**, 23, 209.

⁶⁴ Breslow, R.; Dong, S. D. *Chem. Rev.* **1998**, 98, 1997.

⁶⁵ Vanetten, R. L.; Clowes, G. A.; Sebastian, J. S.; Bender, M. L. *J. Am. Chem. Soc.* **1967**, 89, 3242.

⁶⁶ Takahashi, K. *Chem. Rev.* **1998**, 98, 2013.

⁶⁷ Meier, M.M.; Luiz, M. T. B.; Szpoganicz, B.; Soldi, V. *Thermochim. Acta* **2001**, 375, 153.

⁶⁸ Jiao, H.; Goh, S.H.; Valiyaveetil, S. *Macromolecules* **2002**, 35, 1399.

⁶⁹ Novák, C.; Fodor, M.; Pokol, G.; Izvekov, V.; Sztatisz, J.; Arias, M. J.; Ginés, J. M. *J. Therm. Anal.* **1998**, 51, 1001.

⁷⁰ Yilmaz, V. T.; Karadag, A.; İçbudak, H. *Thermochim. Acta* **1995**, 261, 107.

⁷¹ Hedges, A. R. *Chem. Rev.* **1998**, 98, 2035.

⁷² Krois, D.; Brinker, U. H. *J. Am. Chem. Soc.* **1998**, 120, 11627.

⁷³ Takeo, K.; Kuge, T. *Agr. Biol. Chem.* **1972**, 36, 2615.

⁷⁴ Abelt, C. J.; Lokey, J. S.; Smith, S. H. *Carbohydr. Res.* **1989**, 192, 119.

In the slurry method, a suspension containing up to 40% (w/w) of cyclodextrin is stirred with the guest molecule. As the dissolved cyclodextrin forms a complex and the complex precipitates, more of the cyclodextrin goes into solution to form more complex.

The paste method is most commonly used in large scale industrial processes. This method requires a minimum amount of water (20-30%). The cyclodextrin, the guest, and water are mixed in a reactor, and the highly viscous paste is kneaded until the complex is formed.

In the dry mixing method, the guest with the cyclodextrin is mixed without the addition of water. This method is generally not considered as an efficient one, but works well, if the guest acts as a solvent for the cyclodextrin. This is for example the case with lemon oil.

1.3.4 Methods for Structure Determination of Cyclodextrin Inclusion Complexes

1.3.4.1 Structures in Solution

1.3.4.1.1 NMR Methods

Nuclear magnetic resonance (NMR) spectroscopy is one of the most powerful and versatile methods for the elucidation of the structure of supramolecular host – guest complexes at all.

Accommodation of the guest molecule into the cavity of the host leads to changing of the environment of the guest's and host's observed nuclei. For example, concerning the cyclodextrin protons, the shielding or deshielding is expected only for the inner H3 and H5 protons, whereas the outer H2 and H4 protons will not be affected by the inclusion complex formation. Thus, under the conditions of a fast exchange process, the inclusion is accompanied by the so-called Induced Chemical Shift (ICS). The magnitude of the ICS implies the spacial proximity of the protons and, hence, the mutual guest – host orientation. A typical structural inference is that if only H3 undergoes ICS in the presence of substrate then the cavity penetration is shallow, whereas if H5 also shifts, the penetration is deep.⁷⁵

Nuclear Overhauser Effect⁷⁶ (NOE) is very broadly utilized in the experimental NMR techniques for the geometry determination of CyD ICs.⁷⁷ In this case, the origin of the NOE is a host-guest intermolecular dipole-dipole interaction involving transfer of magnetization from one proton to another one directly through space during the spin-lock time of the experiment. Application of traditional NOE difference methods is limited by the unfavorable tumbling rates τ_c of compounds with molecular masses around 1000- 2000 Da. The critical cross relaxation rate depends - besides on the viscosity of the solvents - on the τ_c of the studied compound and on the

⁷⁵ Connors, K. A. *Chem. Rev.* **1997**, 97, 1325.

⁷⁶ For example see textbook: Claridge, T. D. W. *High-Resolution NMR Techniques in Organic Chemistry- Tetrahedron Organic Chemistry Series*, Vol. 19, Pergamon Press, UK, **1999**.

⁷⁷ (a) Inoue, Y. *Annu. Rep. NMR Spectrosc.* **1993**, 27, 59. (b) Schneider, H-J.; Hacket, F.; Rüdiger, V. *Chem. Rev.* **1998**, 98, 1755.

spectrometer frequency. In consequence, the conventional steady-state NOE is positive only for molecular masses below 1000, and negative for those well above 5000 Da, making the NOESY technique not well suitable for study of CyD ICs. Spin-lock experiments such as the rotating frame NOE (ROESY) overcome this serious limitation by application of an additional excitation pulse; after this one observes the transverse instead of the conventional longitudinal magnetization enhancements. Measurements of NOE enhancement by ROESY are particularly useful for molecules with a motional correlation time τ_c near to or just satisfying the condition $\omega\tau_c = 1$, where ω is the angular Larmor frequency. This condition corresponds to a rather larger molecular system (e. g. CyD ICs), in which the magnitude of conventional NOE enhancement is very small, but an NOE enhancement observed in a rotating frame is always positive and quite large.

In practice, two-dimensional NOE experiments are used for conformational studies of CyD ICs. The spacial proximity (r^{-6} dependence, where r is internuclear distance) of two protons is inferred from their integrated intensity of cross-peaks. However, the underlying relaxation constants also depend on the tumbling and the shape of the molecule. Spin diffusion and contributions from third nuclei as well as processes other than transverse relaxation during spin-locking also complicate a rigorous quantitative interpretation. ROESY experiments may give rise to coherent exchange of magnetization in J -coupled networks by the TOCSY mechanism, leading to further serious complications.⁷⁸ TOCSY cross-peaks have opposite signs of ROESY cross-peaks, and make distance calibration with vicinal or geminal protons difficult, although the TOCSY peaks are distinguishable in a phase-sensitive spectrum. ROESY cross-peaks can also originate from cross-relaxation with other coupled spins. Such “false positives” are misleading since they have the same sign as the ROESY cross-peaks, which one wants to measure. Nevertheless, ROESY cross-peak volumes offer at least semiquantitative information about internuclear distances, or allow the introduction of upper limits for distances between protons separated by more than about 4 Å; protons beyond this cut-off distance give no or only very weak NOE signals.

1.3.4.1.2 Induced Circular Dichroism

Circular Dichroism (CD) spectroscopy is a modified form of absorbance spectrophotometry, in which the difference in absorbance between left and right circularly polarized light ($\Delta A = A_L - A_R$) passing through the sample is measured as a function of wavelength λ .⁷⁹ The designation “Circular Dichroism” is due to historical reasons, when initially circular dichroism studies were made in the visible spectral region and it was found that when viewed by transmitted right- and left-handed light a solution of such a substance would be colored differently.⁸⁰

A symmetric chromophore possessing a plane or center of symmetry becomes optically active upon placing it in the asymmetric field of another chiral molecule. This effect is known as induced optical activity or induced circular dichroism (ICD). The host molecule cyclodextrin is inherently chiral, but transparent to UV-VIS light

⁷⁸ Botsi, A.; Yannakopoulou, K.; Hadjoudis, E.; Perly, B. *J. Org. Chem.* **1995**, *60*, 4017.

⁷⁹ Circular Dichroism of Cyclodextrin Complexes, Krois, D.; Brinker, U. H.; In *Handbook of Cyclodextrins and Their Complexes*, Dodziuk, H., Wiley: New York, **2006**, pp. 289.

⁸⁰ Foss, J. G. *J. Chem. Educ.* **1963**, *40*, 592.

region,⁸¹ where the guest's chromophore is UV-VIS active. Thus, ICD is observed in the chromophore's UV-VIS active region (200-800 nm) upon inclusion into the CyD's cavity. Perturbation theory of induced optical activity for a chromophore included in a chiral host predicts the possibility of three different mechanisms:⁸²

The first mechanism (one electron transfer) derives from the interaction of the electric and magnetic dipole transition moments of the chromophore. The second mechanism (dipole-dipole) arises from the interaction of the electric dipole transition moments of the guest's excited states with the higher energy ones of the macrocycle. The third mechanism involves an interaction of the magnetic dipole transition moment (m) of the chromophore and the electric dipole moment (μ) of the host.

Based on the Kirkwood-Tinoco⁸³ theory of polarizabilities, Harata formulated a rule for the orientation of the chromophore residing inside the cavity of cyclodextrin:⁸⁴ if the transition dipole moment vector of the guest chromophore is aligned parallel to the n-fold C- symmetric axis of cyclodextrin, the sign of the ICD Cotton effect for that transition will be positive, whereas if the vector is aligned perpendicular to the cavity axis, the ICD sign will be negative (Figure 6, left).

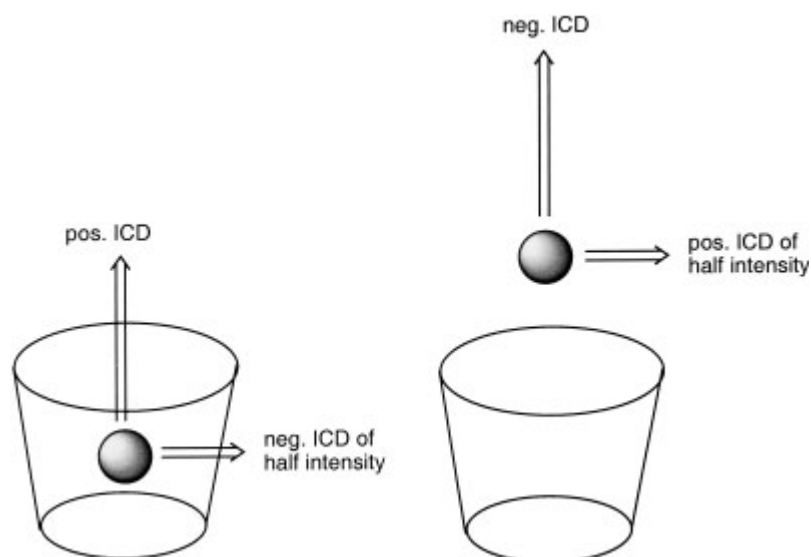


Figure 6. Illustration of the meaning of Harata's (left) and Kodaka's (right) rules.

⁸¹ Due to the presence of only single sigma bonds in cyclodextrins, a significant absorption of the UV light takes place in a far UV spectral region.

⁸² Schellman, J. A. *Acc. Chem. Res.* **1968**, *1*, 147.

⁸³ Tinoco, I. Jr. *Adv. Chem. Phys.* **1962**, *4*, 113.

⁸⁴ Harata, K.; Uedaira, H. *Bull. Chem. Soc. Jpn.* **1975**, *48*, 375.

Kodaka extended the rule for a chromophore located outside the cavity and found a reversal of the ICD signs (Figure 6, right).⁸⁵ Both rules are based on ICD studies of *aromatic* guest's chromophores when mainly the dipole-dipole mechanism of induced optical activity is operative. Thus, the knowledge of the transition dipole moment vector of the guest's chromophore is a prerequisite for the geometry estimation of the CyD IC i.e. the mutual orientation of the guest towards the host.

In accordance with the Lambert–Beer law: $\Delta\varepsilon = \Delta A/(c.d)$, $\Delta\varepsilon$ instead of ΔA is plotted against λ in the ICD spectra. The molar concentration c is usually normalized on the guest molecule, since the host (CyD) is present in an excess and thus, the maximal magnitude of the ICD effect is limited by the amount of the guest. Linearly polarized light – a racemate of left and right circularly polarized lights – becomes elliptically polarized upon passing through the solution of a chiral compound. Therefore, the ellipticity θ is frequently used instead of $\Delta\varepsilon$. There is a simple relationship between the molar ellipticity and $\Delta\varepsilon$: $[\theta] = 3298.2 \Delta\varepsilon$. The dimension of molar ellipticity $[\theta]$ is $\text{deg.cm}^2.\text{dmol}^{-1}$.

1.3.4.2 Structures in the Solid State

X-ray single crystal analysis is without any doubt the most powerful technique for a geometry assessment at all.

Cyclodextrins consist of glucose unit building blocks which form the macrocycle and which are generally in the 4C_1 chair conformation. The structures of native cyclodextrins are fairly rigid due to intramolecular hydrogen bonds between the O-2H and the O-3H of adjacent glucose units. The macrocyclic ring is distorted from an ideal n -fold symmetry in the crystalline state.

The crystal packing of CyD ICs is generally governed by the arrangement of CyD molecules because they dominate the intermolecular contact to form the crystal lattice. However, the packing mode is not unique for a particular CyD but varies according to the guest molecule. There are three packing types, cage type, channel type, and layer type, which are widely observed (Figure 7).

⁸⁵ (a) Kodaka, M. *J. Phys. Chem.* **1991**, 95, 2110. (b) Kodaka, M. *J. Am. Chem. Soc.* **1993**, 115, 3702. (c) Kodaka, M. *J. Phys. Chem. A.* **1998**, 102, 8101.

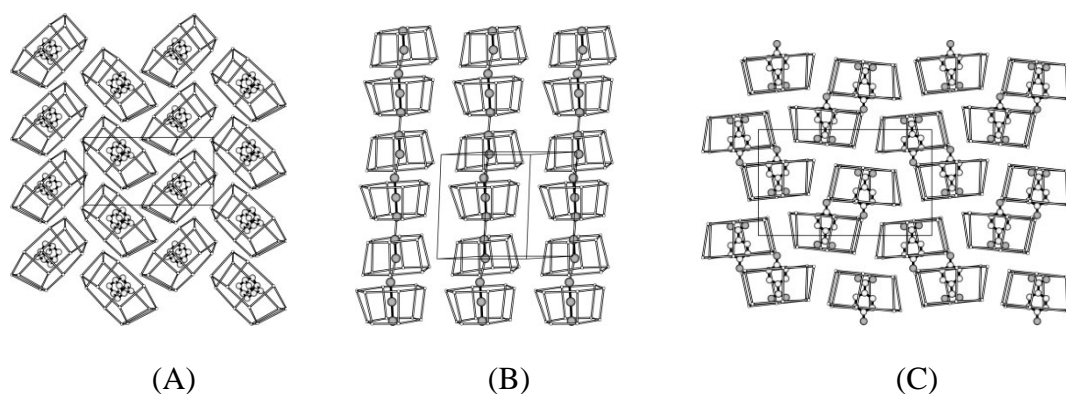


Figure 7. Schematic drawing of crystal packings: (A) cage-type observed in the β -CyD complex with hexamethylenetetramine, (B) head-to-head channel-type observed in the α -CyD complex with iodine-iodide, (C) layer-type observed in the α -CyD complex with *p*-nitrophenol. Adopted from ref. 86.¹³

The cage-type packing structure was observed in complexes of: α -CyD with relatively small guest molecules e.g. water, methanol, propan-1-ol, iodine, smaller carboxylic acids and noble gases; β -CyD with benzene and benzyl alcohol and γ -CyD – hydrate. CyD molecules in the cage-type packing mode are arranged in a “herring-bone” fashion and both ends of the host cavity are closed by adjacent molecules to create an isolated “cage” (Figure 7, A).

The channel-type structure is formed by linear stacking of CyD rings (Figure 7, B). This column-like structure has an infinite cylindrical channel that can accommodate a long molecule such as diethyl ether, sodium hexanoate, methyl orange, potassium acetate, polyiodides, an alkyl chain (octanol) or a linear polymer into the cavity of α -CyD. There are two types of channel-like CyD arrangements, called “head-to-head” and “head-to-tail” (Figure 8).

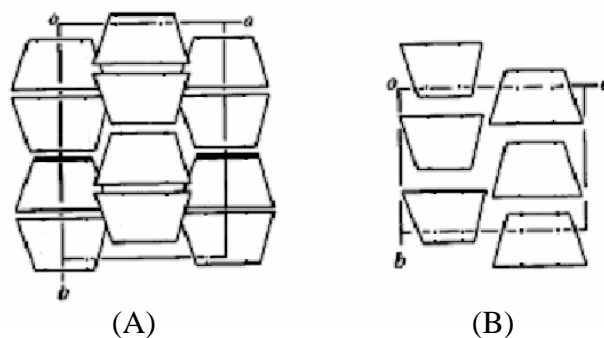


Figure 8. Schematic drawing of channel type packing: (A) head-to-head dimers, (B) head-to-tail stacking.

The first structure is formed by the linear arrangement of head-to-head CyD dimers (Figure 7, B and Figure 8, A). In the dimer unit, the secondary hydroxyl side of two molecules are facing each other and are connected by hydrogen bonds to create a barrel-like cavity. In the head-to-tail packing structure, CyD rings are linearly stacked

⁸⁶ Crystallographic Study of Cyclodextrins and Their Inclusion Complexes, Kazuaki Harata; In *Handbook of Cyclodextrins and Their Complexes*, Dodziuk, H., Wiley: New York, 2006.

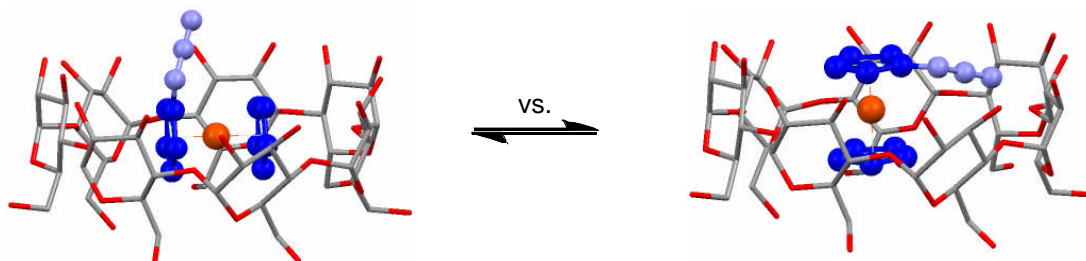
and the primary hydroxyl side faces the secondary hydroxyl side of the next molecule by hydrogen bonds (Figure 8, B).

The layer-type packing structure has been frequently observed when the guest molecule is so large that a part of the molecule cannot be accommodated within the CyD cavity: for example with *p*-disubstituted benzenes included in α -CyD. In these cases the channel type structure is not formed, because the length of the guest molecules does not match the length of the repetition unit in the host channel. On the other side, *p*-nitro, *p*-chloro- and *p*-bromoacetanilides do form channel-type inclusion structures with β -CyD. In the crystal of *p*-nitrophenol@ α -CyD complex, the CyD rings are arranged in a plane to make a molecular layer and two adjacent layers are shifted with respect to each other by half a molecule, showing a brick-work pattern (Figure 7, C). Both ends of the cavity are open to an intermolecular space of the adjacent layers. A part of the guest molecule not included in the host cavity protrudes into the intermolecular space and is in contact with host molecules of the adjacent layer.

The crystallographic studies of CyD ICs have already been reviewed and reference to detailed description of the mentioned complexes may be found therein.⁸⁷

⁸⁷ (a) Saenger, W. *J. Incl. Phenom.* **1985**, 2, 445. (b) Harata, K. *Chem. Rev.* **1998**, 98, 1803.

2. Solvent- and Temperature-Tuned Orientation of Ferrocenyl Azide Inside β -Cyclodextrin



2.1 Abstract

An Induced Circular Dichroism (ICD) solution study on the orientation of ferrocenyl azide within the β -cyclodextrin cavity is described. In DMSO, ferrocenyl azide prefers an axial inclusion, whereas in ethylene glycol and DMSO/H₂O = 50/50 an equatorial alignment dominates. As shown by temperature dependent ICD spectra, at lower temperatures ferrocenyl azide adopts preferentially an equatorial arrangement, whereas at higher temperatures an axial one is favored. Temperature and solvent effects on the co-conformation of ferrocene non-covalently bound to cyclodextrin has never been observed before.

2.2 Introduction

For the study of solution structures of achiral chromophoric guests with chiral host molecules, induced circular dichroism (ICD) has been employed as a sensitive spectroscopic tool. The method is particularly useful for the structural analysis of cyclodextrin (CyD) complexes.¹ Knowledge of solution structures of host-guest complexes contributes to the understanding of molecular recognition phenomena in enzyme-substrate interaction or catalysis. In supramolecular chemistry it also helps to advance structure-reactivity relationships.

In recent years, we have focused on supramolecular carbene chemistry. The reactive species were generated photolytically from diazirine precursors within the cyclodextrin cavity.² In contrast, examples concerning supramolecular nitrene

¹ (a) Zhdanov, Y. A.; Alekseev, Y. E.; Kompantseva, E. V.; Vergeichik, E. N. *Russ. Chem. Rev. (Engl. Transl.)* **1992**, *61*, 563. (b) Circular Dichroism of Cyclodextrin Complexes, Krois, D.; Brinker, U. H.; In *Handbook of Cyclodextrins and Their Complexes*, Dodziuk, H., Wiley, New York, **2006**, pp. 289-298.

² Representative publications: (a) Brinker, U. H.; Buchkremer, R.; Kolodziejczyk, M.; Kupfer, R.; Rosenberg, M.; Poliks, M. D.; Orlando, M.; Gross, M. L. *Angew. Chem., Int. Ed.* **1993**, *32*, 1344. (b) Rosenberg, M. G.; Kam, S. M.; Brinker, U. H. *Tetrahedron Lett.* **1996**, *37*, 3235. (c) Krois, D.; Bobek, M. M.; Werner, A.; Kählig, H.; Brinker, U. H. *Org. Lett.* **2000**, *2*, 315. (d) Rosenberg, M. G.; Brinker, U. H. *J. Org. Chem.* **2001**, *66*, 1517. (e) Knoll, W.; Bobek, M. M.; Giester, G.; Brinker, U. H. *Tetrahedron Lett.* **2001**, *42*, 9161. (f) Rosenberg, M. G.; Brinker, U. H. *J. Org. Chem.* **2003**, *68*, 4819. (g) Krois, D.; Brecker, L.; Werner, A.; Brinker, U. H. *Adv. Synth. Catal.* **2004**, *346*, 1367. (h)

chemistry are rare.³ Because the chemistry of azides as nitrene precursors entrapped in host matrices has not yet been examined extensively, we decided to investigate the ferrocenyl azide FcN₃@ β -CyD complex. Moreover, the chemistry of FcN₃ in solution has already been described.⁴ Here we wish to report about the solution structure of the FcN₃@ β -CyD complex with special emphasis on how solvent properties and temperature influence the alignment of FcN₃ in the β -CyD cavity.

The structures of ferrocene (FcH) – cyclodextrin complexes have been determined by X-ray diffraction analysis.⁵ Naturally, the structure of a solid complex may differ from that complex in a solution.⁶ Because ferrocene β -CyD complexes are barely soluble in water,⁷ studies have been conducted in organic solvents or in mixtures of organic solvents and water. Aprotic polar solvents like DMSO and DMF comprise the best solubilizing properties for CyDs and also their complexes, unfortunately at the expense of low association constants.⁸ Among aqueous solutions, the combination of DMSO/H₂O has been applied.⁹ Ethylene glycol was found to be a preferred solvent compromising relatively good solubilizing and binding properties.^{10,11,12,13}

The alignment of the guest molecule within the CyD host molecule may be inferred from ICD. Thus, Harata established a rule¹⁴ which states that the ICD of a chromophore inside the cyclodextrin's cavity will be positive, when the electric transition dipole moment is aligned parallel to the cyclodextrin's principal axis. In contrast, the ICD will be negative, when the alignment of the transition dipole moment vector is perpendicular to the cyclodextrin's principal axis. Later, Hatano et al.¹⁵ calculated a "transit" angle at 54 degrees, at which the signs of the ICD peaks reverse.¹⁶ Kodaka's treatment shows that the situation is exactly the opposite

Rosenberg, M. G.; Brinker, U. H. In *Adv. Phys. Org. Chem.*, Richard, J. P., Ed.; Academic: New York, **2005**, Vol. 40, pp. 1-47.

³ (a) Tokitoh, N.; Saiki, T.; Okazaki, R. *Chem. Commun.* **1995**, 1899. (b) Tönshoff, C.; Bucher, G. *Eur. J. Org. Chem.* **2004**, 269. (c) Warmuth, R.; Makowiec, S. *J. Am. Chem. Soc.* **2005**, *127*, 1084.

⁴ (a) Abramovitch, R. A.; Azogu, C. I.; Sutherland, R. G. *Chem. Commun.* **1971**, 134. (b) Azogu, C. I.; Offor, M. N. *J. Organomet. Chem.* **1981**, *222*, 275. (c) Steel, C.; Rosenblum, M.; Geyh, A. S. *Int. J. Chem. Kinet.* **1994**, *26*, 631.

⁵ (a) Odagaki, Y.; Hirotsu, K.; Higuchi, T.; Harada, A.; Takahashi, S. *J. Chem. Soc. Perkin Trans. 1*, **1990**, 1230. (b) Liu, Y.; Zhong, R.-O.; Zhang, H.-Y.; Song, H.-B. *Chem. Commun.* **2005**, *17*, 2211.

⁶ Mieusset, J.-L.; Krois, D.; Pacar, M.; Brecker, L.; Giester, G.; Brinker, U. H. *Org. Lett.* **2004**, *6*, 1967.

⁷ (a) Strelets, V. V.; Mamedjarova, I. A.; Nefedova, M. N.; Pysnograeva, N. I.; Sokolov, V. I.; Pospíšil, L.; Hanzlík, J. *J. Elektroanal. Chem.* **1991**, *310*, 179. (b) Wu, J.-S.; Toda, K.; Tanaka, A.; Sanemasa, I. *Bull. Chem. Soc. Jpn.* **1998**, *71*, 1615. (c) Osella, D.; Carretta, A.; Nervi, C.; Ravera, M.; Gobetto, R. *Organometallics* **2000**, *19*, 2791.

⁸ (a) Siegel, B.; Breslow, R. *J. Am. Chem. Soc.* **1975**, *97*, 6869-6870. (b) Matsue, T.; Akiba, U.; Suzufuji, K.; Osa, T. *Denki Kagaku* **1985**, *53*, 508.

⁹ Czarniecki, M. F.; Breslow, R. *J. Am. Chem. Soc.* **1978**, *100*, 7771.

¹⁰ Harada, A.; Takahashi, S. *Chem. Lett.* **1984**, 2089.

¹¹ (a) Harada, A.; Takahashi, S. *J. Chem. Soc., Chem. Commun.* **1984**, 645. (b) Harada, A.; Hu, Y.; Yamamoto, S.; Takahashi, S. *J. Chem. Soc. Dalton. Trans.* **1988**, 729.

¹² (a) Sokolov, V. I.; Bondareva, V. L.; Golovaneva, I. F. *J. Organomet. Chem.* **1988**, *358*, 401. (b) Sokolov, V. I.; Bondareva, V. L.; Golovaneva, I. F. *Organomet. Chem. USSR. (English Translation)* **1988**, *1*, 400.

¹³ Kobayashi, N.; Opallo, M. *J. Chem. Soc. Chem. Commun.* **1990**, 477.

¹⁴ Harata, K.; Uedaira, H. *Bull. Chem. Soc. Jpn.* **1975**, *48*, 375.

¹⁵ Shimizu, H.; Kaito, A.; Hatano, M. *J. Am. Chem. Soc.* **1982**, *104*, 7059.

¹⁶ If the chromophore transition dipole moment adopts this angle, zero rotatory strength was calculated. In a real solution, it may be assumed, no ICD signal should be observed, if the band of the guest's chromophore would consist of only one single transition. And that despite of the presence of a complex!

outside the cyclodextrin cavity.¹⁷ It has to be noted that these rules were derived on the basis of strong $\pi - \pi^*$ transitions of the guest's chromophore. However, they have been successfully validated for weak $n - \pi^*$ transitions of diazirines,¹⁸ azoalkanes¹⁹ and even to weak d-d transitions (400 – 550 nm) of ferrocenes.^{11,20}

Ferrocene produces in ethylene glycol a positive ICD band for β -CyD and a small negative one for γ -CyD in the range of its d-d transition band of FcH.^{11,12} Therefore, two different dominant orientations were proposed for FcH in β -CyD and in γ -CyD. The axial arrangement of ferrocene was attributed to β -CyD and the equatorial one to the FcH@ γ -CyD complex.¹¹ This assignment was corroborated later by comparing the ICD spectra of bridged ferrocenophanes in the presence of β -CyD with those of FcH in β - or γ -CyD.¹³

2.3 Results and Discussion

The stoichiometry of the FcN₃@ β -CyD complex in solution was determined by the method of continuous variation (Figure 1).²¹ Its maximum at 0.5 clearly indicates a 1:1 stoichiometry.

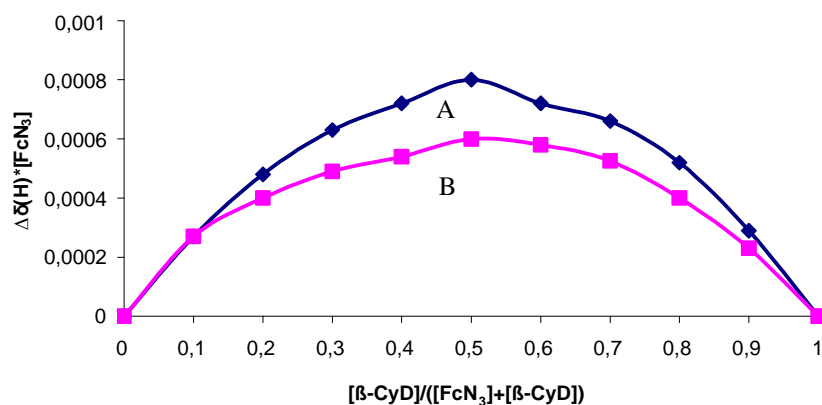


Figure 1. ¹H NMR Job's plot of the FcN₃@ β -CyD complex in *d*₆-DMSO. The change in chemical shift of the α - and β -protons (A and B curves, respectively) of the ferrocenyl azide multiplied by the concentration of ferrocenyl azide is plotted on the ordinate. [FcN₃]+[β -CD] = 0.1 M, T = 27 °C.

The structure of the guest - ferrocenyl azide was determined by X-Ray single crystal analysis (Figure 2).

¹⁷ (a) Kodaka, M. *J. Am. Chem. Soc.* **1993**, *115*, 3702-3705. (b) Kodaka, M. *J. Phys. Chem. A* **1998**, *102*, 8101.

¹⁸ Bobek, M. M.; Krois, D.; Brinker, U. H. *Org. Lett.* **2000**, *2*, 1999.

¹⁹ (a) Zhang, X.; Nau, W. M. *Angew. Chem. Int. Ed.* **2000**, *39*, 544. (b) Mayer, B.; Zhang, X.; Nau, W. M.; Marconi, G. *J. Am. Chem. Soc.* **2001**, *123*, 5240. (c) Zhang, X.; Gramlich, G.; Wang, X.; Nau, W. M. *J. Am. Chem. Soc.* **2002**, *124*, 254. (d) Bakirci, H.; Zhang, X.; Nau, W. M. *J. Org. Chem.* **2005**, *70*, 39.

²⁰ (a) Ueno, A.; Moriwaki, F.; Osa, T.; Hamada, F.; Murai, K. *Tetrahedron Lett.* **1985**, *26*, 899. (b) Matsue, T.; Evans, D. H.; Osa, T.; Kobayashi, N. *J. Am. Chem. Soc.* **1985**, *107*, 3411. (c) Kobayashi, N.; Osa, T. *Chem. Lett.* **1986**, 421. (d) Kobayashi, N.; Osa, T. *Bull. Chem. Soc. Jpn.* **1991**, *64*, 1878. (e) Suzuki, I.; Chen, Q.; Ueno, A.; Osa, T. *Bull. Chem. Soc. Jpn.* **1993**, *66*, 1472.

²¹ Gil, V. M. S.; Oliveira, N. C. *J. Chem. Edu.* **1990**, *67*, 473.

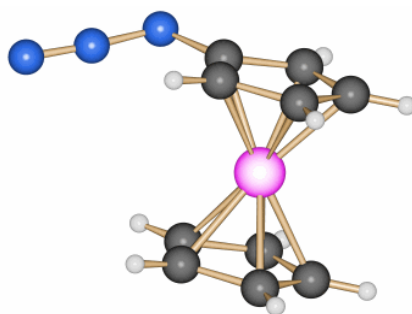


Figure 2. Structure of ferrocenyl azide based on X-Ray single crystal analysis

Also of interest was the effect of the azido functional group on the association constant (K_a) in comparison to unsubstituted ferrocene. ICD titration afforded a K_a for the FcH@ β -CyD complex at 510 M^{-1} .²² We determined K_a of the FcN₃@ β -CyD complex in ethylene glycol by two methods. An iterative Scatchard plot²³ based on ICD titrations afforded a value of $180 \pm 5 \text{ M}^{-1}$. Benesi-Hildebrand treatment²⁴ of the UV-VIS titration data furnished a value of $190 \pm 20 \text{ M}^{-1}$. Thus, the azido group causes K_a to be reduced by a factor of about 3. The association constant for the FcH@ β -CyD complex in DMSO has been determined at 40 M^{-1} and 60 M^{-1} by ICD and cyclic voltamperometric titration, respectively.^{8b} Determination by polarimetry afforded a value of 50 M^{-1} .^{8a} Moreover, the association constant of the FcN₃@ β -CyD complex was determined by ¹H NMR titration in *d*₆-DMSO utilizing a Benesi-Hildebrand plot. This led to $K_a < 5 \text{ M}^{-1}$. Thus, in DMSO, FcN₃ is about 10 times more weakly bound as unsubstituted FcH.

Next, the conformation of FcN₃ in the β -CyD cavity was investigated. The polarization direction of the symmetry forbidden d-d band of FcH has been established by single crystal UV-VIS spectroscopy and was found to be axial along the Cp-Fe-Cp bonds of FcH.²⁵ Inclusion of FcN₃ gives rise to a negative ICD signal in DMSO/H₂O = 50/50 (v/v), but a positive one in DMSO (Figure 3).

²² Sokolov, V. I.; Bondareva, V. L.; Golovanova, I. F. *Organomet. Chem. USSR*. **1989**, 2, 660.

²³ Krois, D.; Brinker, U. H. *J. Am. Chem. Soc.* **1998**, 120, 11627.

²⁴ Benesi, H. A.; Hildebrand, J. H. *J. Am. Chem. Soc.* **1949**, 71, 2703.

²⁵ (a) Yamada, S.; Nakahara, A.; Tsuchida, R. *J. Chem. Phys.* **1954**, 22, 1620. (b) Yamada, S.; Nakahara, A.; Tsuchida, R. *Bull. Chem. Soc. Jpn.* **1955**, 28, 465.

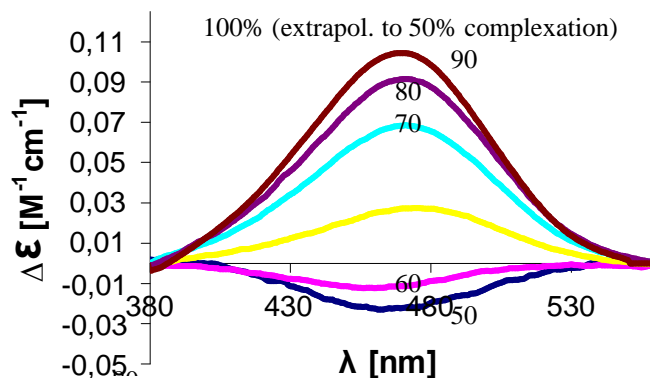


Figure 3. ICD signal dependence on the DMSO content (% v/v) of the aqueous solution. T = 25°C.

A negative band was also observed for ethylene glycol solutions. In contrast, in all solvents studied, FcH produces a positive ICD band (see Supporting Information).

In accordance with Harata's rule, from the band signs it can be assumed that the transition dipole moment of the FcN₃ molecule is oriented parallel to the principal axis of β -CyD in ethylene glycol and DMSO/H₂O = 50/50 (v/v) (Figure 4, B), whereas it is perpendicular for neat DMSO (Figure 4, A).²⁶

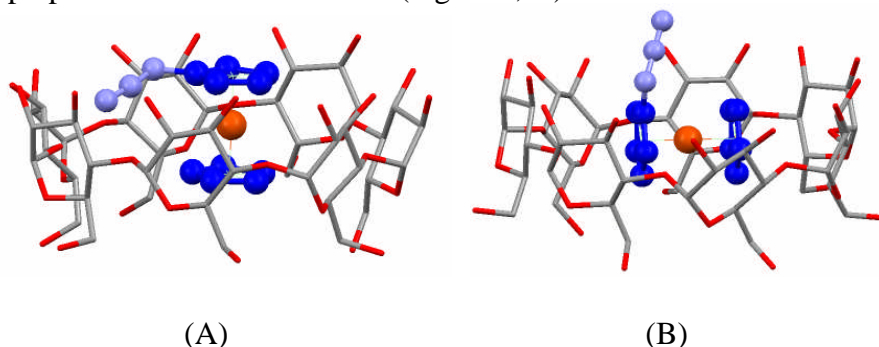


Figure 4. Proposed structures of ferrocenyl azide inside the β -cyclodextrin cavity according to ICD. (A) axial, (B) equatorial arrangement. The geometry of the complex components, each is based on a single crystal X-Ray diffraction analysis (Supporting Information).

Other mechanisms could account for a ICD band reversal as well: In a dynamic equilibrium, two (or more) complex co-conformations can exist. Each one produces a different ICD band. The overlay of these bands is observed as an experimental ICD spectrum. Dependent on the conditions, the differently weighted populations of the co-conformers can lead to an ICD sign reversal as well as to a mutual cancellation of the ICD signals.

Figure 5 represents a search for a suitable ratio of DMSO and H₂O in which the transition dipole moment adopts the above-mentioned transit angle, at which no ICD signal should be observed.

²⁶ The ¹H NMR titration with β -CyD in *d*₅-DMSO caused a change of chemical shift of the α - and β -protons of ferrocenyl azide speaking in favor of inner inclusion. Nevertheless, there exists a risk that the sign reversal observed in the ICD spectra originates from a translation of the guest along the principal axis of the cyclodextrin host.

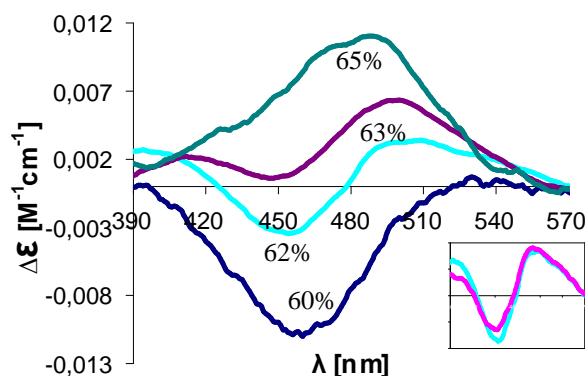


Figure 5. ICD signal dependence on the DMSO content (% v/v) of the aqueous solution. T = 25°C.

At 62 % of DMSO, however, the signal splits into two components with a trough at 455 nm and a hill at 500 nm. This splitting is well known, even from the spectroscopy of chiral ferrocenes and indicates participation of two transitions.²⁷ In order to exclude that the curve profile exhibiting a positive as well as a negative ICD signal at 62% of DMSO arose at random, the measurement was conducted with a lower concentration of the complex (Figure 5, Inset, purple curve). No remarkable concentration effect on the intensity change or wavelength shift was observed.

It is well known that solvents can control the orientation of guest molecules within the CyD cavity.^{20e,28} However, for a ferrocene *non-covalently* bound to cyclodextrin a solvent composition-dependent ICD signal sign reversal is described here for the first time.

Next the temperature effect on the ICD spectrum of the FcN₃@β-CyD complex was investigated (Figure 6).

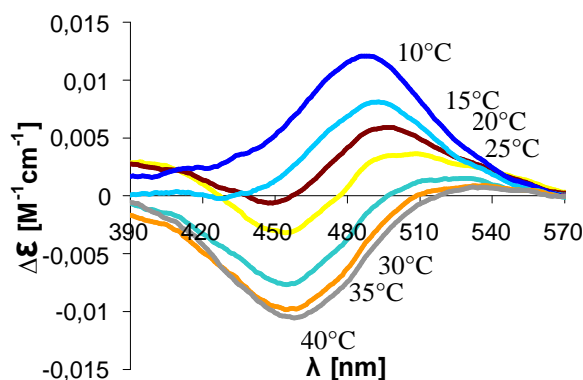


Figure 6. Temperature effect on the ICD spectra sign at a constant solvent composition, DMSO/H₂O = 62/38 (v/v), [FcN₃] = 0.0049 M, [β-CyD] = 0.0496 M.

²⁷ (a) Falk, H.; Hofer, O. *Monatsh. Chem.* **1969**, *100*, 1507. (b) Falk, H.; Lehner, H. *Tetrahedron* **1971**, *27*, 2279.

²⁸ (a) Bortolus, P.; Monti, S. *J. Phys. Chem.* **1987**, *91*, 5046. (b) Kobayashi, N.; Osa, T. *Carbohydr. Res.* **1989**, *192*, 147. (c) De Namor, A. F. D.; Traboulssi, R.; Lewis, D. F. V. *Chem. Commun.* **1990**, 751. (d) Fornasier, R.; Parmagnani, M.; Tonellato, U. *J. Inclusion Phenom. Mol. Recognit. Chem.* **1991**, *11*, 225. (e) Tee, O. S.; Mazza, C.; Lozano-Hemmer, R.; Giorgi, J. B. *J. Org. Chem.* **1994**, *59*, 7602.

At 10 °C the complex produces a positive ICD band within the investigated wavelength range. A temperature increase up to 40 °C caused a continuous sign reversal with a final nearly all negative ICD spectrum (Figure 6). Applying Harata's rule it is assumed that at higher temperatures the ferrocenyl azide adopts preferentially an equatorial arrangement (Figure 4, B) and at lower temperatures an axial one (Figure 4, A) is favored.²⁹ At about 25 °C, we deduce that the molecular axis of ferrocenyl azide adopts the "transit" angle. As mentioned above, population contribution of two co-conformers might account for the ICD sign reversal as well.

A temperature effect on the ICD spectra of ferrocene *covalently* bound to β -CyD has already been described.^{20e} To the best of our knowledge, the here demonstrated temperature effect on the conformation of a *non-covalently* bound guest inside a cyclodextrin has never been observed before.

2.4 Conclusion

In summary, application of Harata's rule on the $\text{FcN}_3 @ \beta\text{-CyD}$ complex allowed inspection of the changes of the orientation of ferrocenyl azide inside the $\beta\text{-CyD}$ cavity caused by temperature and solvent property altering. At lower temperatures ferrocenyl azide adopts axial inclusion, whereas at higher temperatures an equatorial one is preferred. Enhancing the DMSO content in aqueous DMSO solution invoked axial alignment, whereas a higher water content leads to an equatorial one. In ethylene glycol the proposed structure might be similar to the one in DMSO/H₂O. Further insight into the co-conformation variability should come from QM/MM calculations, which are currently in progress.

2.5 Experimental Section

(Supporting Information)

The structures of the complexes presented above the Abstract section and in Figure 4 were drawn on the basis of the single crystal X-Ray structure analysis of the complex components. The structure of $\beta\text{-CyD}$ was adopted from the literature.³⁰ For the determination of the association constants by NMR and ICD titration, the errors of the regression analyses were expressed as standard deviations.

Ferrocenyl azide was prepared according to the literature.³¹ $\beta\text{-CyD}$ was recrystallized two times from water, dried at 80 °C at 15 mm Hg for 1 d. The composition was determined by elemental analysis (97.17 % w/w). Deionized MQ water (conductivity 18 M Ω .cm) was used. Commercial p.a. quality of DMSO and ethylene glycol were used.

Circular dichroism spectra were recorded in thermostated (± 0.5 °C) quartz cuvettes (1 cm path length). For ICD, the integration time was set to 1 second and

²⁹ For simplification, neglectation of a temperature effect on the binding constant was assumed. An increase of temperature could also bring about a relocation of the guest beyond or beneath the CyD's cavity. Thus, the fact that the observed ICD sign reversal may have originated from a translation of the guest along the principal axis of cyclodextrin ultimately cannot be excluded.

³⁰ Steiner, T.; Koellner, G. *J. Am. Chem. Soc.* **1994**, *116*, 5122.

³¹ Nesmeyanov, A. N.; Drozd, V. N.; Sazonova, V. A. *Dokl. Akad. Nauk SSSR* **1963**, *150*, 321.

each spectrum was repeated four times (ICD titrations) and two times for the temperature and solvent dependencies. The averaged spectra were then smoothed according to need and corrected to zero baseline at the longest wavelength. A 250 MHz NMR instrument was used for recording ^1H NMR spectra at 27 °C. The residual solvent peak was set as a reference (DMSO, quintet, $\delta = 2.50$ ppm).

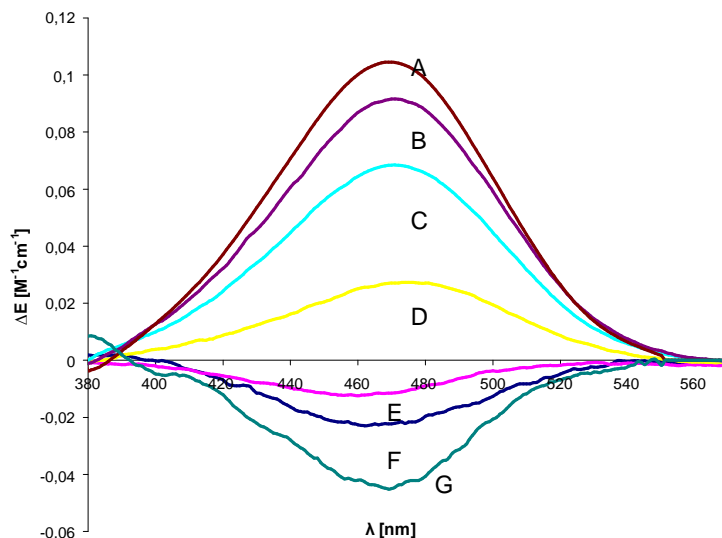


Figure S 1. ICD signal dependence on the DMSO/H₂O solution composition. T = 25 °C. (A) 100 % DMSO, [FcN₃] = 0.0100 M, [β-CyD] = 0.2300 M. Curve multiplied by factor 1.25 (B) 90 % DMSO, [FcN₃] = 0.0079 M, [β-CyD] = 0.1611 M. (C) 80 % DMSO, [FcN₃] = 0.0074 M, [β-CyD] = 0.1320 M. (D) 70 % DMSO, [FcN₃] = 0.0058 M, [β-CyD] = 0.0739 M. (E) 60 % DMSO, [FcN₃] = 0.0040 M, [β-CyD] = 0.0306 M. (F) 50 % DMSO, [FcN₃] = 0.0020 M, [β-CyD] = 0.0051 M. (G) 40 % DMSO, [FcN₃] = 0.0014 M, [β-CyD] = 0.0014 M. Curve multiplied by factor 3.62.

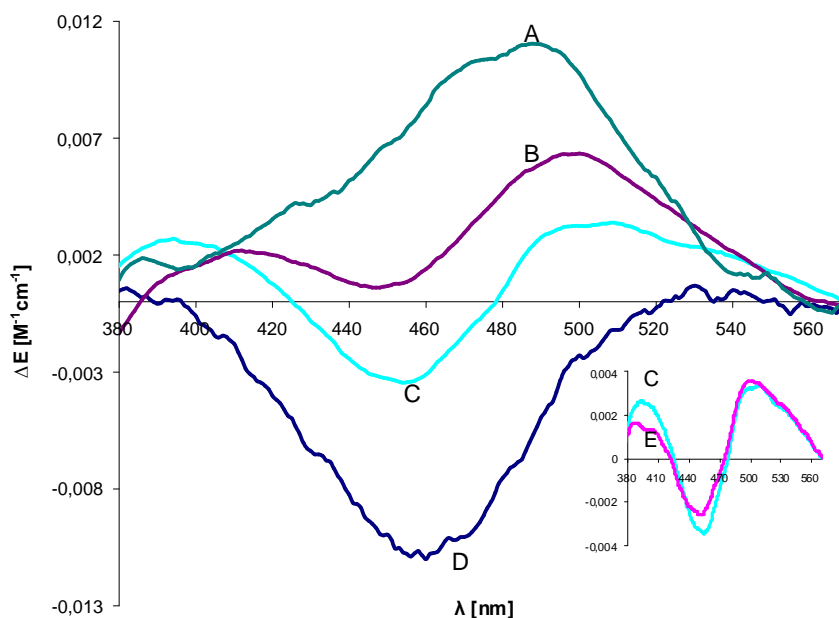


Figure S 2. ICD signal dependence on the DMSO/H₂O solution composition. T = 25 °C. (A) 65 % DMSO (B) 63 % DMSO (C) 62 % DMSO (D) 60 % DMSO (E) 62 % DMSO. Concentrations used for A, B, C: [FcN₃] = 0.0049 M, [β-CyD] = 0.0496 M.; for E: [FcN₃] = 0.0049 M, [β-CyD] = 0.0243 M.; for D: [FcN₃] = 0.0040 M, [β-CyD] = 0.0306 M.

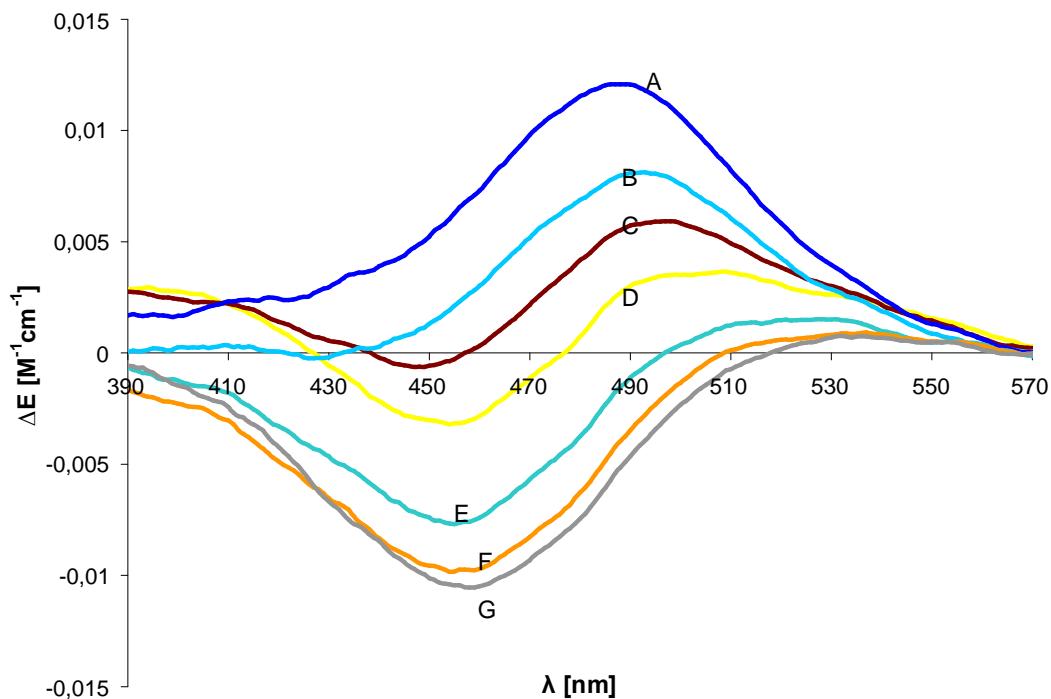


Figure S 3. Temperature effect on the ICD spectra sign. (A) 10 °C. (B) 15 °C. (C) 20 °C. (D) 25 °C. (E) 30 °C. (F) 35 °C. (G) 40 °C. Conditions: DMSO/H₂O = 62/38 (v/v), [FcN₃] = 0.0049 M, [β -CyD] = 0.0496 M.

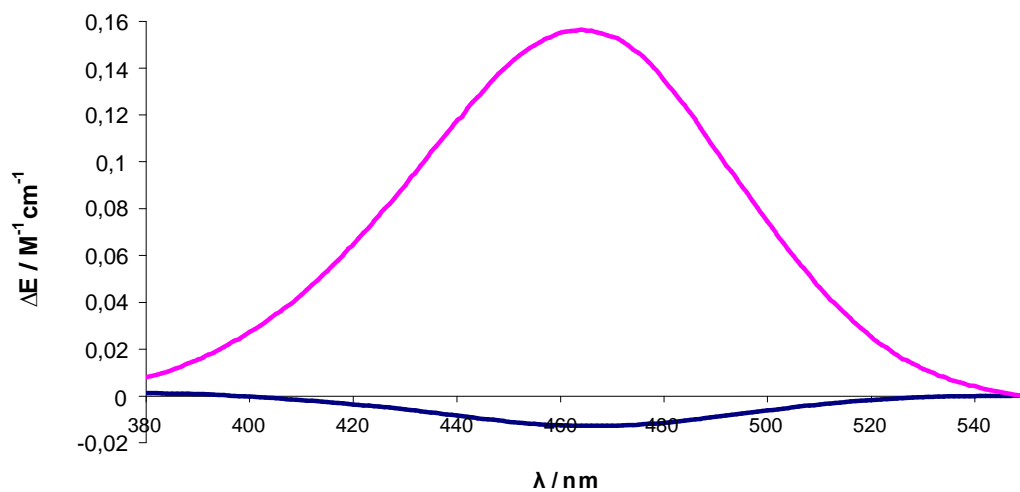


Figure S 4. ICD spectrum of the FcH (—) and FcN₃ (—) in the presence of β -CyD in ethylene glycol. T = 25 °C. [FcH] = [FcN₃] = [β -CyD] = 0.01 M.

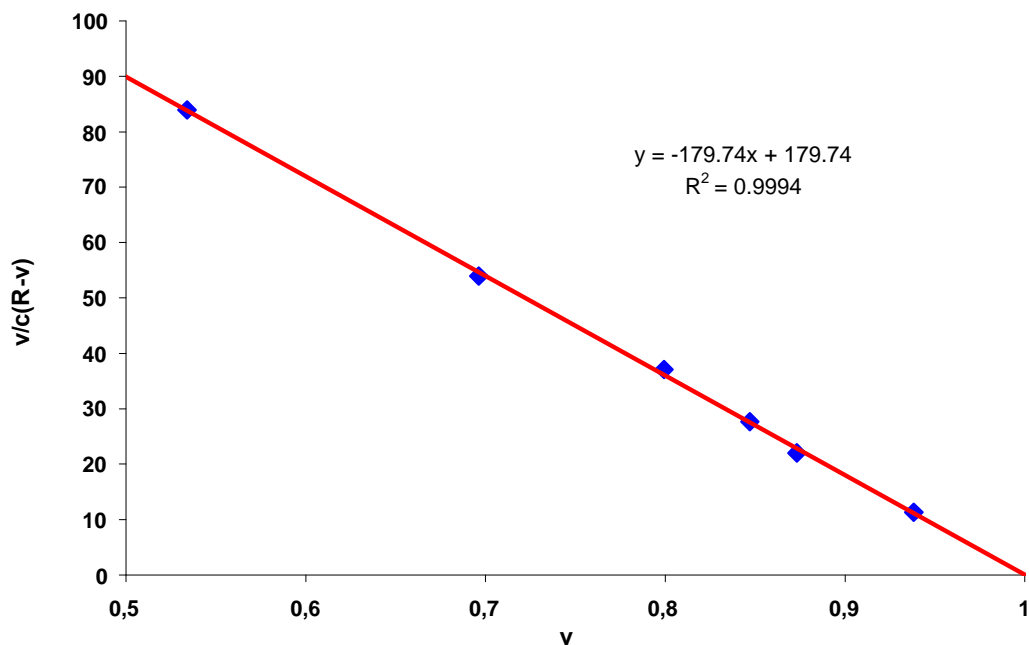


Figure S 5. Scatchard Plot constructed on the basis of the ICD titration of FcN_3 with $\beta\text{-CyD}$ in ethylene glycol. $T = 25\text{ }^\circ\text{C}$. $[\text{FcN}_3] = 0.01\text{ M}$. ($v = \Delta\varepsilon/\Delta\varepsilon_{\text{max}}$, R – mol excess of $\beta\text{-CyD}$, c – constant concentration of the FcN_3 0.01 M).

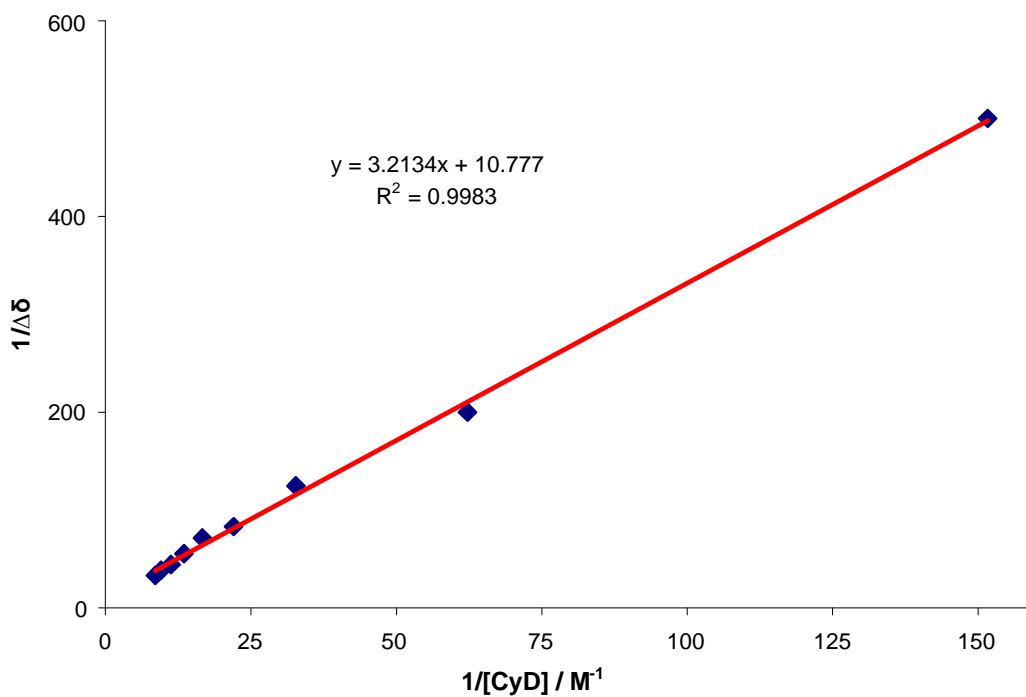


Figure S 6. Benesi-Hildebrand Plot of ^1H NMR titration of FcN_3 with $\beta\text{-CyD}$ in $d_6\text{-DMSO}$. $T = 27\text{ }^\circ\text{C}$. On the ordinate the shift difference of guest β -protons is plotted. $[\text{FcN}_3] = 0.007\text{ M}$.

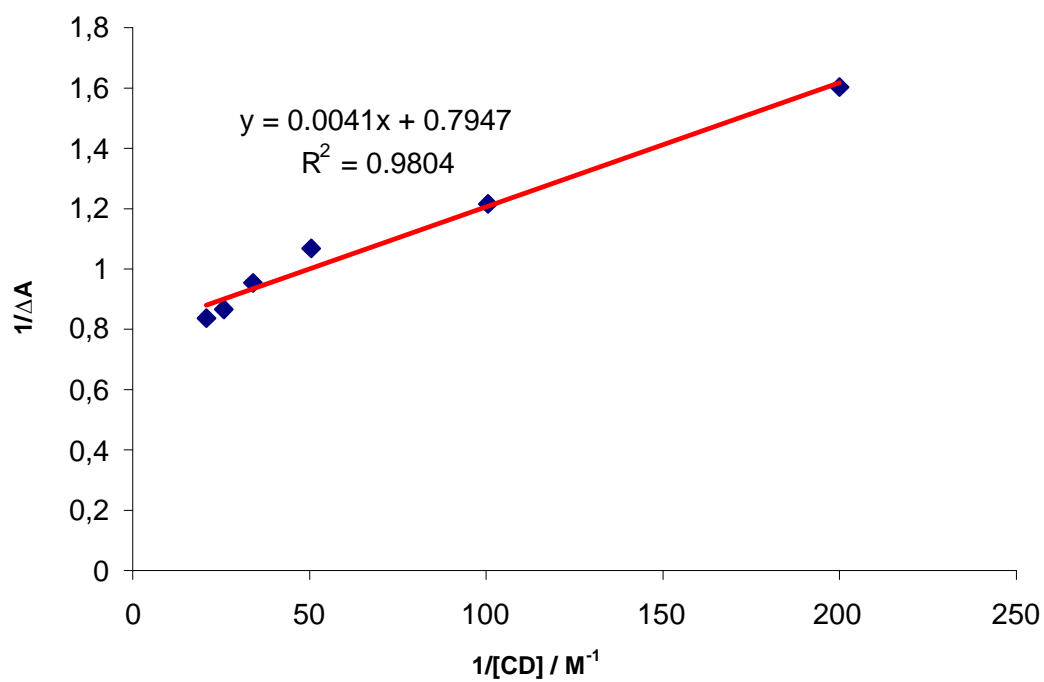


Figure S 7. Benesi-Hildebrand plot of the UV-VIS titration of FcN_3 with β -CyD in ethylene glycol. $T = 25$ °C. The reciprocal difference of the absorbance enhancement of the trough at 381 nm by complex formation is plotted on the ordinate. $[FcN_3] = 0.01$ M.

ORTEP diagram for ferrocenyl azide X-Ray crystallographic data, Crystal Data and Details of Data Collection, positional and thermal parameters, bond distances and angles and ORTEP diagram for ferrocenyl azide.

Crystallographic Structure Determination. X-ray diffraction measurement was performed at 100 K. The single crystal was positioned at 40 mm from the detector and 4102 frames were measured, each for 10 s over a 1° scan for. The data were processed using Denzo-SMN software.³² Crystal data, data collection parameters, and structure refinement details are given in Table S 1.

Complex	Ferrocenyl azide
empirical formula	C ₁₀ H ₉ N ₃ Fe
fw	227.05
space group	<i>P</i> 2 ₁ 2 ₁ 2 ₁
<i>a</i> , Å	7.4498(3)
<i>b</i> , Å	10.6899(4)
<i>c</i> , Å	11.6023(3)
<i>V</i> , Å ³	923.98(6)
<i>Z</i>	4
λ , Å	0.71073
ρ_{calcd} , g cm ⁻³	1.855
crystal size, mm ³	0.07 × 0.07 × 0.03
<i>T</i> , K	100
μ , cm ⁻¹	15.89
Flack parameter	0.000(9)
R1 ^a	0.0148
wR2 ^b	0.0392
GOF ^c	1.067

^a $R1 = \Sigma ||F_o| - |F_c|| / \Sigma |F_o|$, ^b $wR2 = \{ \Sigma [w (F_o^2 - F_c^2)^2] / \Sigma [w (F_o^2)^2] \}^{1/2}$. ^c $GOF = \{ \Sigma [w (F_o^2 - F_c^2)^2] / (n - p) \}^{1/2}$, where *n* is the number of reflections and *p* is the total number of parameters refined.

Table S 1. Crystal Data and Details of Data Collection for Ferrocenyl azide.

The structures was solved by direct methods and refined by full-matrix least-squares techniques. Non-hydrogen atoms were refined with anisotropic displacement parameters. H atoms were inserted in calculated positions and refined using a riding

³² Otwinowski, Z.; Minor, W. Processing of X-ray Diffraction Data Collected in Oscillation Mode. *Macromolecular Crystallography*; **1997**; part A, pp 307.

model. Computer programs: structure solution, SHELXS-97,³³ refinement, SHELXL-97,³⁴ molecular diagrams, ORTEP,³⁵; scattering factors.³⁶

The result of X-ray diffraction study of ferrocenyl azide is shown in Figure S8. The compound crystallized from ether in the orthorhombic noncentrosymmetric $P2_12_12_1$ space group with one molecule of ferrocenylazide in the asymmetric unit. The Cp rings display an eclipsed arrangement with a torsional twist angle $\text{Cp}\cdots\text{Fe}\cdots\text{Cp}$ of 0.4° . The Cp rings are almost parallel to each other, the dihedral angle being at 0.8° . The bond lengths and angles in the ferrocene moiety are normal.³⁷ The azide group is slightly bent with the N1–N2–N3 angle of $172.94(12)^\circ$. This angle and the distribution of electron density over the N_3 moiety [N1–N2 1.2388(12), N2–N3 1.1325(14) Å] are very similar to those in 1,1'-diazidoferrocene.³⁸ The azide group is tilted out of plane from the Cp ring, the torsional angle $\Theta_{\text{C2-C1-N1-N2}}$ being at -22.2° .

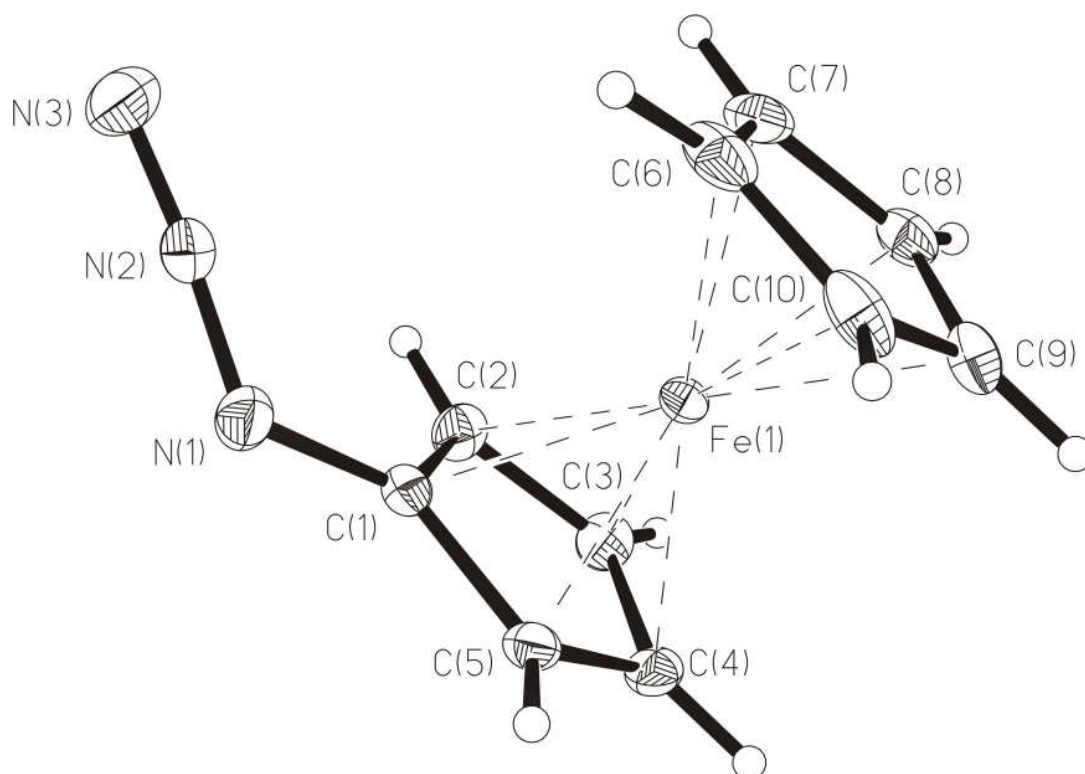


Figure S 8. ORTEP diagram of ferrocenyl azide.

³³ Sheldrick, G. M. *SHELXS-97, Program for Crystal Structure Solution*; University of Göttingen: Göttingen, Germany, 1997.

³⁴ Sheldrick, G. M. *SHELXL-97, Program for Crystal Structure Refinement*; University of Göttingen: Göttingen, Germany, 1997.

³⁵ Johnson, G. K. Report ORNL-5138; Oak Ridge National Laboratory; Oak Ridge, TN, 1976.

³⁶ International Tables for X-ray Crystallography; Kluwer Academic Press: Dordrecht, The Netherlands, 1992; Vol. C, Tables 4.2.6.8 and 6.1.1.4.

³⁷ Zhang, M.; Adaci, Y.; Hirao, T.; Ikeda, I. *Tetrahedron: Asymmetry* **1996**, 7, 451.

³⁸ Shafir, A.; Power, M.P.; Whitener, G.D.; Arnold, J. *Organometallics* **2000**, 19, 3978.

Positional and thermal parameters, Bond distances and angles for ferrocenyl azide

Atom	x	y	z	U(eq)
Fe(1)	484(1)	9614(1)	988(1)	11(1)
N(1)	-162(1)	12435(1)	433(1)	21(1)
N(2)	-436(2)	12410(1)	-620(1)	20(1)
N(3)	-608(2)	12504(1)	-1586(1)	29(1)
C(1)	-693(1)	11329(1)	1041(1)	15(1)
C(2)	-1975(1)	10397(1)	702(1)	18(1)
C(3)	-2072(1)	9510(1)	1617(1)	18(1)
C(4)	-859(1)	9892(1)	2503(1)	18(1)
C(5)	3(1)	11019(1)	2149(1)	16(1)
C(6)	2507(2)	9708(1)	-196(1)	25(1)
C(7)	1246(2)	8766(1)	-517(1)	22(1)
C(8)	1165(2)	7867(1)	388(1)	19(1)
C(9)	2374(1)	8252(1)	1270(1)	20(1)
C(10)	3202(1)	9392(1)	909(1)	23(1)

Table S 2. Atomic coordinates ($\times 10^4$) and equivalent isotropic displacement parameters ($\text{Å}^2 \times 10^3$) for ferrocenyl azide. U(eq) is defined as one third of the trace of the orthogonalized U_{ij} tensor.

Atom	x	y	z	U(eq)
H(2)	-2634	10376	1	21
H(3)	-2816	8788	1634	22
H(4)	-659	9467	3210	21
H(5)	875	11476	2572	20
H(6)	2826	10420	-641	29
H(7)	576	8742	-1213	27
H(8)	435	7139	400	22
H(9)	2591	7826	1975	24
H(10)	4065	9858	1332	28

Table S 3. Hydrogen coordinates ($\times 10^4$) and isotropic displacement parameters ($\text{Å}^2 \times 10^3$) for ferrocenyl azide.

Atom	U11	U22	U33	U23	U13	U12
Fe(1)	10(1)	12(1)	12(1)	-1(1)	1(1)	0(1)
N(1)	32(1)	15(1)	18(1)	1(1)	-4(1)	1(1)
N(2)	25(1)	15(1)	21(1)	1(1)	1(1)	2(1)
N(3)	41(1)	27(1)	20(1)	3(1)	0(1)	-1(1)
C(1)	16(1)	15(1)	14(1)	-1(1)	0(1)	4(1)
C(2)	13(1)	22(1)	17(1)	1(1)	-3(1)	2(1)
C(3)	11(1)	23(1)	20(1)	2(1)	3(1)	0(1)
C(4)	17(1)	24(1)	13(1)	1(1)	3(1)	4(1)
C(5)	18(1)	19(1)	13(1)	-4(1)	-1(1)	4(1)
C(6)	24(1)	17(1)	32(1)	-1(1)	17(1)	-1(1)
C(7)	30(1)	20(1)	18(1)	-3(1)	9(1)	1(1)
C(8)	20(1)	13(1)	22(1)	-4(1)	5(1)	-1(1)
C(9)	15(1)	17(1)	28(1)	-1(1)	1(1)	4(1)
C(10)	11(1)	19(1)	40(1)	-6(1)	5(1)	0(1)

Table S 4. Anisotropic displacement parameters ($\text{\AA}^2 \times 10^3$) for ferrocenyl azide. The anisotropic displacement factor exponent takes the form:
 $-2 \pi^2 [h^2 a^{*2} U_{11} + \dots + 2 h k a^* b^* U_{12}]$

Atom(1)-Atom(2)	distance
Fe(1)-C(1)	2.0331(9)
Fe(1)-C(10)	2.0402(10)
Fe(1)-C(6)	2.0414(10)
Fe(1)-C(2)	2.0418(10)
Fe(1)-C(3)	2.0424(9)
Fe(1)-C(4)	2.0441(10)
Fe(1)-C(7)	2.0480(10)
Fe(1)-C(5)	2.0487(10)
Fe(1)-C(9)	2.0511(11)
Fe(1)-C(8)	2.0571(10)
N(1)-N(2)	1.2388(12)
N(1)-C(1)	1.4326(13)
N(2)-N(3)	1.1325(14)
C(1)-C(5)	1.4261(14)
C(1)-C(2)	1.4352(14)
C(2)-C(3)	1.4252(14)
C(2)-H(2)	0.9500
C(3)-C(4)	1.4295(14)
C(3)-H(3)	0.9500
C(4)-C(5)	1.4246(15)
C(4)-H(4)	0.9500
C(5)-H(5)	0.9500
C(6)-C(10)	1.4225(18)
C(6)-C(7)	1.4269(16)
C(6)-H(6)	0.9500
C(7)-C(8)	1.4239(15)
C(7)-H(7)	0.9500
C(8)-C(9)	1.4242(16)
C(8)-H(8)	0.9500
C(9)-C(10)	1.4283(15)
C(9)-H(9)	0.9500
C(10)-H(10)	0.9500

Table S 5. Bond lengths (Å)

Atom(1)-Atom(2)-Atom(3)	angle
C(1)-Fe(1)-C(10)	122.30(4)
C(1)-Fe(1)-C(6)	107.11(4)
C(10)-Fe(1)-C(6)	40.79(5)
C(1)-Fe(1)-C(2)	41.24(4)
C(10)-Fe(1)-C(2)	158.55(5)
C(6)-Fe(1)-C(2)	122.18(5)
C(1)-Fe(1)-C(3)	68.67(4)
C(10)-Fe(1)-C(3)	159.25(5)
C(6)-Fe(1)-C(3)	158.60(5)
C(2)-Fe(1)-C(3)	40.85(4)
C(1)-Fe(1)-C(4)	68.42(4)
C(10)-Fe(1)-C(4)	122.78(5)
C(6)-Fe(1)-C(4)	158.86(5)
C(2)-Fe(1)-C(4)	68.97(4)
C(3)-Fe(1)-C(4)	40.95(4)
C(1)-Fe(1)-C(7)	122.97(4)
C(10)-Fe(1)-C(7)	68.60(5)
C(6)-Fe(1)-C(7)	40.84(5)
C(2)-Fe(1)-C(7)	106.93(5)
C(3)-Fe(1)-C(7)	122.57(5)
C(4)-Fe(1)-C(7)	158.93(4)
C(1)-Fe(1)-C(5)	40.90(4)
C(10)-Fe(1)-C(5)	106.79(4)
C(6)-Fe(1)-C(5)	122.40(4)
C(2)-Fe(1)-C(5)	69.48(4)
C(3)-Fe(1)-C(5)	69.02(4)
C(4)-Fe(1)-C(5)	40.74(4)
C(7)-Fe(1)-C(5)	159.03(4)
C(1)-Fe(1)-C(9)	158.63(4)
C(10)-Fe(1)-C(9)	40.86(4)
C(6)-Fe(1)-C(9)	68.62(5)
C(2)-Fe(1)-C(9)	158.87(4)
C(3)-Fe(1)-C(9)	122.98(5)
C(4)-Fe(1)-C(9)	107.58(4)
C(7)-Fe(1)-C(9)	68.37(5)
C(5)-Fe(1)-C(9)	122.38(4)
C(1)-Fe(1)-C(8)	159.25(4)

Table S 6. Bond angles [deg]

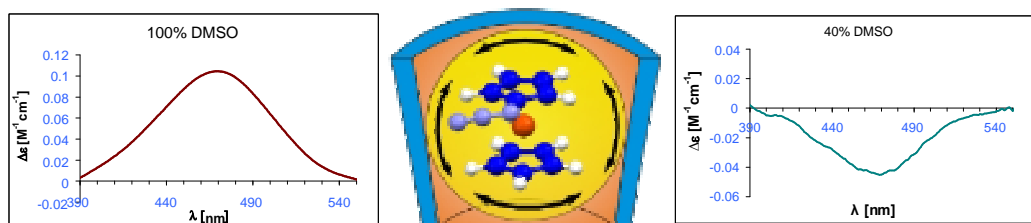
Atom(1)-Atom(2)-Atom(3)	angle
C(10)-Fe(1)-C(8)	68.55(4)
C(6)-Fe(1)-C(8)	68.56(4)
C(2)-Fe(1)-C(8)	122.57(4)
C(3)-Fe(1)-C(8)	107.54(5)
C(4)-Fe(1)-C(8)	122.96(4)
C(7)-Fe(1)-C(8)	40.59(4)
C(5)-Fe(1)-C(8)	158.64(4)
C(9)-Fe(1)-C(8)	40.57(4)
N(2)-N(1)-C(1)	114.91(9)
N(3)-N(2)-N(1)	172.94(12)
C(5)-C(1)-N(1)	122.39(9)
C(5)-C(1)-C(2)	109.11(9)
N(1)-C(1)-C(2)	128.47(9)
C(5)-C(1)-Fe(1)	70.14(5)
N(1)-C(1)-Fe(1)	127.63(7)
C(2)-C(1)-Fe(1)	69.70(6)
C(3)-C(2)-C(1)	106.96(8)
C(3)-C(2)-Fe(1)	69.60(6)
C(1)-C(2)-Fe(1)	69.05(5)
C(3)-C(2)-H(2)	126.5
C(1)-C(2)-H(2)	126.5
Fe(1)-C(2)-H(2)	126.4
C(2)-C(3)-C(4)	108.27(9)
C(2)-C(3)-Fe(1)	69.55(6)
C(4)-C(3)-Fe(1)	69.59(5)
C(2)-C(3)-H(3)	125.9
C(4)-C(3)-H(3)	125.9
Fe(1)-C(3)-H(3)	126.6
C(5)-C(4)-C(3)	108.61(9)
C(5)-C(4)-Fe(1)	69.80(5)
C(3)-C(4)-Fe(1)	69.46(5)
C(5)-C(4)-H(4)	125.7
C(3)-C(4)-H(4)	125.7
Fe(1)-C(4)-H(4)	126.6
C(4)-C(5)-C(1)	107.04(9)
C(4)-C(5)-Fe(1)	69.46(6)
C(1)-C(5)-Fe(1)	68.97(5)
C(4)-C(5)-H(5)	126.5
C(1)-C(5)-H(5)	126.5
Fe(1)-C(5)-H(5)	126.7

Table S 6. Bond angles [deg] (continued)

Atom(1)-Atom(2)-Atom(3)	angle
C(10)-C(6)-C(7)	107.89(9)
C(10)-C(6)-Fe(1)	69.56(6)
C(7)-C(6)-Fe(1)	69.83(6)
C(10)-C(6)-H(6)	126.1
C(7)-C(6)-H(6)	126.1
Fe(1)-C(6)-H(6)	126.1
C(8)-C(7)-C(6)	108.14(10)
C(8)-C(7)-Fe(1)	70.05(6)
C(6)-C(7)-Fe(1)	69.33(6)
C(8)-C(7)-H(7)	125.9
C(6)-C(7)-H(7)	125.9
Fe(1)-C(7)-H(7)	126.3
C(7)-C(8)-C(9)	107.94(9)
C(7)-C(8)-Fe(1)	69.36(6)
C(9)-C(8)-Fe(1)	69.49(6)
C(7)-C(8)-H(8)	126.0
C(9)-C(8)-H(8)	126.0
Fe(1)-C(8)-H(8)	126.7
C(8)-C(9)-C(10)	107.98(10)
C(8)-C(9)-Fe(1)	69.94(6)
C(10)-C(9)-Fe(1)	69.16(6)
C(8)-C(9)-H(9)	126.0
C(10)-C(9)-H(9)	126.0
Fe(1)-C(9)-H(9)	126.5
C(6)-C(10)-C(9)	108.04(10)
C(6)-C(10)-Fe(1)	69.65(6)
C(9)-C(10)-Fe(1)	69.98(6)
C(6)-C(10)-H(10)	126.0
C(9)-C(10)-H(10)	126.0
Fe(1)-C(10)-H(10)	126.0

Table S 6. Bond angles [deg] (continued)

3. Solvent and Temperature Dependent Co-Conformation of Ferrocenyl Azide inside β -Cyclodextrin: Induced Circular Dichroism, Quantum Mechanical, and NMR Studies



3.1 Abstract

A solution study on association constant determination and on the co-conformation of ferrocenyl azide in the β -cyclodextrin cavity is described. The Job's plot proved ferrocenyl azide to form a 1:1 stoichiometric complex with β -cyclodextrin. In d_6 -DMSO, the ferrocenyl azide practically does not bind to β -cyclodextrin ($K_a < 5 \text{ M}^{-1}$), as determined by ^1H NMR titration. In ethylene glycol a moderate binding constant was found ($K_a = 180 \pm 5 \text{ M}^{-1}$) as inferred from Induced Circular Dichroism (ICD). Dramatic temperature and solvent dependence of the ICD spectra were uncovered. In DMSO, a positive peak in the range of d-d ferrocene band was observed, whereas negative one was noticed in DMSO/H₂O = 40/60. 2D ROESY NMR experiments recorded in these solvents allowed a straightforward estimation of the complex geometries accounting for the ICD phenotype variation: the co-conformation is tuned by the solvent.

3.2 Introduction

Cyclodextrins (CyDs) are cyclic oligosaccharides consisting of six (α), seven (β) or eight (γ) glucose units bound together by $\alpha(1 - 4)$ glycosidic bonds.¹ Their truncated cone shape with the hydrophobic cavity allows to accommodate various guest molecules, thus forming a host-guest inclusion complex. These water-soluble cyclic sugars have found very important applications in analytical chemistry²,

¹ (a) Szejtli, J. *Cyclodextrins and Their Inclusion Compounds*; Akadémiai Kiadó: Budapest, **1982**. (b) Szejtli, J. *Cyclodextrin Technology*; Kluwer: Dordrecht, **1988**. (c) Duchêne, D. *New Trends in Cyclodextrins and Derivatives*; Santé: Paris, **1991**. (d) Szejtli, J.; Osa, T. *Comprehensive Supramolecular Chemistry: Cyclodextrins*, Volume 3, Pergamon Press, Elsevier, **1996**. (e) Dodziuk, H. *Cyclodextrins and Their Complexes: Chemistry, Analytical Methods, Applications*; Wiley-VCH: New York, **2006**.

² (a) Li, S.; Purdy, W. C. *Chem. Rev.* **1992**, 92, 1457 and references cited therein. (b) Hedges, A. R. *Chem. Rev.* **1998**, 98, 2035. (c) Lipkowitz, K. B., Pearl, G., Coner, B., Peterson, M. A. *J. Am. Chem. Soc.* **1997**, 119, 600.

catalysis³, drug delivery and pharmacy⁴, photochemistry⁵, food industry⁶ and others.^{7,1c} Moreover, these compounds have been extensively employed to understand host-guest complexation, to develop sensors for binding, and as mimetic systems for enzyme reactivity.^{1,2,8,9} The “structure-activity relationship” plays a dominant role in chromatography, e. g. in chiral separations.^{1c} Moreover, pharmaceutical applications of CyDs for drug protection or targeting now legally require structural characterization of the administered compounds.¹⁰ Thus, the knowledge of the structure of CyD inclusion complexes is of principal importance.

In this chapter, in addition to the term “structure” the term “co-conformation”,¹¹ i.e., the relative orientation of the guest within the host will be used as well.

Induced circular dichroism (ICD) is a sensitive spectroscopic tool used to study the co-conformation of achiral chromophoric guests with chiral host molecules.¹² The method is particularly useful for the structure analysis of natural α -, β -, and γ -cyclodextrins (CyDs) as inherently chiral hosts. The structural information obtained from NMR techniques¹⁰ complements information from ICD and together may afford the most reliable image of the solution structure of cyclodextrin complexes.

In recent years, our group has focused on supramolecular carbene chemistry, where the carbene was generated from diazirine precursors within the cyclodextrin cavity.¹³ In contrast, examples concerning supramolecular nitrene chemistry are rare.¹⁴ Hence, we decided to study organic azides inside cyclodextrins. Since ferrocene has been shown to be a suitable guest for CyDs,¹⁵ we decided to investigate first the ferrocenyl azide $\text{FcN}_3@ \beta\text{-CyD}$ complex.

³ Takahashi, K. *Chem. Rev.* **1998**, *98*, 2013.

⁴ (a) Fromming, K. H.; Szejtli, J. *Cyclodextrins in Pharmacy*, Kluwer: Dordrecht, **1994**. (b) Loftsson, T.; Brewster, M. E. *J. Pharm. Sci.* **1996**, *85*, 1017. (c) Uekama, K.; Hirayama, F.; Irie, T. *Chem. Rev.* **1998**, *98*, 2045.

⁵ Bortolus, P.; Monti, S. *Adv. Photochem.* **1996**, *21*, 1.

⁶ See, for example: (a) Cully, J.; Vollbrecht, H.-R. (SKW Trostberg AG), DE-A 4013367 A1, 1990; *Chem. Abstr.* **1992**, *116*, 40116n. (b) Duby, P.; Huynh-Ba, T. Eur. Pat. Appl. EP 545,085; *Chem. Abstr.* **1993**, *119*, 138068k.

⁷ Szejtli, J. *J. Mater. Chem.* **1997**, *7*, 575.

⁸ Breslow, R.; Dong, S. D. *Chem. Rev.* **1998**, *98*, 1997.

⁹ Saenger, W. *Angew. Chem., Int. Ed.* **1980**, *19*, 344.

¹⁰ Schneider, H.-J.; Hacket, F.; Rüdiger, V.; Ikeda, H. *Chem. Rev.* **1998**, *98*, 1755.

¹¹ Mayer, B.; Zhang, X.; Nau, W. M.; Marconi, G. *J. Am. Chem. Soc.* **2001**, *123*, 5240.

¹² (a) Zhdanov, Y. A.; Alekseev, Y. E.; Kompantseva, E. V.; Vergeychik, E. N. *Russ. Chem. Rev. (Engl. Transl.)* **1992**, *61*, 563. (b) Allenmark, S. *Chirality* **2003**, *15*, 409.

¹³ Representative publications: (a) Brinker, U. H.; Buchkremer, R.; Kolodziejczyk, M.; Kupfer, R.; Rosenberg, M.; Poliks, M. D.; Orlando, M.; Gross, M. L. *Angew. Chem., Int. Ed.* **1993**, *32*, 1344. (b) Rosenberg, M. G.; Kam, S. M.; Brinker, U. H. *Tetrahedron Lett.* **1996**, *37*, 3235. (c) Krois, D.; Bobek, M. M.; Werner, A.; Kählig, H.; Brinker, U. H. *Org. Lett.* **2000**, *2*, 315. (d) Rosenberg, M. G.; Brinker, U. H. *J. Org. Chem.* **2001**, *66*, 1517. (e) Knoll, W.; Bobek, M. M.; Giester, G.; Brinker, U. H. *Tetrahedron Lett.* **2001**, *42*, 9161. (f) Rosenberg, M. G.; Brinker, U. H. *J. Org. Chem.* **2003**, *68*, 4819. (g) Krois, D.; Brecker, L.; Werner, A.; Brinker, U. H. *Adv. Synth. Catal.* **2004**, *346*, 1367. (h) Rosenberg, M. R.; Brinker, U. H. In *Adv. Phys. Org. Chem.*; Richard, J. P., Ed.; Academic: New York, **2005**; Vol. 40, pp 1-47. (i) Rosenberg, M. G.; Brinker, U. H. *Eur. J. Org. Chem.* **2006**, 5423.

¹⁴ (a) Tokitoh, N.; Saiki, T.; Okazaki, R. *Chem. Commun.* **1995**, 1899. (b) Tönshoff, C.; Bucher, G. *Eur. J. Org. Chem.* **2004**, 269. (c) Warmuth, R.; Makowiec, S. *J. Am. Chem. Soc.* **2005**, *127*, 1084. (d) *Idem. ibid.* **2007**, *129*, 1233.

¹⁵ For comparison, the binding constants K_a for adamantane derivatives, regarded as some of the best fitting guests in β -CyD inclusion complexes in H_2O , lie in the range of $10\,000 - 100\,000\ \text{M}^{-1}$ and $16\,500\ \text{M}^{-1}$ (H_2O) for ferrocene@ β -CyD, respectively. (a) Rekharsky, M. V.; Inoue, Y. *Chem. Rev.* **1998**, *98*, 1875, particularly on p. 1908. (b) Wu, J. S.; Toda, K.; Tanaka, A.; Sanemasa, I. *Bull. Chem. Soc. Jpn.* **1998**, *71*, 1615, respectively.

Moreover, the chemistry of FcN₃ in solution without the addition of cyclodextrins has been described in literature.¹⁶

Recently, we reported an ICD study on the orientation of ferrocenyl azide inside β -cyclodextrin with special emphasis on how solvent and temperature influence the co-conformation.¹⁷ In this study, we continued the investigation and also employed quantum mechanical and NMR (2D ROESY) techniques to shed more light on the co-conformation of FcN₃ within the β -CyD cavity. Determination of association constants of the FcN₃@ β -CyD complex in DMSO and ethylene glycol (EG) is also discussed in detail.

Ferrocene forms yellowish 1:2 and 1:1 solid stoichiometric complexes with α -, β -, and γ -CyD, respectively¹⁸. The structure of solid ferrocene (FcH) – cyclodextrin complexes has been determined by X-ray diffraction for the FcH@(α -CyD)₂ complex.¹⁹ The ferrocene longitudinal axis is bent from the α -cyclodextrin principal axis by an angle of approximately 45°. Only recently Liu and coworkers²⁰ succeeded in preparing crystals of FcH@ β -CyD suitable for X-ray analysis.²¹ Here in the solid state the longitudinal Cp-Fe-Cp axis is parallel to the CyD molecular vertical axis.

Ferrocene β -CyDs complexes have been thoroughly investigated in solution as well. Because ferrocene β -CyD complexes are barely soluble in water,^{15b,22} the studies have been conducted in organic solvents or in mixtures of organic solvents and water. Aprotic polar solvents like DMSO and DMF comprise the best solubilizing properties for cyclodextrins and also their complexes.^{1a} Another suitable solvent is ethylene glycol, which is superior among alcohols.²³ Among aqueous solutions, the combination DMSO/H₂O in different proportions has been manifested frequently.²⁴ The association constant K_a in these solvents is, however, in an opposite order, i.e., DMSO ~ DMF < alcohols < water. The highest association takes place in neat water and, therefore, the higher the water content in the mixture of water and organic

¹⁶ (a) Abramovitch, R. A.; Azogu, C. I.; Sutherland, R. G. *Chem. Commun.* **1971**, 134. (b) Steel, C.; Rosenblum, M.; Geyh, A. S. *Int. J. Chem. Kinet.* **1994**, *26*, 631. (c) Azogu, C. I.; Offor, M. N. *J. Organomet. Chem.* **1981**, *222*, 275.

¹⁷ Walla, P.; Arion, V. B.; Brinker, U. H. *J. Org. Chem.* **2006**, *71*, 3274.

¹⁸ (a) Harada, A.; Takahashi, S. *J. Chem. Soc., Chem. Commun.* **1984**, 645. (b) Harada, A.; Hu, Y.; Yamamoto, S.; Takaashi, S. *J. Chem. Soc. Dalton. Trans.* **1988**, 729.

¹⁹ Odagaki, Y.; Hirotsu, K.; Higuchi, T.; Harada, A.; Takahashi, S. *J. Chem. Soc., Perkin Trans. 1*, **1990**, 1230.

²⁰ Liu, Y.; Zhong, R-O.; Zhang, H-Y.; Song, H-B. *Chem. Commun.* **2005**, *17*, 2211.

²¹ The reason why for a long time it was impossible to obtain a suitable FcH@ β -CyD crystal most probably derives from the scarce solubility of the complex in water (*vide infra*). Liu et al. in ref. 20 solved this problem by raising the temperature and thereby increasing the solubility of the complex. The view on earlier unsuccessful attempts to prepare X-ray suitable FcH@ β -CyD crystals can be obtained from the following literature: (a) Klingert, B.; Rihs, G. *J. Chem. Soc., Dalton. Trans.* **1991**, 2749. (b) Higuchi, T. *Organomet. News* **1992**, *3*, 117. (c) Kuwahara, D.; Imashiro, F.; Terao, T. *Chem. Phys. Lett.* **1993**, *204*, 533.

²² (a) Strelets, V. V.; Mamedjarova, I. A.; Nefedova, M. N.; Pysnograeva, N. I.; Sokolov, V. I.; Pospíšil, L.; Hanzlík, J. *J. Elektroanal. Chem.* **1991**, *310*, 179. (b) Osella, D.; Carretta, A.; Nervi, C.; Ravera, M.; Gobetto, R. *Organometallics* **2000**, *19*, 2791.

²³ Harada, A.; Takahashi, S.; *Chem. Lett.* **1984**, 2089.

²⁴ (a) Czarniecki, M. F.; Breslow, R. *J. Am. Chem. Soc.* **1978**, *100*, 7771. (b) Breslow, R.; Czarniecki, M. F.; Emert, J.; Hamaguchi, H. *J. Am. Chem. Soc.* **1980**, *102*, 762. (c) Trainor, G. L.; Breslow, R. *J. Am. Chem. Soc.* **1981**, *103*, 154. (d) Breslow, R.; Trainor, G. L.; Ueno, A. *J. Am. Chem. Soc.* **1983**, *105*, 2139.

cosolvent, the higher the binding constant.²⁵ In the case of water-insoluble ferrocene – CyD complexes, ethylene glycol was found to be a solvent of preference compromising relatively good solubilizing and binding properties.^{23,30,31,32,45}

The alignment of the aromatic guest may be inferred from ICD. Harata's rule²⁶ states that the electronic transitions parallel to the molecular axis of CyDs produce a positive ICD, while those normal to the axis show a negative ICD. If the chromophore resides outside of the cavity, Kodaka's rule²⁷ operates and an opposite ICD relation holds true.

Alignment of the longitudinal molecular axis (Cp-Fe-Cp)²⁸ of ferrocenes within the CyD's cavities has been determined in solution by ICD on the base of the "d-d ferrocene band".^{23,30,31,32} This weak band ($\epsilon < 100 \text{ M}^{-1} \text{ cm}^{-1}$), gaining its intensity mainly through vibronic stealing in the visible area is responsible for the coloring of ferrocene and lies in the range of ca. 350 – 600 nm with a maximum at 442 nm. It consists of two symmetry forbidden singlet transitions and one triplet transition.²⁹ Next, we will deal only with the spin-allowed transitions, readily observed in absorption spectroscopy. The first one at 417 nm possesses some metal-to-ligand charge transfer character, whereas the second one at 470 nm almost pure d-d character.^{29a-d}

Ferrocene produces a positive Cotton effect for β -CyD and a small negative for γ -CyD in the range of the d-d transition band of ferrocene (λ_{max} 442 nm in the absorption spectrum) at $\lambda_{\text{max}} \sim 460 \text{ nm}$ in the ICD spectrum in ethylene glycol.^{23,30,31} Therefore, a different orientation of FcH in β -CyD than in γ -CD was proposed. The longitudinal arrangement of ferrocene was attributed to β -CyD and the transversal to the FcH@ γ -CyD complex. This assignment was corroborated later by comparing the ICD spectra of bridged ferrocenophanes in the presence of β -CyD with those of ferrocene in β - or γ -CyD.³²

3.3 Results

3.3.1 Stoichiometry of FcN₃@ β -CyD Inclusion Complex

²⁵ In spite of a few literature reports about "reversed" effects on the increase of the binding constant caused by organic co-solvent addition (Connors, K. A. *Chem. Rev.* **1997**, *97*, 1325.), this statement can be regarded as a general rule.

²⁶ Harata, K.; Uedaira, H. *Bull. Chem. Soc. Jpn.* **1975**, *48*, 375.

²⁷ (a) Kodaka, M. *J. Am. Chem. Soc.* **1993**, *115*, 3702. (b) Idem. *J. Phys. Chem. A* **1998**, *102*, 8101.

²⁸ Cp- means cyclopentadienyl ligand.

²⁹ (a) Scott, D. R.; Becker, R. S.; *J. Chem. Phys.* **1961**, *35*, 516 and references 1-17 therein. (b) Armstrong, A. T.; Carroll, D. G.; McGlynn, S. P. *ibid.* **1967**, *47*, 1104. (c) Sohn, Y. S.; Hendrickson, D. N.; Gray, H. B. *J. Am. Chem. Soc.* **1971**, *93*, 3603. (d) Nielson, D.; Boone, D.; Eyring, H. *J. Phys. Chem.* **1972**, *76*, 511. (e) Zerner, M. C.; Loew, G. H.; Kirchner, R. F.; Mueller-Westerhof, U. T. *J. Am. Chem. Soc.* **1980**, *102*, 589.

³⁰ Harada, A.; Hu, Y.; Yamamoto, S.; Takahashi, S. *J. Chem. Soc. Dalton Trans.* **1988**, 729.

³¹ (a) Sokolov, V. I.; Bondareva, V. L.; Golovaneva, I. F. *J. Organomet. Chem.* **1988**, *358*, 401. (b) Idem. *Metalloorganicheskaya Khimiya* **1988**, *1*, 716. (English Translation in: *Organomet. Chem. USSR* **1988**, *1*, 400.).

³² Kobayashi, N.; Opallo, M. *J. Chem. Soc., Chem. Commun.* **1990**, 477.

In our hands, ferrocenyl azide formed an unstoichiometric solid complex with β -CyD. Based on the ^1H NMR and elemental analysis, the ratio of FcN_3 to β -CyD was 1:1.1 to 1:1.3. To distinguish whether the non-integer stoichiometry is brought about by the presence of small amounts of a 1:2 complex or not, we determined the stoichiometry in solution by the method of continuous variation³³ (Figure 1).

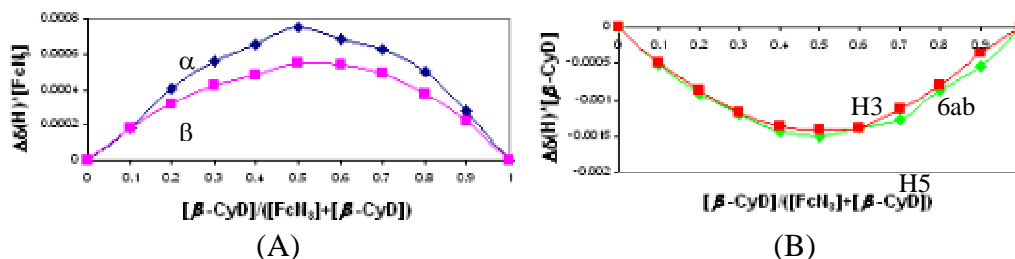


Figure 1. ^1H NMR Job's plot of the $\text{FcN}_3@ \beta\text{-CyD}$ complex in d_6 -DMSO. (A) The change in chemical shift of the α - (dark blue) and β - (pink) protons of ferrocenyl azide multiplied by the concentration of the azide is plotted in the ordinate. (B) The change in chemical shift of the H5 (pale green) and overlapping H3, 6ab (red) protons of β -CyD multiplied by the concentration of the cyclodextrin in the ordinate. Positive values in the ordinate designate downfield shift and negative upfield shift. $[\text{FcN}_3]+[\beta\text{-CyD}] = 0.1 \text{ M}$, $T = 300\text{K}$.

Due to the insolubility of the complex in water, the measurement was performed in d_6 -DMSO.

3.3.2 Association Constants (K_a) Determinations

The effect of the introduction of the azide functional group to ferrocene on the association constant in comparison to unsubstituted ferrocene was investigated. Thus, we determined K_a of the $\text{FcN}_3@ \beta\text{-CyD}$ complex in ethylene glycol by an iterative Scatchard plot,³⁴ based on ICD titration (Figure 2).

³³ Oliveira, N. C.; Victor, M. S. *J. Chem. Edu.* **1990**, 67, 473.

³⁴ Krois, D.; Brinker, U.H. *J. Am. Chem. Soc.* **1998**, 120, 11627.

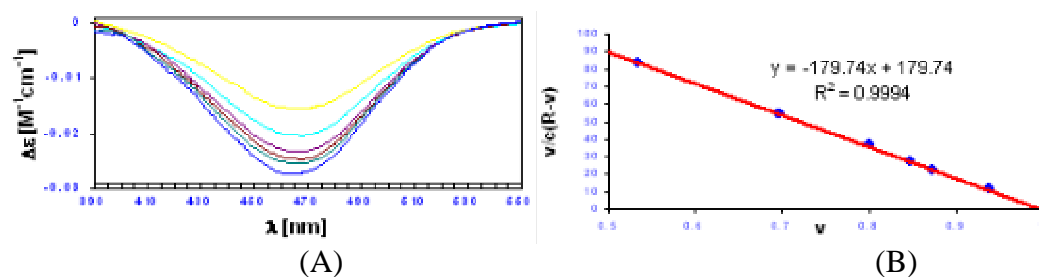


Figure 2. (A) ICD titration of FcN_3 by β -CyD in EG at 25°C . $[\text{FcN}_3]=0.01\text{ M}$. The molar excess of β -CyD used is given with ascending intensity of the ICD signal: 1.17, 2, 3, 4, 5, 10. (B) Scatchard Plot constructed from ICD titration of FcN_3 by β -CyD in EG at 25°C . $[\text{FcN}_3]=0.01\text{ M}$. ($v = \Delta\varepsilon/\Delta\varepsilon_{\text{max}}$, $R =$ mole excess of β -CyD, $c =$ constant concentration of FcN_3 0.01 M).

Determination in EG afforded $K_a = 180 \pm 5\text{ M}^{-1}$ (Figure 2 B).

Furthermore, we were interested in the binding of FcN_3 to β -CyD in DMSO. K_a was determined by ^1H NMR titration (Figure 3).

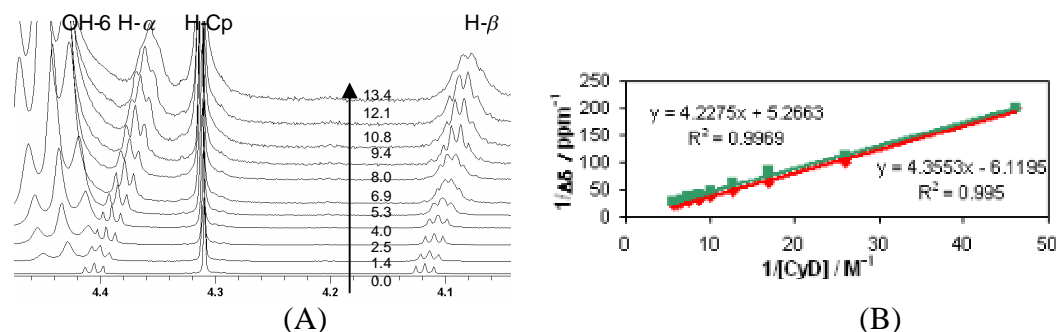


Figure 3. (A) ^1H NMR Titration of FcN_3 by β -CyD in d_6 -DMSO. The numbers beside the arrow mean molar excess of β -CyD. (B) Benesi-Hildebrand Plot based on ^1H NMR titration. $t = 27^\circ\text{C}$, $[\text{FcN}_3]_{\text{av.}} = 0.014\text{ M}$.

The induced changing of the chemical shift of the α - and β - protons of FcN_3 was then treated with a Benesi-Hildebrand plot³⁵ and $K_a < 5\text{ M}^{-1}$ for the $\text{FcN}_3@ \beta$ -CyD complex in d_6 -DMSO was assessed (Figure 3).

K_a of the $\text{FcN}_3@ \beta$ -CyD complex in $\text{DMSO}/\text{H}_2\text{O} = 40/60$ (v/v) was not determined due to the low solubility of the complex.

3.3.3 Solution Co-conformation Studies

In this section, we will deal at first with structural features of low molecular guest molecules FcH and FcN_3 . These structural descriptions are based on X-ray single-crystal analysis and density functional theory (DFT). Having geometrical coordinates of the guest molecules in hand, UV-VIS spectra were calculated using the ZINDO method. These single point calculations afforded invaluable information about the transition dipole moment vectors required for the interpretation of the ICD spectra, which will be shown subsequently. Finally, 2D NMR technique will be utilized for the co-conformation assessment.

³⁵ Benesi, H. A.; Hildebrand, J. H. *J. Am. Chem. Soc.* **1949**, 71, 2703.

3.3.3.1 Structural Features of FcH and FcN₃ Guest Molecules

Ferrocene molecule exists in two conformations – in the D_{5d} (cyclopentadienyls staggered) and D_{5h} (cyclopentadienyls eclipsed) symmetry point groups.³⁶ At -173 °C (100 K), as shown by X-ray single-crystal analysis (Figure 4, A), the cyclopentadienyl rings of FcN₃ are in an eclipsed geometry.

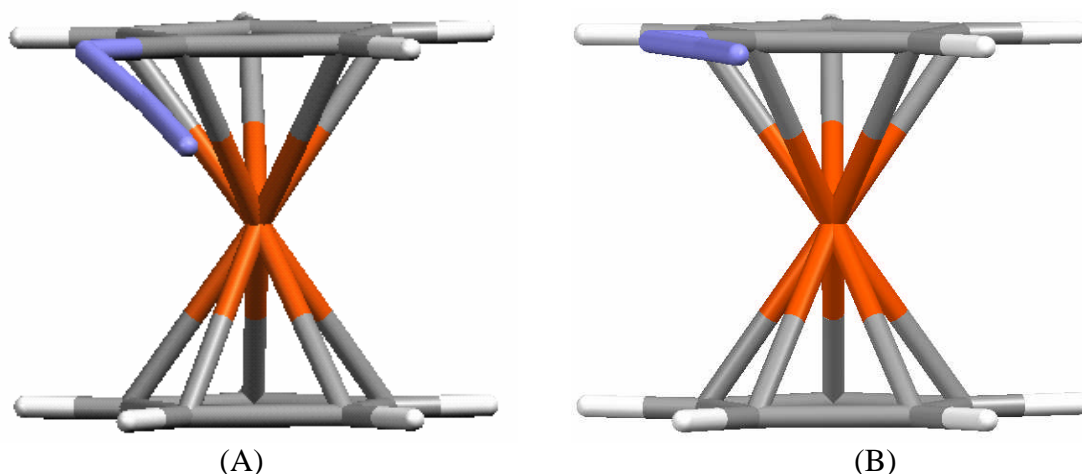


Figure 4. Ferrocenyl azide geometries based on (A) Single-crystal X-ray diffraction. (B) B3LYP/6-31G(d) optimization.

For comparison with the X-ray single-crystal structure, the geometry of FcN₃ was calculated by density functional theory as well. Becke's³⁷ three-parameter hybrid method and the exchange functional of Lee, Yang, and Parr (B3LYP)³⁸ with the 6-31G(d) basic set were used (Figure 4, B). This DFT method already has been successfully applied for calculations of ferrocene geometries.³⁹

In terms of mutual orientation of coplanar cyclopentadienyl rings of FcN₃, the B3LYP/6-31G(d) geometry calculations found the eclipsed geometry as a saddle point of first order, i.e., transition state (Figure 4, B). The azide group at the minimized structure is according to B3LYP/6-31G(d) calculation nearly coplanar with the cyclopentadienyl rings (Figure 4, B), the dihedral angle being $\vartheta(\text{C2-C1-N1-N2}) = 3.02^\circ$; the positive sign means deflection of the azide group towards the iron atom. In contrast to B3LYP/6-31G(d) calculations, the azide group in the single crystal (Figure 4, A) is deflected towards the iron atom downwards by $\vartheta(\text{C2-C1-N1-N2}) = 22.18^\circ$.

The azide group of FcN₃ rotates freely at room temperature rendering the molecule achiral. The rotation may be either in an upwards or downwards sense e.g. outwards or towards the iron atom, respectively. We scanned the energy dependence from the azide group torsion and calculated the rotational barrier to be 2.5 and 3.1 kcal/mol corresponding to upwards and downwards rotation, respectively (Figure 5).

³⁶ Coriani, S.; Haaland, A.; Helgaker, T.; Jørgensen, P. *Chem. Phys. Chem.* **2006**, *7*, 245.

³⁷ Becke, A. D. *J. Chem. Phys.* **1993**, *98*, 5648.

³⁸ Lee, C.; Yang, W.; Parr, R. G. *Phys. Rev. B* **1988**, *37*, 785.

³⁹ Kadkin, O.; Näther, C.; Friedrichsen, W. *J. Organomet. Chem.* **2002**, *649*, 161.

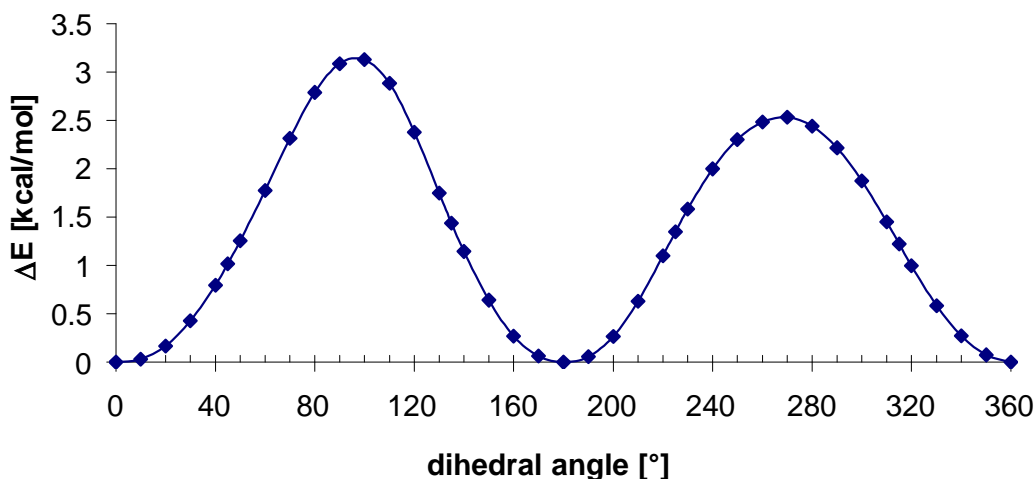


Figure 5. B3LYP/6-31G(d) calculated rotational barrier of the azide group. The barriers at torsions 100° or 270° correspond to downwards or upwards deflection of the azide group, respectively.

Noticeable is the fact, that in the crystal packing (orthorhombic crystal system, $P2_12_12_1$ space group), the azide groups of all FcN_3 molecules in the cell possess an equal orientation (Figure 6).

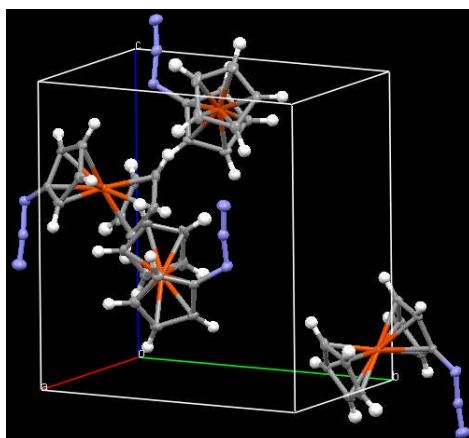


Figure 6. Crystal packing of ferrocenyl azide. For the X-ray single crystal analysis of FcN_3 see ref.¹⁷

3.3.3.2 Calculation of UV-VIS Spectra of FcH and FcN_3 Guest Molecules

The knowledge of the direction of the transition dipole moment vector within the guest molecule's absorption band is a crucial prerequisite for the ICD sign prediction.^{26,27} The polarization direction of the symmetry forbidden d-d band of FcH has been already determined by single crystal UV-VIS spectroscopy and was found to be axial along the Cp-Fe-Cp bond of ferrocene.⁴⁰ However, a question may be asked, whether the axial polarization direction of the d-d band will or will not be affected by

⁴⁰ (a) Yamada, S.; Nakahara, A.; Tsuchida, R. *J. Chem. Phys.* **1954**, 22, 1620. (b) Idem. *Bull. Chem. Soc. Jpn.* **1955**, 28, 465.

the monosubstitution of ferrocene? We sought for the answer in theoretical chemistry: UV-VIS spectra of FcH and FcN₃ guest molecules were calculated by the ZINDO/S^{29e} method, which was parametrized for ferrocene. These calculations afforded information about the required transition dipole moment vectors. The single point ZINDO/S calculations were performed on both X-ray geometry¹⁷ and on the geometry calculated by the B3LYP/6-31G(d) DFT method.

A good agreement between the experimental and predicted UV-VIS spectra of the d-d band was found (Figure 7).

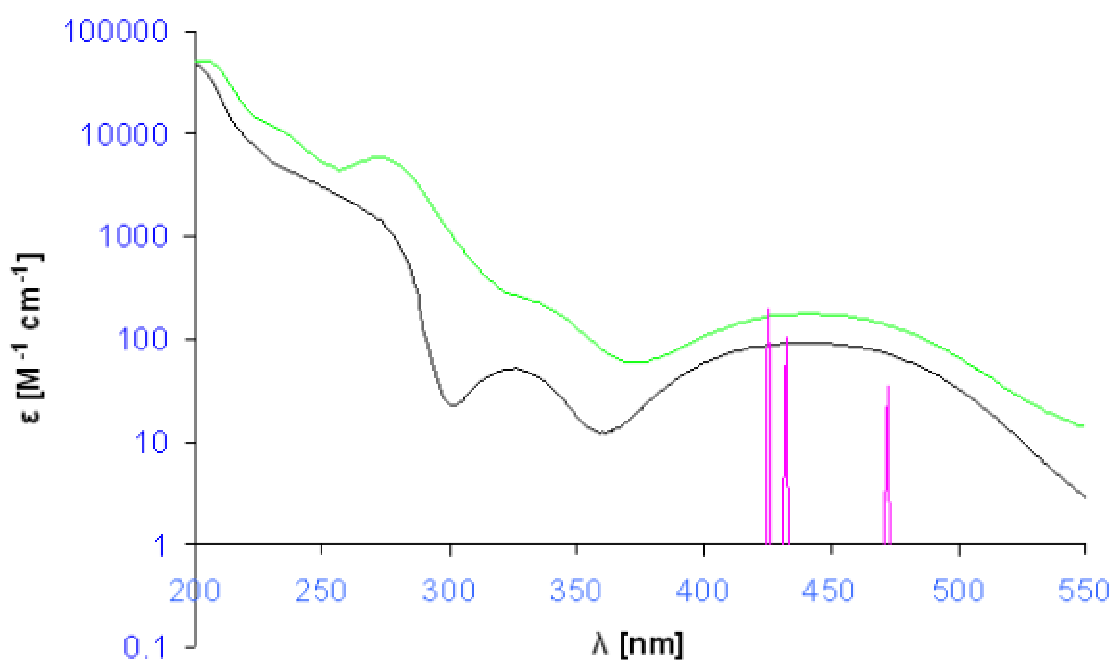


Figure 7. UV-VIS spectra of FcH (—), FcN₃ (—) (light petroleum ether (65-90 °C), concentrations used 3×10^{-3} , 3×10^{-4} , 3×10^{-5} M) and calculated wavelengths of the singlet transitions (—) in the region of the d-d band by ZINDO/S method based on the X-ray structure of FcN₃. The oscillatory strengths of the three transitions were multiplied by a factor of 50000. Only the transitions in the range of the d-d absorption are depicted.

In order to theoretically demonstrate the effect on the wavelength shift and oscillatory strength by attaching the azide group to ferrocene, the calculated ZINDO/S d-d band singlet transitions of FcH and FcN₃ based on various geometries are listed in Table 1.⁴¹

⁴¹ The constrained eclipsed FcN₃ geometry used for subsequent single point ZINDO/S calculations is very suitable for the comparison with the D_{5h} symmetric B3LYP/6-31G(d) optimized FcH, since the distance of the cyclopentadienyl rings in both molecules is equal 3.309 Å. The calculated wavelengths of the d-d transitions are, apart from other descriptors, dependent on this distance. Thus, this way the effect of the azide group attachment may be studied solely.

	Geom.	Symm.	λ [nm]	f	MO# \rightarrow MO#	Orbitals	
FcH	B3LYP/ 6-31G(d)	D5h	470	0.0000	27 \rightarrow 34 (72%)	4A1' \rightarrow 2E1'' (72%)	
			469	0.0000	27 \rightarrow 35 (72%)	4A1' \rightarrow 2E1'' (72%)	
			430	0.0000	29 \rightarrow 34 (50%) 28 \rightarrow 35 (50%)	3E2' \rightarrow 2E1'' (50%) 3E2' \rightarrow 2E1'' (50%)	
			430	0.0000	28 \rightarrow 34 (50%) 29 \rightarrow 35 (50%)	3E2' \rightarrow 2E1'' (50%) 3E2' \rightarrow 2E1'' (50%)	
			482	0.0012	34 \rightarrow 44 (+45%)	34A \rightarrow 44A (+45%)	1a
FcN ₃	B3LYP/ 6-31G(d)	C1	471	0.0000	34 \rightarrow 43 (+61%)	34A \rightarrow 43A (+61%)	1b
			448	0.0002	33 \rightarrow 38 (53%) 36 \rightarrow 38 (+38%)	33A \rightarrow 38A (53%) 36A \rightarrow 38A (+38%)	2
			437	0.0044	35 \rightarrow 43 (35%) 36 \rightarrow 44 (25%)	35A \rightarrow 43A (35%) 36A \rightarrow 44A (25%)	3a
			437	0.0005	36 \rightarrow 43 (+35%) 35 \rightarrow 44 (27%)	36A \rightarrow 43A (+35%) 35A \rightarrow 44A (27%)	3b
			472	0.0007	34 \rightarrow 44 (+58%)	34A \rightarrow 44A (+58%)	
X-Ray	C1	465	0.0000	34 \rightarrow 43 (71%)	34A \rightarrow 43A (71%)		
		432	0.0021	33 \rightarrow 38 (30%) 33 \rightarrow 37 (26%)	33A \rightarrow 38A (30%) 33A \rightarrow 37A (26%)		
		425	0.0039	35 \rightarrow 43 (47%) 36 \rightarrow 44 (+38%)	35A \rightarrow 43A (47%) 36A \rightarrow 44A (+38%)		
		423	0.0001	36 \rightarrow 43 (44%) 35 \rightarrow 44 (38%)	36A \rightarrow 43A (44%) 35A \rightarrow 44A (38%)		

Table 1. ZINDO/S calculated d-d band transition wavelengths of FcH and FcN₃ based on various geometries.

The assignment of the transitions of FcN₃ in Table 1 was made possible by visual comparison of the orbitals involved in the transitions of FcH and FcN₃ based on B3LYP/6-31G(d) geometries (Supporting Information).

Finally, calculations showing the dependence of the d-d transition dipole moment vectors on the dihedral angle $\vartheta(\text{C2-C1-N1-N2})$ were performed (Table 2).

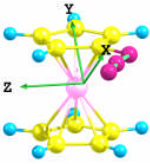
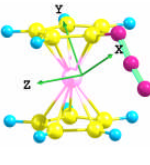
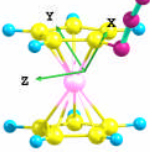
Structure	Azide Dihedral	Transition	Transition Energy	Oscillatory Strength	Transition dipole moment components		
			λ [nm]	f	x	y	z
	0	1a	482.2	0.0013	0.3364	-0.0988	0.0728
		1b	470.1	0	-0.0227	0.0278	-0.0422
		2	448	0.0002	0.0161	0.1454	0.0024
		3a	436.5	0.0038	-0.5692	0.124	-0.1107
		3b	436.5	0.0011	0.313	-0.0487	-0.0117
	90	1a	474.3	0	-0.0187	-0.0008	-0.0046
		1b	470.2	0.0001	0.0716	-0.0245	-0.0014
		2	450.2	0.0003	0.1124	-0.0094	0.1435
		3a	432.4	0	0.0471	-0.0423	0.0218
		3b	432.6	0.0001	0.0513	-0.0571	-0.0076
	270	1a	461.3	0	0.0361	-0.0383	-0.002
		1b	465.7	0	-0.0015	-0.0002	0.0439
		2	508	0.0004	0.0059	-0.0074	0.2034
		3a	423.1	0	0.005	-0.0032	-0.0318
		3b	423.4	0.0001	0.1022	-0.0472	0.0009

Table 2. Dependence of transition energies, oscillatory strengths, and transition dipole moment vector alignment from the torsion angle $\vartheta(\text{C2-C1-N1-N2})$ of the azide group. The maximal absolute values of the transition dipole moment components is marked with red color; the components corresponding to zero oscillatory strength are not marked by color.

3.3.3.3 ICD Studies of *FcH* and *FcN₃* Included in the Cavity of β -CyD

Figure 8 shows the UV-VIS spectra plotted against the ICD spectra of the $\text{FcN}_3@ \beta\text{-CyD}$ complex; ZINDO/S calculated transition frequencies are shown as well.

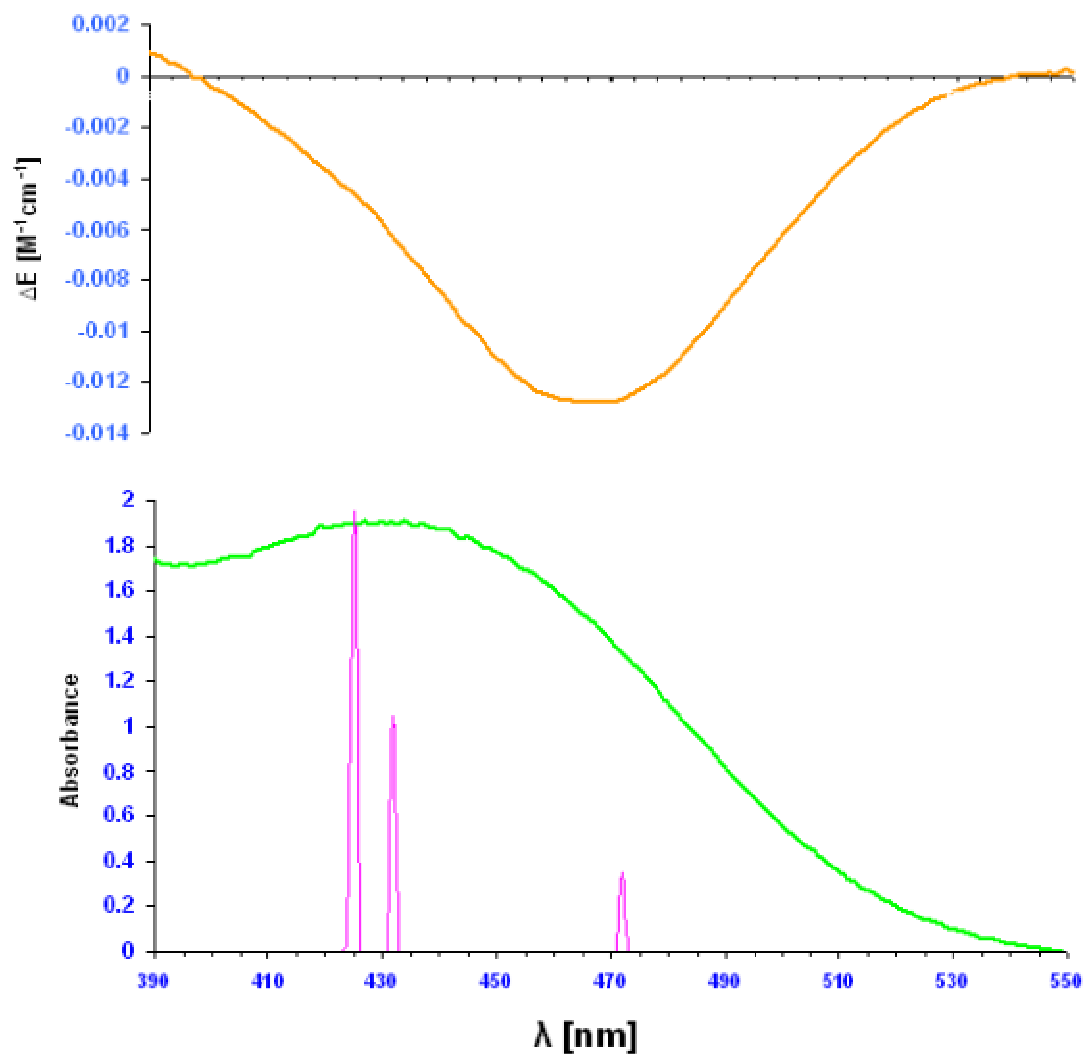


Figure 8. Comparison of ICD (top) and UV-VIS spectra (bottom) of $\text{FcN}_3@ \beta\text{-CyD}$ complex in EG. $T = 25\text{ }^\circ\text{C}$. $[\text{FcN}_3] = [\beta\text{-CyD}] = 0.01\text{ M}$. The ZINDO/s calculated frequencies of d-d transitions of FcN_3 are based on X-ray geometry and are depicted as pink spikes. The oscillatory strengths are multiplied by a factor of 500.

Figure 9 - Figure 11 depict the ICD spectra of FcH and FcN_3 in the presence of $\beta\text{-CyD}$ in EG, DMSO, and DMSO/ $\text{H}_2\text{O} = 40/60$ (v/v), respectively.

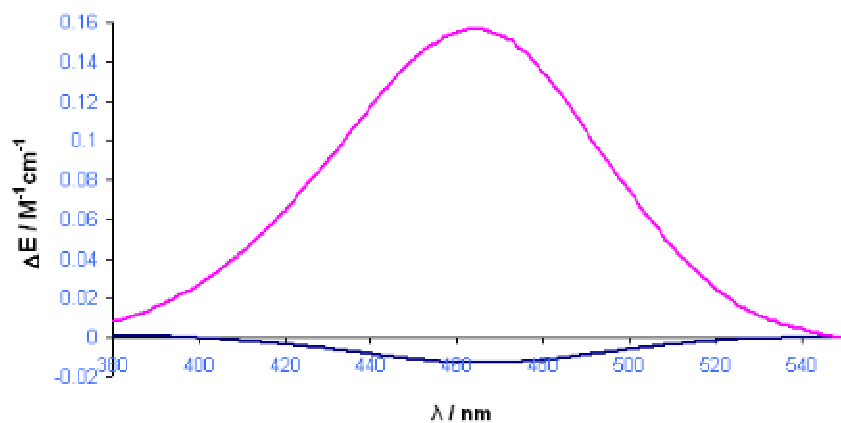


Figure 9. ICD spectrum of FcH (---) and FcN₃ (----) in the presence of β -CyD at 25 °C in EG. [FcH] = [FcN₃] = [β -CyD] = 0.01 M.

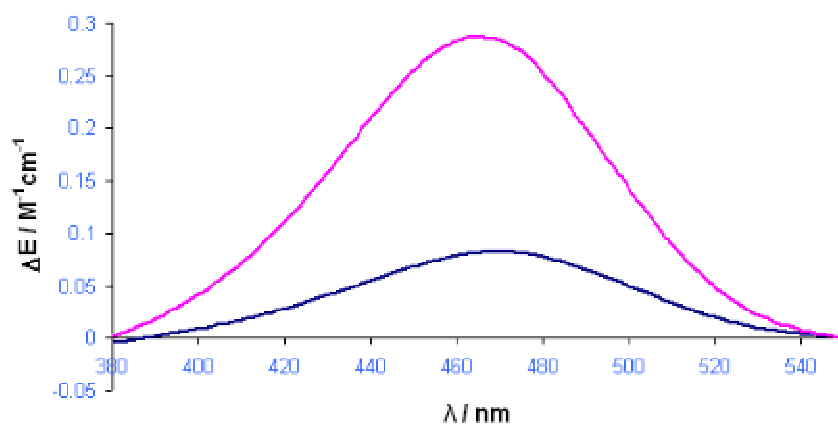


Figure 10. ICD spectrum of FcH (---) and FcN₃ (----) in the presence of β -CyD at 25 °C in DMSO. [FcH] = [FcN₃] = 0.01 M, [β -CyD] = 0.23 M.

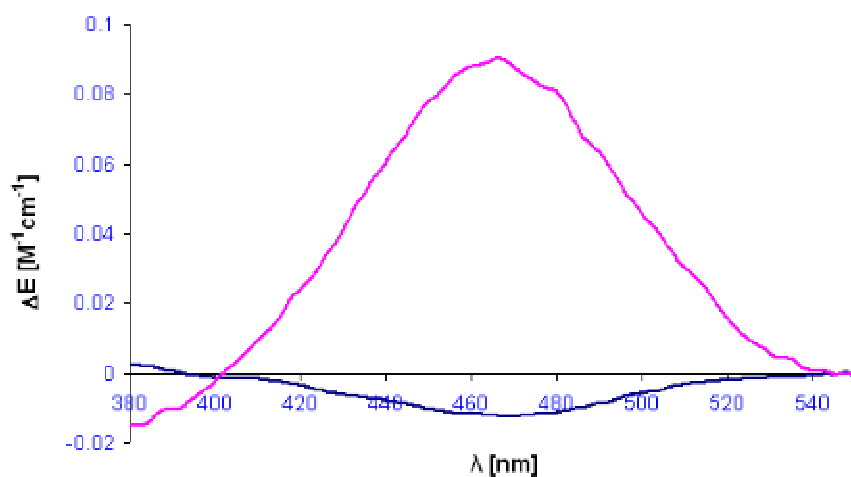


Figure 11. ICD spectrum of FcH (---) and FcN₃ (----) in the presence of β -CyD at 25 °C in DMSO/H₂O = 40/60 (v/v). [FcH] = [FcN₃] = [β -CyD] = 0.0014 M.

The maxima of the ferrocene d-d band are slightly red shifted (465 -> 470 nm) upon substitution of ferrocene by the azide group (Figure 9 - Figure 11). This effect of the azide group attachment is somewhat more distinct in the ICD rather than in the absorption spectra (Figure 7).

Addition of water to the DMSO solution of the $\text{FcN}_3@ \beta\text{-CyD}$ complex caused a reversal of the ICD signs (compare Figure 10 and Figure 11). Continual tuning of the ICD phenotype by addition of water to DMSO is illustrated in Figure (Figure 12).

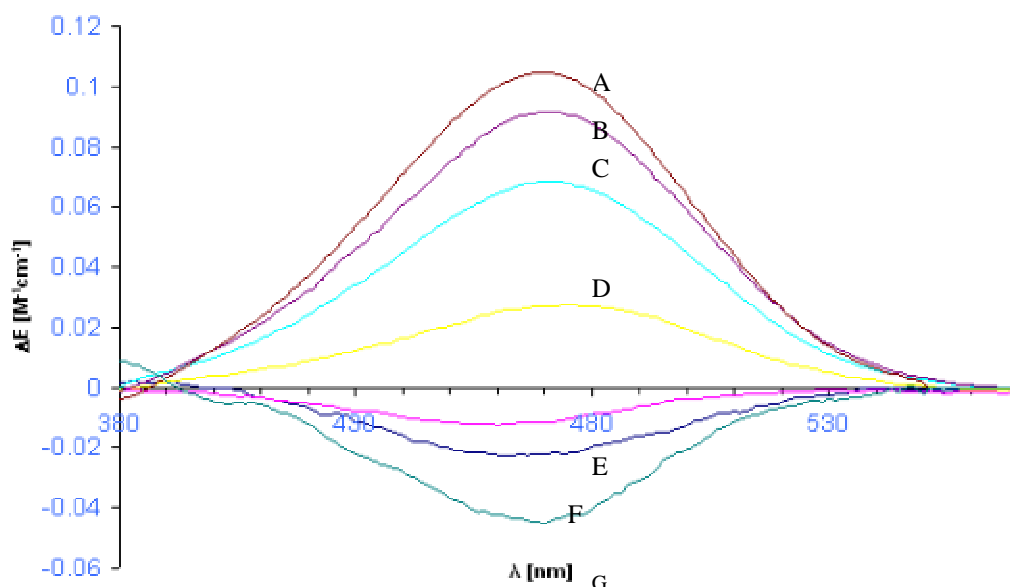


Figure 12. ICD signal dependence on the DMSO/H₂O solution composition. T = 25°C. (A) 100 % DMSO, [FcN₃] = 0.0100 M, [β-CyD] = 0.2300 M. Curve multiplied by factor 1.25 (B) 90 % DMSO, [FcN₃] = 0.0079 M, [β-CyD] = 0.1611 M. (C) 80 % DMSO, [FcN₃] = 0.0074 M, [β-CyD] = 0.1320 M.. (D) 70 % DMSO, [FcN₃] = 0.0058 M, [β-CyD] = 0.0739 M. (E) 60 % DMSO, [FcN₃] = 0.0040 M, [β-CyD] = 0.0306 M. (F) 50 % DMSO, [FcN₃] = 0.0020 M, [β-CyD] = 0.0051 M. (G) 40 % DMSO, [FcN₃] = 0.0014 M, [β-CyD] = 0.0014 M. Curve multiplied by factor 3.62.

At 70 % DMSO content there is still a positive ICD peak while at 60 % already a negative one (Figure 12, Curves D, E). We “refined” the interval of the curves between 70 % and 60 % DMSO content (Figure 13).

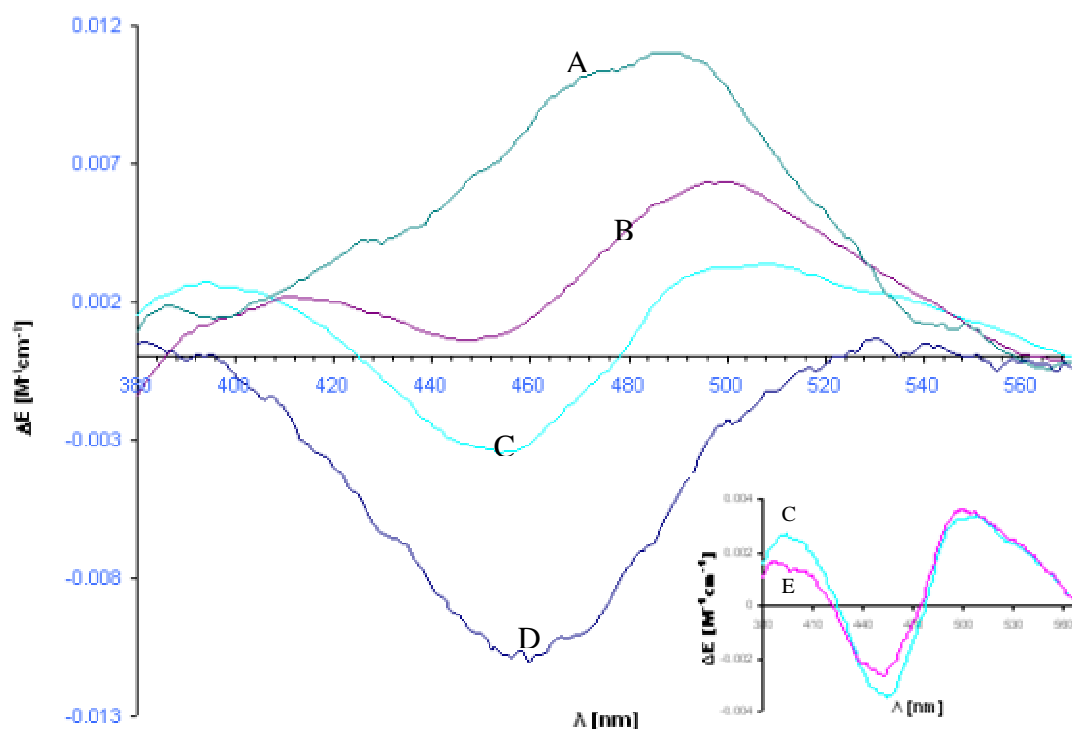


Figure 13. ICD signal dependence on the DMSO/H₂O solution composition. T = 25°C. (A) 65 % DMSO (B) 63 % DMSO (C) 62 % DMSO (D) 60 % DMSO (E) 62 % DMSO. Concentrations used for A, B, C: [FcN₃] = 0.0049 M, [β-CyD] = 0.0496 M.; for E: [FcN₃] = 0.0049 M, [β-CyD] = 0.0243 M.; for D: [FcN₃] = 0.0040 M, [β-CyD] = 0.0306 M.

At 62 % DMSO content the signal is splitted into two components with a trough at 455 nm and a hill at 500 nm (Figure 13, Curve C). With increasing amounts of DMSO the trough moved up to positive values with consequent blue shift of the original negative peak in Figure 12, curve G->F->E from 470 to 460 nm and continued in Figure 13 to 453 nm (Curve C). Simultaneously, the hill with the maximum at 470 nm shifted red to 476 nm (Figure 12, curves A->B->C->D) and continued to 500 nm in Figure 13, curves A->B->C. Note, the maxima of the complexes are at 470 nm regardless whether hill or trough (Figure 12, curves A, G). In order to exclude that the curve profile exhibiting positive as well negative ICD signs (Figure 13, Curve C) arose randomly, the measurement was conducted with another concentration of the complex (Inset in Figure 13, Curves C and E). No remarkable concentration effect on the intensity change and no ICD signal sign reversal were observed.

As a next step we investigated the temperature effect on the ICD spectrum of the FcN₃@β-CyD complex (Figure 14).

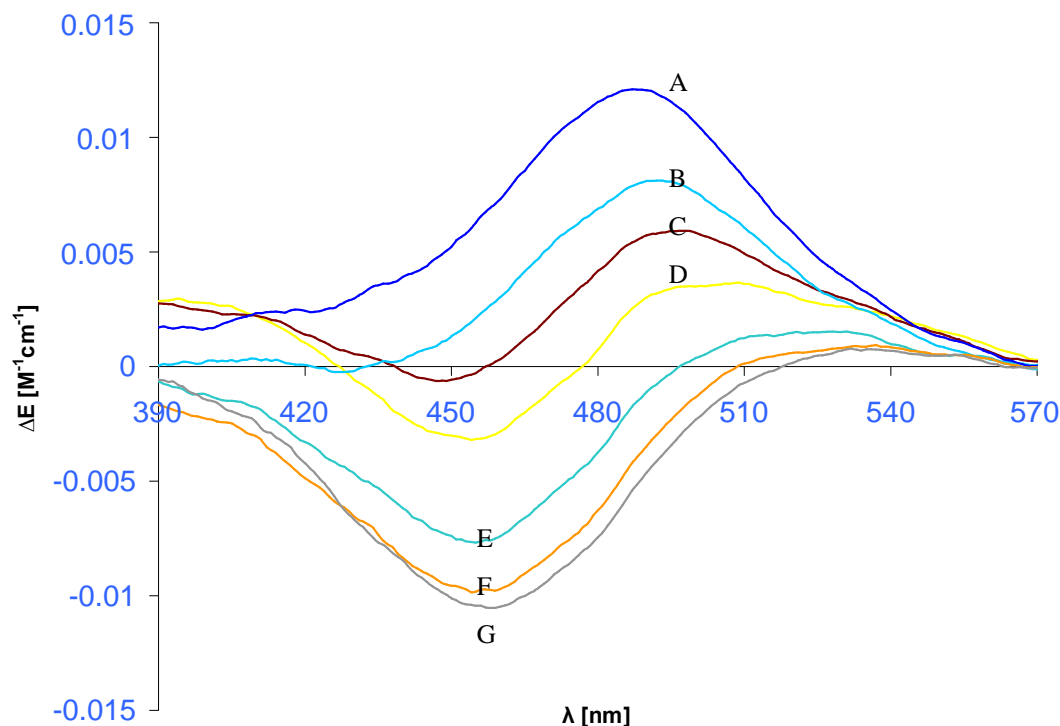


Figure 14. Temperature effect on the ICD spectra sign. (A) 10°C. (B) 15°C. (C) 20°C. (D) 25°C. (E) 30°C. (F) 35°C. (G) 40°C. Conditions: DMSO/H₂O = 62/38 (v/v), [FcN₃] = 0.0049 M, [β -CyD] = 0.0496 M.

The ICD spectra possess two maxima, one hill ($\lambda_{\max} = 487$ nm) at the lowest used temperature at 10 °C and a trough ($\lambda_{\min} = 458$ nm) at highest temperature at 40°C (Figure 14, Curves A and G). At highest experimental temperature at 40°C (Curve G) the curve shows two maxima, one trough at 458 nm and one flat hill at 533 nm. When lowering the temperature the trough's wavelength shifted gradually to 447 nm with a simultaneous intensity increase (Curves G \rightarrow C). With increasing temperature the flat hill at 533 nm shifted to 487 nm together with an intensity enhancement (Curves D \rightarrow G). At 25 °C the curve is split into two components - the hill at $\lambda_{\max} = 505$ nm and the trough at $\lambda_{\min} = 455$ nm (Curve D). At 15 °C and lower temperatures the trough is not observable anymore (Curve B \rightarrow A).

3.3.3.4 Study of the Solution Co-conformation by 2D ROESY Spectroscopy

To shed more light on the conformational changes induced by solvents, the anticipated complex was investigated by 2D ROESY experiments in the solvents corresponding to those used in the ICD studies. For this purpose, the assignment of the FcN₃ protons was ascertained in the following way:

- 1) Investigation of the 2D NMR sSpectra of acetyl ferrocene (AcFc) has shown that ${}^2J_{\text{Cl-Ha}} < {}^3J_{\text{Cl-Hb}}$ (HMBC spectra in Supporting Information).

- 2) The knowledge of point 1 was used for the evaluation of the ^1H , ^{13}C , HSQC, HMBC NMR spectra of FcN_3 recorded in d_6 -DMSO and CDCl_3 (Supporting Information).

Upon recording the 2D ROESY spectra, broad signals resulting from overlapping of H3 and H6 of the β -CyD protons were observed (Figure 15).

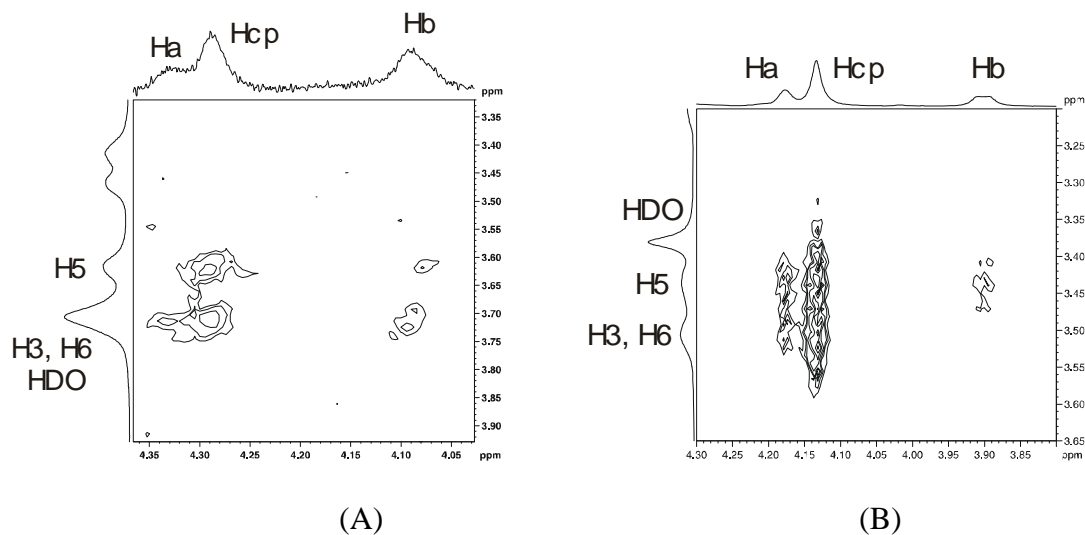


Figure 15. 2D ROESY of the $\text{FcN}_3@ \beta\text{-CyD}$ complex (a) in d_6 -DMSO / $\text{D}_2\text{O} = 40 / 60$ (v/v). $[\text{FcN}_3] = [\beta\text{-CyD}] = 0.0014$ M. (b) in d_6 -DMSO. $[\text{FcN}_3] = [\beta\text{-CyD}] = 0.22$ M. $T = 27$ °C, 600 MHz, mixing time 600 ms.

3.4 Discussion

The maximum of the mole fraction at 0.5 in the Job's plot clearly and straightforwardly indicates a 1:1 stoichiometry (Figure 1). The shallow profile suggests weak binding of ferrocenyl azide to β -CyD in the polar aprotic solvent d_6 -DMSO. Thus, the small excess of β -CyD in the isolated solid complex most probably stems from a co-precipitation of β -CyD together with the $\text{FcN}_3@ \beta\text{-CyD}$ complex.^{1a}

No new peaks in the ^1H NMR spectra of the Job's plot were observed, which points to a fast equilibrium exchange. Concerning the guest molecule, both α - and β -protons experienced an upfield shift. The maximums observed were 0.028 and 0.022 ppm, respectively. Interestingly, only a very small downfield shift of 0.004 ppm for the Cp-Ring protons was observed. The upfield shift of the α - and β - protons of FcN_3 indicates shielding by the inner cyclodextrin cavity protons.⁴² On the other side, the downfield shift indicates an interaction with highly electronegative atoms such as oxygen.⁴² Therefore, the upfield shift experienced by the Cp-protons might be brought about by the proximity with the glycosidic oxygens of the cyclodextrin.

There are a few literature reports concerning the determination of the K_a of the $\text{FcH}@ \beta\text{-CyD}$ complex in EG. In one of them,⁴³ $K_a = 510 \text{ M}^{-1}$ was determined by ICD

⁴² Veiga, F. J. B.; Fernandes, C. M.; Carvalho, R. A.; Geraldes, C. F. G. C. *Chem. Pharm. Bull.* **2001**, *49*, 1251 and citations therein.

⁴³ Sokolov, V. I.; Bondareva, V. L.; Golovaneva, I. F. *Metalloorganicheskaya Khimiya* **1989**, *2*, 1252. (English Translation in: *Organomet. Chem. USSR*. **1989**, *2*, 660).

titration in EG by treating the data by a Benesi-Hildebrand plot.³⁵ The same authors, applying the same procedure, reported in another journal a value of 410 M⁻¹.^{31a} Takahashi reported values of 83, 77, and 83 M⁻¹ determined by ICD, UV-VIS and optical rotation titrations, respectively.²³ The experimental data were treated by a Benesi-Hildebrand plot as well, but no diagrams or graphs were shown. Therefore, we set as a reference K_a at 460 M⁻¹, the arithmetic average of the two values by Sokolov.^{31a, 43} Thus, the introduction of the azide group to ferrocene caused a reduction of the equilibrium constant by a factor of 2.5.

The association constant for the FcH@β-CyD complex in DMSO has been determined at 40 M⁻¹ and at 60 M⁻¹ by ICD and cyclic voltamperometric titration, respectively.⁴⁴ Determination by polarimetry afforded a value of 50 M⁻¹.⁴⁵ We used the arithmetic average of these three values, i.e., 50 M⁻¹ as a reference value of K_a for the FcH@β-CyD complex in DMSO. ¹H NMR titration of FcN₃ by β-CyD in *d*₆-DMSO afforded a value of K_a < 5 M⁻¹ (Figure 3). In a direct plot (not shown), due to the low association constant, saturation was not achieved and only a straight line was obtained. Thus, in DMSO FcN₃ binds more than 10 times weaker than unsubstituted ferrocene does.

As mentioned above by considerations about the Job's plot (Figure 1), also by ¹H NMR titration H-α and H-β of FcN₃ experience an upfield shift and the H-Cp a downfield shift (Figure 3, A). The corresponding maximal observed values of induced shift were 0.049, 0.038, and 0.003 ppm, respectively. Noticeable is the line broadening of all guest protons with increasing concentration of β-CyD. Line broadening indicates retardation of the rate of exchange between guest and host. Moreover, the β-protons of FcN₃ experience a triplet to multiplet conversion. Considering the prolonged residence with motional restriction of FcN₃ inside the cavity, the splitting of the triplet is probably evoked by a different chiral environment to which each β-proton is exposed. This chiral environment thus renders the C-H protons of the guest diastereotopic. Splitting of guest's protons by the inclusion into cyclodextrin cavity is a phenomenon, which has been observed commonly and has been reported also for the rotaxane of a 1,1'-disubstituted ferrocene thread in the *per-O*-alkylated β-CyD.⁴⁶

In both solvents used, a lowering of the binding constant upon attaching the azide functionality onto ferrocene was observed. The reason for this lowering is conceivable, since the dimension of the azide group is comparable with the dimension of the cyclopentadienyl ring of ferrocenyl azide and thereby, the inclusion of FcN₃ is hindered by a steric factor. Moreover, the azide group is freely rotating at room temperature (the evidence is being for example the chemical equivalence of α-, α'- and β-, β'- protons and carbons of FcN₃ in the NMR), which enhances the flexibility of the whole molecule and thus hampers the binding. In general, apolar guests tend to be more firmly held in the CyD cavity than polar guests.^{15a} The azide group is polar and invokes enhancement of the polarity in comparison to unsubstituted ferrocene. Presumably, this electronic effect also contributes to the lowering of binding constant.

Theoretical calculations confirmed an almost barrierless rotation of the azide group in the FcN₃ molecule; the rotational barrier being 2.5 and 3.1 kcal/mol (Figure 5). The barrier of the azide group leading to *cis*- and *trans*-isomerisation of vinyl

⁴⁴ Matsue, T.; Akiba, U.; Suzufuji, K.; Osa, T. *Denki Kagaku* **1985**, *53*, 508.

⁴⁵ Siegel, B.; Breslow, R. *J. Am. Chem. Soc.* **1975**, *97*, 6869.

⁴⁶ Skinner, P. J.; Blair, S.; Katakya, R.; Parker, D. *New J. Chem.* **2000**, *24*, 265.

azide has already been calculated to be 5 kcal/mol based on B3LYP/ 6-311G++G(d,p) calculations.⁴⁷

In the crystal, the azide group of FcN₃ is bent towards the iron atom by the angle $\angle(\text{C2-C1-N1-N2}) = 22.18^\circ$ (Figure 4, A and Figure 6). Because according to the DFT calculation the azide group is coplanar with the cyclopentadienyl ring (Figure 4, B), the bending in the crystal is probably evoked by forces of lattice energy, which in the ferrocene lattice is of the order of 10 kcal.mol⁻¹.⁴⁸ Upon crystallization from achiral conformer mixtures of FcN₃, only one enantiomeric conformer is observed in the crystal cell (Figure 6). Thus, in the solid state the molecules of FcN₃ precipitated as a chiral enantioconformer arbitrarily designated "R", since the azide group is oriented "to the right". Most probably, in the crystal chosen for the diffraction analysis, only one enantioconformer was present. The crystallization experiment was repeated again, but instead of ether, methanol was used. Identical packing in the crystal was found (not shown), consisting of only chiral "R" enantioconformers. We did not investigate further, whether the whole macroscopic batch of crystals exhibit chirality or whether it is achiral. This would be done for example by measuring the solid sample by circular dichroism.

It is known, that the substitution of a ferrocene by an electron-withdrawing group causes a bathochromic shift of the d-d band, whereas an electron-releasing group produces a hypsochromic shift.⁴⁹ In our case, no bathochromic or hypsochromic shift of the d-d band (circa 350-600 nm) of FcN₃ versus FcH could be observed in the UV-VIS spectra (Figure 7). This is conceivable, since the azide group possesses a negative inductive and a positive mesomeric effect,⁵⁰ which apparently cancel out each other. Monosubstitution of ferrocene leads to its symmetry disruption and the d-d band gains allowance (increase of the d-d band absorption in electronic spectra). This has already been shown by calculating the UV-VIS spectra of aminoferrocene by semi-empirical method.^{29b} As expected, attaching the azide group to ferrocene caused a hyperchromic effect and the extinction coefficient of the d-d band maximum at 445 nm increased from 91 (unsubstituted ferrocene) to 181 M⁻¹cm⁻¹ (ferrocenyl azide) (Figure 7). The integrated (350-600 nm) oscillatory strength of the d-d band approximately doubled from 0.002 (FcH) to 0.004 (FcN₃).

The ZINDO/S calculations based on B3LYP/6-31G(d) FcN₃-optimized geometry found five singlet transitions at 482 nm (f=0.0012), 471 nm (f=0.0000), 448 nm (f=0.0002), 437 nm (f=0.0044), 437 nm (f=0.0005) in the d-d ferrocene band range (Table 1). Since FcN₃ possesses C₁ symmetry, all the participated orbitals and transitions possess A symmetry. Upon the substitution of ferrocene by the azide group, the doubly degenerate ferrocene's transition E₁" at 470 nm loses double degeneracy and splitted into two transitions of symmetry A at 482 nm (f=0.0012) and 471 nm (f=0.0000). Analogously, the E₂" transition at 430 nm changed into A transitions at 437 nm (f=0.0044) and 437 nm (f=0.0005). A new transition at 448 nm (f=0.0002) was formed which involved single electron excitation into unoccupied molecular orbitals of the azide group (Orbitals # 37 and # 38, see also Supporting Information). Thus, a small bathochromic shift of the d-d band resulted from attaching the azide group onto ferrocene. From this theoretical aspect, the azide group behaves

⁴⁷ Badawi, H. M. *THEOCHEM* **2002**, 579, 11.

⁴⁸ Braga, D.; Grepioni, F. *Organometallics* **1992**, 11, 711.

⁴⁹ For example: (a) Toma, Š.; Gáplovský, A.; Hudeček, M.; Langfelderová, Z. *Monatsh. Chem.* **1985**, 116, 357. (b) Toma, Š.; Gáplovský, A.; Pavlík, I. *ibid.* **1985**, 116, 479.

⁵⁰ Patai, S., Ed., *The Chemistry of the Azido Group*; Wiley: London, 1971, p. 203.

as an electron-withdrawing group. The hyperchromic effect was brought about as well (Transitions 1a, 2, 3a, 3b).

Single point ZINDO/S calculations revealed further that the transition energies and oscillatory strengths are dependent on the dihedral angle $\vartheta(\text{C2-C1-N1-N2})$ of FcN_3 (Table 2). The attachment of the azide group onto ferrocene leads to the deflection of the transition dipole moment vectors of the d-d band in comparison to axially polarized d-d transitions of unsubstituted ferrocene.⁴⁰ Moreover, the deflection of the vectors is dependent on the dihedral angle $\vartheta(\text{C2-C1-N1-N2})$. For simplification, only four extreme cases of FcN_3 conformations: azide coplanar with cyclopentadienyl ring, i.e., $\vartheta(\text{C2-C1-N1-N2}) = 0^\circ$ or 180° ; azide perpendicular to the cyclopentadienyl ring, i.e., $\vartheta(\text{C2-C1-N1-N2}) = 90^\circ$ or 270° were considered in Table 2. The transitions 1a and 3a possess intensity and are x-polarized, only if the azide group is coplanar with the cyclopentadienyl ring. The transition 1b gains small intensity ($f = 0.0001$) only if the azide torsion is 90° and then is polarized in the x, y – plane, the vector pointing prevalently in the x – direction. Energy of transition 2, which involves single electron excitation into unoccupied azide group orbitals # 37 and 38, exhibited the strongest sensitivity against the azide torsion; the shift being 60 nm going from 0° (448 nm) to a 270° (508 nm) azide dihedral angle. Also, the polarization direction of transition 2 is strongly dependent on the azide torsion angle. Polarization along the y – axis is experienced if the azide group is coplanar with the cyclopentadienyl ring, whereas x, z- and almost z- polarized when the azide torsion is 90° and 270° , respectively. Transition 3b is the most intensive if the azide group is coplanar with the cyclopentadienyl ring, and in all studied cases polarized in the x, y-plane. Transition 2 involving orbitals of the azide group, was overlapping with the d-d transitions and exhibited a complex polarization pattern depending strongly on the azide group torsion.

The maxima of the d-d band of FcN_3 are shifted from 435 nm in UV-VIS spectra to 466 nm in ICD spectra (Figure 8). This is a well known phenomenon even in the spectroscopy of chiral ferrocenes⁵¹ and indicates an overlapping of two or more bands differently weighted in VIS and ICD spectra, respectively. These calculated transitions (the band's components) are depicted by pink spikes (Figure 8, bottom).

Ferrocene produces in all cases positive ICD peaks suggesting an axial co-conformation (Figure 9 - Figure 11).^{23,26,30,31,32} An inclusion of FcN_3 produces a negative ICD sign in EG and DMSO/ H_2O , but a positive sign in DMSO (Figure 9 - Figure 11). In DMSO/ $\text{H}_2\text{O} = 62/38$ (v/v) mixture, the ICD spectrum is split into two components with a negative sign at 455 nm and a positive at 500 nm (Figure 13, Curve C).

The interpretation of the ICD sign solvent dependencies as well as the splitting at 62 % DMSO content may be done in a four ways:

- 1) In terms of Harata's rule, i.e., the guest is located only inside the CyD cavity, and the solvent tunes its rotational orientation (co-conformation).
- 2) In terms of Kodaka's rule, i.e., the moving of the guest along the C7-symmetric axis of the CyD is tuned by the solvent.

⁵¹ (a) Falk, H.; Hofer, O. *Monatsh. Chem.* **1969**, *100*, 1507. (b) Falk, H.; Lehner, H. *Tetrahedron* **1971**, *27*, 2279.

- 3) In a dynamic equilibrium, two (or more) complex co-conformations can exist. Each one produces a different ICD band. The overlay of these bands is observed as an experimental ICD spectrum. Dependent on the conditions, the differently weighted populations of the co-conformers can lead to an ICD sign reversal as well as to a mutual cancellation of the ICD signals.
- 4) Inclusion by CyD leads to motional restriction of the FcN₃'s azide group and thus rendering the enantioconformers chiral. Simultaneously, the CyD discriminates the enantiomeric conformers of the guest molecule FcN₃, i.e., variation in the binding of each enantioconformer in dependence on the solvent. This phenomena has already been described for inclusion of pyrene, benzophenone, 4-helicene, and 1,1'-binaphthyl in CyDs.⁵²

In the previous ICD studies on solution co-conformation of substituted ferrocenes – CyD complexes,^{23,30,31,32,17,53} it was assumed, that the substitution of the ferrocene did not have any effect on the deflection of the polarization direction of the d-d band transition dipole moment vector. This approximation made the co-conformation estimations possible, simply based on the ICD spectra by applying Harata's rule.

However, the attachment of functional groups (especially those in conjugation with the aromatic ring) may lead to a strong influence on the transition dipole moment vector of the d-d ferrocene band. This was demonstrated here with the azide group. Moreover, due to the low rotational barrier of many functional groups attached to ferrocene (conformational mobility), its disposition upon inclusion into the CyD cavity cannot be estimated straightforwardly only based on ICD spectra. For these purposes, the most exact co-conformation assessment would be amenable for example via application of the coupled strategy of docking calculations with subsequent computation and comparison of the ICD spectra.^{11,54}

Since the ICD study did not allow a straightforward estimation of the solution co-conformation of the FcN₃@ β -CyD complexes, we employed the 2D ROESY NMR technique to clarify the question.

Although the line broadening and overlapping of the H3 and H6 protons of CyD in the ROESY spectra complicated the interpretation, we finally successfully estimated the solution structures of the complex based on both studied solvents (Figure 16 and Figure 17).

⁵² (a) Kano, K. *J. Phys. Org. Chem.* **1997**, *10*, 286. (b) Allenmark, S. *Chirality* **2003**, *15*, 409, and references cited therein.

⁵³ Han, Y.; Cheng, K.; Simon, K. A.; Lan, Y.; Sejwal, P.; Luk, Y-Y. *J. Am. Chem. Soc.* **2006**, *128*, 13913.

⁵⁴ Marconi, G.; Mayer, B. *Pure Appl. Chem.* **1997**, *69*, 779.

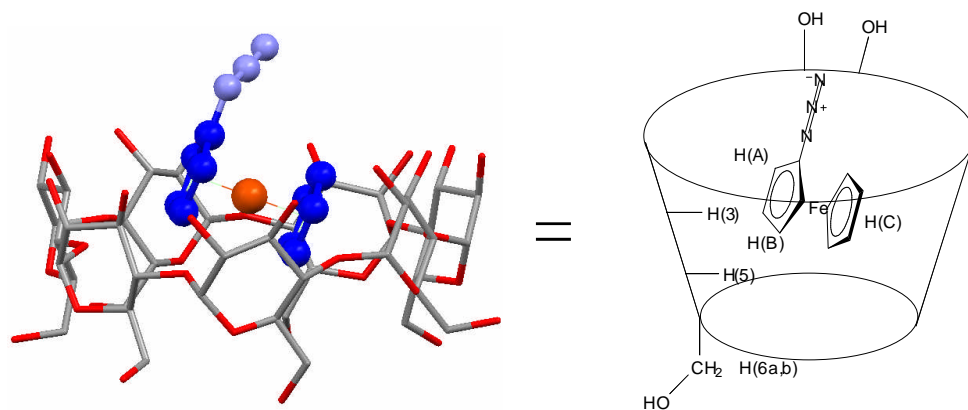


Figure 16. Proposed disposition of FcN_3 within the β -CyD cavity in $\text{DMSO}/\text{H}_2\text{O} = 40/60$ (v/v) according to 2D ROESY. The hydrogen atoms are omitted for clarity.

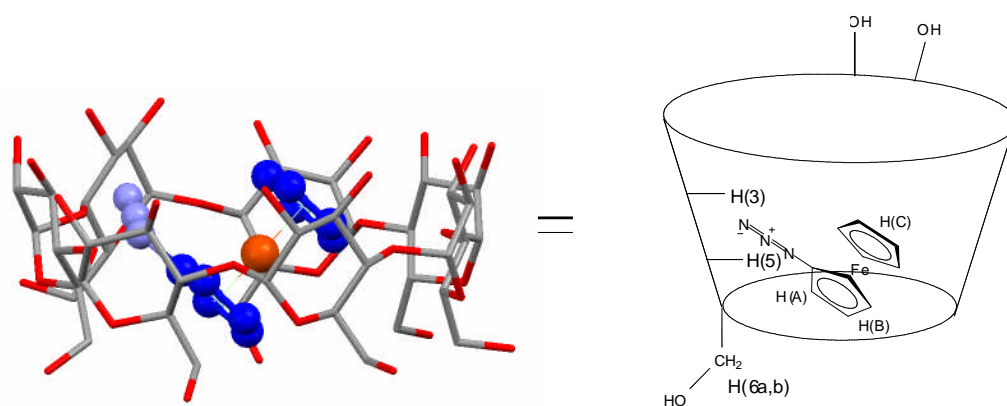


Figure 17. Proposed disposition of FcN_3 within the β -CyD cavity in d_6 -DMSO according to 2D ROESY. The hydrogen atoms are omitted for clarity.

In the d_6 -DMSO/ $\text{D}_2\text{O} = 40/60$ (v/v) solvent system, FcN_3 has cross-peaks with all of its protons with H3 (H6) and H5 of the β -CyD (Figure 15, A). The spacial proximity of these guest – host protons is directly proportional to the intensity of the cross-peaks. In d_6 -DMSO/ D_2O (Figure 15, A) the signal's intensities diminish in this order: $(\text{Hcp} + \text{H5}) = (\text{Hcp} + \text{H3}, (\text{H6})) > (\text{Ha} + \text{H3}, (\text{H6})) = (\text{Hb} + \text{H3}, (\text{H6})) > (\text{Hb} + \text{H5}) > (\text{Ha} + \text{H5})$. Since in this solvent mixture the H3 and H5 protons of the β -CyD cannot be distinguished, two different limiting conformations of the FcN_3 molecule within the β -CyD could be proposed. The first one concerning the interaction of the guest protons with the H3 protons and the second one with H6.⁵⁵ However, only the first one was taken into account (Figure 16) since the proposed position of the guest according to the second one (not shown) would place the guest outside the strongly binding hydrophobic cavity at the bottom part of the cyclodextrin. At this position no forces could hold the guest in the vicinity of the CyD and thus the complex would be unable to exist.

⁵⁵ The study of the solution structure of cyclodextrin complexes based on 2D ROESY conducted in d_6 -DMSO has already been described in: Forgo, P.; Vincze, I.; Kövér, K. E. *Steroids* **2003**, 68, 321, but we did not dare to neglect the interaction with the H6 protons as these authors have done, because observation of the cross-peak of the guest with H6 protons of the β -CyD is very common in the case of classical small molecules like ours or those used in the above mentioned reference.

In the ROESY spectrum recorded in d_6 -DMSO (Figure 15, B) the integrated cross-peak signals are in a different order: (Hcp + H5) = (Hcp + H3, (H6)) > (Ha + H5) > (Ha + H3, (H6)) = (Hb + H5) > (Hb + H3, (H6)). We proposed the conformation of the complex (Figure 15, B) assuming the cross-peak (Ha + H3, (H6)) arose mainly by a Ha – H3 interaction and the weak cross-peak (Hb + H3, (H6)) by a Ha – H6 interaction, while upon assuming interaction of H3 only, no disposition of the ferrocenyl azide could reflect the ROESY's cross-peaks origin. Also, the Job's plot (Figure 1) and ^1H -NMR titration (Figure 3) speaks in favor of this structure since a maximal shift was observed on the Ha guest protons. Thereby we placed the Ha protons in the neighborhood of the H5 protons, with which it has the strongest signal in the ROESY spectrum (Figure 15, B). Moreover, in the ^1H guest part of the ROESY spectra (Figure 15, B), the Hb proton is split into two broad singlets and therefore each of the Hb protons must experience a different chiral environment, one Hb proton to H6 and the second one to H5. To achieve this, the guest molecule must be twisted in the perpendicular plane to the longitudinal axis of FcN_3 .

Note in $\text{DMSO}/\text{D}_2\text{O} = 40/60$ (v/v) the guest is located in the upper part of the β -CyD cavity (Figure 16) whereas in neat DMSO at the bottom part (Figure 17). We deduce the increasing of the DMSO content not only rotates, but also lifts the ferrocenyl azide to the upper rim of the cyclodextrin.

Thus, the 2D ROESY technique allowed to explain the ICD spectra. The co-conformation is tuned by the solvent, accounting for the observed ICD sign variation. The same holds true for the temperature effect, since the electronic circular dichroism is not sensitive to temperature,⁵⁶ and thus, the changing phenotype of the ICD spectra reflects conformational changes. Since the d-d band of FcN_3 has a negative sign in EG as well as in $\text{DMSO}/\text{H}_2\text{O} = 40/60$, the co-conformation of the complex may be similar in both solvents (Figure 16).

3.5 Conclusion

The binding affinity of ferrocenyl azide towards β -CyD was investigated by means of ICD and NMR titrations. Special emphasis was put on the influence of solvents. To investigate the effect of the azide group, the association constants were compared with those of the unsubstituted ferrocene- β -cyclodextrin complexes. It is already well known that the solvent controls the orientation of the guest molecule within the CyD cavity.⁵⁷ Herein, we present a novel example based on ICD and 2D ROESY studies of the $\text{FcN}_3@ \beta$ -CyD complex. The ROESY techniques afforded information allowing a straightforward proposal of the solution structures in two solvents – DMSO and $\text{DMSO}/\text{H}_2\text{O} = 40/60$ (v/v). The co-conformation is tuned by these solvents, as was corroborated by the ICD study. In ethylene glycol the proposed structure might be similar to the one in $\text{DMSO}/\text{H}_2\text{O}$, due to the identical ICD sign. Finally, the temperature has a substantial effect on the orientation of the guest within the host's cavity.

⁵⁶ Mori, T.; Ko, Y. H.; Kim, K.; Inoue, Y. *J. Org. Chem.* **2006**, *71*, 3232.

⁵⁷ (a) Bortolus, P.; Monti, S. *J. Phys. Chem.* **1987**, *91*, 5046-5050. (b) Kobayashi, N.; Osa, T. *Carbohydr. Res.* **1989**, *192*, 147. (c) De Namor, A. F. D.; Traboulssi, R.; Lewis, D. F. V. *Chem. Commun.* **1990**, *10*, 751. (d) Fornasier, R.; Parmagnani, M.; Tonellato, U. *J. Inclusion Phenom. Mol. Recognit. Chem.* **1991**, *11*, 225. (e) Oswald S. T.; Charles, M.; Rafael, L.-H.; Javier, B. G. *J. Org. Chem.* **1994**, *59*, 7602.

3.6 Experimental Section

(Supporting Information)

General Remarks

Ferrocenyl azide was prepared according to the literature.⁵⁸ β -CyD (available from American Maizo Co., Hammond, Ind.) was recrystallized two times from water, dried at 80°C at 15 mm Hg for 1 d and the composition determined by elemental analysis (97.17 % w/w). Deionized MQ water (conductivity 18 M Ω .cm) was used. Commercial p.a. quality DMSO and ethylene glycol were used.

UV-Vis spectra were recorded with a Perkin-Elmer Lambda 7 spectrometer. Circular dichroism spectra were recorded with a CD6 circular dichrograph (I.S.A. Jobin-Yvon), in thermostated (\pm 0.5 °C) quartz cuvettes (1 cm path length). In ICD, the integration time was set to 1 second and each spectrum was repeated four times (ICD titrations) and the other measurements twice. The averaged spectra (accumulation mode) were then smoothed according to need either through 9 or 25 points and corrected to zero baseline at longest wavelength.

Microsoft Excell[®] was used for constructing diagrams. For the determination of the association constants by NMR and ICD titration, the errors of the regression analysis expressed as standard deviations from the fitted data were estimated by treating as a single data set.

The NMR measurements were conducted with Bruker Avance Spectrometers (250, 400, and 600 MHz). The temperature was kept constant at 300K and the residual solvent peak was set as a reference (*d*₆-DMSO, quintet, δ = 2.50 ppm; CDCl₃, singlet, δ = 7.26 ppm).

Theoretical Section

The density functional theory was employed for geometry optimization of FcH and FcN₃ molecules: Becke's³⁷ three-parameter hybrid method and the exchange functional of Lee, Yang, and Parr (B3LYP)³⁸ with the 6-31G(d) basic set implemented in the Gaussian 03 Program package.⁵⁹ The single point ZINDO/S⁶⁰

⁵⁸ Nesmeyanov, A. N.; Drozd, V. N.; Sazonova, V. A. *Dokl. Akad. Nauk SSSR* **1963**, *150*, 321.

⁵⁹ Frisch, M. J.; Trucks, G. W.; Schlegel, H. B.; Scuseria, G. E.; Robb, M. A.; Cheeseman, J. R.; Montgomery, J. A., Jr.; Vreven, T.; Kudin, K. N.; Burant, J. C.; Millam, J. M.; Iyengar, S. S.; Tomasi, J.; Barone, V.; Mennucci, B.; Cossi, M.; Scalmani, G.; Rega, N.; Petersson, G. A.; Nakatsuji, H.; Hada, M.; Ehara, M.; Toyota, K.; Fukuda, R.; Hasegawa, J.; Ishida, M.; Nakajima, T.; Honda, Y.; Kitao, O.; Nakai, H.; Klene, M.; Li, X.; Knox, J. E.; Hratchian, H. P.; Cross, J. B.; Bakken, V.; Adamo, C.; Jaramillo, J.; Gomperts, R.; Stratmann, R. E.; Yazyev, O.; Austin, A. J.; Cammi, R.; Pomelli, C.; Zakharski, J. W.; Ayala, P. Y.; Morokuma, K.; Voth, G. A.; Salvador, P.; Dannenberg, J. J.; Zakrzewski, V. G.; Dapprich, S.; Daniels, A. D.; Strain, M. C.; Farkas, O.; Malick, D. K.; Rabuck, A. D.; Raghavachari, K.; Foresman, J. B.; Ortiz, J. V.; Cui, Q.; Baboul, A. G.; Clifford, S.; Cioslowski, J.; Stefanov, B. B.; Liu, G.; Liashenko, A.; Piskorz, P.; Komaromi, I.; Martin, R. L.; Fox, D. J.; Keith, T.; Al-Laham, M. A.; Peng, C. Y.; Nanayakkara, A.; Challacombe, M.; Gill, P. M. W.; Johnson, B.; Chen, W.; Wong, M. W.; Gonzalez, C.; Pople, J. A. *Gaussian 03, revision C.02*; Gaussian, Inc.: Wallingford, CT, 2004.

calculations for electronic spectra prediction were conducted with the HyperChem⁶¹ program package. The configuration interaction included seven occupied molecular orbitals and thirteen unoccupied as has been originally demonstrated with ferrocene by the ZINDO method.⁶⁰ The σ - σ and π - π overlap weighting factors used were 1.267 and 0.585, respectively.

The optimization of FcH (D^{5h} Symmetry) was conducted without any restraint and the ground state was confirmed by vibrational analysis.

Constraint was applied to FcN₃ for all conducted optimizations (Figure S 1):

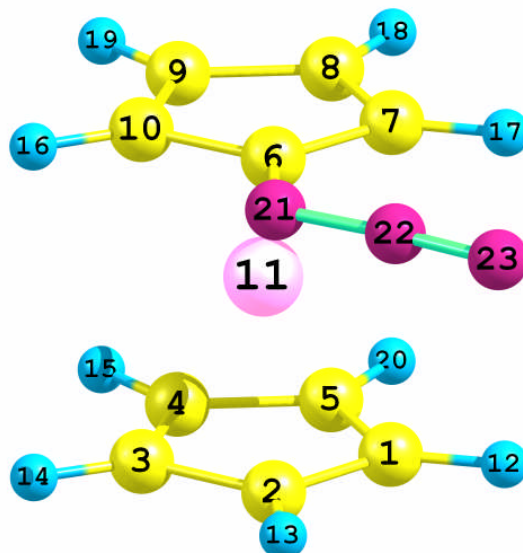


Figure S 1. B3LYP/6-31G(d) optimized geometry of FcN₃ constrained to the eclipsed conformation.

Restraint to the “eclipsed” conformation was applied as follows: four sets of dihedral angles were kept constrained at 0 degrees during the optimization of the geometry - (H12-C1-C7-H17, H20-C5-C8-H18, H15-C4-C9-H19 and H14-C3-C10-H16).

For the azide group rotational barrier determination, the dihedral angle ϑ (C7-C6-N21-N22) was scanned, starting at $\vartheta = 0^\circ$, 36 steps of 10 degrees size were optimized. To obtain the self consistent field energy (RB+HF-LYP) at $\vartheta = 45, 135, 225$ and 315° , a second scan was conducted starting with $\vartheta = 45$ degrees, performing 4 steps of 90 degrees size.

⁶⁰ Zerner, M. C.; Loew, G. H.; Kirchner, R. F.; Mueller-Westerhof, U. T. *J. Am. Chem. Soc.* **1980**, *102*, 589.

⁶¹ HyperChem(TM) Professional 7.5, Hypercube, Inc., 1115 NW 4th Street, Gainesville, Florida 32601, USA.

Cartesian Coordinates of Optimized Molecules

FcH (D5h Symmetry)

C	0.00000000	1.21460000	1.65460000
C	1.15520000	0.37530000	1.65460000
C	0.71390000	-0.98260000	1.65460000
C	-0.71390000	-0.98260000	1.65460000
C	-1.15520000	0.37530000	1.65460000
Fe	0.00000000	0.00000000	0.00000000
C	1.15520000	0.37530000	-1.65460000
C	0.00000000	1.21460000	-1.65460000
C	-1.15520000	0.37530000	-1.65460000
C	-0.71390000	-0.98260000	-1.65460000
C	0.71390000	-0.98260000	-1.65460000
H	0.00000000	2.29700000	1.64580000
H	2.18460000	0.70980000	1.64580000
H	1.35010000	-1.85830000	1.64580000
H	-1.35010000	-1.85830000	1.64580000
H	-2.18460000	0.70980000	1.64580000
H	2.18460000	0.70980000	-1.64580000
H	0.00000000	2.29700000	-1.64580000
H	-2.18460000	0.70980000	-1.64580000
H	-1.35010000	-1.85830000	-1.64580000
H	1.35010000	-1.85830000	-1.64580000

Number of imaginary frequencies: 0

Sum of electronic and zero-point energies=	-1650.532760
Sum of electronic and thermal energies =	-1650.524215
Sum of electronic and thermal energies=	-1650.523271
Sum of electronic and thermal free energies=	-1650.567284

FcN₃ - azide group dihedral angle (ϑ) not constrained

H	-0.66817700	-2.07132000	1.78068800
C	-1.16007000	-1.62987700	0.92348000
C	-0.80857400	-1.84565600	-0.44304400
H	-2.75103900	-0.35309600	1.84998300
H	-0.00204700	-2.47142200	-0.80322000
C	-1.69307300	-1.07182400	-1.25340600
H	-1.67018300	-1.01575100	-2.33396100
C	-2.59182000	-0.37803600	-0.38806700
H	-3.37815500	0.29896200	-0.69584000
C	-2.26143200	-0.72218900	0.95818800
Fe	-0.65019300	0.14724700	0.02753500
C	1.29633000	0.72417300	-0.31450300
C	0.94432200	0.92061000	1.05978800
H	0.41525300	1.52914000	-2.20564800
H	1.43391200	0.47651400	1.91673000
C	-0.16059800	1.82530400	1.09171800
H	-0.66138200	2.18069800	1.98266400
C	-0.49459700	2.17041300	-0.25210300
H	-1.29424600	2.83068900	-0.56065500
C	0.40040000	1.48289500	-1.12535600
N	2.35501400	-0.03406100	-0.87110700
N	3.07159900	-0.67332400	-0.09256400
N	3.80992200	-1.30514800	0.50841000

Number of imaginary frequencies: 1 (-15.6602 cm⁻¹)

Sum of electronic and zero-point energies=	-1814.115231
Sum of electronic and thermal energies=	-1814.104762
Sum of electronic and thermal energies=	-1814.103818
Sum of electronic and thermal free energies=	-1814.151945

FeN₃ - azide group dihedral angle (ϑ) constrained

$$\vartheta = 0$$

H	-0.68865300	-2.06776000	1.78465000
C	-1.17804500	-1.62344500	0.92748500
C	-0.83122200	-1.84480400	-0.43931000
H	-2.75502700	-0.32975800	1.85480000
H	-0.03069500	-2.47794900	-0.79998400
C	-1.70987800	-1.06396400	-1.24924900
H	-1.68845600	-1.00976700	-2.32993800
C	-2.60038500	-0.36020200	-0.38340700
H	-3.38084400	0.32359100	-0.69108000
C	-2.27071200	-0.70528200	0.96280800
Fe	-0.65327300	0.14741200	0.02776900
C	1.29863100	0.70626600	-0.31876000
C	0.94982100	0.90734400	1.05565800
H	0.42099000	1.51481500	-2.21012100
H	1.43688700	0.46029700	1.91249900
C	-0.14616500	1.82293300	1.08770900
H	-0.64169300	2.18511400	1.97887300
C	-0.47938300	2.16822600	-0.25621900
H	-1.27341400	2.83541200	-0.56443800
C	0.40763600	1.47064500	-1.12973700
N	2.34560000	-0.06801900	-0.87549500
N	3.08726100	-0.67282700	-0.09288100
N	3.84488400	-1.27815600	0.51136000

Number of imaginary frequencies: 1 (-12.9484 cm⁻¹)

Sum of electronic and zero-point energies=	-1814.115202
Sum of electronic and thermal energies=	-1814.104738
Sum of electronic and thermal enthalpies=	-1814.103794
Sum of electronic and thermal free energies=	-1814.151901

$$\vartheta = 90$$

H	-1.51166200	-1.45134700	2.17820600
C	-1.74658900	-1.19271200	1.15391600
C	-1.21614500	-1.83064600	-0.00728500
H	-3.16474300	0.53160200	1.36636000
H	-0.50120200	-2.64308200	-0.01606500
C	-1.75972900	-1.17999300	-1.15535100
H	-1.53633000	-1.42766100	-2.18492600
C	-2.62431600	-0.13711900	-0.70411300
H	-3.18030500	0.54663300	-1.33243400
C	-2.61613900	-0.14500700	0.72393500
Fe	-0.71705000	0.15833300	0.00068100
C	1.31725100	0.25747200	-0.01079700
C	0.79800800	0.90028300	1.15772500
H	0.98660600	0.64737100	-2.19514900
H	1.01136000	0.62399300	2.18158500
C	-0.05129400	1.96025400	0.72025700
H	-0.60383600	2.63347800	1.36249300
C	-0.05941000	1.96776700	-0.70757900
H	-0.61981000	2.64783000	-1.33570700
C	0.78476700	0.91276200	-1.16614700
N	2.17790200	-0.88808200	-0.02431600
N	3.39881500	-0.66599000	-0.00181800
N	4.53825600	-0.63219200	0.01621700

Number of imaginary frequencies: 2 (-67.755 cm^{-1}) and (-26.3747 cm^{-1})

Sum of electronic and zero-point energies=	-1814.110254
Sum of electronic and thermal energies=	-1814.100646
Sum of electronic and thermal enthalpies=	-1814.099702
Sum of electronic and thermal free energies=	-1814.145309

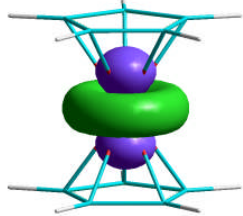
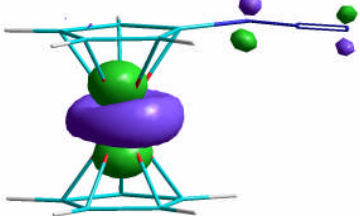
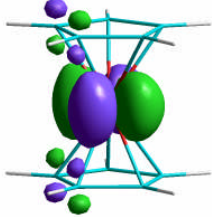
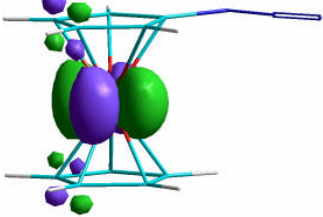
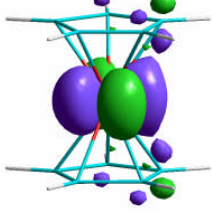
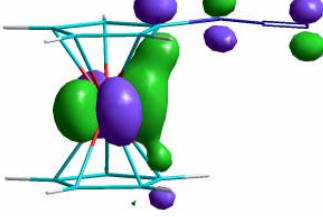
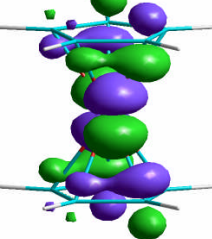
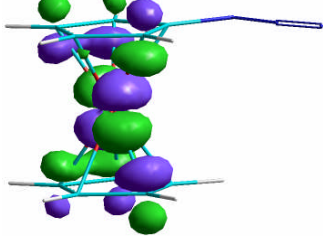
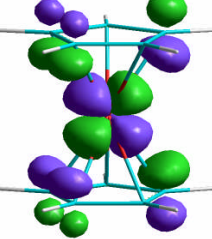
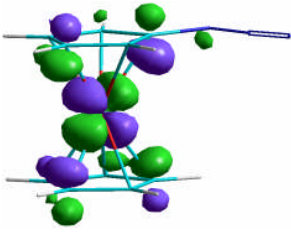
$$\vartheta = 270^\circ$$

H	0.83667200	-1.62461300	-2.20380400
C	1.11807900	-1.47389600	-1.16967700
C	0.37988100	-1.92360600	-0.03427300
H	3.03615400	-0.32323300	-1.31495100
H	-0.54539800	-2.48257900	-0.05901300
C	1.07938100	-1.51075500	1.13912000
H	0.76508700	-1.69423800	2.15837400
C	2.25450200	-0.81213400	0.72917700
H	2.99192400	-0.36674000	1.38429200
C	2.27828100	-0.78915400	-0.69858700
Fe	0.58422200	0.13143800	0.00177400
C	-1.26022500	1.02298500	-0.01689300
C	-0.50371400	1.43381800	-1.15872300
H	-0.86903400	1.24106800	2.17976700
H	-0.79402600	1.29935600	-2.19211700
C	0.68619000	2.05925000	-0.68385800
H	1.47706900	2.46592500	-1.30043800
C	0.66220600	2.03973000	0.74389400
H	1.43106800	2.42866700	1.39861600
C	-0.54304500	1.40321300	1.16102500
N	-2.60829900	0.54703800	-0.05143300
N	-2.82904600	-0.66607800	-0.00360000
N	-3.19530000	-1.74634500	0.03159400

Number of imaginary frequencies: 2 (-43.2544 cm^{-1}) and (-24.2627 cm^{-1})

Sum of electronic and zero-point energies=	-1814.111350
Sum of electronic and thermal energies=	-1814.101711
Sum of electronic and thermal enthalpies=	-1814.100767
Sum of electronic and thermal free energies=	-1814.146703

Figures of FcH and FcN₃'s orbitals participating in d-d transitions calculated by the ZINDO/S method

MO #	FcH (D_{5h} Symmetry)	MO #	FcN ₃ (C_1 Symmetry)
27		34	
28		35	
29		36	
34		43	
35		44	

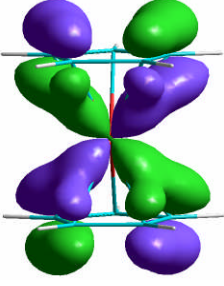
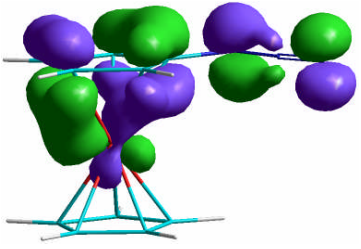
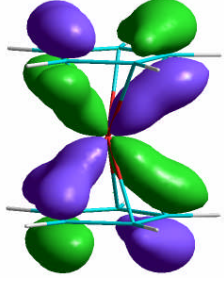
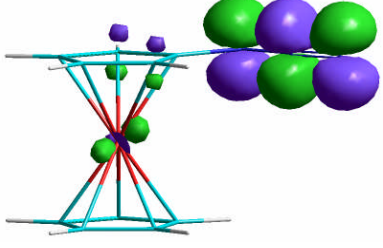
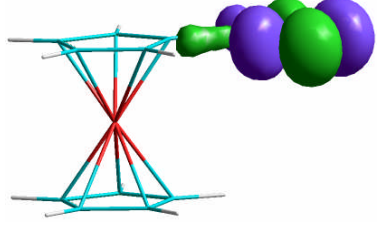
25		33	
26		-	-
-	-	37	
-	-	38	

Figure S 2. Single point ZINDO/S calculation of orbitals involved in the d-d transitions of FcH and FcN₃. A Gouraud shaded surface with an orbital contour value 0.05 was used for visualization.

NMR Spectra of Acetyl Ferrocene

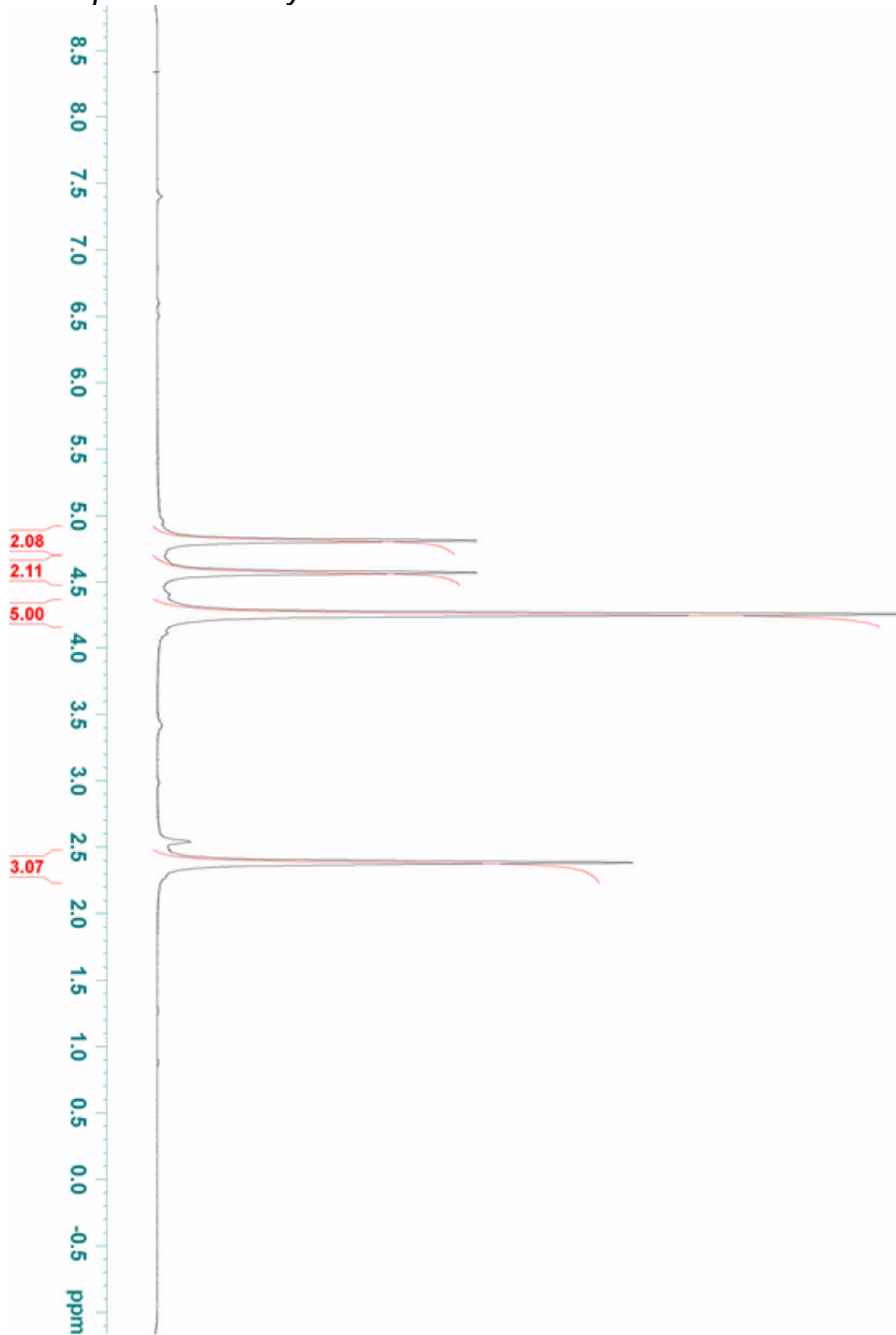


Figure S 3. 600 MHz ^1H NMR Spectrum of acetyl ferrocene in d_6 -DMSO at 300K.



Figure S 4. 600 MHz ^{13}C NMR Spectrum of acetyl ferrocene in d_6 -DMSO at 300K.

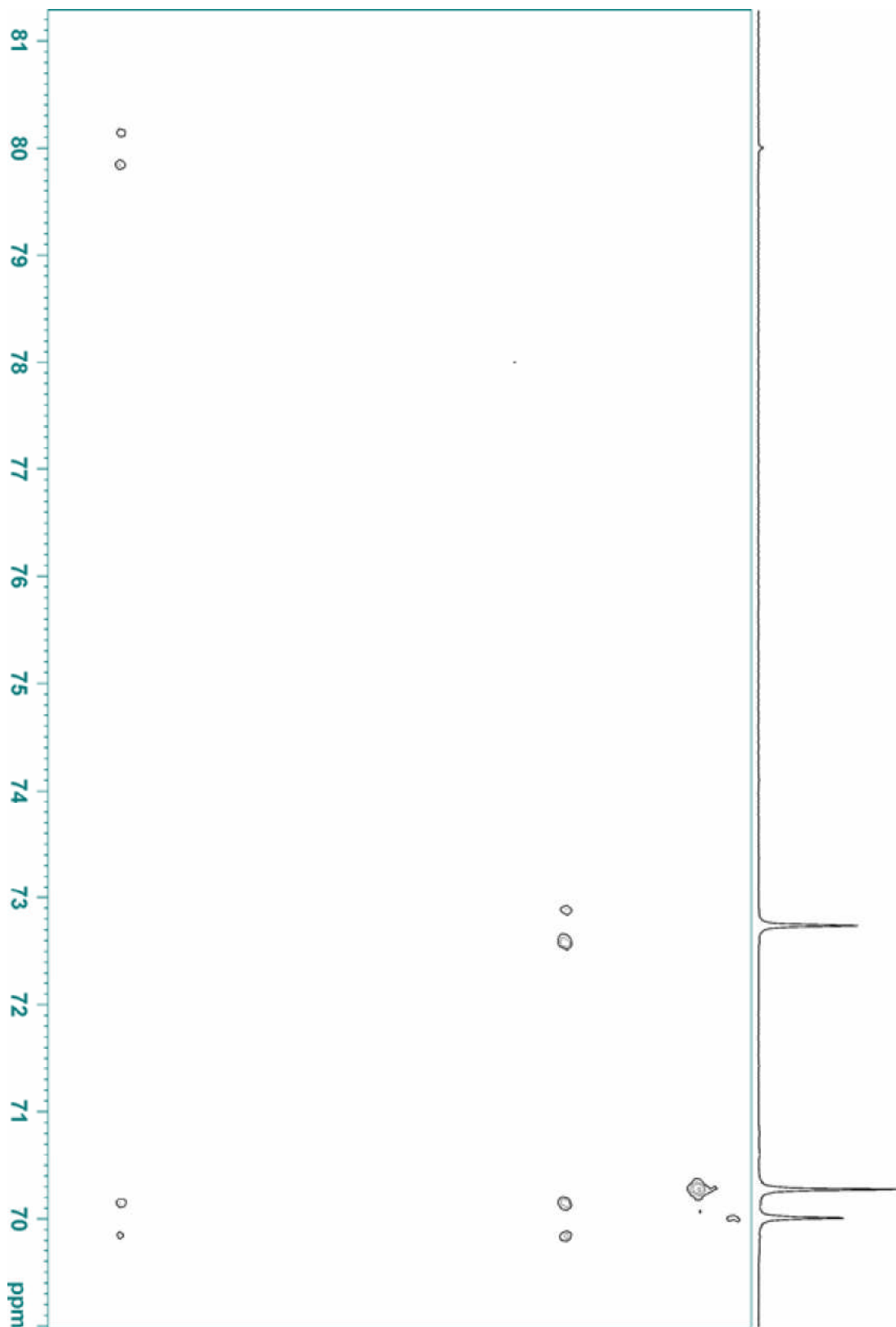


Figure S 5. 600 MHz 2D INADEQUATE NMR Spectrum of acetyl ferrocene in *d*₆-DMSO at 300K.

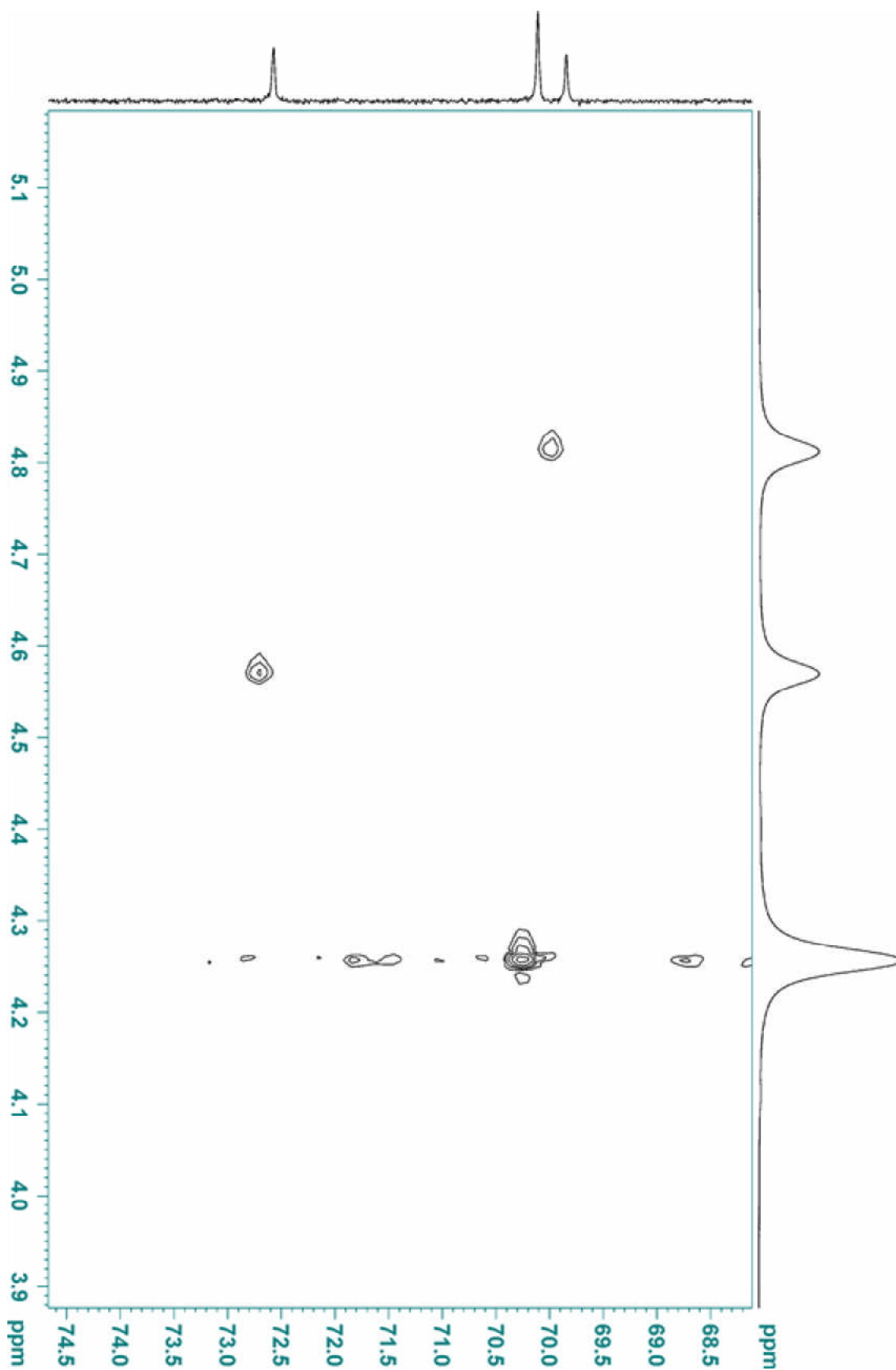


Figure S 6. 600 MHz HSQC NMR Spectrum of acetyl ferrocene in d_6 -DMSO at 300K.

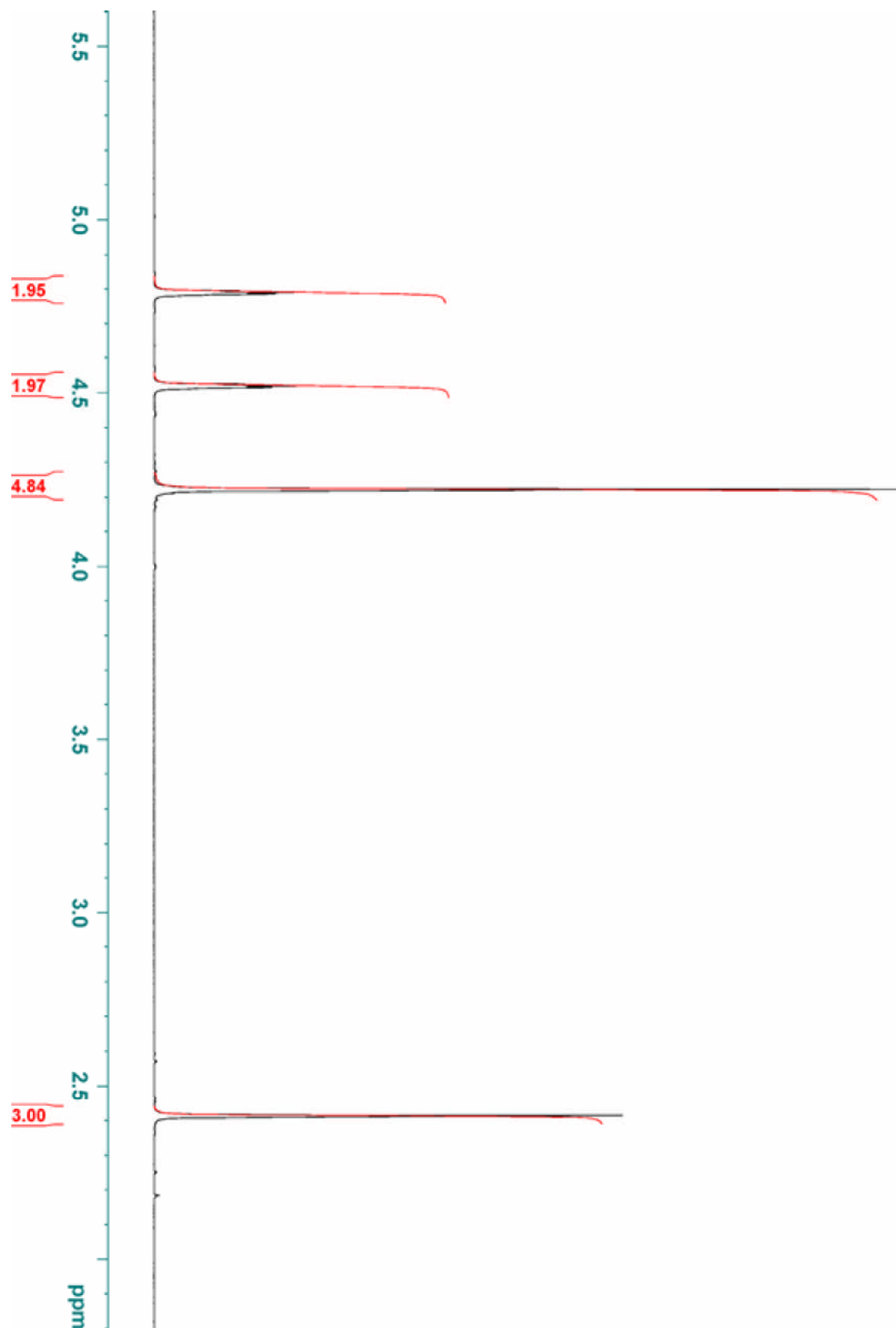


Figure S 7. 400 MHz ^1H NMR Spectrum of acetyl ferrocene in CDCl_3 at 300K.

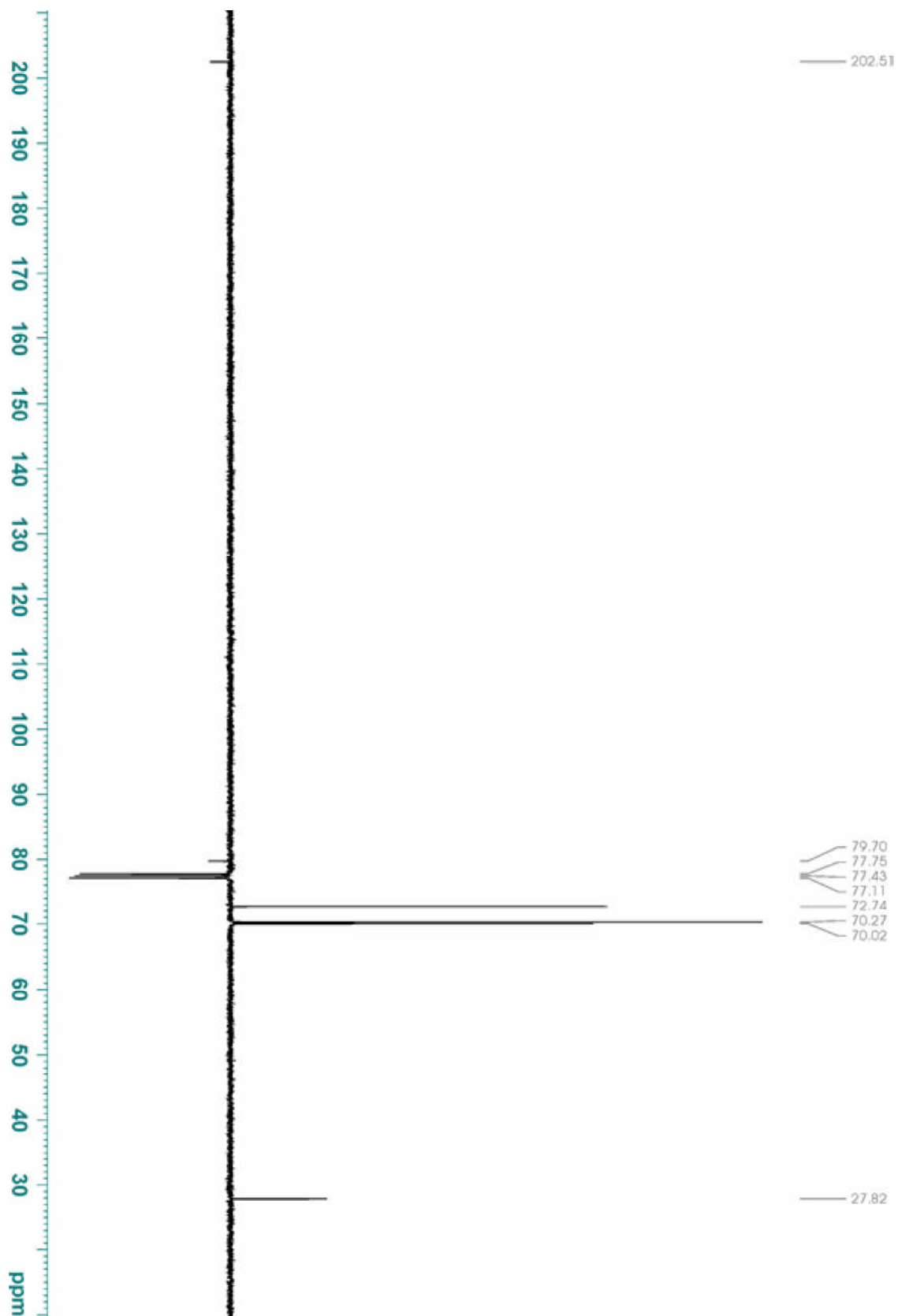


Figure S 8. 400 MHz ^{13}C (JMOD) NMR Spectrum of acetyl ferrocene in CDCl_3 at 300K.

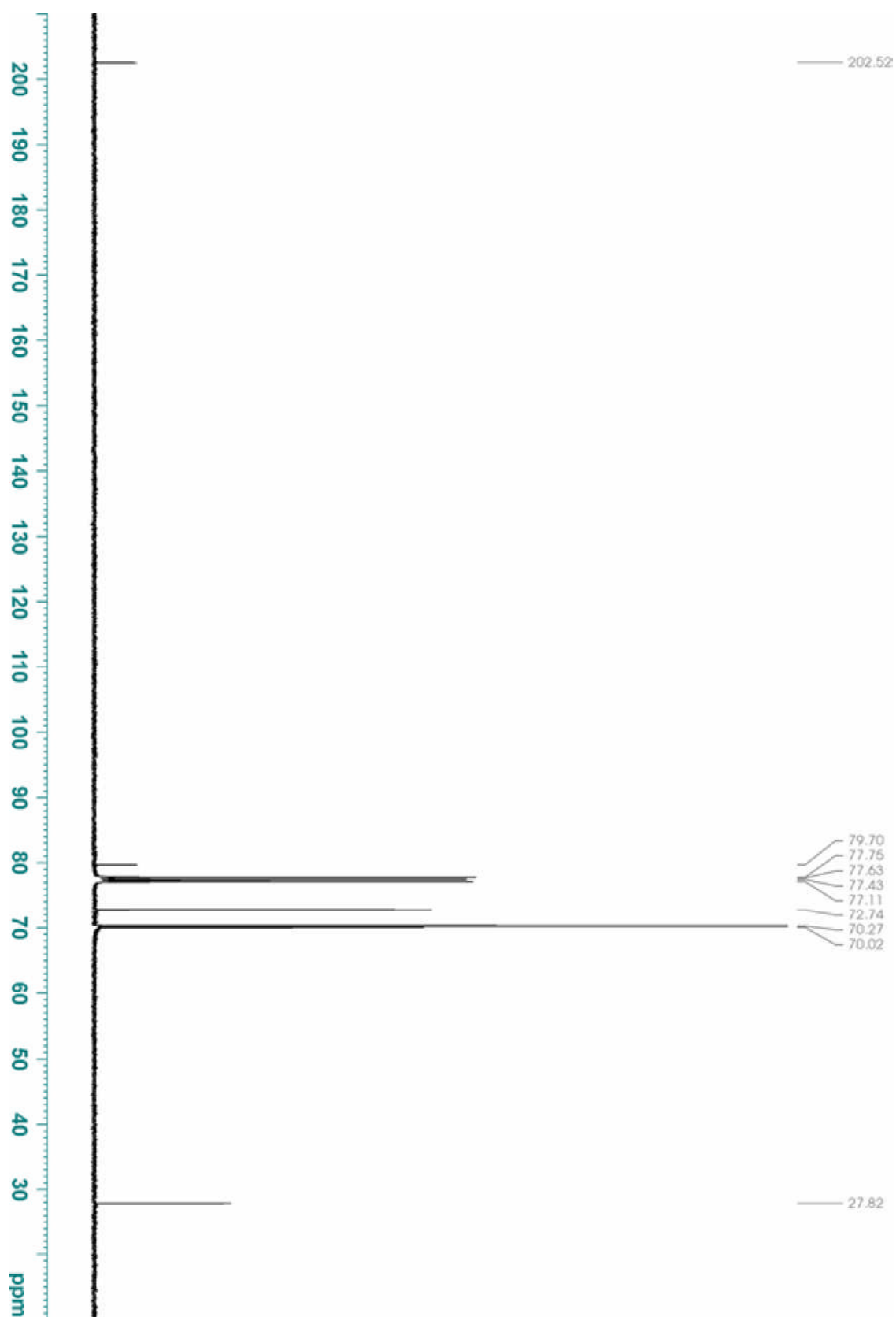


Figure S 9. 400 MHz ^{13}C NMR Spectrum of acetyl ferrocene in CDCl_3 at 300K.

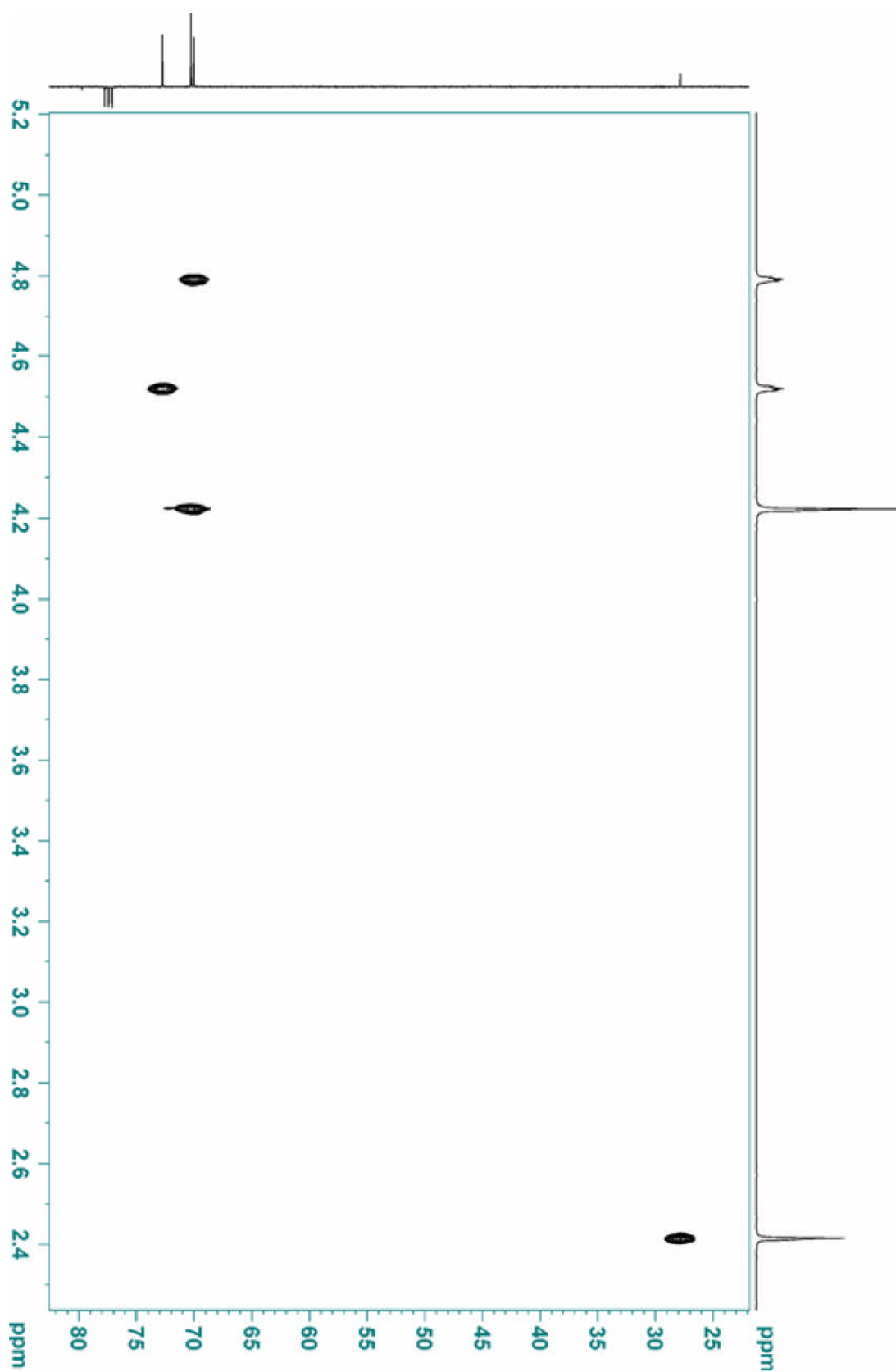


Figure S 10. 400 MHz HSQC NMR Spectrum of acetyl ferrocene in CDCl₃ at 300K.

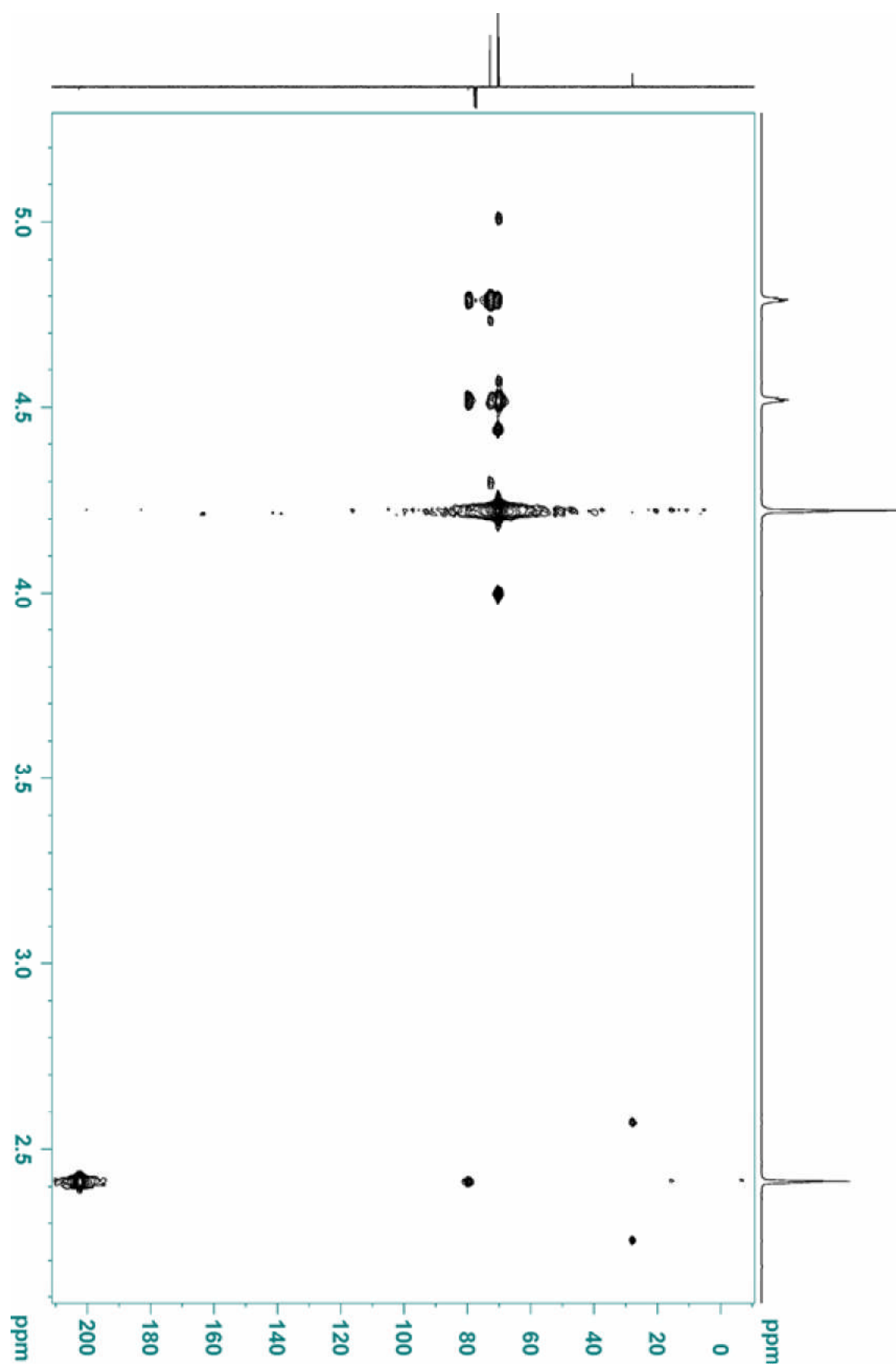


Figure S 11. 400 MHz HMBC NMR Spectrum of acetyl ferrocene in CDCl_3 at 300K.

NMR Spectra of Ferrocenyl Azide

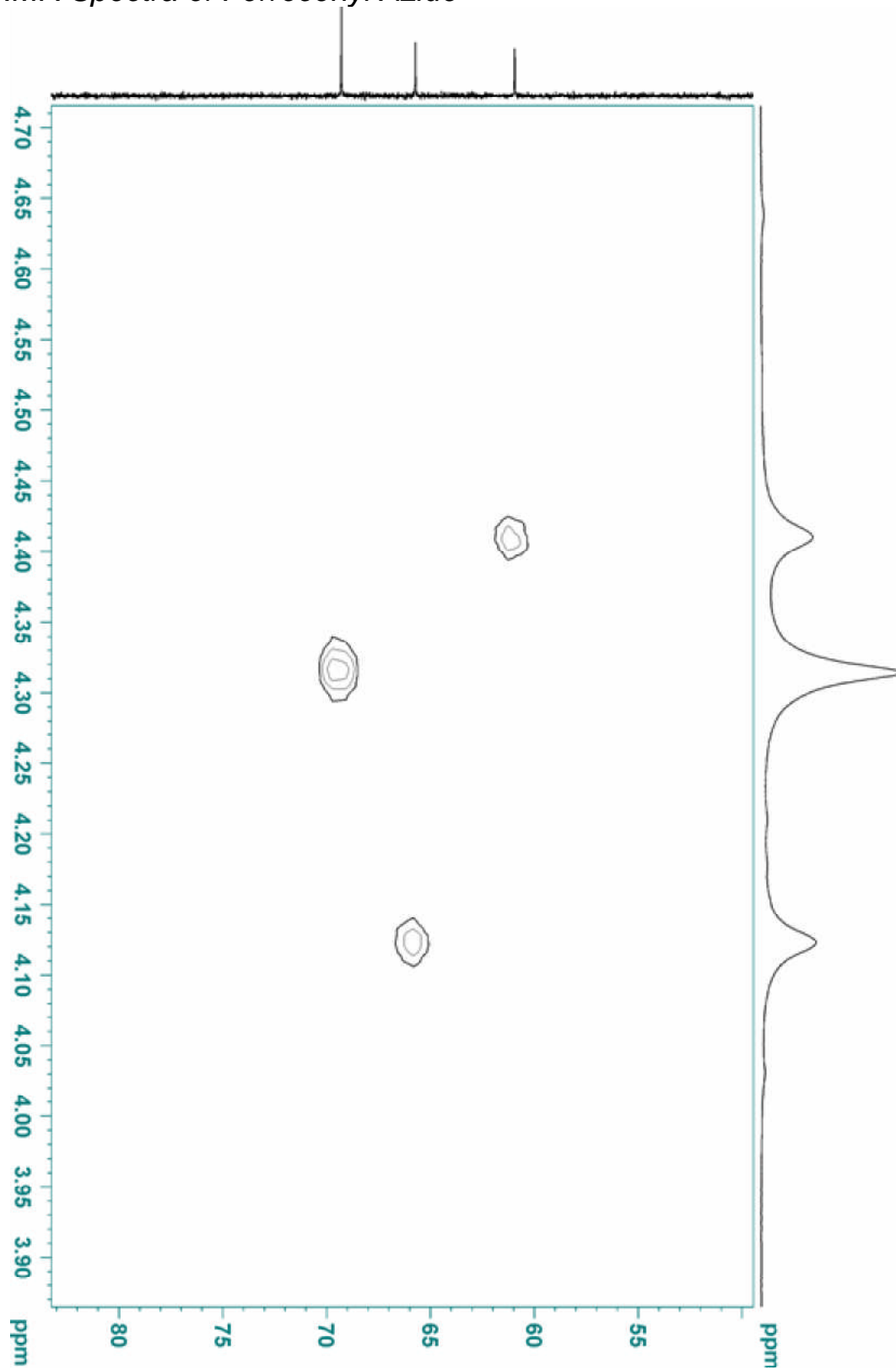


Figure S 12. 400 MHz HSQC NMR Spectrum of ferrocenyl azide in d_6 -DMSO at 300K.

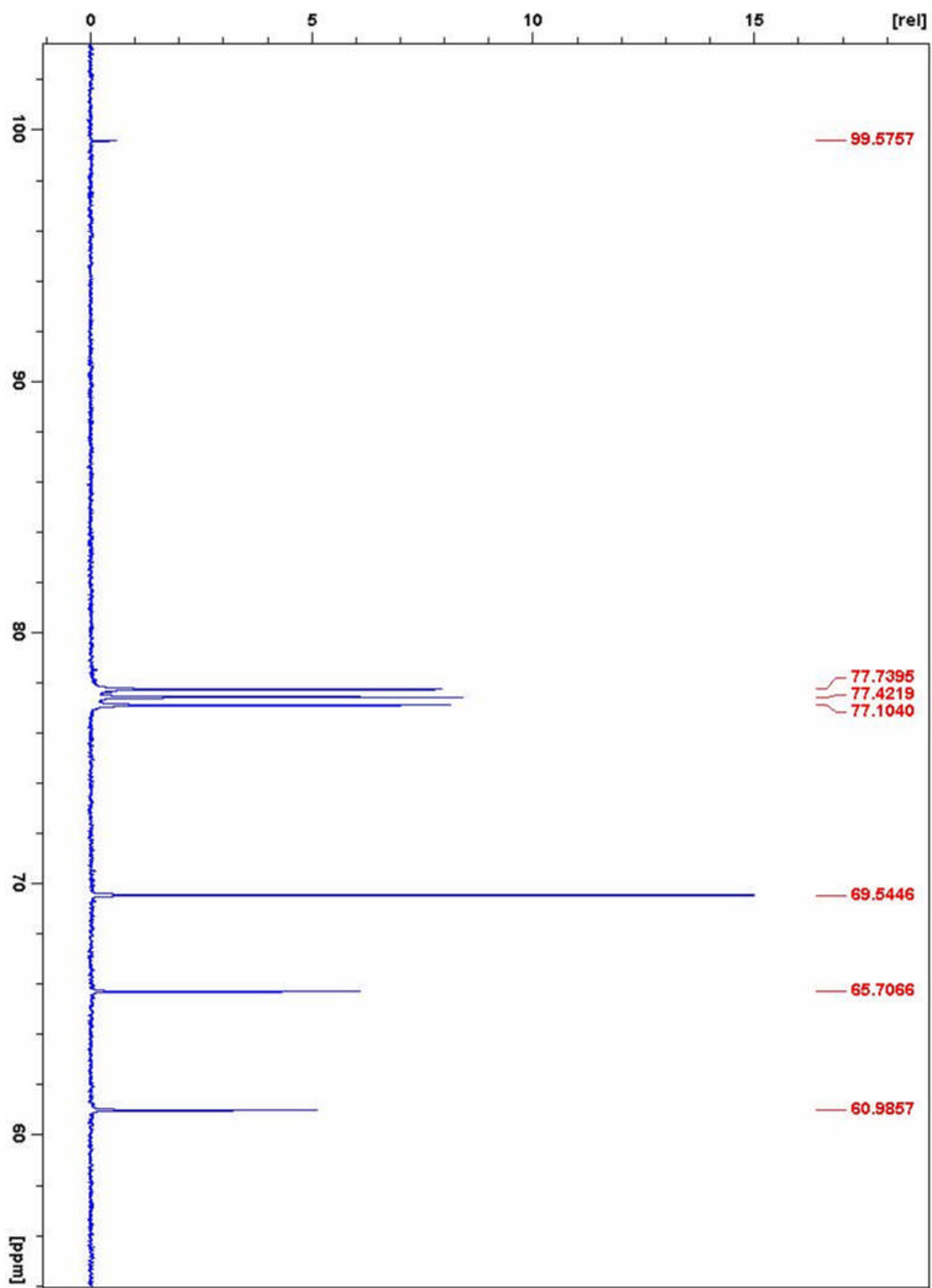


Figure S 13. 400 MHz ^{13}C NMR Spectrum of ferrocenyl azide in CDCl_3 at 300K.

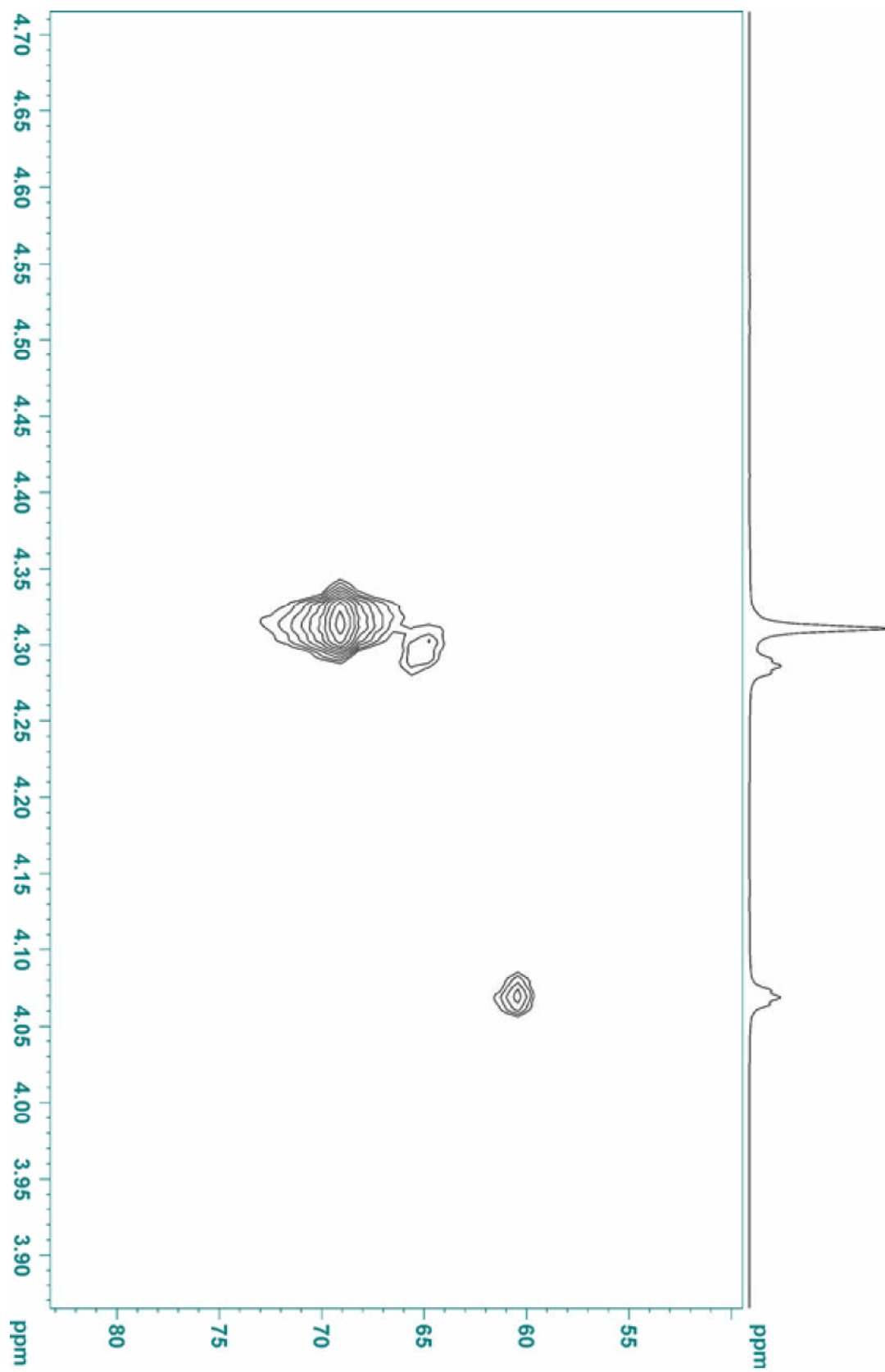


Figure S 14. 400 MHz HSQC NMR Spectrum of ferrocenyl azide in CDCl₃ at 300K.

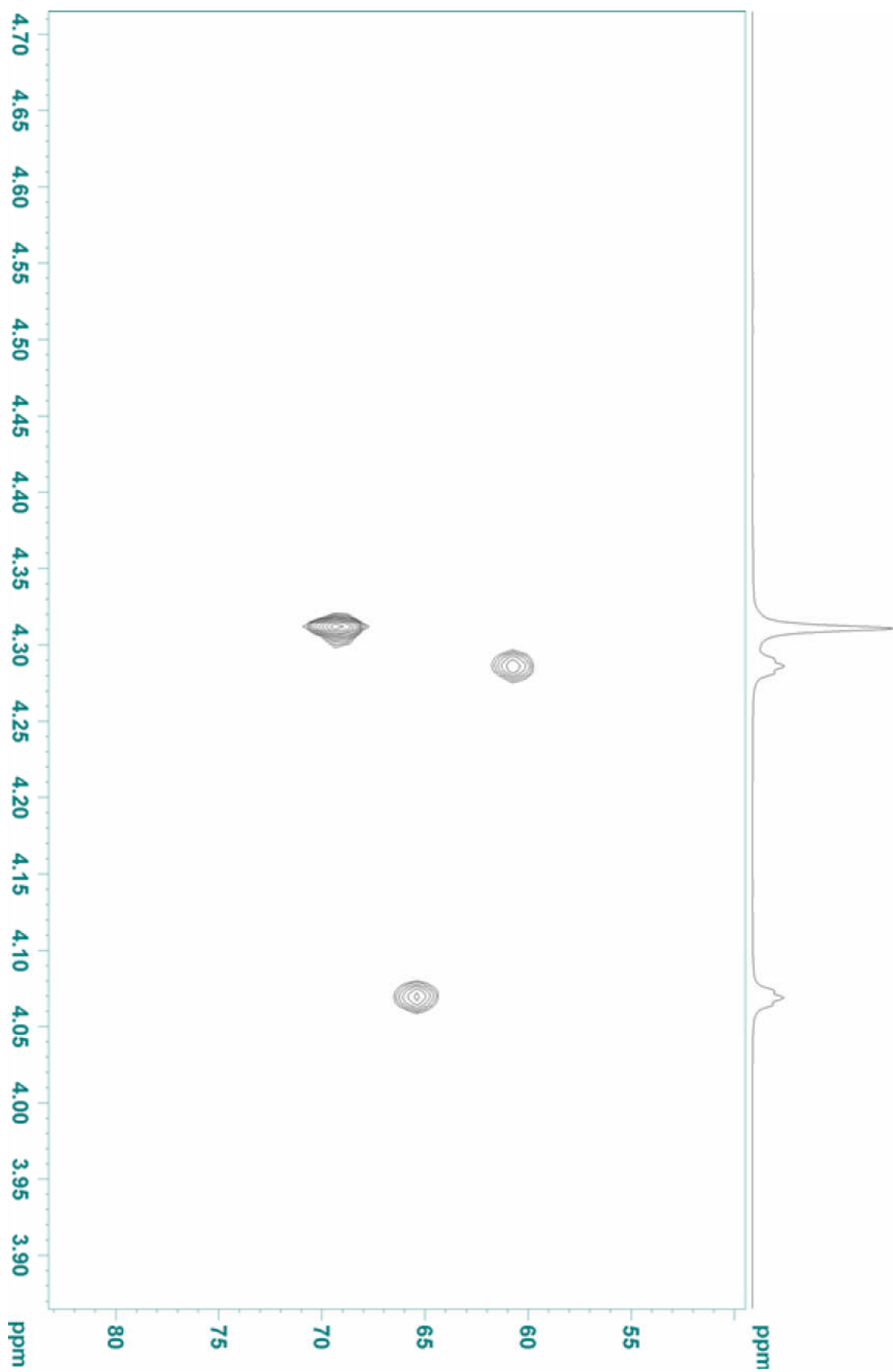
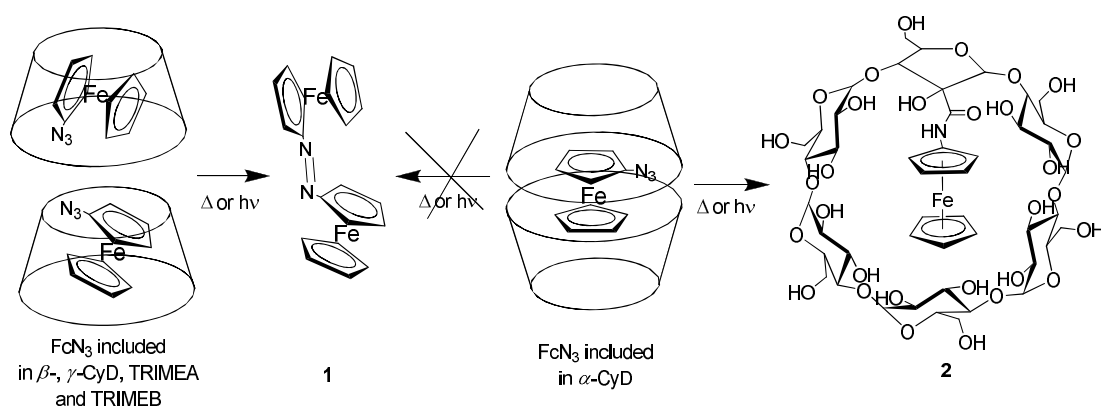


Figure S 15. 400 MHz HMBC NMR Spectrum of ferrocenyl azide in CDCl_3 at 300K.

4. Structure–Chemistry Relationship in Ferrocenyl Azide–Cyclodextrin Complexes



4.1 Abstract

Solid complexes of ferrocenyl azide (FcN₃) with native cyclodextrins (α-, β-, γ-CyDs) and modified CyDs (2,3,6-per-*O*-methyl- α- and β-CyDs (TRIMEA and TRIMEB, respectively)) were decomposed. The resulting product distribution provided a new reaction pathway of ferrocenyl nitrene. Inclusion of FcN₃ by β-, and γ-CyDs, TRIMEA and TRIMEB lead to the formation of azoferrocene **1**, whereas inclusion in α-CyD afforded ferrocenyl amine and a novel compound **2**.

4.2 Introduction

Finding new reaction pathways inside host molecules is of increasing interest in Organic Chemistry, since in a confined space, reactive species cannot react indiscriminately. Cyclodextrins (CyDs) have successfully been used in supramolecular carbene chemistry to modify the reaction course of included precursors.¹ However, there are only a few reports concerning supramolecular nitrene chemistry.² Hence, we set out to extend this interesting field to also generate nitrenes within the confined space of other molecules. As a guest, we used ferrocenyl azide

¹ Representative publications: (a) Brinker, U. H.; Buchkremer, R.; Kolodziejczyk, M.; Kupfer, R.; Rosenberg, M.; Poliks, M. D.; Orlando, M.; Gross, M. L. *Angew. Chem., Int. Ed.* **1993**, *32*, 1344. (b) Rosenberg, M. G.; Kam, S. M.; Brinker, U. H. *Tetrahedron Lett.* **1996**, *37*, 3235. (c) Krois, D.; Bobek, M. M.; Werner, A.; Kählig, H.; Brinker, U. H. *Org. Lett.* **2000**, *2*, 315. (d) Rosenberg, M. G.; Brinker, U. H. *J. Org. Chem.* **2001**, *66*, 1517. (e) Knoll, W.; Bobek, M. M.; Giester, G.; Brinker, U. H. *Tetrahedron Lett.* **2001**, *42*, 9161. (f) Rosenberg, M. G.; Brinker, U. H. *J. Org. Chem.* **2003**, *68*, 4819. (g) Krois, D.; Brecker, L.; Werner, A.; Brinker, U. H. *Adv. Synth. Catal.* **2004**, *346*, 1367. (h) Rosenberg, M. G.; Brinker, U. H. In *Adv. Phys. Org. Chem.*; Richard, J. P., Ed.; Academic: New York, **2005**; Vol. 40, pp 1-47. (i) Rosenberg, M. G.; Brinker, U. H. *Eur. J. Org. Chem.* **2006**, 5423.

² (a) Tokitoh, N.; Saiki, T.; Okazaki, R. *Chem. Commun.* **1995**, 1899. (b) Tönshoff, C.; Bucher, G. *Eur. J. Org. Chem.* **2004**, 269. (c) Warmuth, R.; Makowiec, S. *J. Am. Chem. Soc.* **2005**, *127*, 1084. (d) *ibid.*, *idem.* **2007**, *129*, 1233.

(FcN₃) because of its size and the known chemistry of the corresponding nitrene.³ Native (α -, β -, γ -CyDs) and modified 2,3,6-per-*O*-methyl- α - and β -CyDs, TRIMEA and TRIMEB, respectively were applied as hosts. Our interest was also focused on the structure of the complexes. Thus, for comparison, the unsubstituted ferrocene (FcH) - TRIMEB complex was investigated as well. Both, the ferrocene guests and hosts were chosen intentionally, since they tend to form crystals suitable for X-ray analysis.

4.3 Results and Discussion

As inferred from X-ray analysis, ferrocene adopts an axial alignment inside native β -CyD.⁴ Surprisingly, equatorial inclusion was found within TRIMEB (Figure 1).

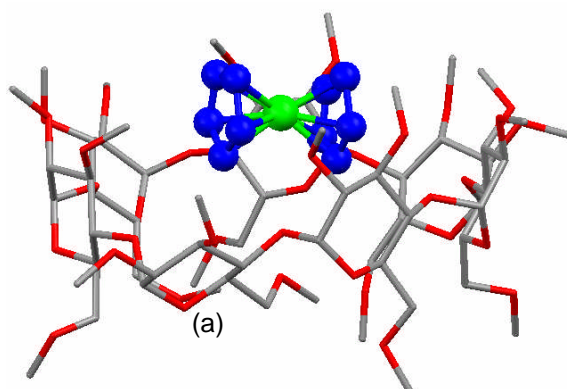


Figure 1. X-ray single crystal structure of the FcH@TRIMEB complex.

The FcH@TRIMEB complex crystallizes in the chiral orthorhombic space group $P2_12_12_1$. Analysis of short contacts revealed that the driving forces of the complexation are mainly van-der-Waals interactions. Only one C-H...O hydrogen bond between the proton of ferrocene and the glycosidic oxygen was observed (not shown). Both, the host and guest are distorted through an induced fit. The host forms an ellipsoid with one glucose unit (Figure 1, marked (a)) deflected out of the cone. Ferrocene is not in the eclipsed conformation, but distorted by a dihedral angle of 15°. The distance between the two cyclopentadienyls of ferrocene is compressed from 3.41⁵ to 3.27 Å, similarly as found in the inclusion by native β -CyD.⁴

The FcN₃@TRIMEB complex crystallizes in the chiral monoclinic space group $P2_1$ (Figure 2).

³ Abramovitch, R. A.; Azogu, C. I.; Sutherland, R. G. *Chem. Commun.* **1971**, 134.

⁴ Liu, Y.; Zhong, R-O.; Zhang, H-Y.; Song, H-B. *Chem. Commun.* **2005**, 17, 2211.

⁵ Braga, D.; Grepioni, F. *Organometallics* **1992**, 11, 711.

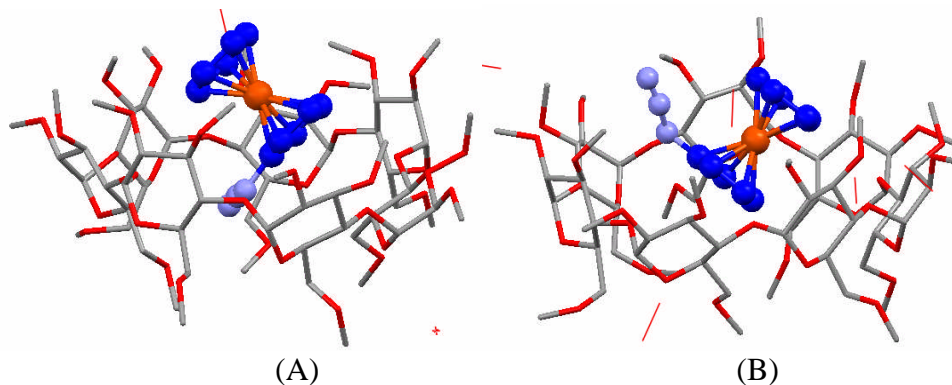


Figure 2. X-ray single crystal structure of the FcN₃@TRIMEB complex.

The asymmetric unit consists of two crystallographically independent TRIMEB molecules, each of them accommodating a molecule of ferrocenyl azide with an approximately 50% occupancy along with a number of lattice methanol molecules. A superposition of the two independent molecular structures of TRIMEB, indicates that both molecules have close conformations (Figure 3).

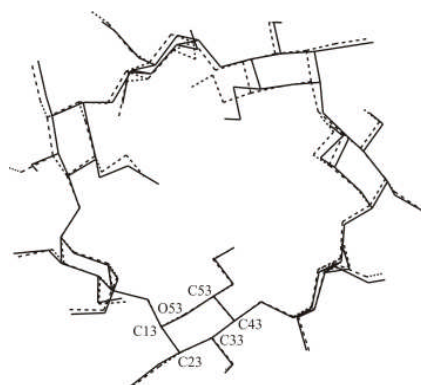


Figure 3. Superposition of structures of two crystallographically independent TRIMEB molecules.

The main difference between the two host-guest pairs in the independent part of the unit cell consists in the different orientation of the ferrocenyl azide molecules with respect to the cyclodextrin cavity. While the azide group of ferrocenyl azide in the first CyD points towards the inner cavity (Figure 2, A), the same group in the second inclusion complex is directed outside the host cavity (Figure 2, B). At the same time, essential differences in the character of intermolecular interactions in these two pairs of complexes were not observed. In the absence of conditions required for hydrogen bond formation, the shortest intermolecular contacts in host-guest pairs are equal or even larger than the sum of the van-der-Waals radii.

According to B3LYP/6-31G(d) calculations, the azide group at the minimum is coplanar with the cyclopentadienyl ring.^{6b} The first inclusion mode of FcN₃ inside TRIMEB (Figure 2, A) did not have any effect on the deflection of the azido group from the co-planarity with the cyclopentadienyl ring. However, in the second mode (Figure 2, B), the deflection by 32° even surpasses the value found for the angle in

⁶ (a) Walla, P.; Arion, V. B.; Brinker, U. H. *J. Org. Chem.* **2006**, *71*, 3274. (b) Walla, P.; Brecker, L.; Brinker, U. H. *manuscript in preparation*.

neat solid FcN_3 (22°),^{6b} where an “eclipsed” (in terms of the two cyclopentadienyl rings) conformation was observed.⁶ In contrast, the entrapment by TRIMEB had no effect on this dihedral distortion. However, the distance between the cyclopentadienyl rings in the A-type mode is elongated from 3.291^{6b} to 3.322 Å and compressed to 3.283 Å in the B-type inclusion mode, as compared with the X-ray structure of neat solid FcN_3 .^{6b}

Furthermore, we investigated the solution structures of the complexes by Induced Circular Dichroism (ICD) and 2D ROESY techniques.⁷ In the ICD, the positive peak in the range of 400-550 nm indicates axial alignment of the Cp-Fe-Cp vector and the negative one an equatorial alignment.⁸ Both, the FcH and $\text{FcN}_3@$ TRIMEB complexes exhibit negative peaks of these d-d bands (Figure 4).

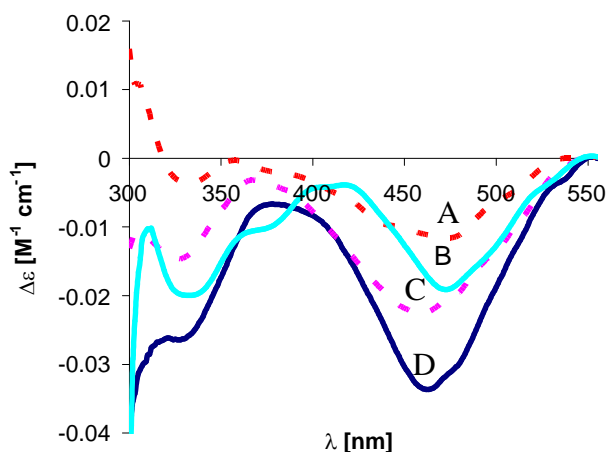


Figure 4. Induced Circular Dichroism spectra of TRIMEB complexes with FcH (dashed lines) and FcN_3 (solid lines). Curves (C, D) for methanol, (B) for H_2O and (A) for $\text{H}_2\text{O}/\text{EtOH} = 80/20$ (v/v), 27°C . The concentrations are given in the Supporting Information.

Thus, ferrocene most probably adopts an equatorial alignment inside the TRIMEB. In the case of the $\text{FcN}_3@$ TRIMEB complex, however, it is not possible to straightforwardly estimate the co-conformation of the non-rigid guests, since the orientation of the flexible functional group controls the orientation of the transition dipole moment vector of the parent guest molecule.^{6b} Inspection of the 2D ROESY spectra of the $\text{FcN}_3@$ TRIMEB complex (Supporting Information) revealed multiple cross-signals between guest and host protons; the most intense being those between the guest and inner cavity protons. The two concomitant structures depicted in Figure 2 would explain the observed cross-peaks. Equatorial alignment of FcN_3 inside TRIMEB would also contribute to the interpretation of the observed cross-peaks.

FcN_3 possesses a C_1 molecular symmetry and the existence of two enantiomers of FcN_3 could be proposed, leading to the chemical nonequivalence of the α -, α' - and β -, β' - protons. However, neat FcN_3 is achiral (no optical rotation observed) and in the ^1H NMR spectra two triplets (2H each) belonging to the α - and β - protons of the substituted cyclopentadienyl ring were observed (Figure 5, A).

⁷ Dodziuk, H. (Ed.), *Cyclodextrins and Their Complexes: Chemistry, Analytical Methods, Applications.*, Wiley: New York, **2006**.

⁸ (a) Harada, A.; Takahashi, S.; *J. Inclusion Phenom.* **1984**, *2*, 791. (b) Harada, A.; Takahashi, S.; *Chem. Lett.* **1984**, 2089. (c) Harada, A.; Hu, Y.; Yamamoto, S.; Takahashi, S. *J. Chem. Soc. Dalton Trans.* **1988**, 729. (d) Kobayashi, N.; Opallo, M. *J. Chem. Soc., Chem. Commun.* **1990**, 477.

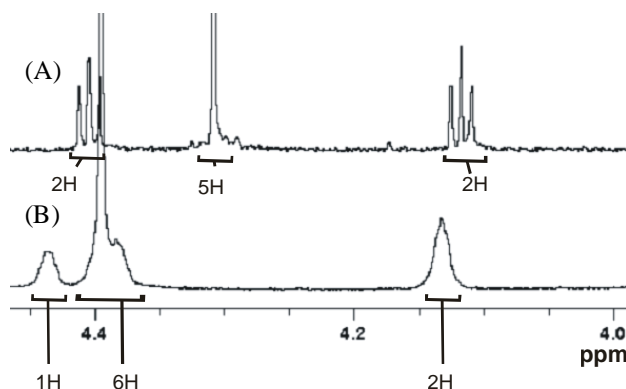


Figure 5. ^1H NMR spectra of (A) FcN_3 in $\text{DMSO-}d_6$, 250 MHz (B) FcN_3 @TRIMEB complex in D_2O . 400 MHz, $c(\text{FcN}_3) = 3.7$ mM, $c(\text{TRIMEB}) = 14.4$ mM, $[\text{H}]/[\text{G}] = 3.9$, 27 °C.

This chemical equivalence of the α -, α' - and β -, β' - protons is caused by free rotation of the azido group. The α -, α' - and β -, β' - protons are chemically equivalent, but not magnetically equivalent, thus forming an AA'B₅CC' spin system. We have observed, upon addition of TRIMEB, that the α - and α' - protons of FcN_3 became chemically nonequivalent, whereas the β - protons retained the unsplit triplet pattern (Figure 5, B). Since no new signals appeared in the spectrum, a fast exchange process in respect to the NMR time scale must take place. The splitting of α - and α' - protons might have been caused probably by freezing of the azide group rotation upon inclusion into the cavity of TRIMEB. As a consequence, FcN_3 becomes chiral and the ABC₅DD' pattern is observed. In other words, *three* species contribute to the observed splitting pattern, i.e. (*L*)- FcN_3 @TRIMEB, (*R*)- FcN_3 @TRIMEB, and free unbound FcN_3 .⁹ At this stage, however, we cannot state, which species contributes preferably, i.e., which enantiomer exhibits a higher affinity towards TRIMEB.

Furthermore were the association constants (K_a) of the FcH and FcN_3 @TRIMEB complexes determined in CD_3OD by the ^1H NMR titration (Supporting Information). A $K_a = 53 \pm 5 \text{ M}^{-1}$ was found for the FcH @TRIMEB complex and a $K_a = 37 \pm 3 \text{ M}^{-1}$ for the FcN_3 @TRIMEB complex. The value of $K_a = 30 \text{ M}^{-1}$ for the FcH @TRIMEB complex has already been determined by HR-DOSY technique.¹⁰ Thus, FcN_3 binds approximately 1.4 times more weakly to TRIMEB in CD_3OD than FcH .

FcN_3 decomposes quickly at around 80 °C,³ a lower temperature than observed for typical stable aryl azides, e.g., phenyl azide decomposes over 130°C. This behavior allows to conduct the thermal decomposition of the FcN_3 -cyclodextrin complexes. The decompositions takes place faster than the release of the guest molecule out of the cavity. Table 1 summarizes the thermal and photochemical decomposition of FcN_3 at different conditions.

⁹ The designation (*L*) and (*R*) accounts for the two chiral enantiomers, see Supporting Information.

¹⁰ Skinner, P. J.; Blair, S.; Katakya, R.; Parker, D. *New J. Chem.*, **2000**, *24*, 265.

Exp.	Complex		Yield of isolated products (%)			
			FcH	FcN=NFc	FcNH ₂	FcN-CyD
1	G (solid)	Δ	9	47	-	-
2	G@(α-CyD) ₂	Δ	<0.5	-	60	9
		hν		-	53	3 ^a
3	G@β-CyD	Δ		5	22	No ^b
		hν		8	27	
4	G@γ-CyD	Δ	4	4	19	Yes ^c
		hν	1	2	9	
5	G@TRIMEA	Δ	4	12	-	Yes ^d
6	G@TRIMEB	Δ	7	2	-	

G=FcN₃. ^aHPLC yield. ^bNo modification of β-CyD observed. ^cComplex mixture of products. ^dInsertion detected by ESI-MS.

Table 1. Product distribution upon solid state decompositions of ferrocenyl azide–cyclodextrin complexes.

FcN₃ forms a complex of 1:2 stoichiometry with a α-CyD (Table 1, Exp. 2). However, with its permethylated analogue (TRIMEA) surprisingly a 1:1 stoichiometry was proven by a Job's plot¹¹ (Figure 6).

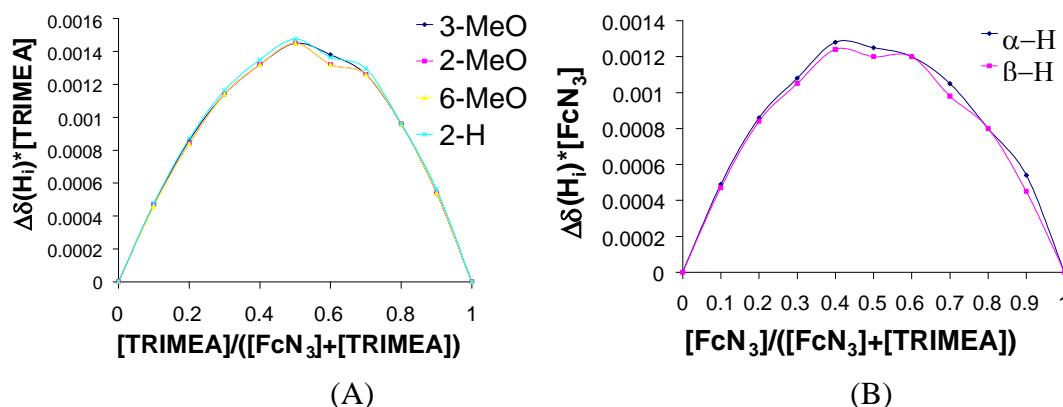


Figure 6. Job's plots for the FcN₃@TRIMEA complex based on ¹H NMR induced chemical shifts in CDCl₃ at 300 K. (A) based on host protons. Protons 3H-4H and 4H-5H were overlapping in the ¹H NMR spectra. (B) based on α- and β- guest's protons. [FcN₃]₀+ [TRIMEA]₀ = 0.1 M. Both charts stem from the same measurement.

The maximum at a mole fraction of 0.5 for the host protons indicates a 1:1 stoichiometry (Figure 6, A), whereas the maximum at 0.4 for the guest protons may indicate a contribution of a 1:2 complexation¹² (Figure 6, B). The decomposition of the FcN₃ – CyDs complexes was carried out in the solid phase (Table 1). Ferrocene (FcH), Azoferrocene (FcN=NFc), and aminoferrocene (FcNH₂) are typical

¹¹ Gil, V. M. S.; Oliveira, N. C. *J. Chem. Educ.* **1990**, *67*, 473.

¹² (a) Caron, L.; Tilloy, S.; Monflier, E.; Wieruszski, J-M.; Lippens, G.; Landy, D.; Fourmentin, S.; Surpateanu, G. *J. Inclusion Phenom.* **2000**, *38*, 361. (b) Giastas, P.; Mourtzis, N.; Yannakopoulou, K.; Mavridis, I. M. *J. Inclusion Phenom.* **2002**, *44*, 247. (c) Bratu, I.; Gavira-Vallejo, J. M.; Hernanz, A. *Biopolymers* **2005**, *77*, 361.

decomposition products.³ In all cases, a C-N bond was cleaved simultaneously with the N-N bond, giving rise to FcH formation to a lesser (Experiments 2, 3 and 4(hv) in Table 1) or to a larger (Experiments 1, 4(Δ) in Table 1) extent. Only in the FcN₃@(α -CyD)₂ decomposition (Exp. 2 in Table 1), no FcN=NFc was formed, instead, aminoferrocene and novel compound **2** were isolated¹³ (Figure 7).

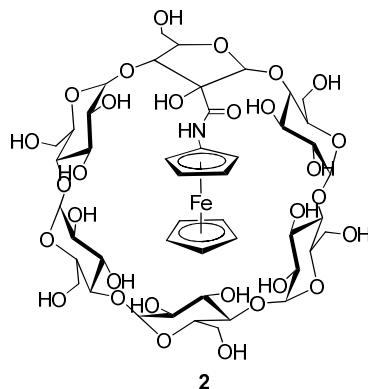


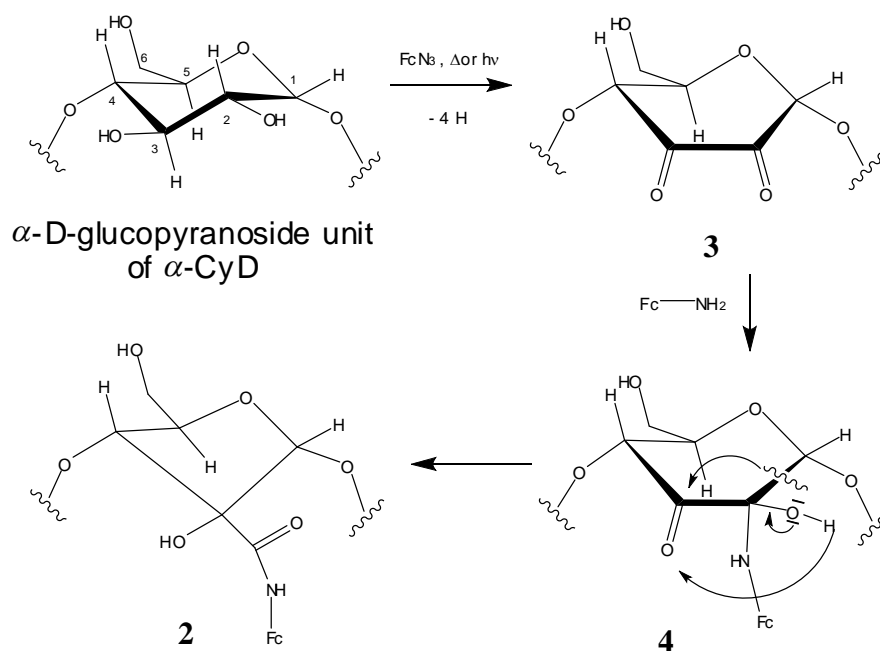
Figure 7. Structure of the product formed upon decomposition of the solid FcN₃@(α -CyD)₂ complex.

Instead of the expected nitrene insertion into the C-H bonds of α -CyD, an unusual glucopyranose – furanose conversion took place. The molecular weight of product **2** is by two units smaller than the molecular weight of a product, which would be formed by insertion of ferrocenyl nitrene into α -CyD. This means that two hydrogen atoms were eliminated in the reaction of intervening ferrocenyl nitrene with α -CyD providing the final product **2**.

A similar rearrangement of methyl β -D-glucopyranoside to 2-carboxy- β -D-pentofuranoside was reported by Theander et al.¹⁴ Methyl β -D-glucopyranoside underwent an oxidation with oxygen under alkaline conditions and afforded an intermediate dione which rearranged to the final 2-carboxy- β -D-pentofuranoside. Based on this benzilic acid type rearrangement, a tentative mechanism explaining the formation of **2** is proposed in Scheme 1:

¹³ Structure **2** was proven by 2D NMR, IR, and ESI-HRMS techniques.

¹⁴ Ericsson, B.; Lindgren, B. O.; Theander, O. *Carbohydr. Res.* **1985**, *141*, 307.



Scheme 1. A possible mechanism explaining the formation of **2**, Fc = ferrocenyl.

The oxidation of the α -D-glucopyranose unit to dione **3** requires a removal of four hydrogen atoms. Due to the 1:2 stoichiometry and geometry of the $\text{FcN}_3@(\alpha\text{-CyD})_2$ complex, in a first stage the ensuing ferrocenyl nitrene abstracts two of the four hydrogen atoms in its neighborhood, i.e., at C3-H and O2-H of the α -D-glucopyranose unit. FcNH_2 may be formed in this oxidative step. At this time, the fate of the residual two hydrogen atoms is uncertain. They are either liberated in molecular form or may be bound to a nitrogen molecule released from the decomposition of the azide group. Diazene might have been formed in this step. The intervening dione **3** then adds FcNH_2 and gives **4**, which rearranges to the final product **2**.

Interestingly, the ensuing ferrocenyl nitrene seems to abstract hydrogens only from the hydroxyl groups of native cyclodextrins, since no formation of FcNH_2 was detected in the reaction with permethylated derivatives (Exp. 5 and 6 in Table 1).

Finally, the ground state of ferrocenyl nitrene was investigated with electron paramagnetic resonance (EPR) spectroscopy. Since aryl nitrenes possess a triplet ground state,¹⁵ it would be interesting to find out whether ferrocenyl nitrene also has a triplet ground state and how the iron atom influences the multiplicity of the nitrene. Thus, a 1 to 3 mole percent solutions of ferrocenyl azide in various solvents were photolyzed in a quartz EPR tube at 77 K and subsequently EPR spectra were recorded between 10 – 50 K. Four types of solvents were used: toluene, a mixture of ether - pentane - ethanol (5:5:2), ether - pentane (1:1) and fluorolube. The absence of any signals below 15 kG indicated that a triplet state of ferrocenyl nitrene was not present. These results point to the likelihood that the ferrocenyl nitrene is being formed, but that it exists in an EPR silent, singlet ground state rather than a triplet ground state. This might be attributed to the iron atom, because ferrocene can behave as a triplet sensitizer as well as a quencher.¹⁶

¹⁵ (a) Smolinsky, G.; Wasserman, E.; Yager, W. A. *J. Am. Chem. Soc.* **1962**, *84*, 3220. (b) Brinen, J. S.; Singh, B. *J. Am. Chem. Soc.* **1971**, *93*, 6623. (c) Platz, M. S. Nitrenes. In *Reactive Intermediate Chemistry*; Moss, R. A.; Platz, M. S.; Jones, M. Jr., Eds.; Wiley: New York, **2004**; Chapter 11, p. 501.

¹⁶ Richards, J. H. *J. Paint Technol.* **1968**, *39*, 569.

4.4 Conclusion

In summary, we have found that ferrocene in a solid state takes on an equatorial alignment inside the cavity of TRIMEB, in contrast to an axial orientation in native β -CyD. Ferrocenyl azide adopts a bimodal disposition within the cavity of TRIMEB. The solution structures of FcH and FcN₃-TRIMEB complexes seem to be consistent with those in the solid state, as inferred from ICD and 2D ROESY measurements. As inferred from ¹H NMR measurements, the AA'B₅CC' spin system pattern of FcN₃ changes into an ABC₅DD' pattern upon addition of TRIMEB, due to the hindering of the rotation of the azide group. Finally, a new unusual reaction pathway of the ferrocenyl nitrene generated within the cavity of α -CyD was uncovered. Instead of a hoped-for nitrene C-H bond insertion into H3 or H5, a novel pyranose-furanose conversion took place.

4.5 Experimental Section

(Supporting Information)

The NMR spectra were recorded with a 250, 400 or 600 MHz Bruker Avance Spectrometer. The assignments of the shifted protons in the 2D ROESY spectra were secured by the consecutive recording of COSY, HMQC and HMBC spectra.

IR – Spectra were measured on a Bruker Vertex 70 in KBr discs.

UV-VIS and CD spectra were recorded with a Perkin-Elmer Lambda 7 spectrometer and a CD6 Circular Dichrograph (I.S.A. Jobin-Yvon), respectively, in thermostated quartz cuvettes (0.1 - 1 cm path length).

Melting points were measured on a Leica Galen III Kofler type melting point microscope and are uncorrected.

Analytical RP-HPLC analysis was performed using a HP1090 instrument equipped with RI-detector HP1047 and interface 35900E (Agilent). The instrument was equipped with an auto-injector and was run with the HP ChemStation (Rev. A.08.03; 2000) software.

ESI-MS Spectra were recorded in positive mode on a Bruker Daltonics HTC Plus, ESI-ion trap.

ESI-HRMS Spectra were recorded in positive mode on a Thermo Scientific LTQ Orbitrap XL™ Hybrid Mass Spectrometer.

Thin layer chromatography was done on Merck (a) Silica gel 60 F₂₅₄ plates (Art. 1.05554) (b) Aluminium oxide 60 F₂₅₄ neutral plates (Art. 1.05550) (c) HPTLC RP-18 without fluorescent indicator (Art. 15037).

TRIMEA,¹⁷ TRIMEB,¹⁸ FcN₃,¹⁹ FcNH₂,¹⁹ and FcN=NFc²⁰ were prepared according to the literature. Water was highly purified using a Milli-Q system (Millipore®). Other chemicals were obtained from commercial sources.

Preparation of FcN₃@(native)CyDs complexes

The long-necked beaker with a magnetical stirring bar was filled with saturated aqueous solutions of CyDs and FcN₃ in Et₂O was added. The mixture was stirred magnetically and argon was bubbled through via a long needle for approximately 7 h at RT. A yellow-orange suspension was formed upon a few minutes. Time by time the mixture was sonicated by dipping the beaker into an ultrasonic cleaner, in order to break up the clumps. The mixture was filtered via syner funnel of porosity # 4 and the filter cake washed with a very small amount of water to remove the coprecipitated CyD. The filter with the cake was dried overnight in desiccator over CaCl₂ at RT at around 10 mm Hg. Next day, the solid cake was turned to a powder and was dried at < 0.5 mm Hg. The composition of the product complexes was at first investigated by a 250 MHz ¹H NMR spectrum in *d*₆-DMSO. In this solvent, the complexes were totally

¹⁷ Schomburg, G.; Deege, A.; Hinrichs, H.; Hübinger, E.; Husmann, H. *J. High Resolut. Chromatogr.* **1992**, *15*, 579.

¹⁸ Schurig, V.; Jung, M.; Schmalzing, D.; Schleimer, M.; Duvekot, J.; Buyten, J. C.; Peene, J. A.; Mussche, P. *J. High Resolut. Chromatogr.* **1990**, *13*, 470.

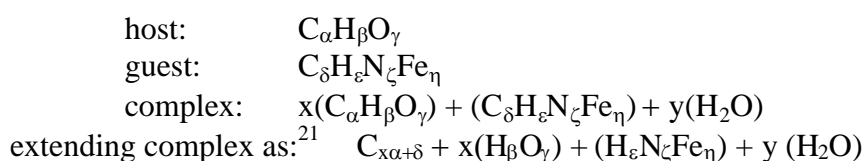
¹⁹ Nesmeyanov, A. N.; Drozd, V. N.; Sazonova, V. A. *Dokl. Akad. Nauk SSSR* **1963**, *150*, 321.

²⁰ Nesmeyanov, A. N.; Sazonova, V. A.; Romanenko, V. I. *Dokl. Akad. Nauk SSSR* **1964**, *157*, 922.

dissociated, i.e., the ^1H NMR spectra pattern can be sought as a sum of the neat componets (^{13}C NMR as well). Therefore, the NMR spectra description are not given explicitly. The same holds true for IR Spectra recorded with KBr discs. From ^1H NMR, no ether was present in the complexes. The product complexes did not melt sharply, but gradually over a range of 50 – 300 °C, which indicates participation of complex processes.

The exact yield and stoichiometry determinations were inferred from elemental analysis of the complexes and the calculations were done as follows:

Designation of molecular formulas of:



$$\text{then we can write: } \frac{w(\text{C}_{found})}{w(\text{N}_{found})} = \frac{\frac{(x\alpha + \delta) \times 12.011}{FW(\text{Complex})}}{\frac{\zeta \times 14.007}{FW(\text{Complex})}} \quad (1),$$

where w designates the atomic composition obtained from elemental analysis.

$$\text{Rearranging (1) we obtain: } x\alpha + \delta = \frac{\frac{w(\text{C}_{found})}{w(\text{N}_{found})} \times \zeta \times 14.007}{12.011}$$

and finally we get the stoichiometry of the host x as:

$$x = \frac{\left(\frac{\frac{w(\text{C}_{found})}{w(\text{N}_{found})} \times \zeta \times 14.007}{12.011} \right) - \delta}{\alpha} \quad (2)$$

Now, knowing the host to guest ratio, we can approach to calculate the number of water molecules y . Two possible ways (a) and (b) of calculations were tested:

- a) The amount of water y was iteratively varied, until the square difference between the calculated elemental composition of nitrogen and experimentally found value converged to a minimum.

²¹ In terms of stoichiometry the guests were set to 1.

- b)** The amount of water y was iteratively varied, until the sum of the square differences between the calculated C/H/N and experimentally found C/H/N analysis converged to a minimum.

Finally, the third method **(c)** was tested. The equations (1) and (3) were not employed in the calculation, since the amounts of host x and water y were directly iteratively varied (two parameters varied), until the sum of the square differences between the calculated C/H/N and experimentally found C/H/N analysis gave a minimum.

There were no remarkable differences, between the host and water content obtained from all methods. Arbitrarily, Table S 1 lists the results from the first method **(a)**.

The calculations were done with Microsoft[®] Excel. For the iteration, the Solver add-in was used. The spreadsheet for these yield and stoichiometry calculations is attached to the attached CD as “Yield_Stoichiometry.xls” file.

Table S 1 summarizes the reaction conditions, yields, and stoichiometries.

Experiment Designation	CyD	n(FcN ₃) [mmol] in Et ₂ O [mL]	Eq. of CyD	Stoichiometry from ¹ H NMR FcN ₃ /CyD	C/H/N Analysis [%]	Stoichiometry from C/H/N Analysis FcN ₃ /CyD/H ₂ O	Yield [%] ^a
PW056	α	0.5 in 7	7.4	1 / ~2.6	43.30/6.08/1.36	1/2.8/	91
PW098	α	0.55 in 5	6	^b	43.43/5.96/1.49	1/2.6/	88
PW163	α	0.88 in 5	6.3	1 / ~2	43.03/5.98/1.77	1/2.1/	81
PW037	β	0.48 in 4	5	1 / ~1.2	42.81/5.59/2.43	1/1.23/5.9	76
PW043	β	0.953 in 10	5	1 / ~1.2	43.28/5.93/2.28	1/1.34/5.1	69
PW122	γ	0.661 in 2.5 ^c	4	1 / ~1.9/ ~0.4) ^d	43.27/5.87/2.74	- ^e	80

^aThe yield is based on C/H/N Analysis and was calculated as: Y = 100% x n(guest included in the complex) / n(starting amount of the guest), where n means molar amount.

^bBroadening of the lines, not resolvable. Indication of decomposition, possible paramagnetic species present.

^cTHF used instead of Et₂O.

^d0.4 eq. of THF present in the sample. This explains the higher amount of γ -CyD component in the sample. Assuming 1:1 stoichiometry of THF@ γ -CyD complex, 1:1 stoichiometry of FcN₃@ γ -CyD complex may be then deduced.

^eNot eligible to calculate because of the presence of THF.

Table S1. Preparation of FcN₃@(native)CyDs complexes.

Photolysis of FcN₃@(all)CyD complexes

Photolyses were carried out in flasks of Pyrex glassware equipped with a septum. The solid material was accurately weighed in as a fine powder (100 - 300 mg) and evenly distributed on the inner surface of the flask. Then the flask filled with the samples was deaerated and Ar saturated several times on a vacuum line. The flask was rotated in a cooling bath (thermostatted water) situated below a medium pressure mercury lamp (Heraeus TQ718-Z4, 700 W, doped with FeI₂). Photolysis was done for 1-2 days depending on the sample amount. Then a few milligrams of sample were dissolved in *d*₆-DMSO and a 250 MHz ¹H NMR spectrum was taken to demonstrate the complete loss of the FcN₃ guest.

Thermolysis of FcN₃@(all)CyD complexes

Thermolysis was carried out analogously as the photolysis. 100 – 300 mg of solid material (case of β- and γ-CyD complexes) or 100 mg – 20 grams (case of α-CyD complex) were thermolyzed by immersing the flask into a thermostatted (85 °C) oil bath under light exclusion for 1 d, when the ¹H NMR analysis indicated complete FcN₃ decomposition.

Work-up of the reaction upon the decompositions of FcN₃@(native)CyDs complexes

Separation of low molecular weight ferrocene derivatives from cyclodextrins was performed by dissolving the solid in water (100 mL) and dichloromethane (100 mL) followed by continuous extraction with the appropriate apparatus (100 mL for the extraction of liquids of higher density). After 24 h the dichloromethane was replaced by a new portion, thus giving a first fraction, and after 48 h a second dichloromethane extract was collected. The solvent from combined extracts was removed with rotatory evaporator and the solid residue separated by preparative layer chromatography (0.75 mm neutral Alumina, 20 x 20 cm plate). The yellow ferrocene band and the violet azoferrocene band were scraped off together. Upon extracting from the sorbent with a DCM/MeOH mixture the solvent was evaporated and thoroughly dried at 0.01 mm Hg. The sample was weighted by precise analytical balances and analyzed by a 250 MHz ¹H NMR spectrum in CDCl₃. The yellow-brown aminoferrocene band was scraped off and analysed in the same manner. The yields are given in the main Chapter and in Table S 2.

Experiment	Complex		Yield of isolated products (%)			
			FcH	FcN=NFc	FcNH ₂	FcN-CyD
1	G (solid)	Δ	9	47	-	-
2	G@(α-CyD) ₂	Δ	<0.5	-	60	9
		hν		-	53	3 ^a
3	G@β-CyD	Δ	<0.5	5	22	No ^b
		hν		8	27	
4	G@γ-CyD	Δ	<0.5	4	4	Yes ^c
		hν		1	2	
5	G@TRIMEA	Δ	4	12	-	Yes ^d
6	G@TRIMEB	Δ	7	2	-	

G=FcN₃. ^aHPLC yield. ^bNo modification of the β-CyD observed. ^cComplicated mixture of products. ^dInsertion detected by ESI-MS.

Table S 2. Product distribution upon solid state decompositions of ferrocenyl azide–cyclodextrin complexes.

The water from the water phase upon continual extraction was evaporated and analyzed by RP-HPLC (Table S 3). The CyD fraction, stemming from the decomposition of the FcN₃@β-CyD complex, was a white solid and was found to be intact β-CyD as shown by RP-HPLC. Upon the decomposition of the FcN₃@γ-CyD complex, a yellowish colored solid was isolated, which indicated a possible modification of γ-CyD by ferrocenyl nitrene. A complex mixture of products was found by HPLC analysis (Figure S 1 and Figure S 2). Due to the complexity of the mixture, a separation into the components was not carried out.

CyD	Column	Eluent H ₂ O / CH ₃ OH [% v/v]	Retention time t _R [min] ^a
α	(A)	90 / 10	9.2
β			14.7
Modified CyD (2)			6.9
α	(B)	90 / 10	15.9
Modified CyD (2)			9.9
α	(C)	95 / 5	7.2
α		90 / 10	4.1
β		95 / 5	5.4
Modified CyD (2)		95 / 5	8.4
γ		90 / 10	5.7
		90 / 10	4.2

^aRetention times of RI detector

(A) Nucleosil 300-5, RP-C8, 290 x 4 mm, 0.7 mL/min, t = 40 °C.

(B) Nucleosil 100-5, RP-C18, 250 x 4 mm, 0.5 mL/min, t = 40 °C.

(C) Shandon Hypersil, 5 micron, 150 x 3 mm, 0.5 mL/min, t = 40 °C.

Table S 3. Representative data for RP-HPLC analysis.

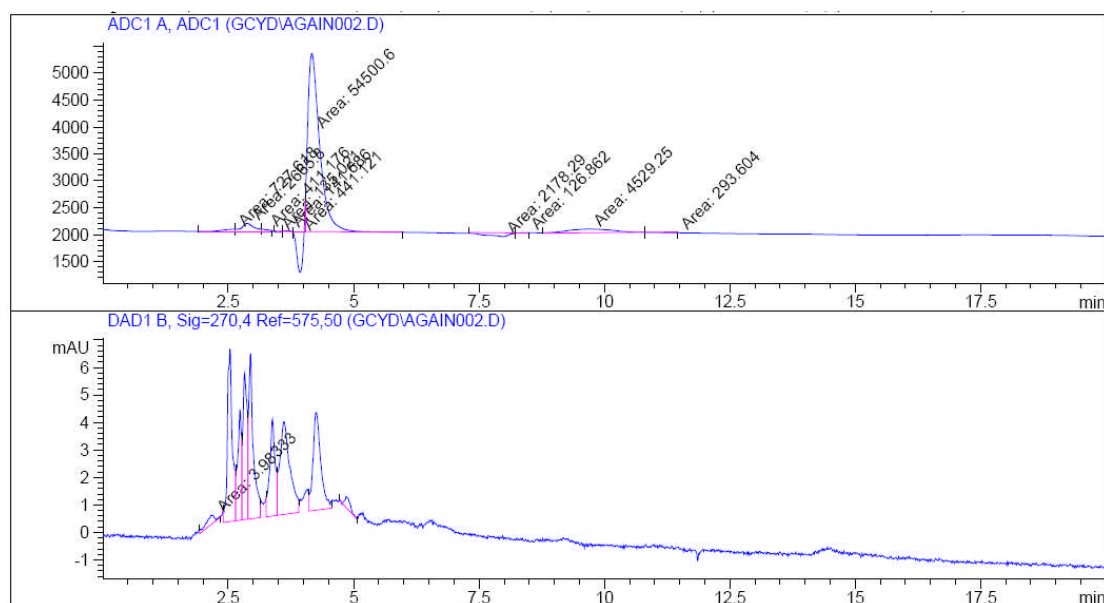


Figure S 1. RP-HPLC Chromatogram of the CyD fraction upon photolysis of the FcN₃@ γ -CyD complex. Upper window for RI Detection, bottom for 270 nm UV detection. Column C in Table S 3 was used.

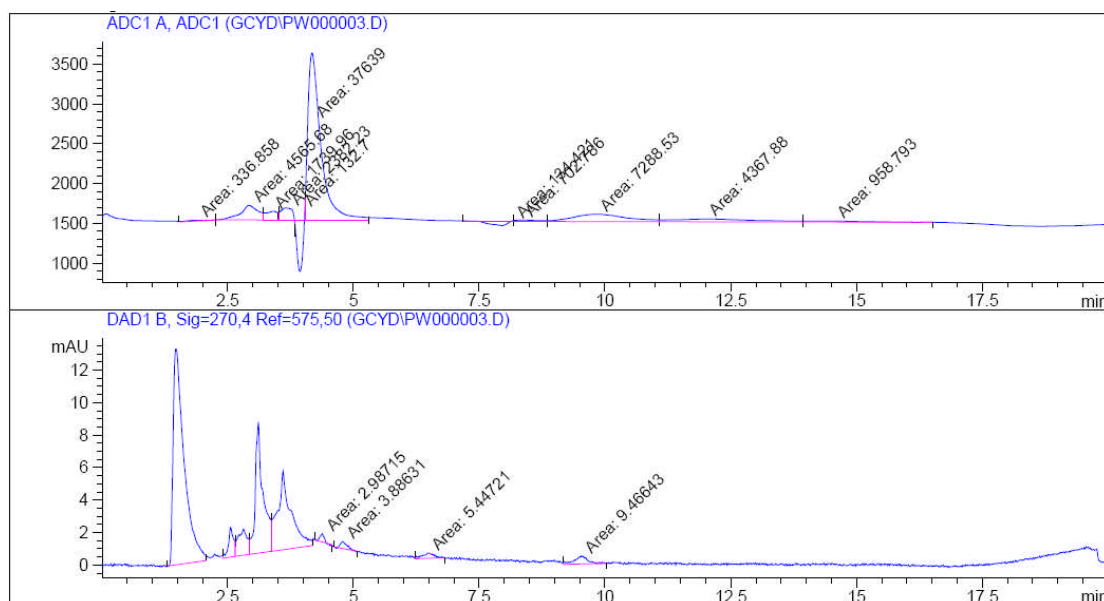


Figure S 2. RP-HPLC Chromatogram of the CyD fraction upon thermolysis of the $\text{FcN}_3@ \gamma\text{-CyD}$ complex. Upper window for RI Detection, bottom for 270 nm UV detection. Column C in Table S 3 was used.

In the case of the $\text{FcN}_3@(\alpha\text{-CyD})_2$ decomposition, a yellowish solid was isolated as well. Only one new peak was found by HPLC (“Modified CyD (2)” in Table S 3 and Figure S 3).

The product was isolated by a Merck LiChroprep[®] RP-C18, 25 - 40 μm , (4 x 45 cm column) medium pressure chromatography (eluent $\text{H}_2\text{O}/\text{MeOH} = 95/5$ (v/v)).

Characterization of the novel product 2

The structure in Figure S 3 was inferred from 2D NMR analysis (COSY, HSQC, HMBC, ROESY, TOCSY in Figure S 4 - Figure S 17).

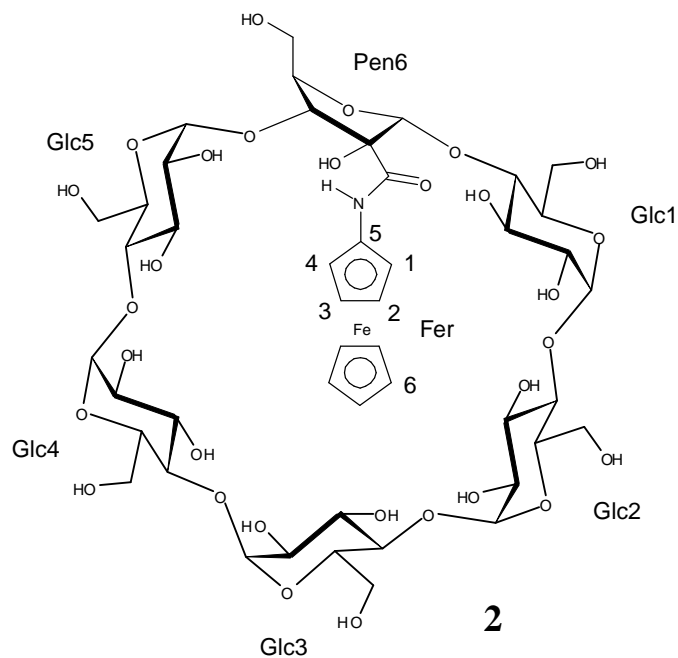


Figure S 3. Structure of the product formed upon decomposition of solid $\text{FcN}_3@(\alpha\text{-CyD})_2$ complex. m.p. 279 - 283 °C (with decomposition). $[\alpha]_D^{20} = +93.8$, $[\alpha]_{578}^{20} = +95.7$, $[\alpha]_{546}^{20} = +99.5$ (c 0.67, H_2O). TLC (RP-C18, $R_f = 0.84$ for **2** in $\text{MeOH}/\text{H}_2\text{O} = 2/1$; 0.56 for $\alpha\text{-CyD}$). TLC (SiO_2 , $R_f = 0.5$ for **2**, 0.25 for $\alpha\text{-CyD}$, 0.23 for $\beta\text{-CyD}$, 0.21 for $\gamma\text{-CyD}$). Solvent 2-propanol : ethylacetate : water = 1:1:1).

Compound **2** characterization based on 2D NMR techniques is summarized in Table S 4 and Table S 5.

600 MHz, DMSO- <i>d</i> ₆ , 20 mg/0.7 mL, 300 K								
		1	2	3	4	5	6a	6b
Glc1	H	4.855	3.432	3.852	3.276	3.540	3.64	3.498
	C	102.35	72.43	74.33	78.12	73.15	60.35	
	OH	-	5.716	5.535	-	-	4.359	
Glc2	H	4.694	3.164	3.734	3.358	3.294	3.664	3.555
	C	99.60	72.60	73.38	82.69	72.74	61.02	
	OH	-	4.703	5.494	-	-	4.501	
Glc3	H	4.702	3.187	3.593	3.337	3.331	3.665	3.550
	C	101.62	71.91	72.34	80.86	71.97	60.67	
	OH	-	5.430	5.078	-	-	4.425	
Glc4	H	4.876	3.348	3.728	3.189	3.361	3.535	3.442
	C	102.90	72.87	73.40	81.97	72.12	60.57	
	OH	-	6.062	5.275	-	-	4.408	
Glc5	H	4.956	3.516	3.938	3.387	3.409	3.668	3.562
	C	100.13	72.54	73.69	82.57	73.06	61.45	
	OH	-	5.878	5.840	-	-	4.524	
		1	2	3	4	5a	5b	6
Pen6	H	5.404	-	4.082	4.283	3.575	3.444	-
	C	109.14	83.95	86.30	87.33	62.30	169.15	
	OH	-	6.458	-	-	5.058	-	
		1	2	3	4	5	6	
Fer	H	4.846	3.992	4.011	4.991	-	4.199 (5H)	
	C	61.15	64.28	64.46	61.84	94.34	69.61 (5C)	
	NH	-	-	-	-	9.389	-	

Table S 4. Compound **2** characterization based on 2D NMR techniques.

600 MHz, D₂O, 30 mg/0.7 mL, 300 K

		1	2	3	4	5	6a	6b
Glc1	H	5.067	3.699	4.067	3.695	3.722	3.824	3.775
	C	101.83	72.05	74.23	76.65	73.08	60.28	
Glc2	H	4.909	3.532	3.980	3.545	3.520	3.830	3.780
	C	99.22	71.56	73.20	81.68	72.41	60.20	
Glc3	H	4.911	3.460	3.592	3.465	3.626	3.80	3.79
	C	101.15	71.33	72.34	80.04	71.60	61.20	
Glc4	H	5.071	3.616	3.988	3.405	3.541	3.721	3.619
	C	102.43	72.07	73.10	80.88	71.68	60.36	
Glc5	H	5.062	3.730	4.068	3.616	3.750	3.835	3.785
	C	102.23	71.37	73.42	81.37	71.40	60.12	
		1	2	3	4	5a	5b	6
Pen6	H	5.479	-	4.158	4.443	3.82	3.81	-
	C	108.47	83.73	86.55	85.81	61.70		168.68
		1	2	3	4	5	6	
Fer	H	4.93 br	4.37 br	4.37 br	4.93 br	-	4.40 br (5H)	
	C	62.83	66.1 br	66.1 br	62.83	n.d.	69.9 br (5C)	

Table S 5. Compound **2** characterization based on 2D NMR techniques.

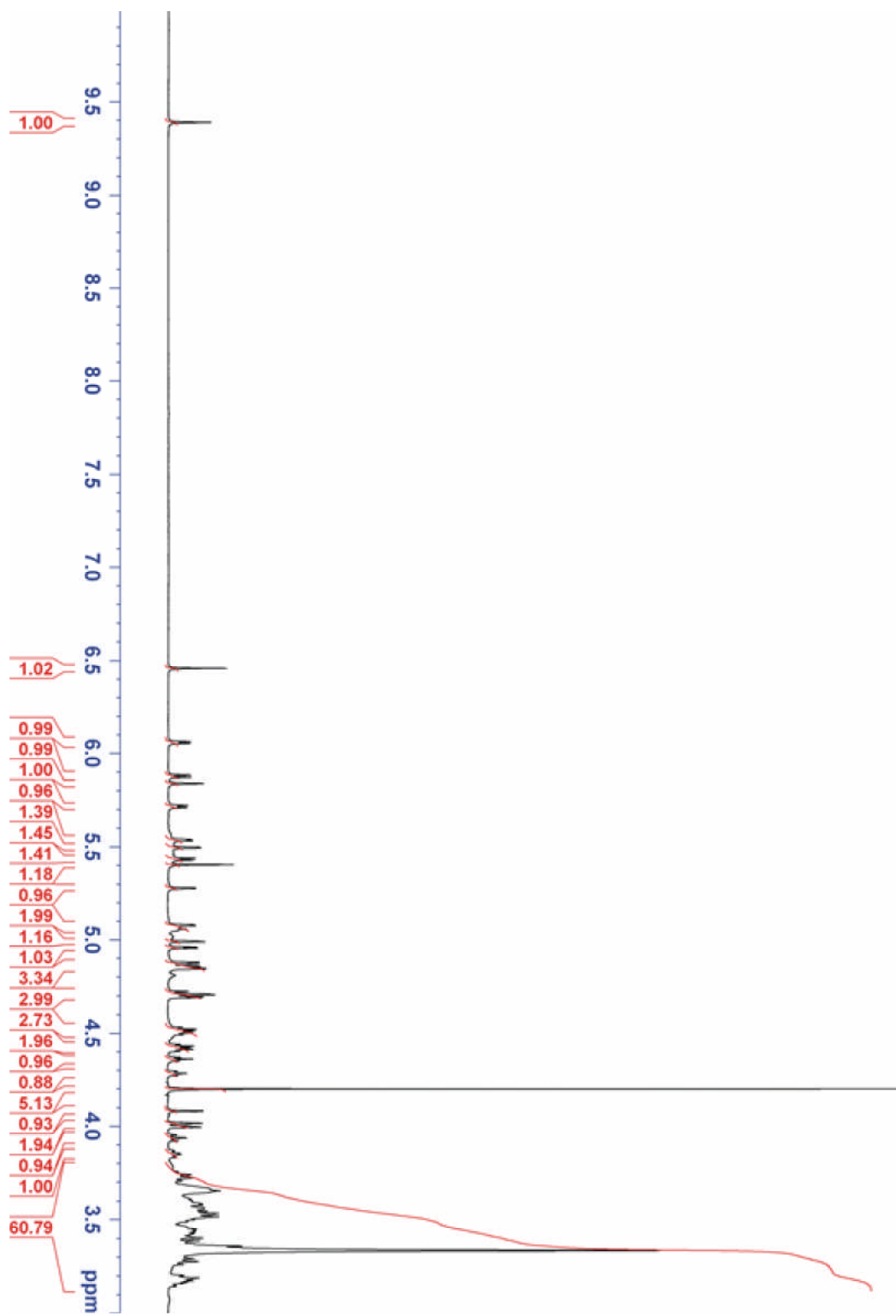


Figure S 4. 600 MHz ¹H NMR spectrum of 2 in DMSO-*d*₆.

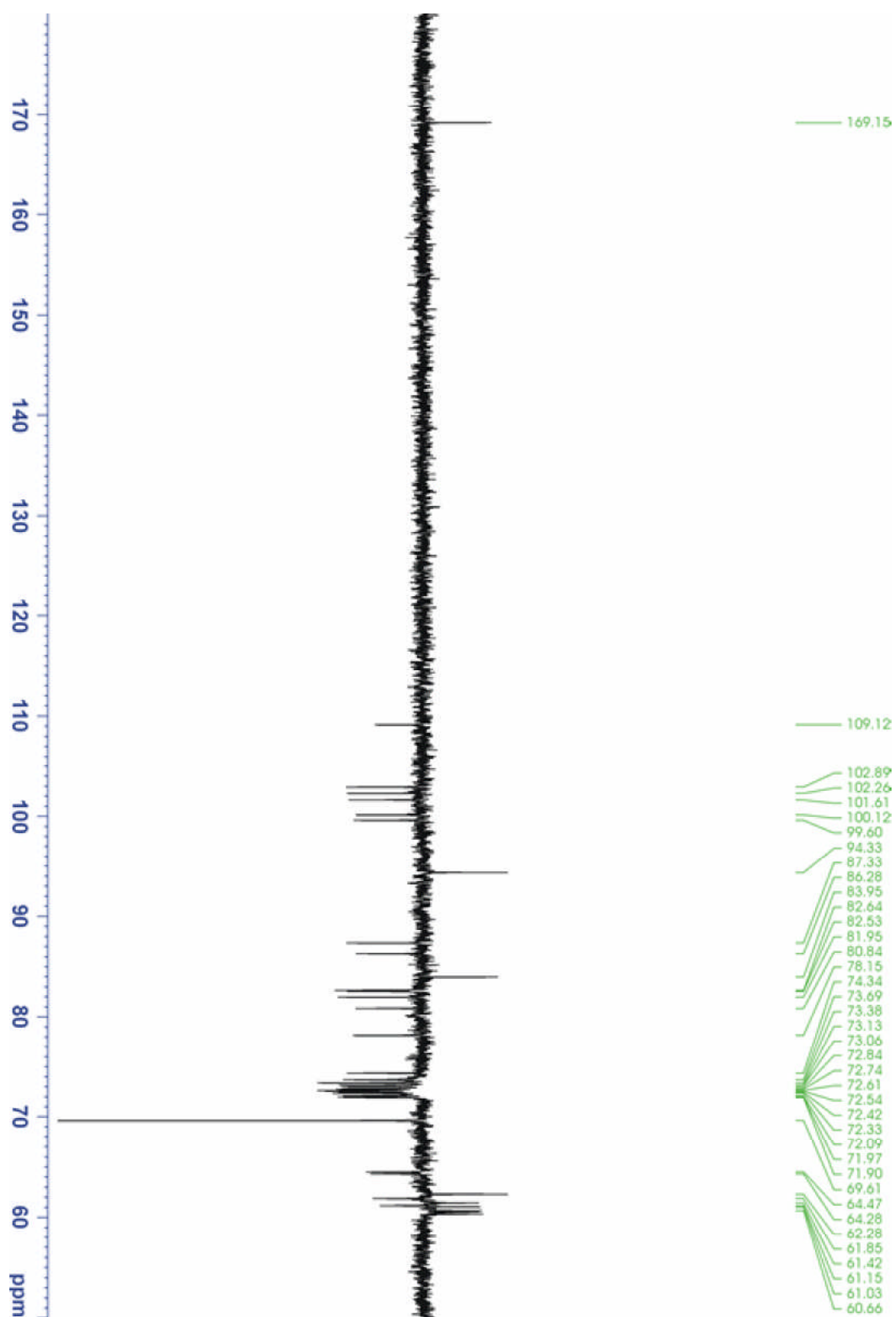


Figure S 5. 600 MHz ^{13}C NMR spectrum of **2** in $\text{DMSO-}d_6$.

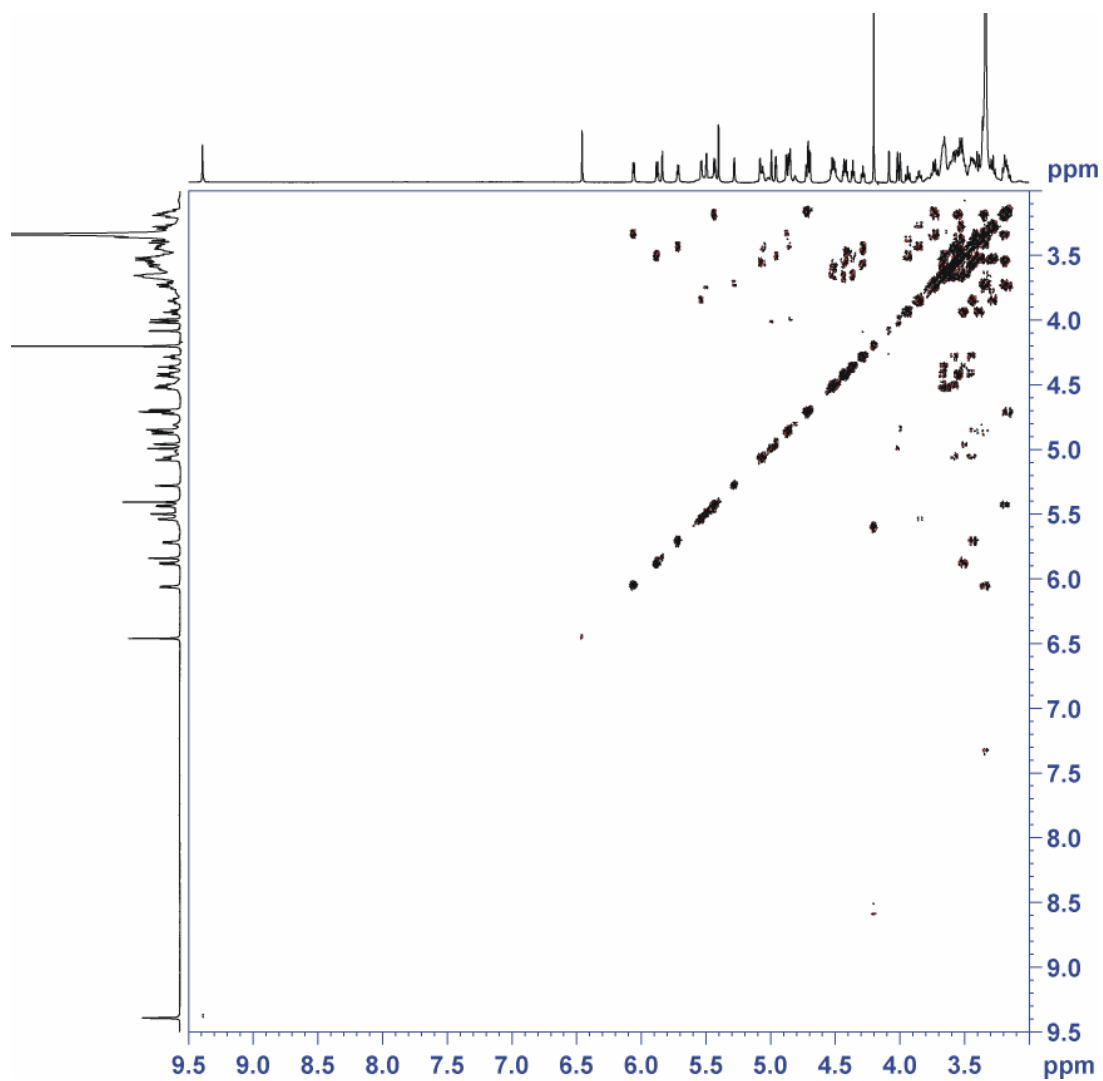


Figure S 6. 600 MHz DQF COSY spectrum of **2** in DMSO-*d*₆.

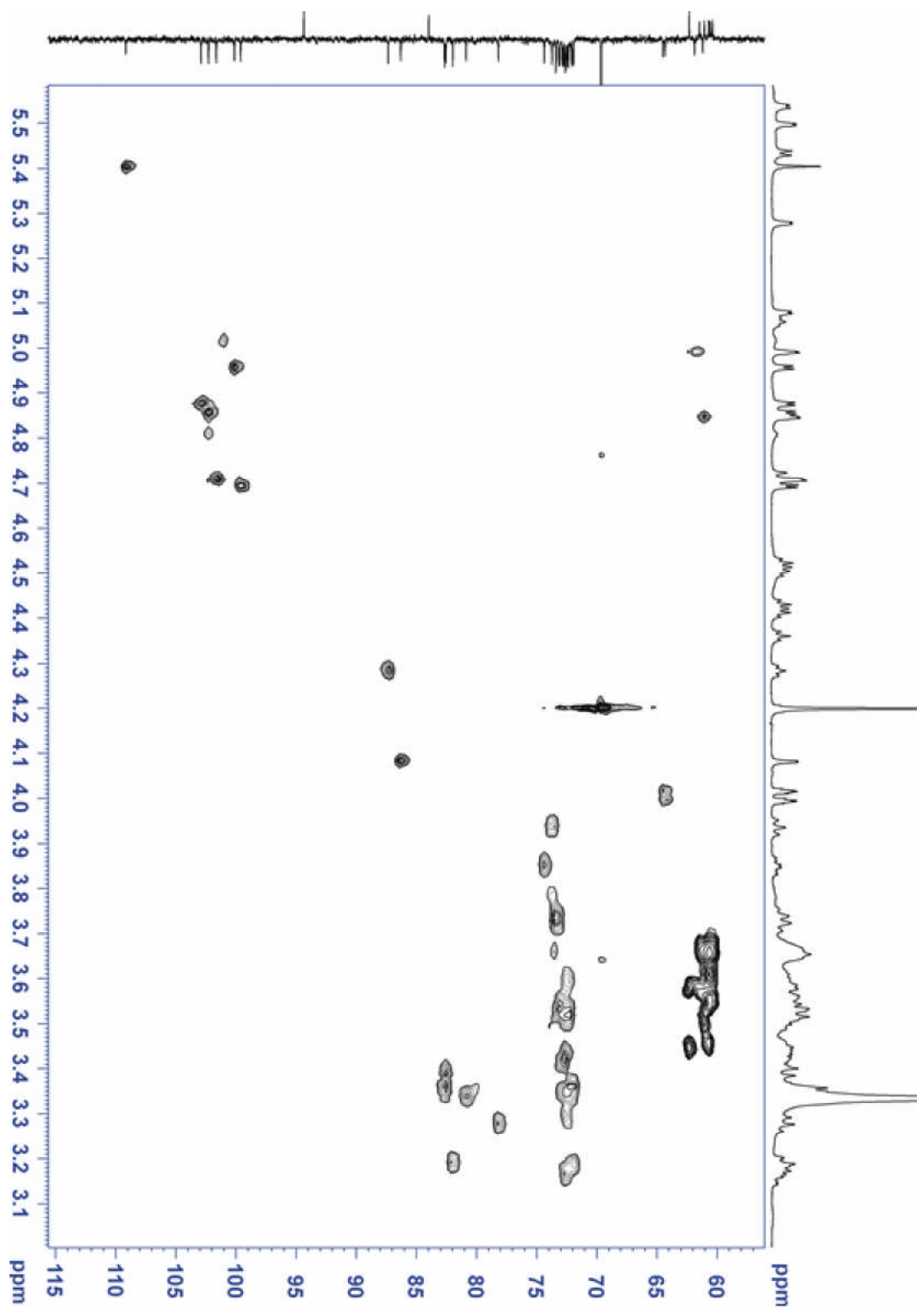


Figure S 7. 600 MHz HSQC spectrum of **2** in $\text{DMSO-}d_6$.

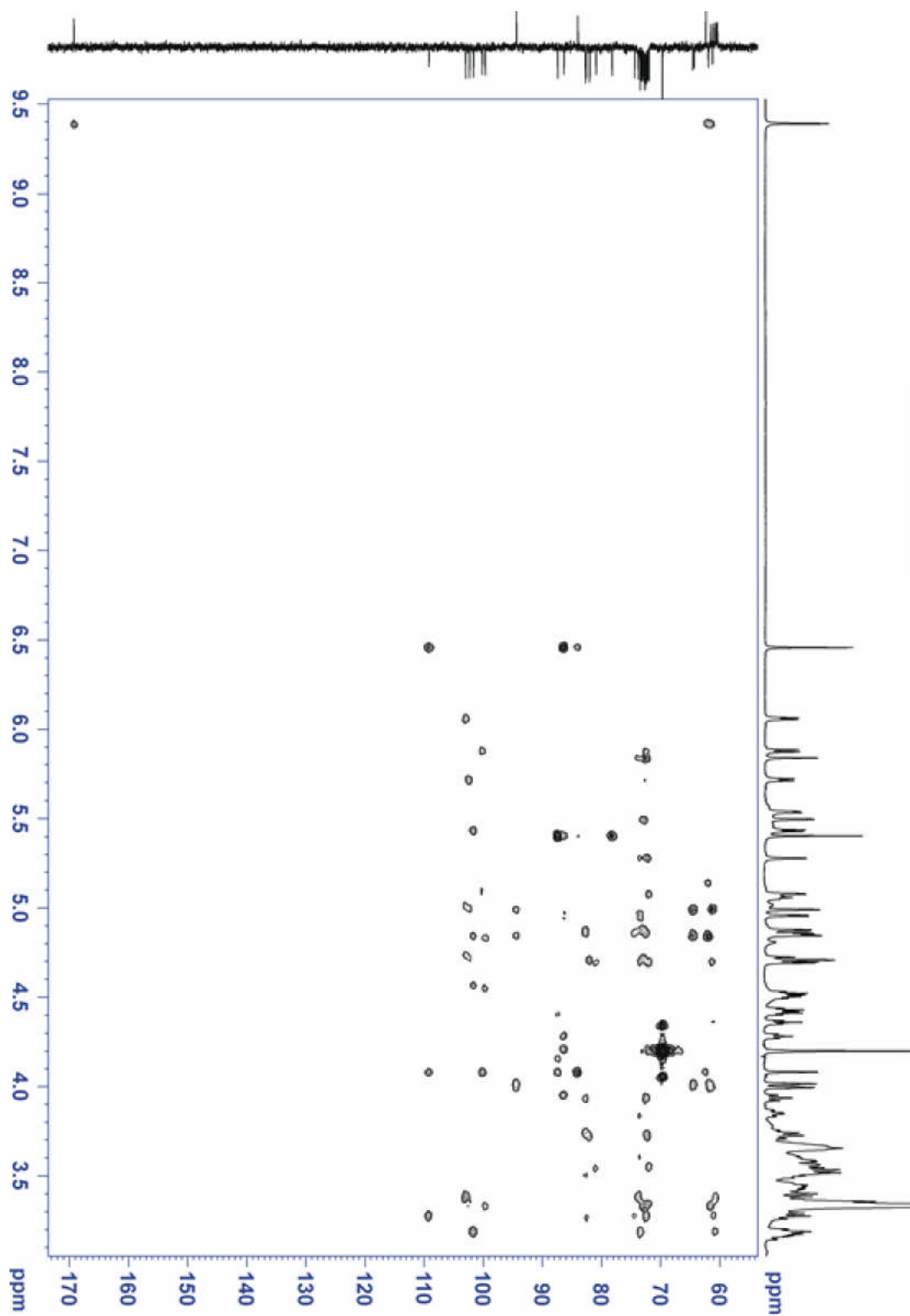


Figure S 8. 600 MHz HMBC spectrum of **2** in $\text{DMSO-}d_6$.

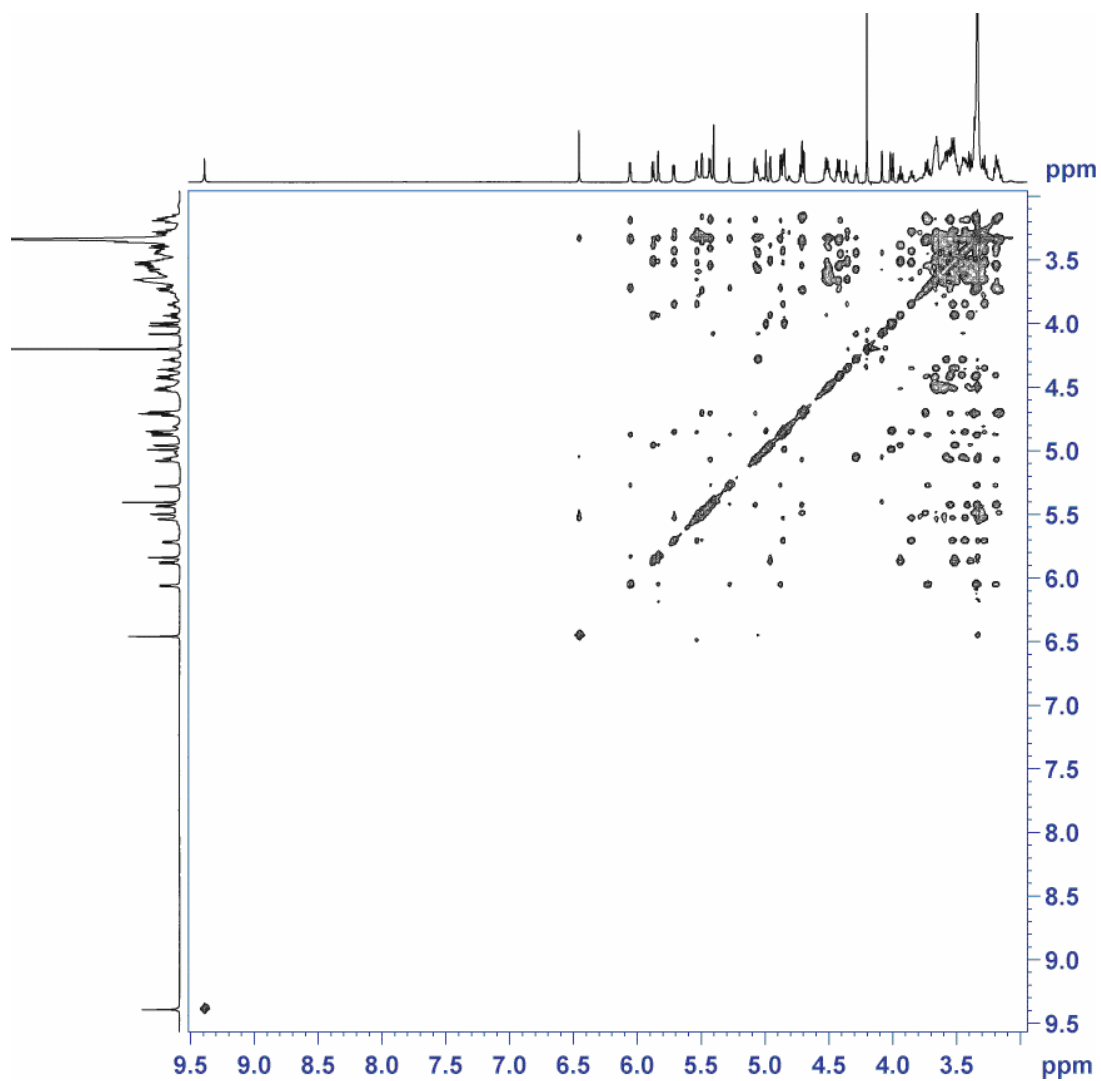


Figure S 9. 600 MHz TOCSY spectrum of **2** in DMSO- d_6 .

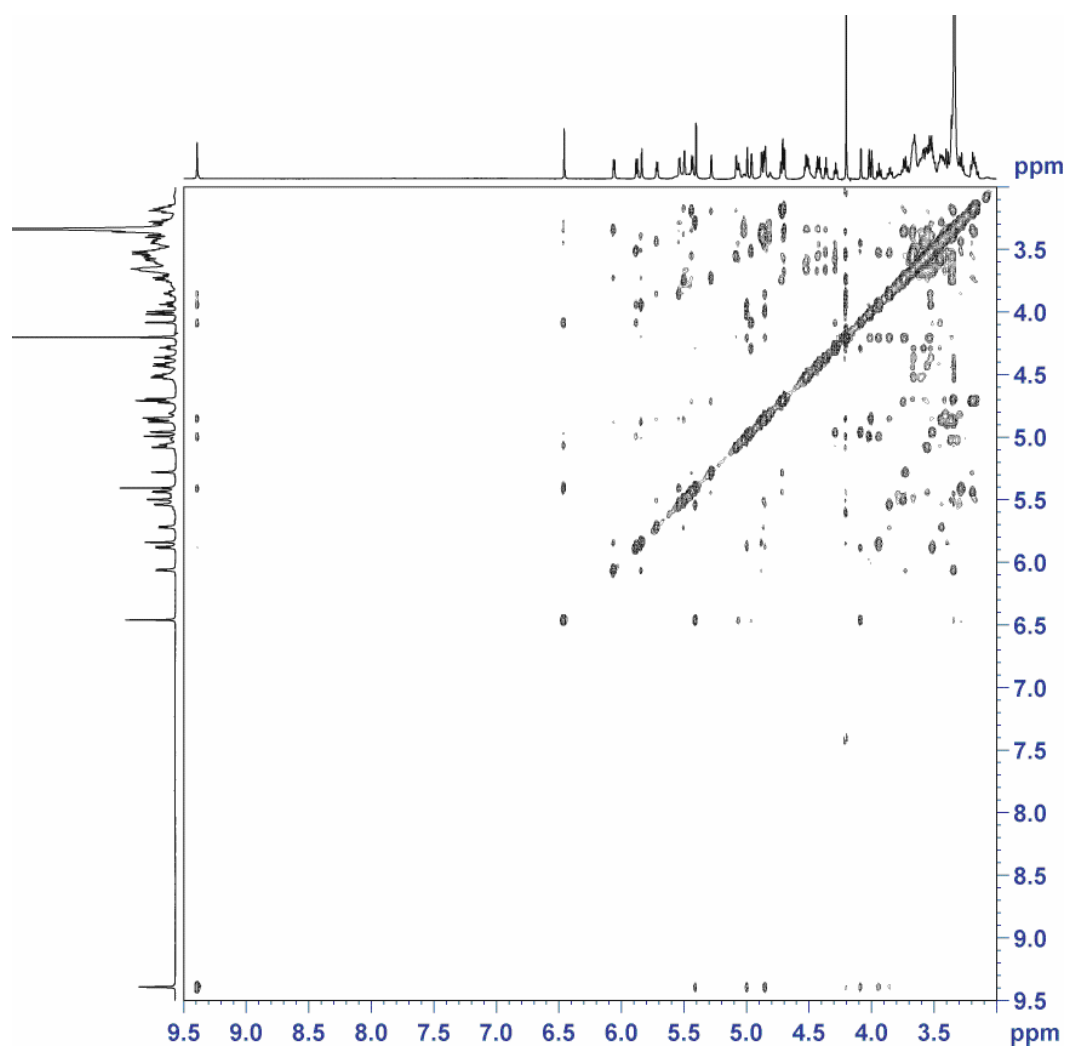


Figure S 10. 600 MHz ROESY spectrum of **2** in DMSO- d_6 .

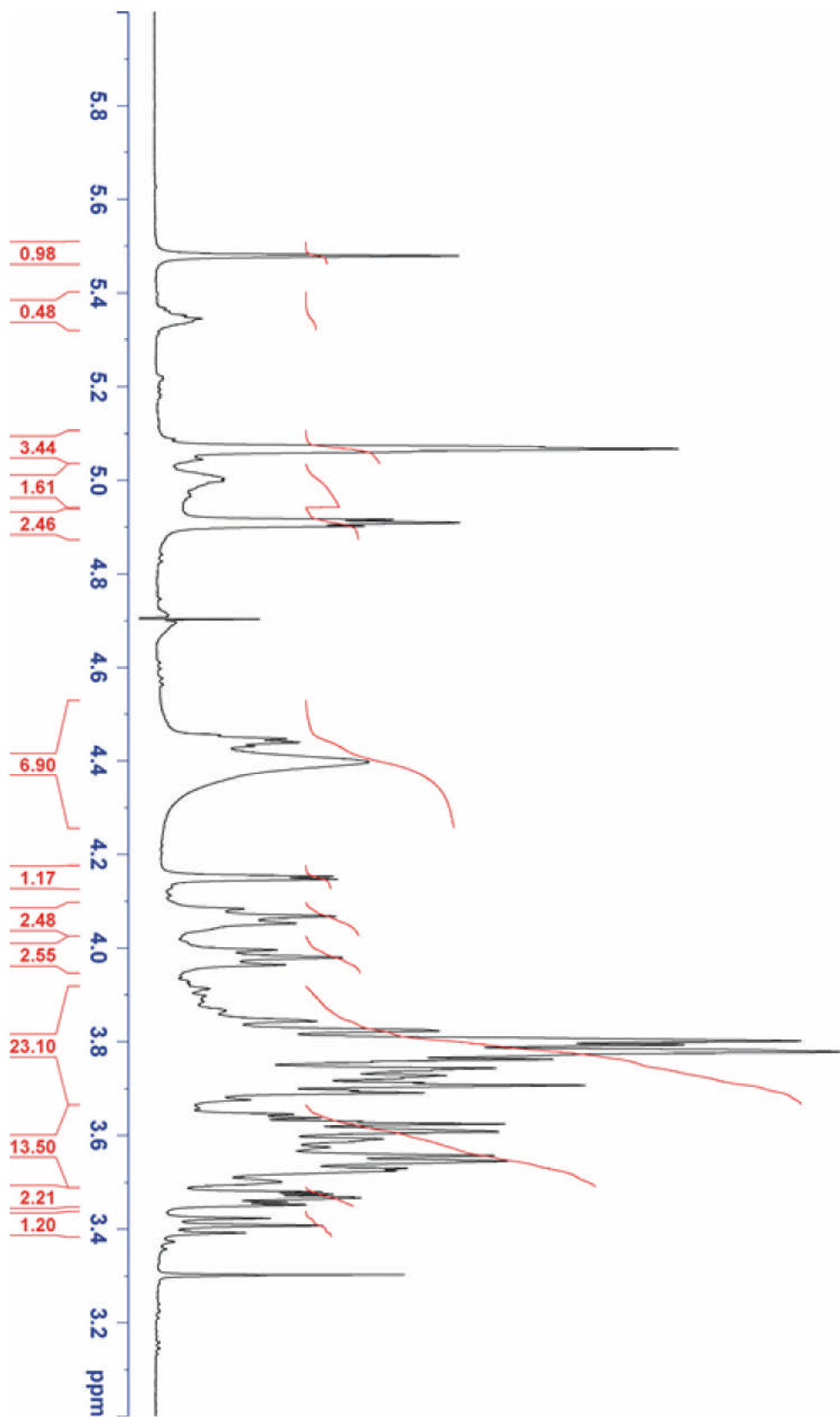


Figure S 11. 600 MHz ^1H NMR spectrum of 2 in D_2O .

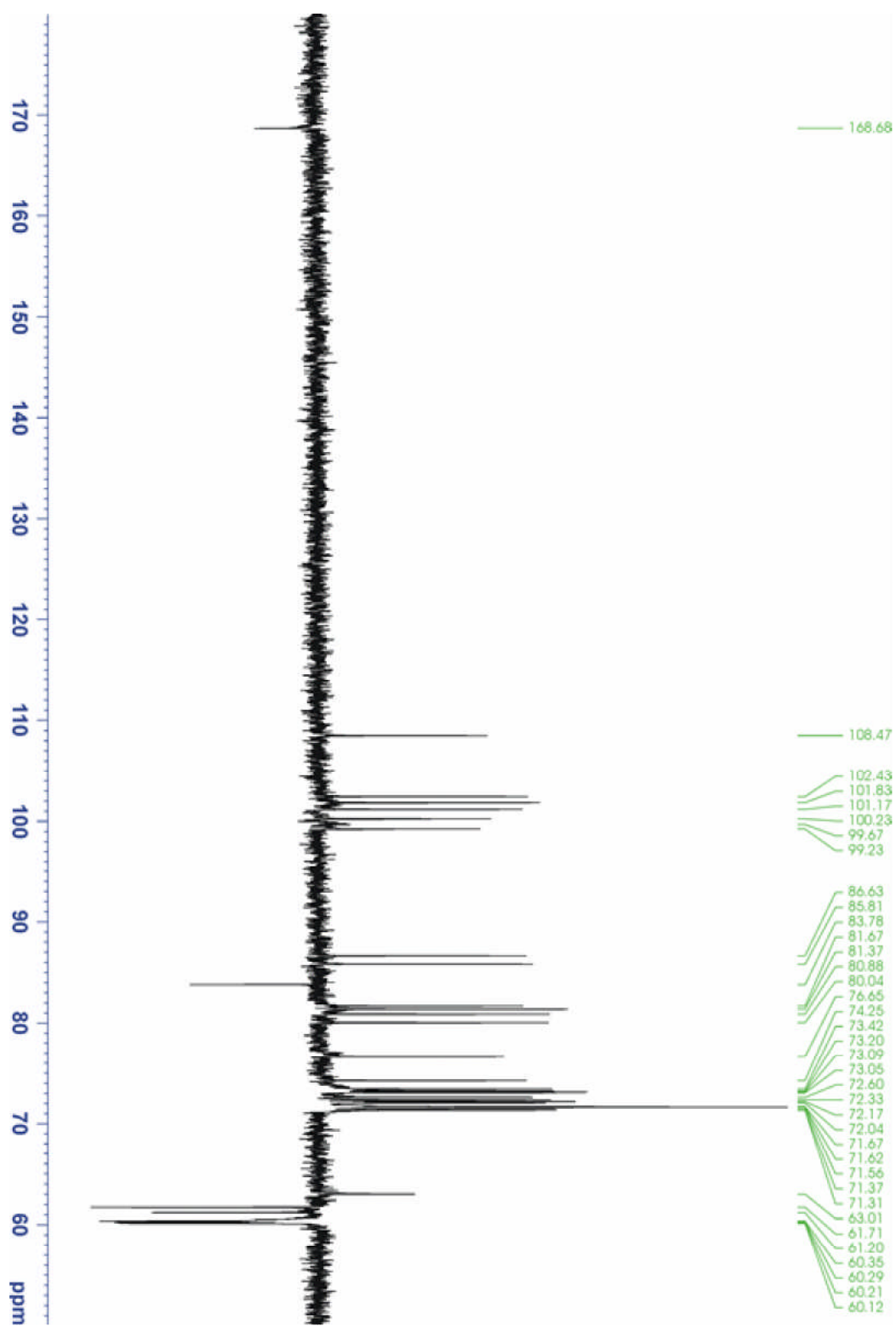


Figure S 12. 600 MHz ^{13}C NMR spectrum of **2** in D_2O .

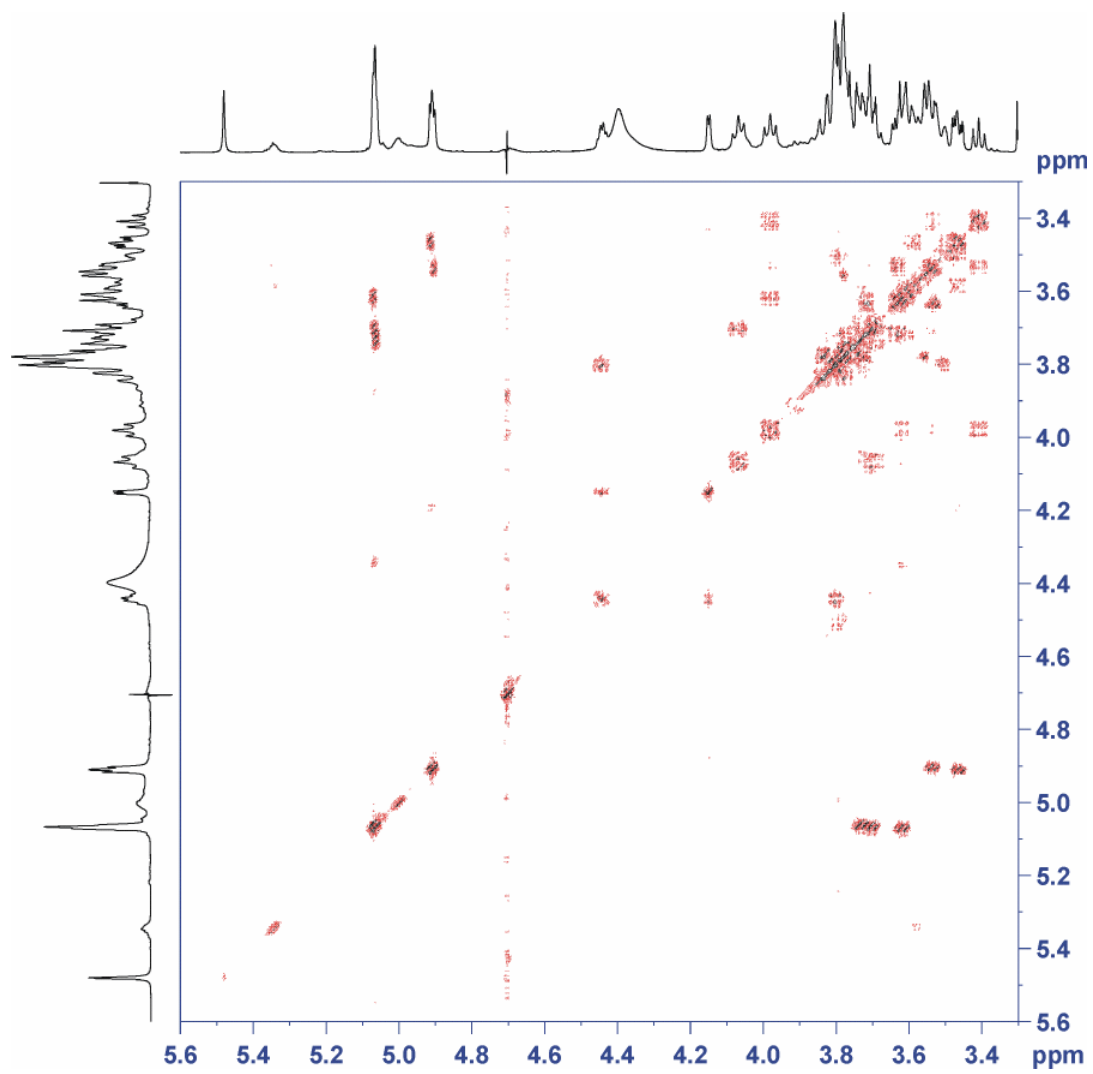


Figure S 13. 600 MHz DQF-COSY spectrum of **2** in D₂O.

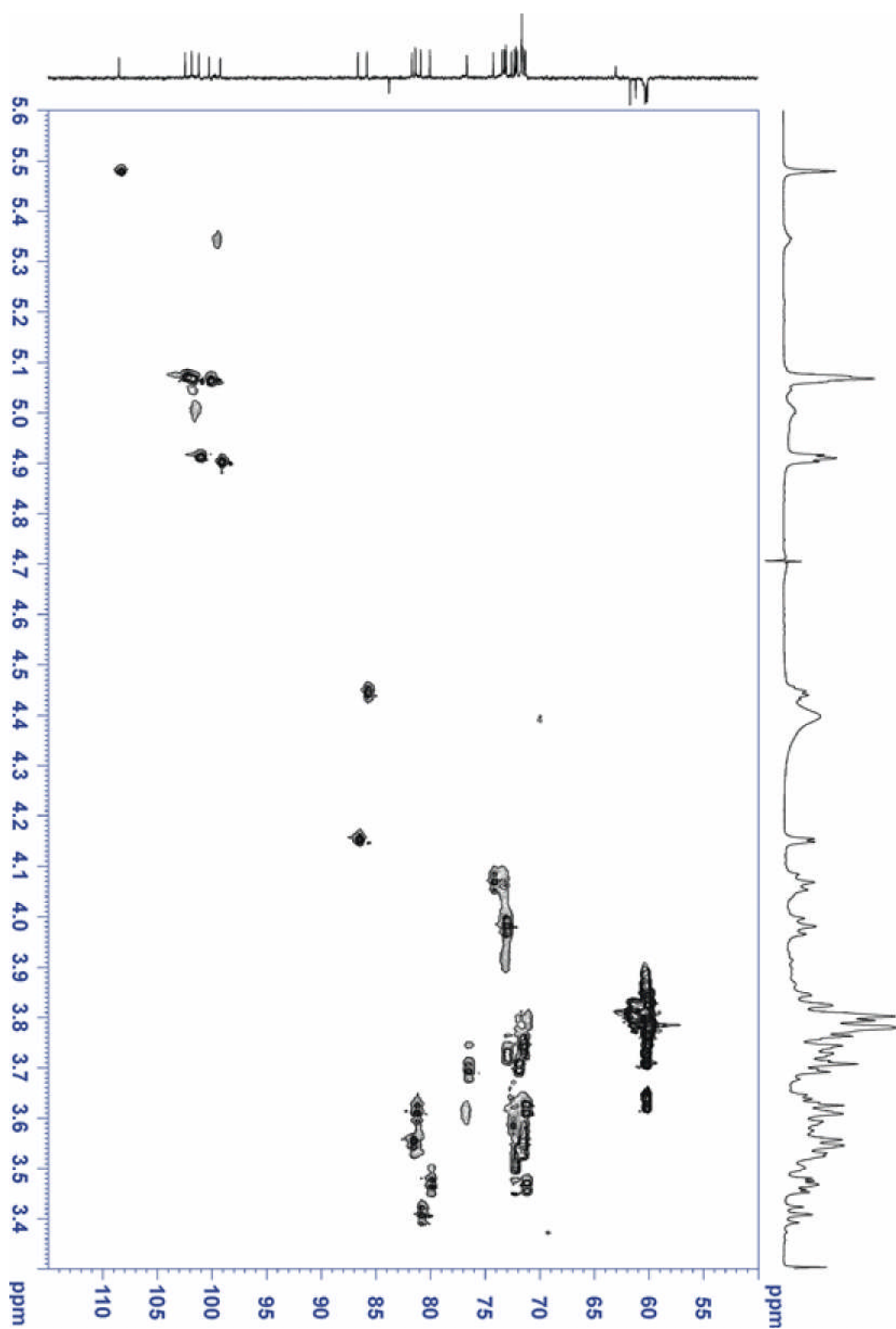


Figure S 14. 600 MHz HSQC spectrum of 2 in D_2O .

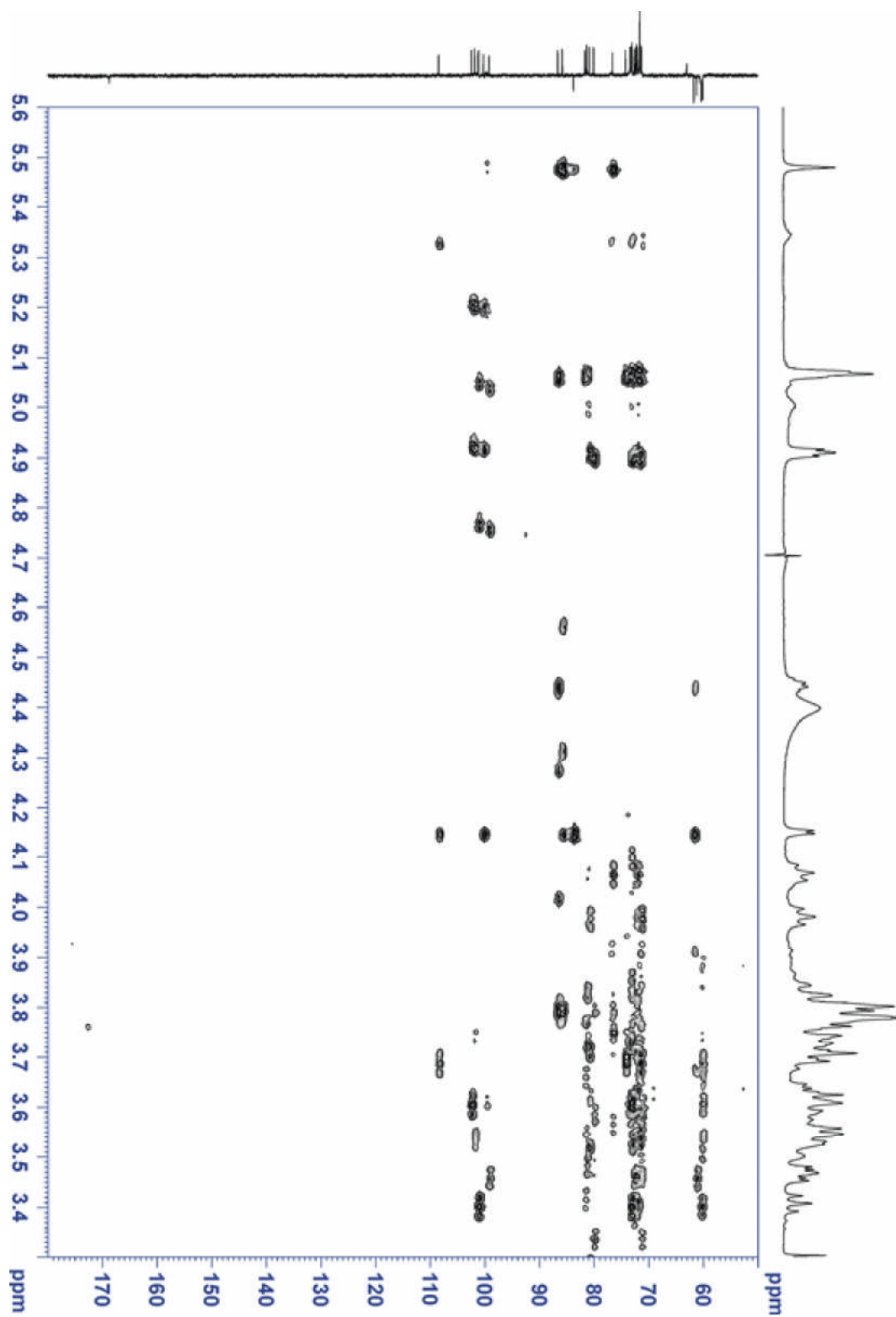


Figure S 15. 600 MHz HMBC spectrum of **2** in D_2O .

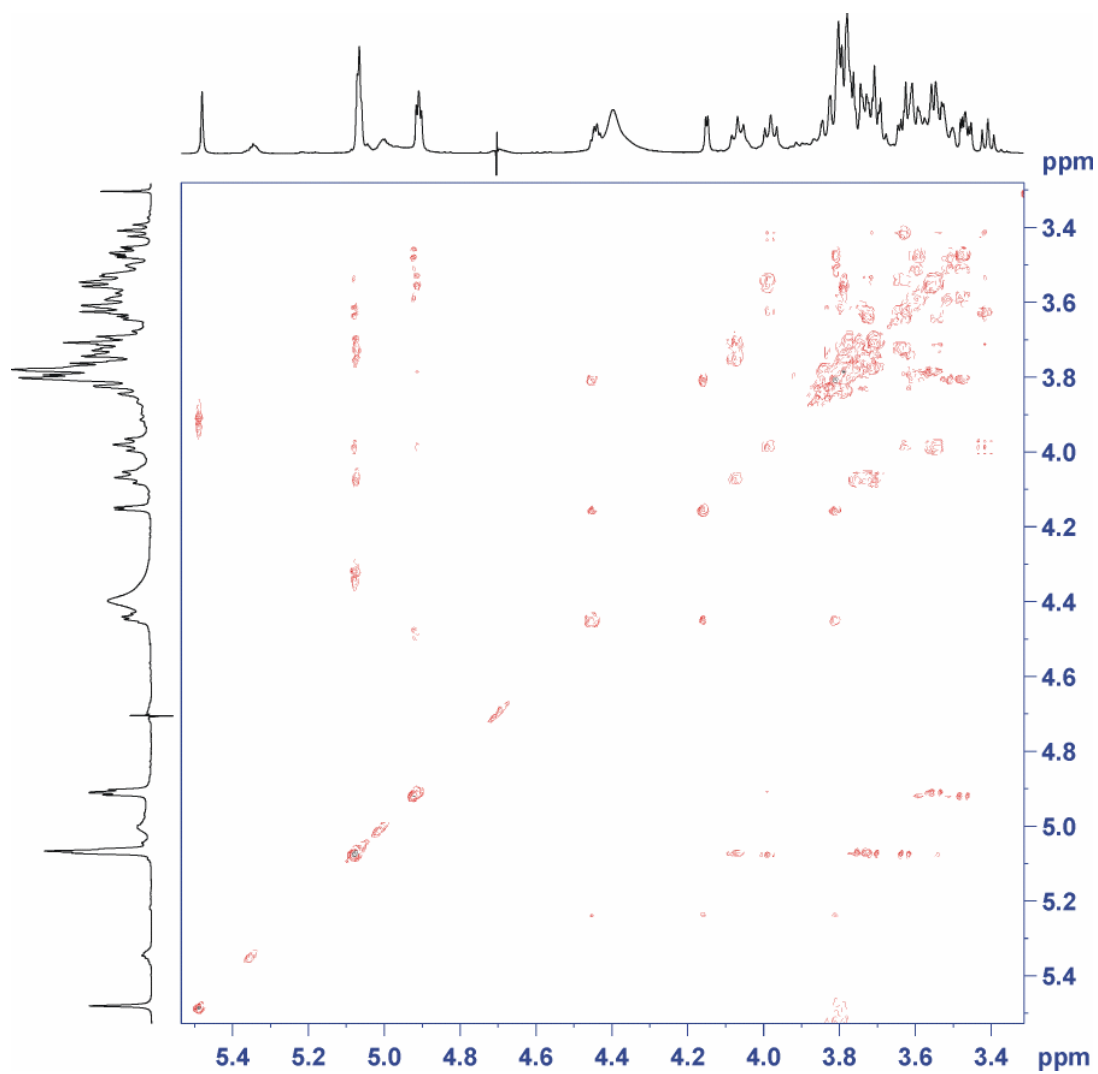


Figure S 16. 600 MHz TOCSY spectrum of **2** in D₂O.

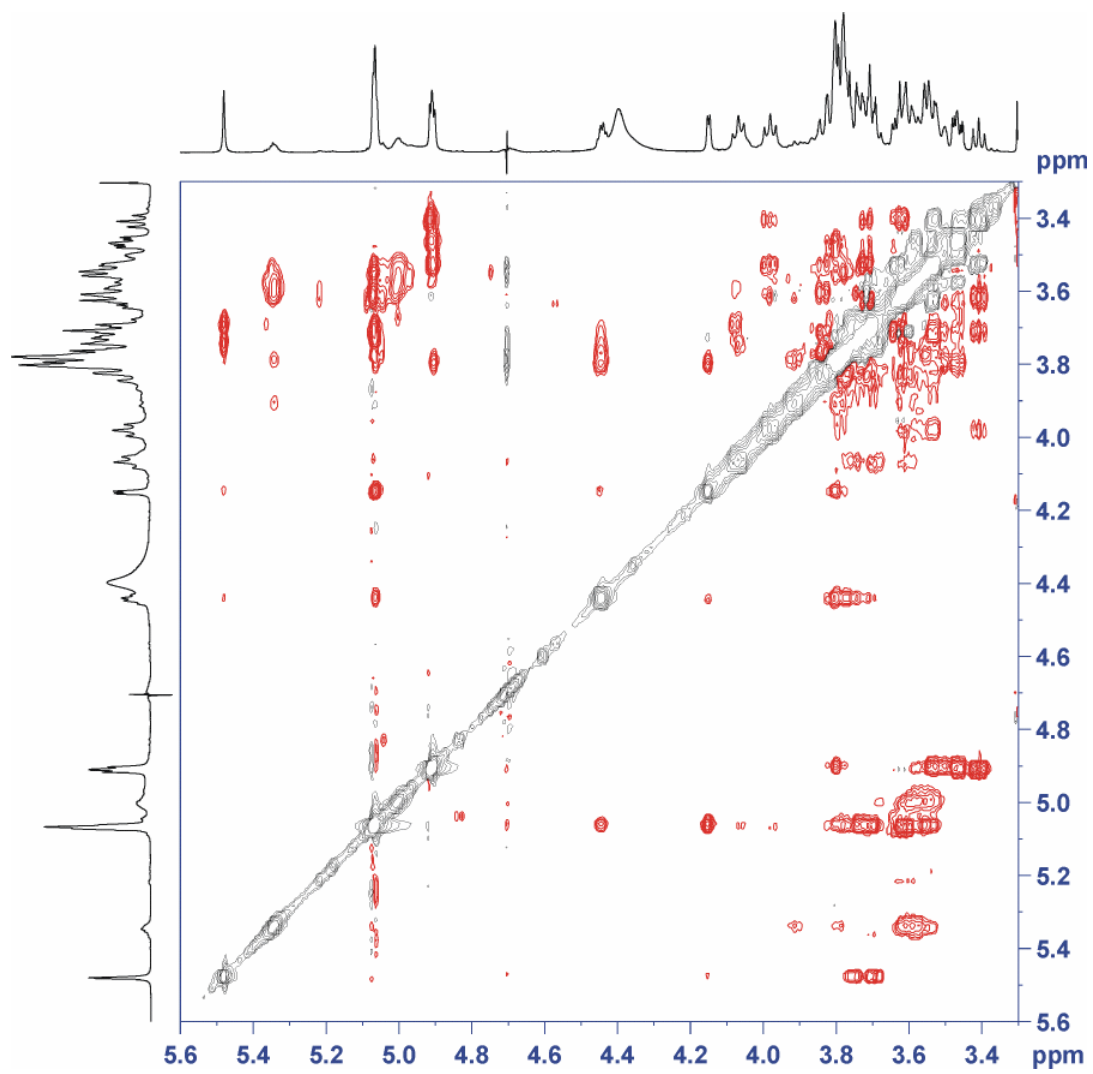


Figure S 17. 600 MHz 2D ROESY spectrum of **2** in D₂O.

IR Spectra unequivocally confirmed the presence of the amide II²² band at 1578 cm⁻¹ (Figure S 18). The amide I²² band at 1640 cm⁻¹ is overlapping with the band stemming from the α -CyD moiety, but due to the enhanced intensity of this band we may deduce its presence. Table S 6 shows the peak list of α -CyD and compound **2**.

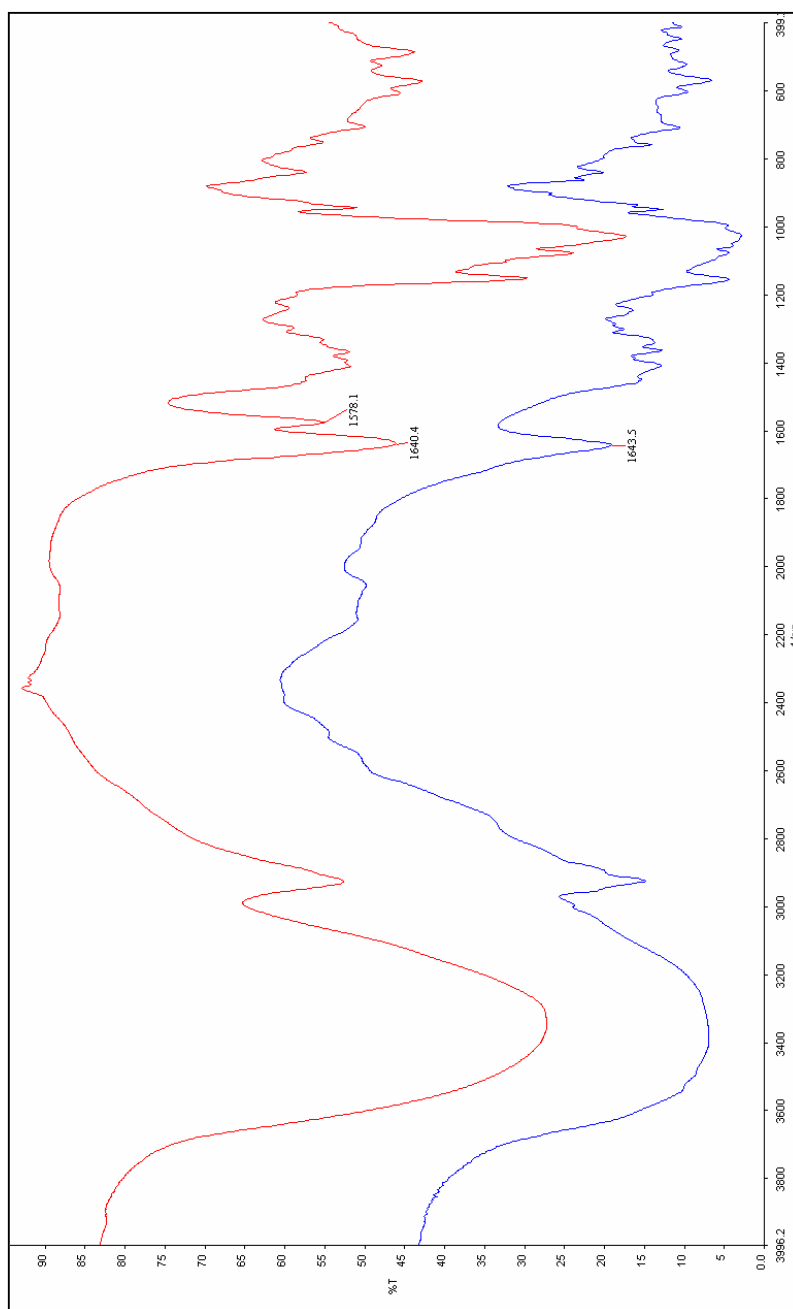


Figure S 18. IR Spectra of **2** (left red curve) compared with α -CyD (right blue curve).

²² Amide I = $\nu_{\text{CO, stretching}} + \nu_{\text{NH, bending}} + \nu_{\text{CN, stretching}}$. Amide II = $\nu_{\text{NH, bending}} + \nu_{\text{CN, stretching}}$. For example, the IR spectra of ferrocenyl acetamide are described in: Heinze, K.; Schlenker, M. *Eur. J. Inorg. Chem.* **2004**, 2974.

Peak List of α -CyD Spectrum				Peak List of 2 Spectrum			
Abscissa units: 1/cm				Abscissa units: 1/cm			
Ordinate units: %T				Ordinate units: %T			
No.	Abscissa	Ordinate	Type	No.	Abscissa	Ordinate	Type
1	3855.39	40.928	Peak	1	3349.99	27.212	Peak
2	3401.20	6.9074	Peak	2	2928.34	52.685	Peak
3	2927.52	14.793	Peak	3	2064.91	88.177	Peak
4	2058.32	49.775	Peak	4	1640.38	46.102	Peak
5	1643.47	19.089	Peak	5	1578.09	55.052	Peak
6	1450.62	15.305	Peak	6	1413.35	51.798	Peak
7	1411.05	12.904	Peak	7	1369.69	51.934	Peak
8	1365.84	12.706	Peak	8	1299.75	58.862	Peak
9	1342.73	13.649	Peak	9	1241.56	59.441	Peak
10	1303.88	17.512	Peak	10	1154.10	29.670	Peak
11	1247.48	16.434	Peak	11	1079.47	23.920	Peak
12	1157.61	4.4116	Peak	12	1030.94	17.213	Peak
13	1078.44	4.4223	Peak	13	946.61	50.930	Peak
14	1026.91	2.8488	Peak	14	841.10	57.309	Peak
15	951.46	12.652	Peak	15	752.88	55.244	Peak
16	938.58	15.789	Peak	16	707.84	49.932	Peak
17	864.93	22.467	Peak	17	608.93	45.496	Peak
18	842.53	20.074	Peak	18	573.94	42.858	Peak
19	761.35	14.070	Peak	19	527.82	47.866	Peak
20	710.75	10.499	Peak	20	487.94	43.749	Peak
21	605.10	9.5708	Peak				
22	570.92	6.5479	Peak				
23	524.24	9.6385	Peak				
24	483.17	10.684	Peak				
25	449.08	10.378	Peak				
26	414.22	10.358	Peak				

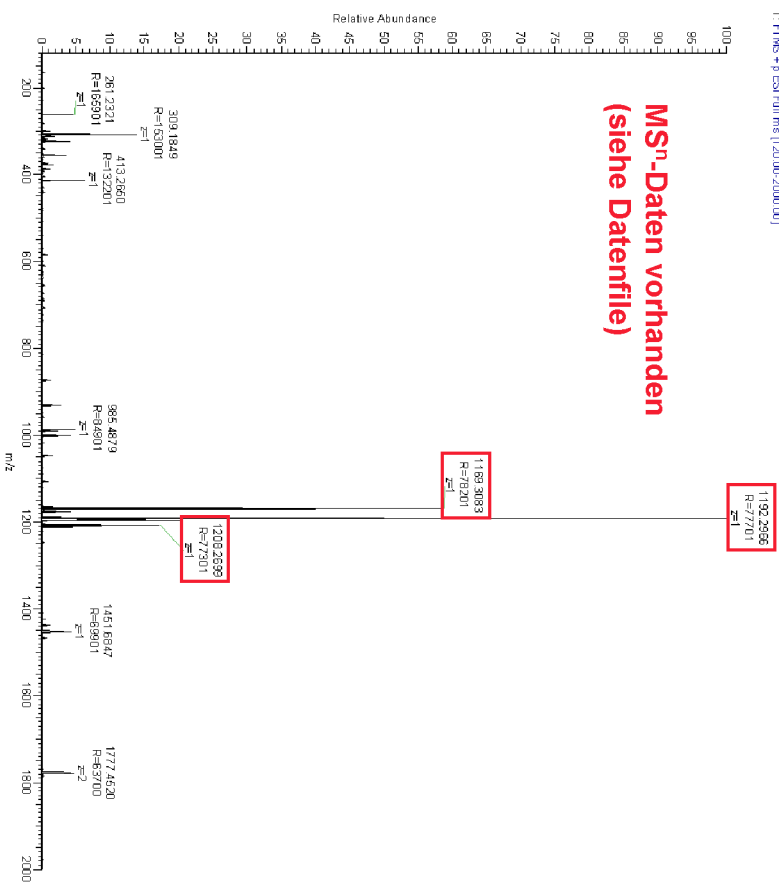
Table S 6. IR spectra peaks lists of α -CyD (left) and product **2** (right).

The molecular composition was collaborated by ESI-HRMS analysis (Figure S 19 - Figure S 23).

Orbitrap – Results – PW230

Orbitrap, direct infusion, PW230:

PW230.D1_48 RT:0.21 Acq.1 NL:218E7
T: FIMS + e-ESI Full.ms [120.00-2000.00]



Elemental composition

Mass: 1169.30835

Id	Formula	Delta pp
1	C ₄₈ H ₆₇ O ₃₀ N ₁₂ Fe ₁	-0.711
2	C ₄₇ H ₆₅ O ₂₇ N ₁₂ Fe ₁	-0.945
3	C ₄₄ H ₆₄ O ₃₀ N ₁₂ Fe ₁	1.346

Elemental composition

Mass: 1192.29663

Id	Formula	Delta pp
1	C ₄₈ H ₆₇ O ₃₀ N ₁₂ Fe ₁	-1.947
2	C ₄₈ H ₆₅ O ₃₀ N ₁₂ Fe ₁	-3.984
3	C ₄₄ H ₆₄ O ₂₇ N ₁₂ Fe ₁	-4.104

Elemental composition

Mass: 1208.28990

Id	Formula	Delta pp
1	C ₄₈ H ₆₇ O ₃₀ N ₁₂ Fe ₁ K ₁	-2.474
2	C ₅₀ H ₆₅ O ₂₈ Fe ₁ K ₁	4.605
3	C ₄₄ H ₆₄ O ₂₇ N ₁₂ Fe ₁ K ₁	-4.807

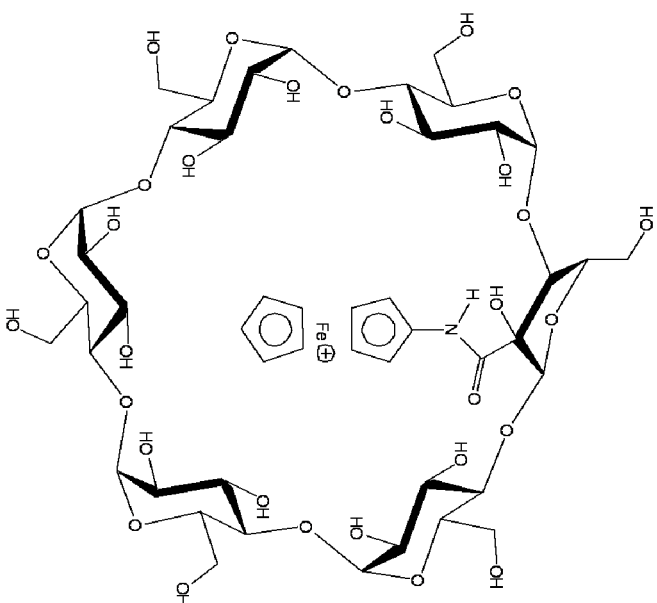
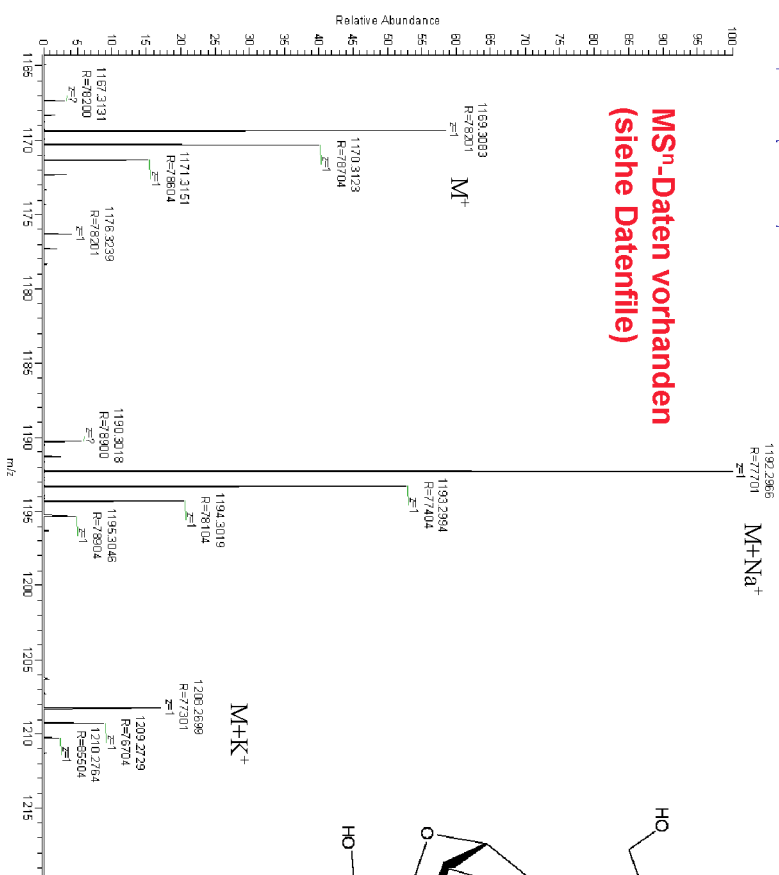
Figure S 19. HRMS-ESI spectrum of product 2.

Orbitrap – Results – PW230

Orbitrap, direct infusion, PW230:

PW230.DI.468 RT:0.21 Acq:1 NL:213E7
T: FTMS +p-ESI Full.ms [120.00-2000.00]

**MSⁿ-Daten vorhanden
(siehe Datenfile)**



Chemical Formula: $C_{48}H_{67}FeNO_{30}$
Exact Mass: 1169.30973

Figure S 20. HRMS-ESI spectrum of product 2.

Orbitrap – Results – PW230

Orbitrap, direct infusion, PW230, MS/MS 1169.3:

PW030_01 #217 RT: 3.90 A4.1 NL: 4.31E5
 F: FTMS +p ESI Full ms2 1169.310@dcd55.00 [32000+200.00]

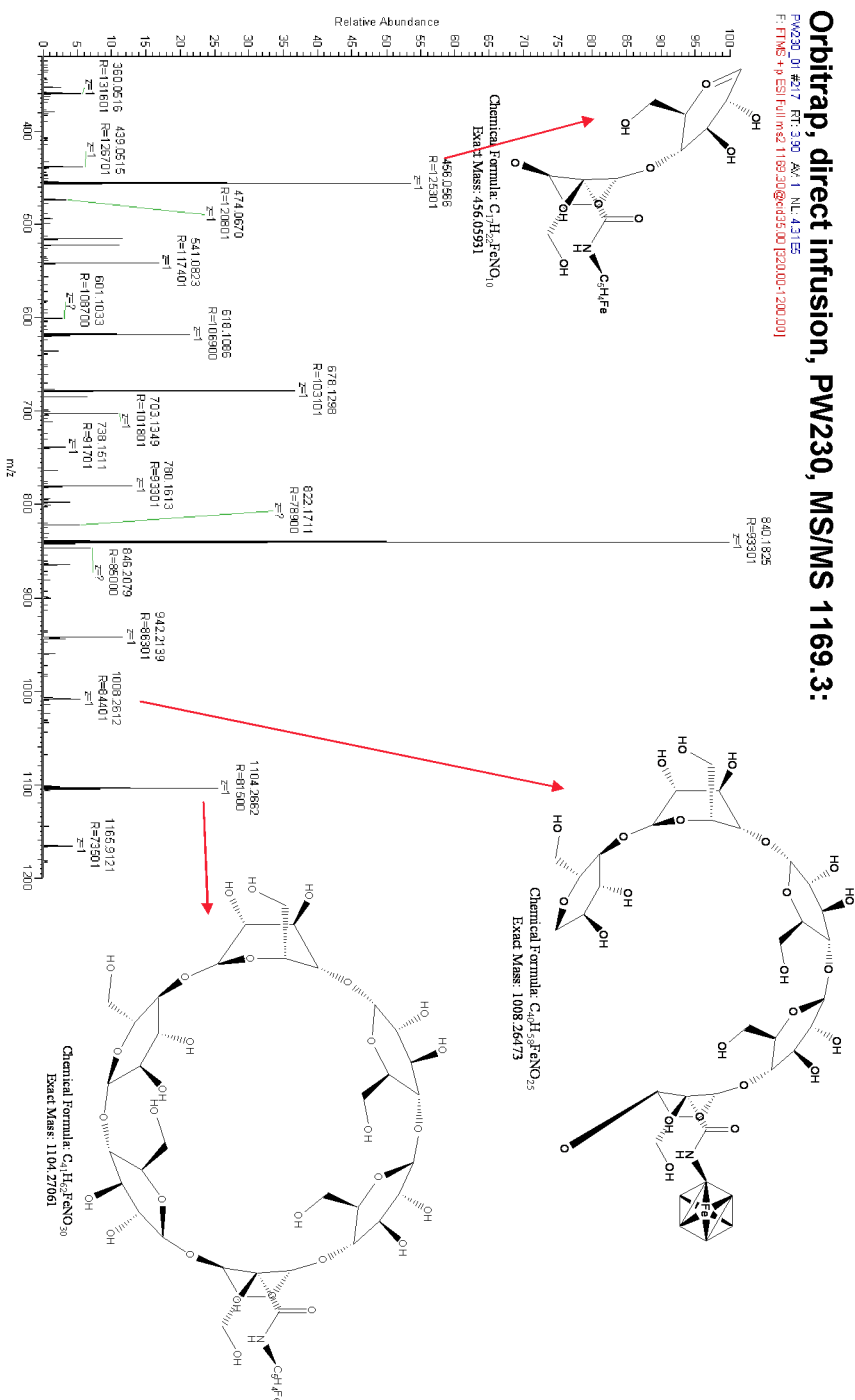


Figure S 21. HRMS-ESI spectrum of product 2.

Orbitrap – Results – PW230

Orbitrap, direct infusion, PW230, MSn 1192.2:

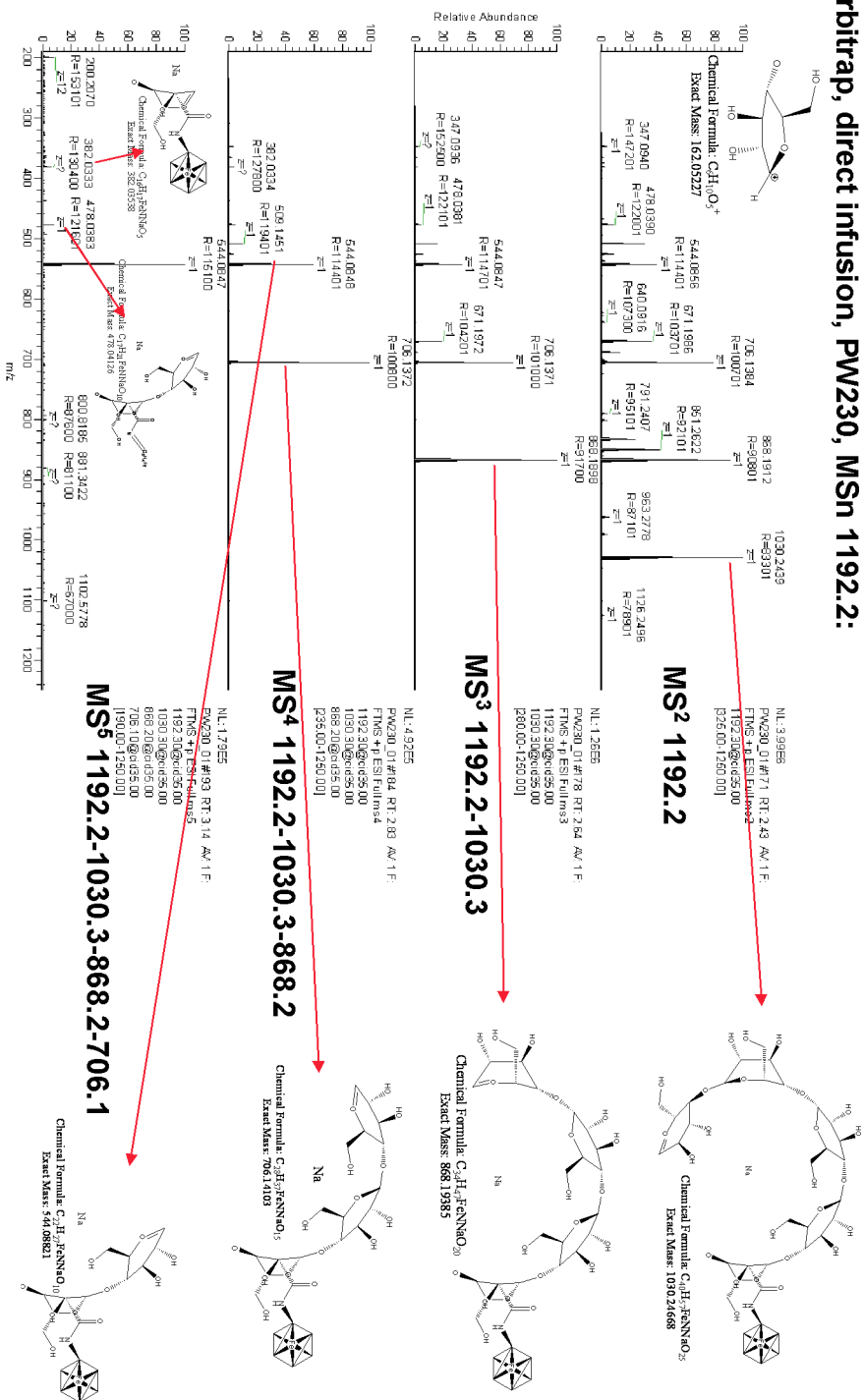
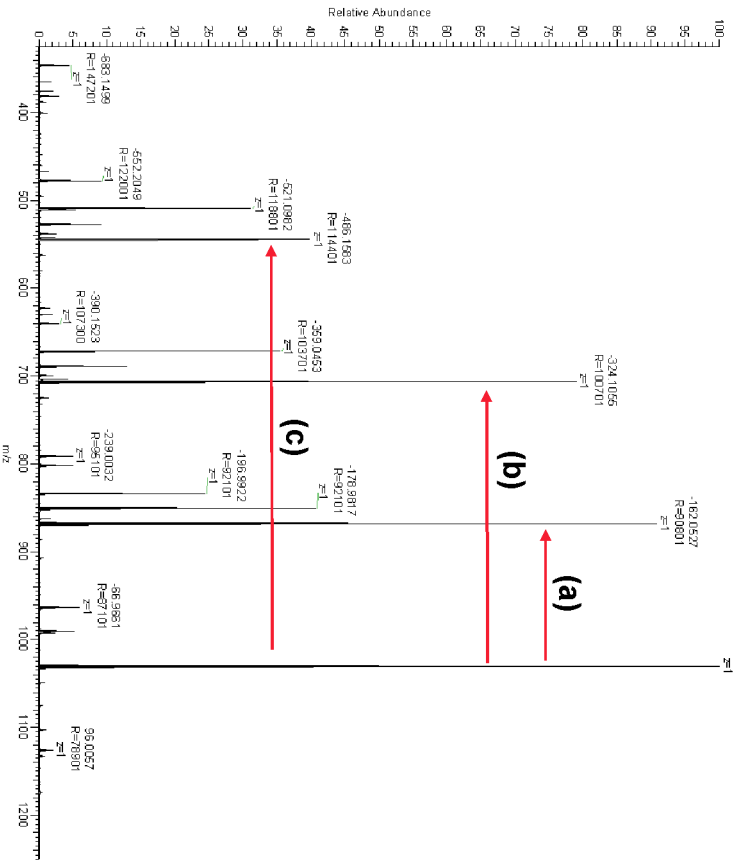


Figure S 22. HRMS-ESI spectrum of product 2.

Orbitrap – Results – PW230

Orbitrap, direct infusion, PW230, MS/MS 1169.3, label relativ zu 1030:

PW230_01_#171 RT: 2.43 min NL: 33985
F: FTMS +p ESI Full ms2 1192.20@q1955.00 | 925.00+1250.00



(a)

Elemental composition	Formula	Delta (m)
Single mass	$C_9 H_{10} O_5$	-0.094
Max. results	$C_9 H_{18} O_7 N_1$	-2.774
	$C_7 H_{11} N_3 S_3 K_1$	-3.201

(b)

Elemental composition	Formula	Delta (m)
Single mass	$C_{12} H_{20} O_{10}$	-0.177
Max. results	$C_{18} H_{22} O_7 N_1 F_1$	0.391
	$C_{10} H_{14} O_8 N_1 S_3 K_1$	n.d.m.c.

(c)

Elemental composition	Formula	Delta (m)
Single mass	$C_{22} H_{35} O_4 N_2 F_1 S_3 K_1$	-0.000
Max. results	$C_{18} H_{30} O_{15}$	-0.141
	$C_{31} H_{32} O_4 N_2$	0.373

Figure S 23. HRMS-ESI spectrum of product 2.

The UV-VIS Spectra show a typical ferrocene pattern (Figure S 24).

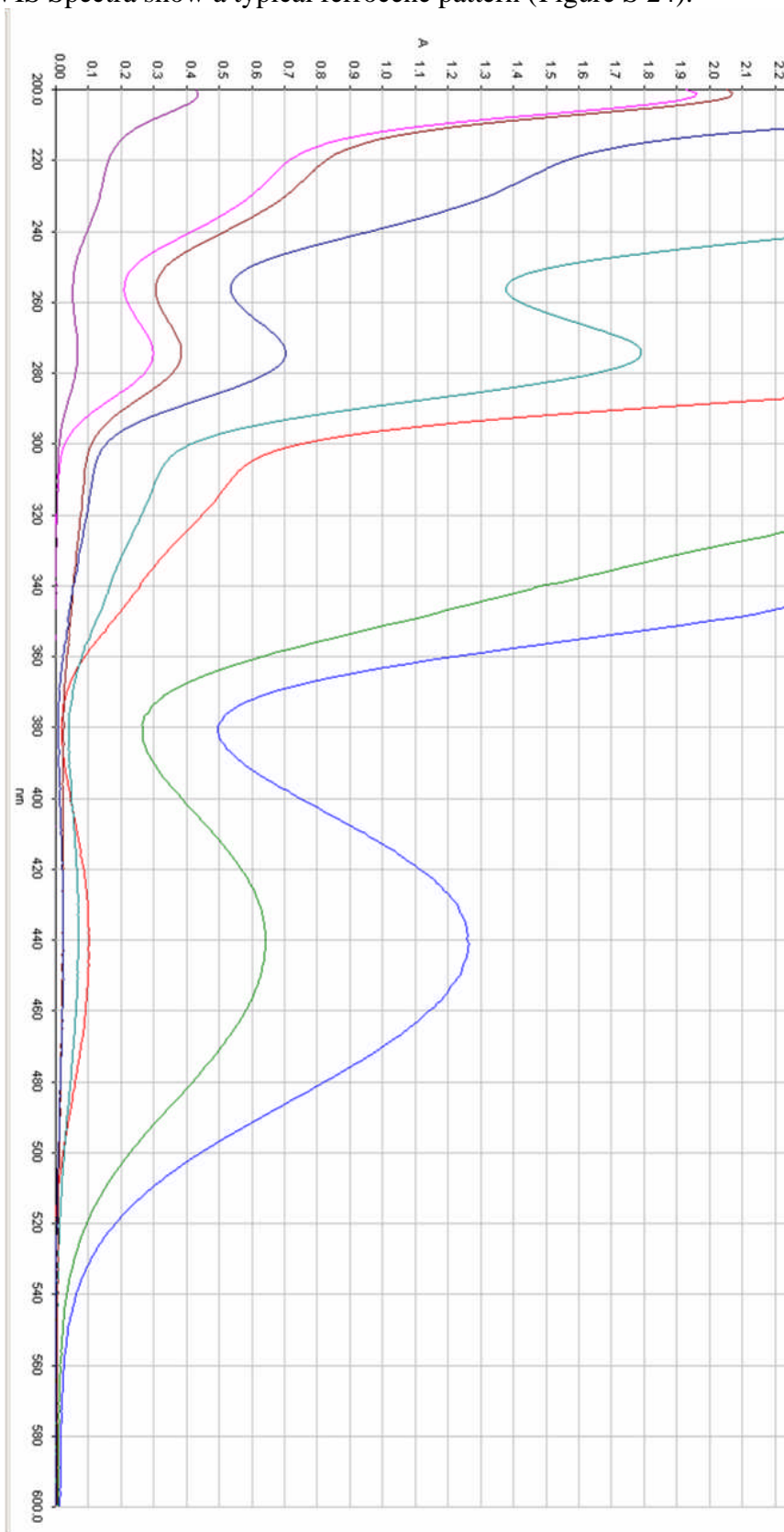


Figure S 24. UV-VIS Spectra of compound 2.

01.sp	1 cm cell length, (5.64×10^{-3} M)
02.sp	1 mm cell length, (5.64×10^{-3} M)
03.sp	0.5 cm cell length, (5.64×10^{-3} M)
04.sp	1 mm cell length, (5.64×10^{-4} M)
05.sp	0.5 cm cell length, (5.64×10^{-4} M)
06.sp	0.5 cm cell length, (1.13×10^{-4} M)
07.sp	1 cm cell length, (1.13×10^{-4} M)
08.sp	1 mm cell length, (1.13×10^{-4} M)

Spectra recorded in H₂O

λ [nm] (ϵ [$M^{-1} \text{ cm}^{-1}$]): 440 (230), 315sh (880),
275 (6250), 230sh (12500), 201 (38500).

Preparation of FcN₃@TRIMEA and TRIMEB complexes

A flask was filled with FcN₃ and modified CyD. Methanol was added and the content dissolved. The flask was stoppered and kept in the freezer at -25°C for at least 24 h. Large orange crystals precipitated afterwards. The flask was transferred to the cooling bath (-21°C) and the supernatant quickly sucked off by a syringe. At the temperature of the cooling bath, the septum was replaced by a water aspirator and “freeze dried” for 4 h. The water aspirator was then replaced by an oil pump and freeze drying continued overnight. The stoichiometry of the orange-yellow solid product was investigated by 250 MHz ¹H NMR in CDCl₃. The yield was determined by elemental analysis based on the nitrogen content. Table S 7 summarizes preparations of the complexes.

Experiment Designation	CyD	n(FcN ₃) [mmol]	Eq. of CyD	V(CH ₃ OH) [mL]	Stoichiometry from ¹ H NMR FcN ₃ /CyD	C/H/N Analysis [%]	Yield [%] ^a
PW195	TRIMEB	0.56	1	3.5	1/~1.4	52.47/7.18/2.19	72
PW235	TRIMEB	3.28	1.04	18	1/~1.3	52.60/7.52/2.20	85
PW199	TRIMEA	0.275	3.17	4	1/~3	52.61/7.39/1.33	76
PW228	TRIMEA	0.705	2.51	8	1/~2.4	52.47/7.68/1.48	89

^aThe yield is based on C/H/N Analysis and was calculated as: $Y = 100\% \times n(\text{guest included in the complex}) / n(\text{starting amount of the guest})$, where n means molar amount.

Table S7. Preparation of FcN₃ complexes with TRIMEA and TRIMEB.

General remarks on the work-up of the reactions after decomposition of the FcN₃@TRIMEA and TRIMEB Complexes

Since, the weight fraction of FcN₃ within the high molecular weight complexes with TRIMEA and TRIMEB hosts is a quite small, the photochemical decomposition was not carried out, because very large amount of the complex would be required to obtain a weightable amount of low mass ferrocene decomposition products. Moreover, utilizing larger amounts of photolyzed material leads to thick layers of the starting material and thus not to complete conversion. The thermal decomposition was done as described above with the native cyclodextrin complexes.

Work-up of the reaction after the decompositions of the FcN₃@TRIMEB complex

490 mg of the yellow-orange solid complex of FcN₃@TRIMEB was thermolyzed at 85-90°C for 2 d. After the decomposition, the color of the solid was brown. A TLC analysis (on Silica gel as well as on Aluminium oxide) indicated the presence of FcH, FcN=NFc, but did not confirm the presence of FcNH₂ unambiguously, i.e., only a very slight spot was visible with 254 nm light. A visualization reagent colored the spot to red, whereas the reference spot of FcNH₂ afforded a brown-yellowish color. A tailing brownish band overlapping with the TRIMEB spot was observed, possibly indicating the presence of a compound formed by modification of the host by ensued ferrocenyl nitrene. The separation was carried out by BIO-BEADS[®] SX3 gel permeation chromatography (100 g filling, 2.5 x 90 cm column, eluent DCM). Eight colored bands developed:

- 1st dark brown (57 mg, brown solid insoluble in DCM!, probably polymers)
- 2nd orange band (401 mg, orange solid)
- 3rd orange-brownish band (4 mg, brown solid)
- 4th green band (4 mg, brown solid)
- 5th grey band (2 mg, black-grey solid)
- 6th red-pink band (5 mg, brown-red solid)
- 7th violet band (1 mg, violet solid)
- 8th yellow band (3 mg, yellow solid)

Each fraction was analysed by TLC.

In the second one, the already mentioned tailing brownish band overlapping with the TRIMEB spot was observed, possibly indicating the presence of a compound formed by a modification of the host by ensued ferrocenyl nitrene.

ESI-MS analysis confirmed the mass of 1627.5 m/z, indicating a possible insertion of the nitrene into a C-H bond of the host. All attempts to separate the compound from TRIMEB failed. Moreover, during separations the product decomposed.

The presence of the known FcN=NFc was observed in the fractions number 6 (6 colored spots on TLC) and 7 (two spots on TLC). 1 mg of FcN=NFc was obtained from these fraction by analytical thin layer chromatography (0.25 mm Silica, 20 x 20 cm).

According to TLC, fraction 7 contained pure ferrocene (7 % yield).

In no fraction, as inferred from ¹H NMR, the presence of FcNH₂ could not be confirmed.

Work-up of the reactions after the decompositions of the FcN₃@TRIMEA complex

435 mg of the yellow solid complex of FcN₃@TRIMEA was thermolyzed for 2 d at 85 °C. Upon the decomposition, the color of the solid had turned brown. A TLC analysis (on Silica as well as on Alumina) indicated the presence of FcH, FcN=NFc, but did not confirm the presence of FcNH₂. A tailing brownish band overlapping with a TRIMEA spot was observed as in the case of the TRIMEB complex, possibly indicating the presence of a compound formed by modification of the host by ensued ferrocenyl nitrene. The separation was carried out by BIO-BEADS[®] SX3 gel permeation chromatography as well. 1.1 mg of FcH (4 % yield) and 3.2 mg of FcN=NFc (12 % yield) were isolated. In general, the reaction mixture upon decomposition of FcN₃@TRIMEA in comparison to FcN₃@TRIMEB, was “cleaner”, in terms of the number of compounds formed.

X-ray crystallographic analysis

X-ray diffraction measurements were performed on a Bruker X8 APEXII CCD diffractometer with graphite monochromated MoK α radiation, $\lambda = 0.71073 \text{ \AA}$ at 100(2) K. The single crystal was positioned at 40 mm from the detector and 1020 frames were measured, each for 30 s over 1° scan width. The data were processed using SAINT software.²³ The structure was solved by direct methods and refined by full-matrix least-squares techniques. Non-hydrogen atoms were refined with anisotropic displacement parameters, except the ferrocene carbon atoms and, three disordered methoxy groups and the oxygen atom of lattice water molecules, which is partially populated. H atoms were placed in geometrically calculated positions and refined as riding atoms in the subsequent least squares model refinements. The positions of the hydrogen atoms of methanol molecules with partial occupancy have been calculated. The isotropic thermal parameters were estimated to be 1.2 times the values of the equivalent isotropic thermal parameters to which hydrogens were bound. The disorder in three methoxy groups was solved by restraining the C–O bonds at 1.41 Å (within a standard deviation of 0.02 Å). The following computer programs were used: structure solution, SHELXS-97,²⁴ refinement, SHELXS-97,²⁵ molecular diagrams;²⁶ Computer: Pentium IV; scattering factors were taken from the literature.²⁷ Details of crystal data, data collection and refinement are as follows:

The crystal FcH@TRIMEB as yellow prism was prepared by mixing a methanolic solution of FcH with an aqueous solution of TRIMEB and letting slowly evaporate the methanol at RT.

²³ Bruker Programs SAINT-NT, version 6.0; SAINT, version 7.12A; Bruker AXS: Madison, WI, USA, 2003.

²⁴ Sheldrick, G.M. SHELXS-97: *Program for Crystal Structure Solution*, University of Göttingen, Germany, 1997.

²⁵ Sheldrick, G.M. SHELXL-97: *Program for Crystal Structure Refinement*, University of Göttingen, Germany, 1997.

²⁶ Mercury 1.4, <http://www.ccdc.cam.ac.uk/mercury>.

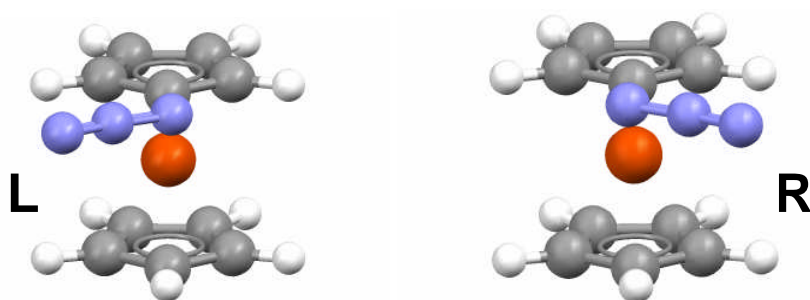
²⁷ *International Tables for X-ray Crystallography*; Kluwer: Dordrecht, The Netherlands, 1992, Vol. C, Tables 4.2.6.8 and 6.1.1.4.

Crystal data: $C_{73}H_{122}FeO_{35}$, $M_r = 1615.57$, orthorhombic, $P2_12_12_1$, $a = 11.1495(3)$, $b = 25.1200(6)$, $c = 28.9405(7)$ Å, $V = 8105.5(4)$ Å³, $Z = 4$, $\mu(\text{MoK}\alpha) = 0.274$ mm⁻¹, 130890 measured reflections, 14308 independent, $R_{\text{int}} = 0.069$, $R(F) = 0.0379$, $wR(F^2) = 0.1016$, Flack parameter $-0.011(12)$.

The crystal $\text{FcN}_3@$ TRIMEB was grown from a methanolic solution at -25 °C. Orange prisms were obtained.

Crystal data: $C_{69.57}H_{122.93}Fe_{0.5}N_{1.5}O_{36.64}$, $M_r = 1594.64$, monoclinic, $P2_1$, $a = 18.0831(5)$, $b = 22.8248(7)$, $c = 23.6495(7)$ Å, $\beta = 110.865(2)^\circ$, $V = 9121.1(5)$ Å³, $Z = 4$, $\mu(\text{MoK}\alpha) = 0.168$ mm⁻¹, 65007 measured reflections, 31328 independent, $R_{\text{int}} = 0.053$, $R(F) = 0.0958$, $wR(F^2) = 0.2843$, Flack parameter $-0.01(3)$.

R- and L- designation of the enantiomeric conformers of FcN_3



ICD spectra of FcH and FcN_3 – TRIMEB complexes

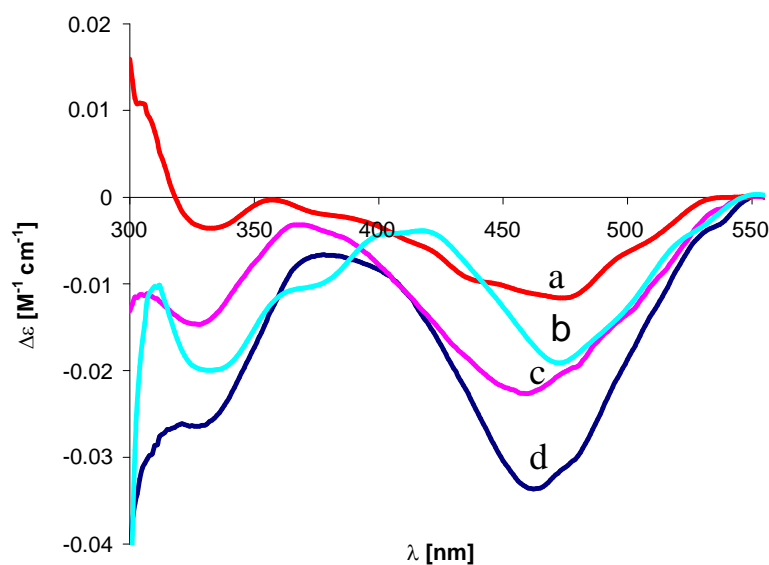


Figure S 25. Induced Circular Dichroism spectra of FcH (a, c) and FcN_3 (b, d) @ TRIMEB complexes in methanol (c, d), H_2O (b) and $\text{H}_2\text{O}/\text{EtOH} = 80/20$ (v/v) (a). $c(\text{FcH}) = 0.26$ mM (a), 30 mM (c); $c(\text{FcN}_3) = 3.7$ mM (b), 30 mM (d); $c(\text{TRIMEB}) = 0.9$ mM (a), 14.5 mM (b), 100 mM (c, d), 27 °C.

2D ROESY spectrum of the $\text{FcN}_3@$ TRIMEB complex

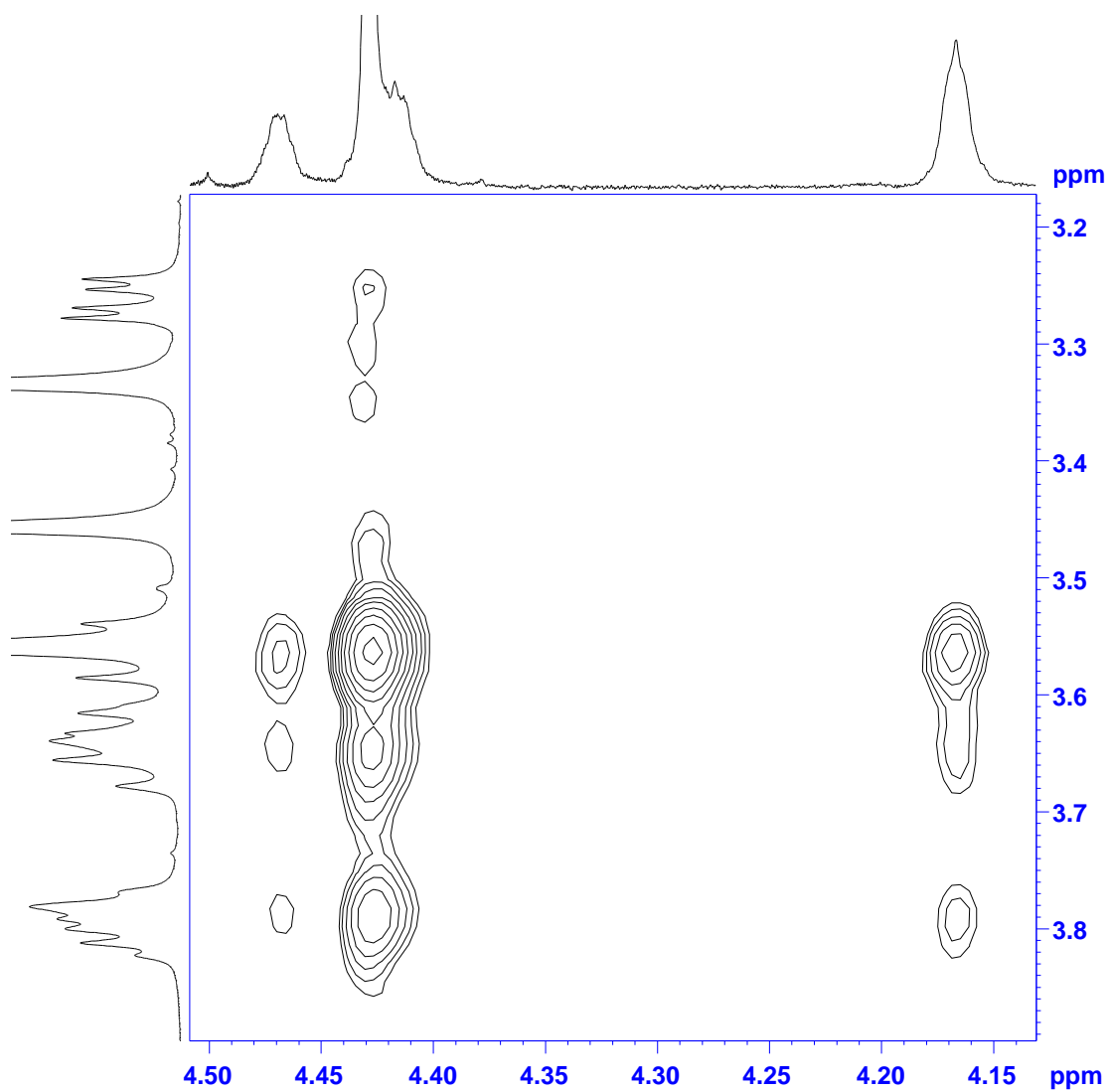


Figure S 26. 400MHz 2D ROESY Spectrum of the $\text{FcN}_3@$ TRIMEB complex in D_2O at 300 K. $c(\text{FcN}_3) = 3.7 \text{ mM}$, $c(\text{TRIMEB}) = 14.4 \text{ mM}$, $[\text{H}]/[\text{G}] = 3.9$. Mixing time 400 ms.

Determination of K_a for the FcH@TRIMEB complex in CD_3OD by 1H NMR titration

5.8 mg of TRIMEB was weighed up into a NMR tube and dissolved in 0.726 mL CD_3OD (Hamilton Syringe used, the level of liquid in the NMR tube was then 53 mm) to afford a 0.0056 M solution. 250 MHz 1H NMR spectra were recorded. Ferrocene was added portionwise directly into the same NMR tube and a 1H NMR spectrum was recorded each time after the addition. The molar excess of ferrocene was inferred from integration; H-1 peak of TRIMEB was used as a reference proton. Only the induced chemical shift of the H-3 inner cavity proton of TRIMEB was plotted against the molar concentration of ferrocene, because the other host's protons signal changed their phenotype during the titration, or induced a small shift. K_a was determined by a curve fitting procedure according to the literature²⁸ with one exception; instead of Microsoft[®] Solver, global minimalization algorithms implemented within the program package OptWorks: Excel[®] were applied²⁹. The statistics for nonlinear regression was obtained from Add-In: SolvStat.³⁰ The best fit was obtained for $K_a = 53 \pm 5 M^{-1}$ and $\Delta\delta_{max} = 0.0407 \pm 0.0013$ (Figure S 27).

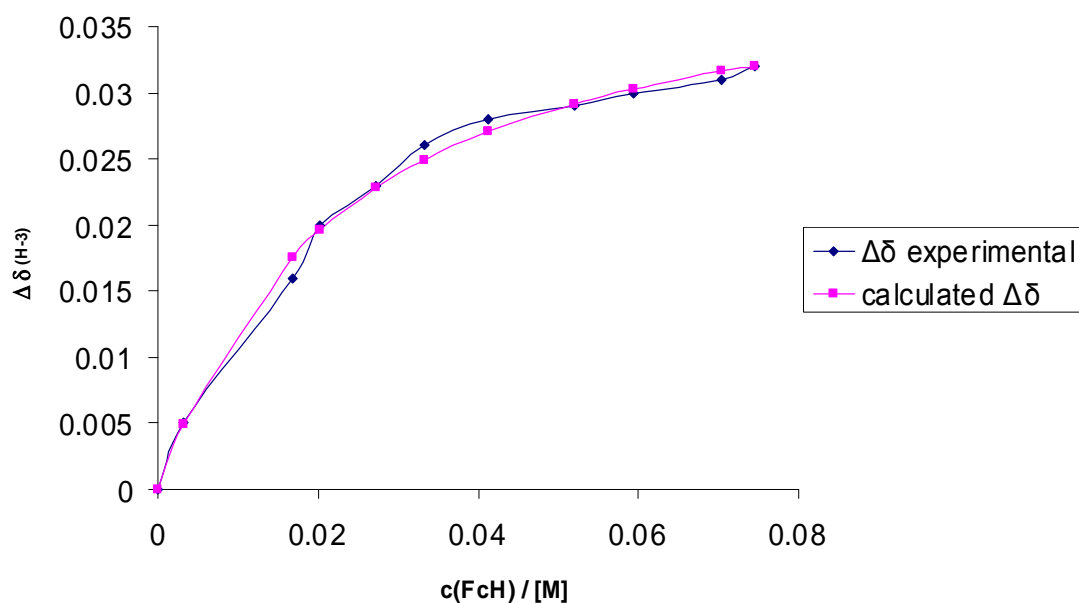


Figure S 27. Direct plot of nonlinear curve fitting for the determination of K_a of the FcH@TRIMEB complex in CD_3OD by 1H NMR titration.

²⁸ Mieusset, J.-L.; Krois, D.; Pacar, M.; Brecker, L.; Giester, G.; Brinker, U. H. *Org. Lett.* **2004**, *6*, 1967.

²⁹ Pi Blue Software, Inc., <http://www.piblue.com>.

³⁰ Billo, E. J. *Excel for Scientists and Engineers: Numerical Methods*. Wiley: New Jersey, 2007.

Determination of K_a for the $FcN_3@TRIMEB$ complex in CD_3OD by 1H NMR titration

The determination was performed in analogy as for the $FcH@TRIMEB$ complex. The TRIMEB Concentration was kept constant at 0.0082 M. The best fit was obtained for $K_a = 37 \pm 3 M^{-1}$ and $\Delta\delta_{max} = 0.0296 \pm 0.0009$ (Figure S 28).

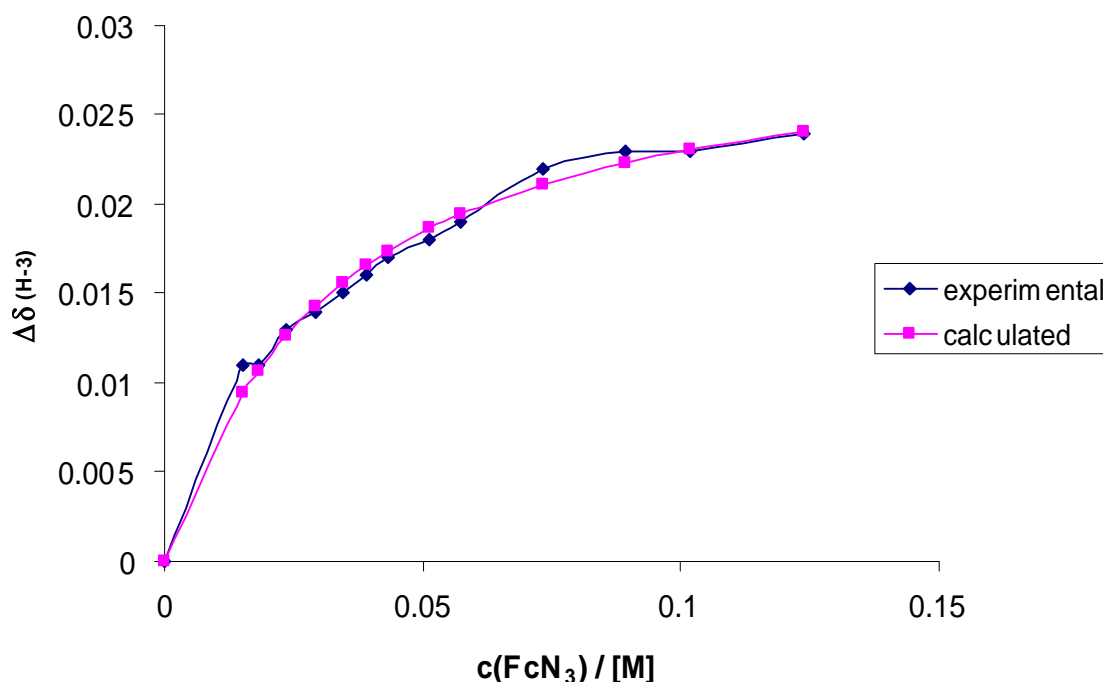


Figure S 28. Direct plot of nonlinear curve fitting for the determination of K_a of the $FcN_3@TRIMEB$ complex in CD_3OD by 1H NMR titration.

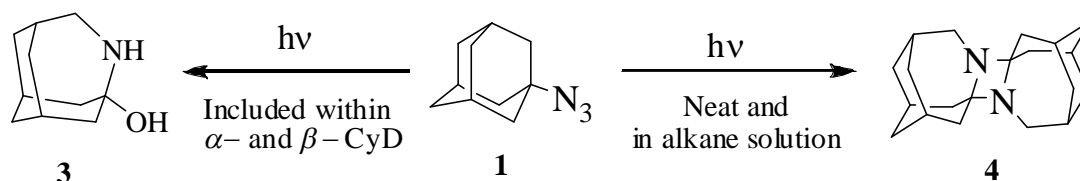
Electron Paramagnetic Resonance (EPR) Studies

CW EPR spectra were acquired with an ESP580 Bruker X-band (9.5 GHz) spectrometer. The system was equipped with an Oxford CF935 cryostat, operating with an Oxford Instruments ITC 502 controller referenced to boiling $N_2(l)$.

From the solid ferrocenyl azide sample, a 1 to 3 mole percent solutions of ferrocenyl azide in toluene were made and placed in a quartz EPR tube for analysis. Except for one initial open sample, all samples were freeze/pump/thawed three times and sealed before irradiation, so any gas bubbles observed after irradiation could be presumed to be nitrogen. The solution was irradiated at 77 K by a hand-held mercury arc lamp for 5-7 min prior to analysis to generate the ferrocenyl nitrene intermediate. Although color and temperature changes can be misleading, it appeared that the color of the sample changed upon irradiation from a clearly yellow color to a yellow-brown color. After irradiation, the sample was removed from liquid nitrogen and plunged immediately into a cryostat operating at 50 K. The temperature of the cryostat was then lowered to 10-30 K, depending on the experiment. The spectrum (ranging from 0 to 12-15 kGauss) revealed no signal, excepting a small, short-lived, strangely shaped signal at around $g = 2$. The exact nature of this signal is unknown, but it is not suggestive of a triplet sublevel transition and may have been a cavity background signal. This procedure was repeated a number of times improving upon any

shortcomings that we could imagine in our protocol. Every time the irradiated sample was removed from the cryostat after the experiment and examined while the solution melted. In every case, copious gas evolution was observed, consistent with the evolution of N₂ gas from the ferrocenyl azide decomposition. Speculating that the absorption spectrum of toluene may have effectively prevented the irradiation of the azide, another solvents were tried. EPA, a mixture containing 5 of parts ether, 5 of parts pentane, and 2 of parts alcohol, forms a nice, clear glass at low temperature, and the absorption spectrum of this solvent clearly cannot interfere with the irradiation of the azide. Experiments carried out in identical fashion using EPA as a solvent also proved unsuccessful but showed copious gas evolution, consistent with the evolution of N₂ gas from the ferrocenyl azide decomposition. In order to rule out hydrogen abstraction from the alcohol of the solvent by the nitrene intermediate, more experiments with yet another solvents, 50/50 ether/pentane and fluorolube were tried. These experiments also gave no signal but showed copious gas evolution, consistent with the evolution of N₂ gas from the ferrocenyl azide decomposition. Lastly, in an attempt to rule out that the hand held arc lamp just didn't have enough intensity to degrade the azide significantly, the sample was irradiated in-situ at 30 K with an eximer laser operating at 308 nm. A systematic study was done, collecting spectra after each series of cumulatively increasing laser shots, ranging from 1 to 100 laser pulses. No signal was obtained and some observable gas evolution was noted afterward upon melting the sample.

5. Study of the Structure and Photochemical Decomposition of the Adamantane Azides Included in α - and β -Cyclodextrin



5.1 Abstract

The products formed upon the photolysis of the adamantane azides with and without supramolecular encapsulation by cyclodextrins (CyDs) were studied. Neat 1-adamantane azide (**1**), or in an alkane solution decomposes to dimerization product **4**, whereas included in the cavity of CyDs, only **3** was formed as a sole product in high yield. Moreover, for the first time, an Induced Circular Dichroism (ICD) study of an alkyl azide included in the CyD cavity is reported. 1- and 2-adamantane azides form 1:1 inclusion complexes (ICs) with β -CyD, but 1:2 ICs with α -CyD. **1** forms a stronger IC with β -CyD in H₂O/EtOH = 8/2 at 293 K ($K_a = 20240 \pm 1000 \text{ M}^{-1}$) than 2-adamantane azide (**5**) does ($K_a = 7450 \pm 400 \text{ M}^{-1}$). A cooperative binding for the **5**@ α -CyD complex is suggested, due to the negligible $K_{a1} = 1 \pm 0.4 \text{ M}^{-1}$ and high $K_{a2} = 21758 \pm 3680 \text{ M}^{-1}$ values in H₂O/EtOH=9/1. As inferred from a 2D ROESY study in D₂O, **1** is accommodated at the upper rim of β -CyD, with the azide group pointing downwards into the cavity. On the other hand, in D₂O two principal orientations of 2-adamantane azide inside the cavity of β -CyD were found. In the solid state, as inferred from an X-ray single crystal analysis, **5** exhibits a bimodal orientation within β -CyD as well.

5.2 Introduction

Cyclodextrins (CyDs) are well-known cyclic oligosaccharides of α -D-glucose units connected through glycosidic α -1,4 bonds. The truncated cone-shaped structures possess a hydrophobic central cavity filled with energetically unfavored water molecules, which can be readily substituted by appropriate less polar guest molecules.¹ This ability to include organic molecules has been long recognized in the pharmaceutical and food industry, making CyDs very interesting and promising molecules.²

¹ Connors, K.A. *Chem. Rev.* **1997**, 97, 1325.

² Szejtli, J. *Chem. Rev.* **1998**, 98, 1743.

Azides have served as nitrene precursors for quite some time.³ Nitrenes are generated by elimination of nitrogen using thermal or photochemical methods. These highly reactive intermediates may immediately react with surrounding molecules and this property has been utilized for photoaffinity labeling studies.^{4,5}

It has been already demonstrated that reactive carbene intermediates included in cyclodextrins can alter dramatically reaction pathways.⁶ A question can be cast, whether in a similar situation the pathway of a nitrene intermediate may be altered as well? In the present paper, we would like to demonstrate for the first time, how the supramolecular enclosure of the adamantly nitrenes by cyclodextrins can alter their reaction pathways. Concerning photoaffinity labeling, our next interest is to investigate the *structure* of the products formed upon a possible insertion of the nitrene into the encapsulating host molecule.

To extend our knowledge about these novel supramolecular aggregates, determinations of the association constants of **1** and **5** with α - and β -CyDs based on the induced circular dichroism (ICD) were conducted. Correlations of the geometry inferred from 2D ROESY technique with Induced Circular Dichroism (ICD) spectra are described.

5.3 Results

5.3.1 Chemistry of the Adamantane Azides – Cyclodextrin Complexes

Photodecomposition of 1-adamantane azide (**1**) leads to the formation of bridge-head imine **2**, which depending on conditions, can either react with surrounding water to form 4-azahomoadamantan-3-ol (**3**) or in absence of water dimerizes in a head-to-tail fashion to azetidine **4** (Scheme 1).⁷

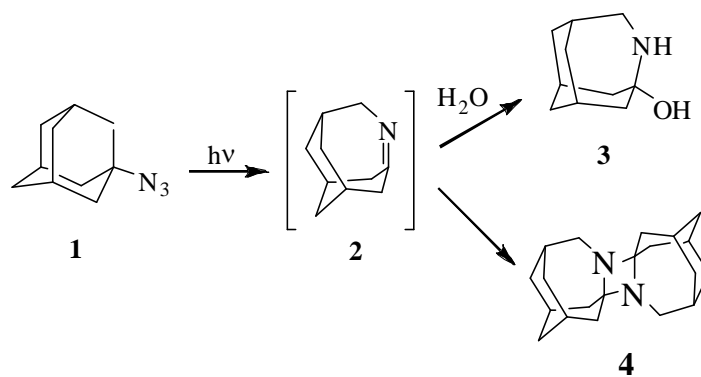
³ (a) Lwowski, W. *Nitrenes*, Interscience Publishers: London, **1970**. (b) Scriven, E.F.V. *Azides and Nitrenes*, Academic Press: New York, **1984**.

⁴ (a) Lwowski, W. *Annals of the New York Academy of Sciences* **1980**, *346*, 491. (b) Vodovozova, E. *L. Biochemistry* (Moscow), **2007**, *72*, 1.

⁵ Bräse, S., Gil, C., Knepper, K., Zimmermann, V. *Angew. Chem., Int. Ed.* **2005**, *44*, 5188.

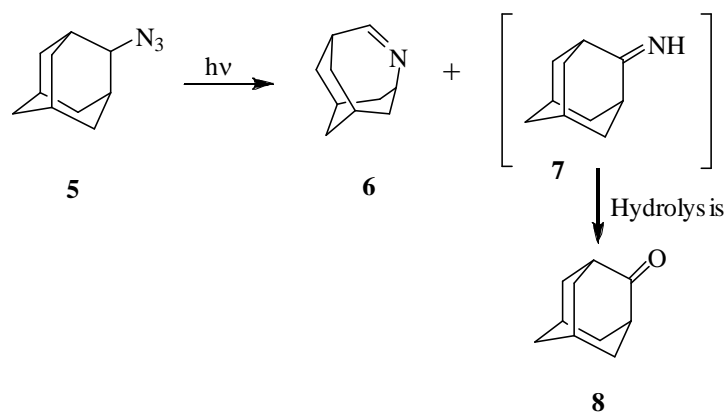
⁶ Brinker, U.H.; Buchkremer, R.; Kolodziejczyk, M.; Kupfer, R.; Rosenberg, M.; Poliks, M.D.; Orlando, M.; Gross, M.L. *Angew. Chem., Int. Ed.* **1993**, *32*, 1344.

⁷ (a) Quast, H.; Eckert, P. *Liebigs Ann. Chem.* **1974**, 1727. (b) Dunkin, I. R.; Shields, C. J.; Quast, H.; Seiferling, B. *Tetrahedron Lett.* **1983**, *24*, 3887. (c) Michl, J.; Radziszewski, G. J.; Downing, J. W.; Wiberg, K. B.; Walker, F. H.; Miller, D. R.; Kovacic, P.; Jawdosiuk, M.; Bonacic-Koutecky, V. *Pure Appl. Chem.* **1983**, *55*, 315.



Scheme 1. Photolyses products of **1**.

Photolysis of 2-adamantane azide (**5**) affords 4-azahomoadamant-4-ene (**6**) and labile imine **7**, which upon work-up hydrolyzes to adamantanone (**8**) (Scheme 2).⁸



Scheme 2. Photolyses products of **5**.

In our hands, photolysis of either solid **1** or in alkane solution also afforded solely **4** (Table 1, Entries 1, 2).

Entry		Yield (%) ^a			
		3	4	6	8
1	1 (solid state)	-	84	-	-
2	1 (alkane sol.)	-	88	-	-
3	1 @(α -CyD) ₂	94 ^b	-	-	-
4	1 @ β -CyD	91	traces	-	-
5	5 (solid state)	-	-	84	15
6	5 (alkane sol.)	-	-	87	5
7	5 @(α -CyD) ₂	-	-	81	10
8	5 @ β -CyD	-	-	77	23

a) The yields were determined by quantitative analytical GC-FID

b) Traces of 1-adamantane amine and adamantane-1-ol were detected by GC-MS

Table 1. Products of photolyses of 1- and 2-adamantane azides (**1**) and (**5**), respectively.

⁸ Sasaki, T.; Eguchi, S.; Toi, N. *J. Org. Chem.* **1979**, *44*, 3711.

In contrast, photolysis of solid **1**@CyD afforded solely **3** (Entries 3, 4). However, photolysis of **5** under similar conditions lead to a major formation of **6** and a minor formation of **8** (Entries 5-8).

5.3.2 Single Crystal Structure of 2-Adamantane azide@ β -Cyclodextrin Complex

The β -cyclodextrin (β -CyD) – 2-adamantane azide ($C_{10}H_{15}N_3$) inclusion complex crystallizes from a hot aqueous – ethanolic solution as white prisms of the composition 2β -CyD \cdot 0.75 $C_{10}H_{15}N_3$ \cdot 21.5 H_2O in the triclinic non-centrosymmetric space group $P1$ (Figure 1).

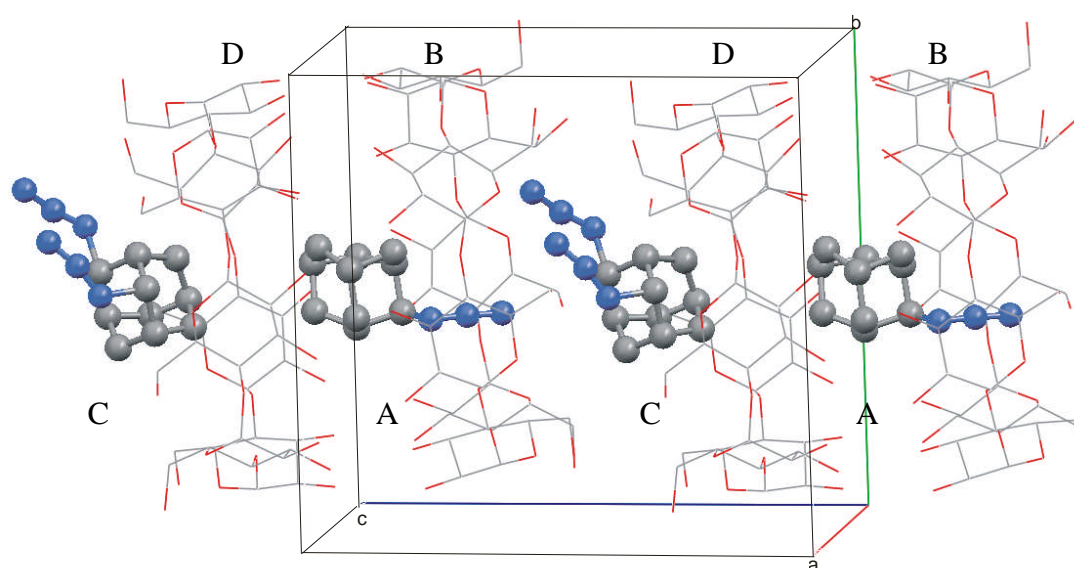


Figure 1. X-ray single crystal structure of the **5**@ β -CyD complex. Hydrogen and water molecules were removed for clarity. Two crystallographically independent β -CyD molecules B and D are present in the unit cell. The guest molecule C is disordered over two positions.

The unit cell consists of two crystallographically independent molecules of β -CyD (Figure 1, B and D), the first accommodating molecule of **5** (Figure 1, A) with approximately 25% occupancy, and the second molecule of **5** (Figure 1, C) with approximately 50% occupancy which is disordered over two positions with site occupation factors 0.5 : 0.5.

5.3.3 Theoretical Study of the Adamantane Azides

Gas phase geometries of the **1** and **5** were optimized by Density Functional Theory (DFT) (Figure 2A and Figure 3).

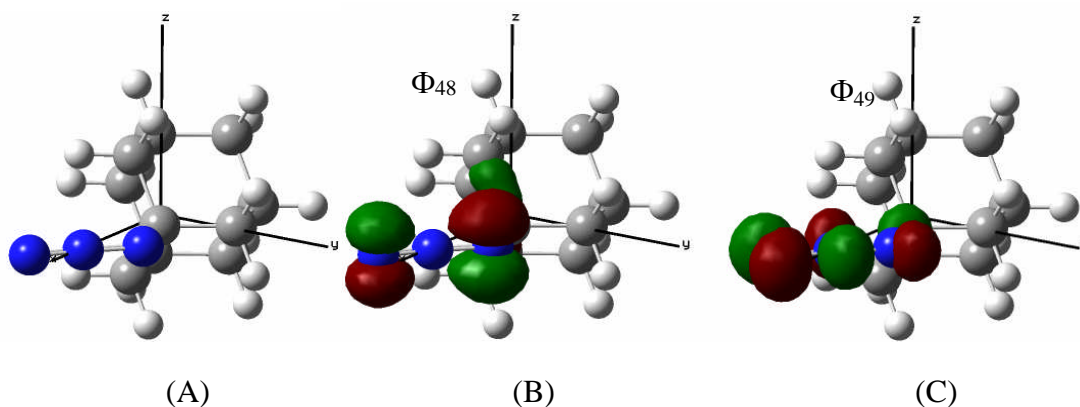


Figure 2. (A) B3LYP/6-31G(d) optimized geometry of **1**; (B) HOMO, (C) LUMO orbitals involved in the TD/B3LYP/6-31G(d) calculated transition at 283 nm based on B3LYP/6-31G(d) optimized geometry (Isosurface value 0.07).

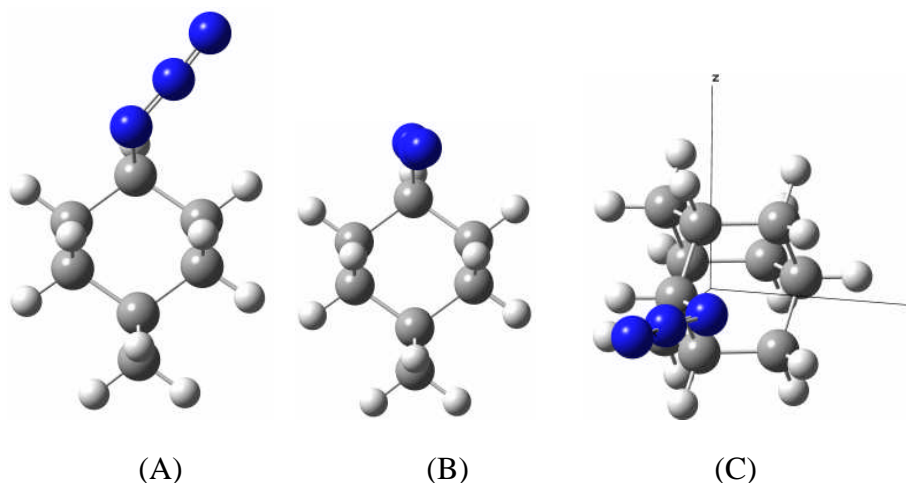


Figure 3. B3LYP/6-31G(d) Optimized geometries of **5**. (A) and (B) ground state geometric conformers. (C) C_s symmetric transition state between the two enantiomeric conformers of (A).

Becke's⁹ three-parameter hybrid method and the exchange functional of Lee, Yang, and Parr (B3LYP)¹⁰ with the 6-31G(d) basic set were used. The aim of geometry optimization was on one side the correlation with the X-ray structure (Figure 1). On the other side, single point calculations of UV-VIS spectra were calculated subsequently in order to obtain information about the transition dipole moment vectors necessary for the ICD spectra interpretation. These single electron vertical transitions of **1** and **5** were computed by two methods – single excitation configuration interaction (CIS)¹¹ and time-dependent DFT (TD)¹² (Table 2 and Table 3, respectively).

⁹ Becke, A. D. *J. Chem. Phys.* **1993**, 98, 5648.

¹⁰ Lee, C.; Yang, W.; Parr, R. G. *Phys. Rev. B* **1988**, 37, 785.

¹¹ Foresman, J. B.; Head-Gordon, M.; Pople, J. A.; Frisch, M. J. *J. Phys. Chem.* **1992**, 96, 135.

¹² Casida, M. E.; Jamorski, C.; Casida, K. C.; Salahub, D. R. *J. Chem. Phys.* **1998**, 108, 4439.

Method	Transit. Energy	Orbitals Involved	Orbital Coeff.	Oscillatory strength	Transition dipole moment components		
	λ [nm]				x	y	z
CIS	281	28 \rightarrow 49	-0.10531	0.0001	-0.0002	0.0004	-0.0249
		40 \rightarrow 49	0.10877				
		46 \rightarrow 49	-0.13772				
		48 \rightarrow 49	0.64961				
		48 \rightarrow 51	0.11208				
TD	283	48 \rightarrow 49	0.68405	0.0000	-0.0005	0.0001	-0.0205

Table 2. CIS(fc)/6-31G(d) and TD/B3LYP/6-31G(d) vertical transitions for **1** at the B3LYP/6-31G(d) ground-state optimized geometry (Figure 2). Only the highest wavelength transition is shown.

Method	Transit. Energy	Orbitals Involved	Orbital Coeff.	Oscillatory strength	Transition dipole moment components		
	λ [nm]				x	y	z
CIS	280	27 \rightarrow 49	-0.10677	0.0001	0.0000	0.0000	-0.0229
		40 \rightarrow 49	0.13669				
		45 \rightarrow 49	-0.15303				
		48 \rightarrow 49	0.63976				
		48 \rightarrow 51	0.12317				
TD	283	48 \rightarrow 49	0.68331	0.0000	0.0000	0.0000	-0.0194

Table 3. CIS(fc)/6-31G(d) and TD/B3LYP/6-31G(d) vertical transitions for **5** at the B3LYP/6-31G(d) transition-state optimized geometry (Figure 3, C). Only the highest wavelength transition is shown.

The single point calculations of **5** (Table 3) were performed on its C_s symmetric geometry (Figure 3, C), because this is the time-averaged geometry experienced in solution. It means, due to the quick flipping of the azide group between the two enantiomeric conformers of A (Figure 3) the molecule renders achiral.

5.3.4 Determination of Association Constants Based on ICD

The strength of the adamantane azides (**1** and **5**) - (α - and β -) cyclodextrin complexes were investigated by means of Induced Circular Dichroism in aqueous – ethanolic solutions at 293 K. Complexation of **1** by β -CyD produced a negative sign of the ICD with the minimum at 285 nm (Figure 4).

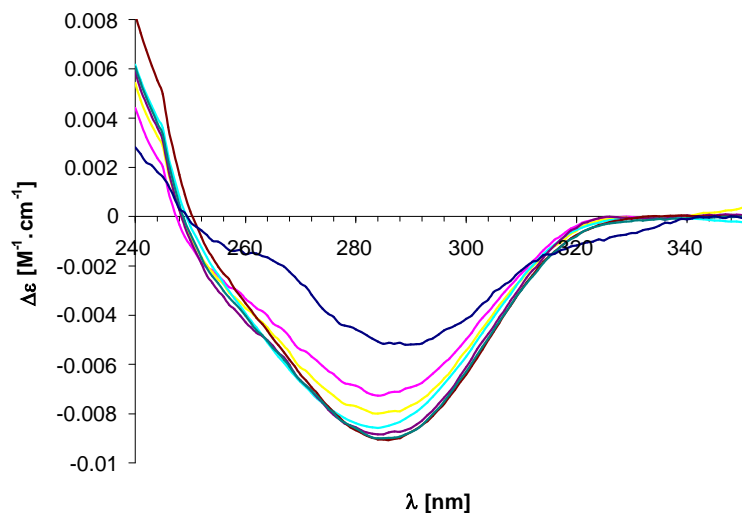


Figure 4. ICD of **1** by complex formation with β -CyD in water with 20% v/v ethanol at 293 K. The observed concentration dependencies were utilized to elucidate the types of complexes formed and to determine the corresponding association constants.

Evaluation of the data was conducted by utilizing the iterative Scatchard plot assuming a 1:1 stoichiometry (Figure 5).^{13,14}

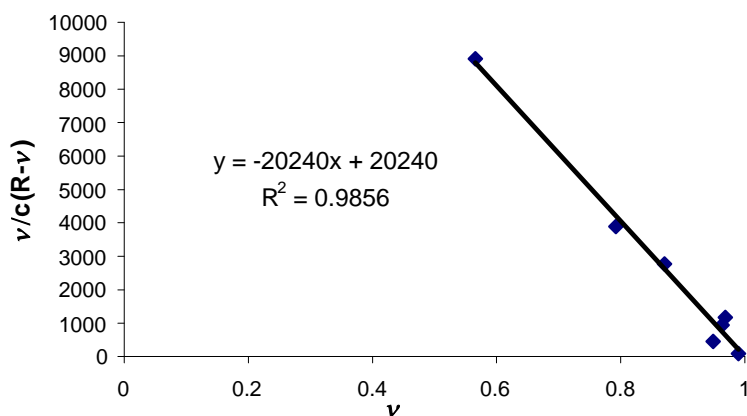


Figure 5. Scatchard plot for the determination of K_a of the **1**@ β -CyD in EtOH / H₂O = 80/ 20 (v/v) at 293K. $K_a(\mathbf{1}@\beta\text{-CyD}) = 20240 \pm 1000 \text{ M}^{-1}$.

ICD of the **5**@ β -CyD afforded a negative sign of the peak at 285 nm as well (Figure 6).

¹³ Krois, D.; Brinker, U.H. *J. Am. Chem. Soc.* **1998**, *120*, 11627.

¹⁴ Bobek, M.M.; Krois, D.; Brinker, U.H. *Org. Lett.* **2000**, *2*, 1999.

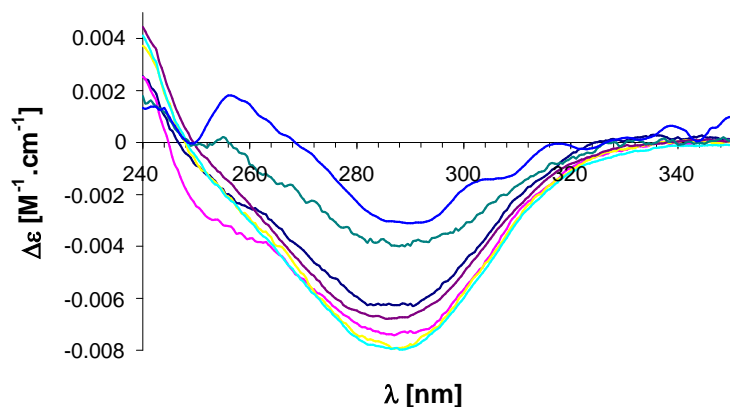


Figure 6. ICD of **5** by complex formation with β -CyD in water with 20% v/v ethanol at 293 K. The observed concentration dependencies were utilized to elucidate the types of complexes formed and to determine the corresponding association constants.

Data treatment by an iterative Scatchard plot lead to the K_a determination (Figure 7).

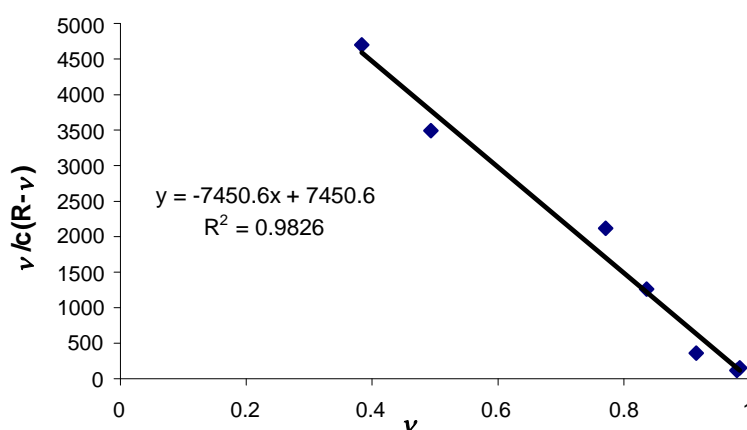


Figure 7. Scatchard plot for the determination of association constant of the **5**@ β -CyD in EtOH / H₂O = 80/ 20 (v/v) at 293K. $K_a(\mathbf{5}@\beta\text{-CyD}) = 7450 \pm 400 \text{ M}^{-1}$.

Induced circular dichroism of **1** by complex formation with α -CyD produced two bands – a positive peak with a maximum at 283 nm and a negative peak with a minimum at 317 nm (Figure 8).

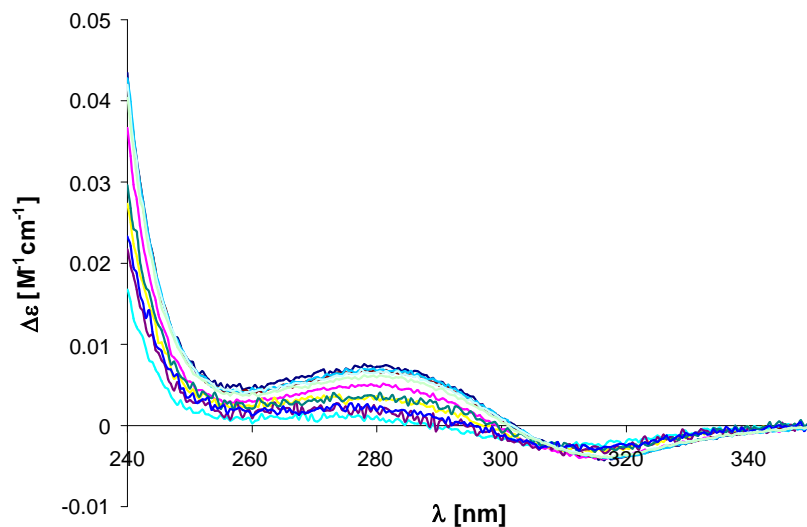


Figure 8. ICD spectra of **1** by complex formation with α -CyD in water with 10% ethanol at 293 K.

The ICD spectra upon complex formation of **5** by α -CyD exhibited only a negative sign of peaks with a minimum at 285 nm (Figure 9).

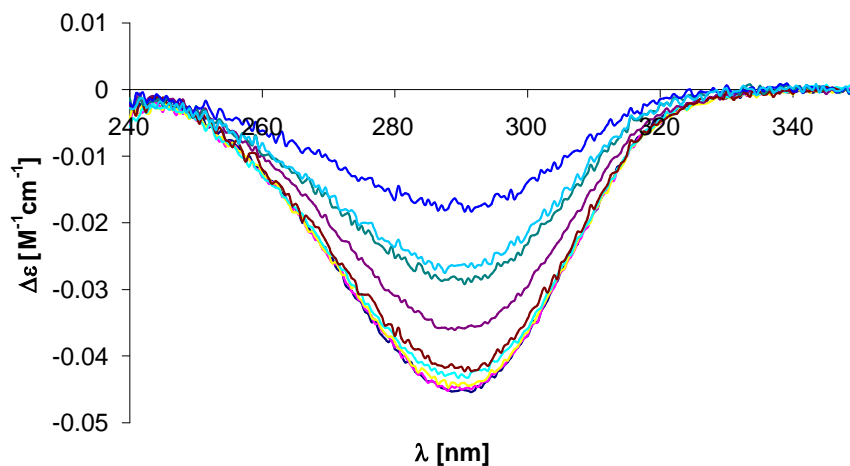
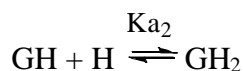
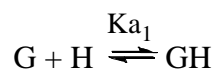


Figure 9. ICD spectra of **5** by complex formation with α -CyD in water with 10% ethanol at 293 K.

Treating the ICD spectral data of Figure 8 and Figure 9 by a Schatchard plot lead to a curved phenotype (not shown), indicating a higher stoichiometry. In our hands, solid 1:2 stoichiometric complexes of **1** and **5** with α -CyD were isolated (Table 1, Entries 3 and 7; see also supporting information). Thus the ICD data were treated by the model of a stepwise 1:1 and 1:2 binding, described as follows:



$$K_{a1} = \frac{[GH]}{[H][G]} \rightarrow [GH] = K_{a1}[G][H] \quad (1)$$

$$K_{a2} = \frac{[GH_2]}{[GH][H]} \rightarrow [GH_2] = K_{a2}[GH][H] \quad (2)$$

Rearranging of equations (1) and (2) lead to the cubic equation (3):

$$[H]^3 + \{2[G]_0 - [H]_0 + \frac{1}{K_{a2}}\}[H]^2 + \left\{\frac{[G]_0 - [H]_0 + 1/K_{a1}}{K_{a2}}\right\}[H] - \frac{[H]_0}{K_{a1}K_{a2}} = 0 \quad (3)$$

The equilibrium concentration [H] was solved analytically¹⁵ by the method of Tartaglia.¹⁶ Then, utilizing equations (1) and (2), theoretically calculated ICD spectra were obtained from equation (4):

$$\Delta\varepsilon = \frac{[GH]}{[G]_0} \Delta\varepsilon_{\max}(GH) + \frac{[GH_2]}{[G]_0} \Delta\varepsilon_{\max}(GH_2) \quad (4)$$

In a final step, the calculated ICD spectral data were fitted to the experimental ones, until the sum of their square differences (χ^2) reached a minimum. Since the Generalized Reduced Gradient algorithm¹⁷ in our hands landed in the false minima, we utilized the global optimization protocols “Genetic Algorithm and Simulated Annealing”.¹⁸ Each result obtained by this global protocol was further refined by the iterative gradient method.

The best global optimization fits of the ICD titration of α -CyD complexes are summarized in Table 4.

¹⁵ Al-Soufi, W.; Cabrer, P. R.; Jover, A.; Budal, R. M.; Tato, J. V. *Steroids* **2003**, *68*, 43.

¹⁶ Herbison-Evans, D. *Solving Quartics and Cubics for Graphics*. In: Paeth A, editor. Graphics Gems V, Academic Press, Chesnut Hill; **1995**, p. 3–15. Available on the WEB (<http://linus.socs.uts.edu.au/~don/pubs/solving.html>) as Technical Report TR94-487, Basser Department of Computer Science, University of Sydney, Australia.

¹⁷ Frontline Systems Inc., P.O. Box 4288, Incline Village, NV 89450, USA. The algorithm is included in MS Excel as the Solver Add-in.

¹⁸ Algorithms included in the program package OptWorks: Excel[®], Pi Blue Software, Inc., <http://www.piblue.com>.

Complex	K_{a1} [M ⁻¹]	K_{a2} [M ⁻¹]	$\Delta\varepsilon_{\max(1:1)}$ [M ⁻¹ cm ⁻¹]	$\Delta\varepsilon_{\max(1:1)}$ [M ⁻¹ cm ⁻¹]	χ^2
1 @(α -CyD) ₂	1 ± 0.4	21758 ± 3680	-0.4941 ± 0.0420	0.0093 ± 0.0002	1.30659x10 ⁻⁷
5 @(α -CyD) ₂	0.34 ± 0.08	2545035 ± 1317452	-34 ± 5	-0.0440 ± 0.0009	1.41633x10 ⁻⁵

Table 4. Best global fits of the ICD titration data for **1** and **5**@ α -CyD in EtOH/H₂O = 90/10 (v/v) at 293 K.

5.3.5 2D ROESY Spectra of Adamantane Azide – Cyclodextrin Complexes

The geometry of the complexes of **1** and **5** with β -CyD in D₂O solutions were inferred from 2D ROESY measurements conducted at 300 K (Figure 10 and Figure 11).

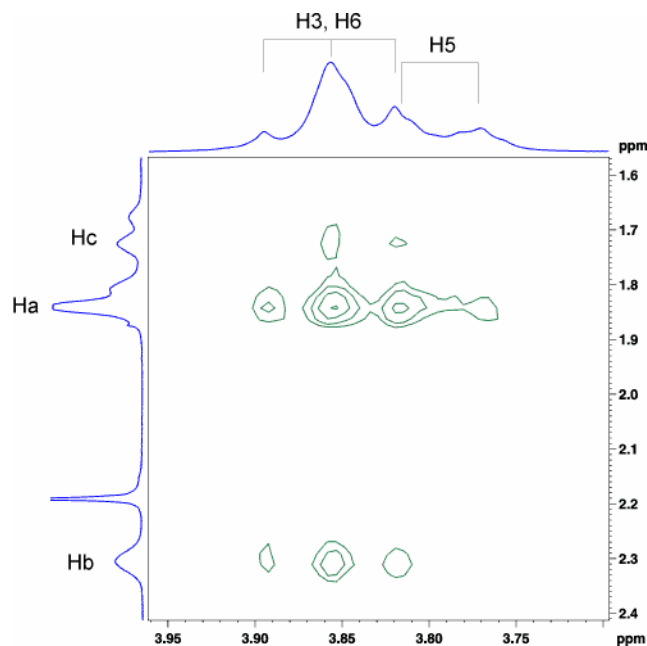


Figure 10. 250 MHz 2D ROESY spectra of **1**@ β -CyD in D₂O. Mixing time 600 ms.

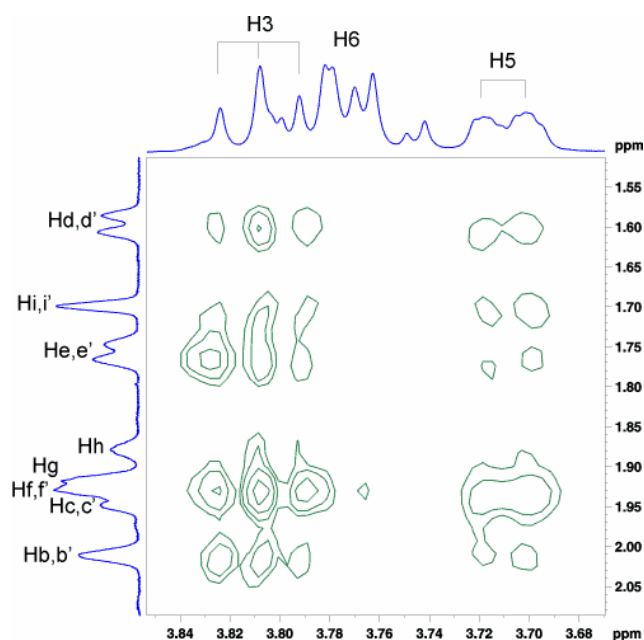


Figure 11. 600 MHz 2D ROESY spectra of **5**@ β -CyD in D₂O. Mixing time 300 ms.

5.4 Discussion

5.4.1 Chemistry of the Adamantane Azide – Cyclodextrin Complexes

The photolysis of **1** in the solid state or in an alkane solvent afforded 1,3-diazetidene **3** via the unstable bridgehead imine **2** (Scheme 1 and Entries 1, 2 in Table 1).⁷

However, upon photolysis of the solid **1**@ β -CyD or **1**@(α -CyD)₂ complexes, 4-azahomoadamantan-3-ol (**3**) was formed as a sole product. Hence, the use of cyclodextrins has altered significantly the reaction pathway of the nitrene intermediate generated from **1** inside the host cavity. The ensuing nitrene lacks the ability of interacting with other nitrenes or their precursors. Instead, in a first stage intermediate **2** is formed, which due to the inclusion is not able to dimerise to **4**. Intermediate imine **2** reacts with in cyclodextrin co-entrapped water molecules and affords 4-azahomoadamantan-3-ol (**3**) as the sole product in high yield. We have to note that photolysis of **1** in aqueous alcohols leads to the formation of **3** as well.⁷

In contrast, for **5**, the use of α - and β - cyclodextrins does not change the reaction pathway of the nitrene: **6** and **7** are formed in a similar ratio as in classical solution chemistry (Scheme 2 and Entries 5-8 in Table 1).

ESI MS and HPLC analyses of the CyD fraction upon the photodecomposition of **1**- and **5**@CyD ICs have clearly proved *no* formation of modified CyDs. Consequently, there is no covalent interaction between the azide and concomitantly the corresponding nitrene and its host molecule. This is in stark contrast to the

decomposition conducted with the aziadamantane - α -CyD inclusion complex, where a chemospecific insertion of adamantanylidene into the CyD's C-3-OH and C-2-OH bonds takes place.¹⁹

5.4.2 Single Crystal Structure of the 2-Adamantane Azide@ β -Cyclodextrin Complex

The cyclodextrin molecules in the crystal form channels with the dimers arranged in a head-to-head type (Figure 1, for details see the *.cif file in the Supporting Information). The guest molecule A is entrapped between the upper apertures (heads) of cyclodextrins D and B, which are mutually oriented head-to-head. The azido group of A penetrates deeply into the cavity of B. On the other hand, the disordered guest C is not really included, only physically entrapped between B and D, which are in this case tail-to-tail oriented, e.g., the adamantane scaffold of C is located in the bottom aperture (tail) of the D-cyclodextrin.

According to DFT calculations, **5** can exist in two geometric minima (Figure 3, A and B) with A being 3 kcal.mol⁻¹ more stable than B. In the **5**@ β -CyD single crystal, the guest takes only the more stable conformation A. The crystal packing energy is apparently not sufficient to force the azide group to bent and thus to exist in conformation B in the cavity of β -CyD.

5.4.3 Theoretical Study of Adamantane Azides

For both investigated adamantane azides, only one electronic transition above 220 nm was found by both methods with the maxima at around 280 nm, independently on the size of configuration interaction (other transitions are not shown) (Table 2 and Table 3).

As illustrated in the case of **1** (Figure 2, B and C), the orbitals involved in the 283 nm transition (Table 2, TD method) are of $\pi_z - \pi_y^*$ nature. This TD calculation corroborates the former finding of a “perpendicular” $\pi_y - \pi_x^*$ transition in alkyl azides and azoimide.²⁰ As inferred from the transition dipole moment components shown in Table 2 and Table 3, the transitions around 280 nm are *z* polarized (perpendicularly to the plane (C-N-N), where the azide group is positioned) for both investigated geometries of **1** and **5**. Both methods – CIS and TD afforded similar results in terms of transition dipole moment vectors and energy of the $\pi_z - \pi_y^*$ transition.

¹⁹ Krois, D.; Bobek, M.M.; Werner, A.; Kählig, H.; Brinker, U.H. *Org. Lett.* **2000**, *2*, 315.

²⁰ Closson, W. D.; Gray, H. B. *J. Am. Chem. Soc.* **1963**, *85*, 290. The arbitrary designation of π orbitals in terms of reference axes x, y, z in our system are y, z, x, respectively.

5.4.4 Determination of Association Constants Based on ICD

The Scatchard plot linearity of both adamantane azides - β -CyD complexes indicates a 1:1 stoichiometry (Figure 5 and Figure 7). The higher value of the association constant K_a ($\mathbf{1}@\beta\text{-CyD}$) = $20240 \pm 1000 \text{ M}^{-1}$ reveals that $\mathbf{1}$ is accommodated more tightly in the host cavity than $\mathbf{5}$; $K_a(\mathbf{5}@\beta\text{-CyD}) = 7450 \pm 400 \text{ M}^{-1}$. The signs of the ICD Cotton effect for $\mathbf{1}$ - and $\mathbf{4}@\beta\text{-CyD}$ are both negative.

For the $\mathbf{1}@(\alpha\text{-CyD})_2$ complex, the first step in the binding process is practically negligible ($K_{a1} = 1 \text{ M}^{-1}$) and only the second one is dominating ($K_{a2} = 21758 \text{ M}^{-1}$) (Table 4). This may be an indication of cooperative binding,²¹ which for example has been described for the binding of 4-biphenyl carboxylate to α -CyD.²² The ICD spectra are split to two bands – one with the maximum at 283 nm and the second one trough at 317 nm (Figure 8). Together with the isodichroic point at 306 nm, this is an indication of the presence of two species – the 1:1 and 1:2 complexes. The first - step 1:1 complex contributes to the ICD spectra by a negative sign ($\Delta\varepsilon_{\max(1:1)} = -0.4941 \text{ M}^{-1} \text{ cm}^{-1}$ in Table 4) and the 1:2 complex by a positive ICD sign ($\Delta\varepsilon_{\max(1:1)} = 0.0093 \text{ M}^{-1} \text{ cm}^{-1}$ in Table 4).

The circular dichroism spectra of inherently chiral azides have already been reported.²³ To the best of our knowledge, the maximal ever-reported absolute value of $\Delta\varepsilon = 2.27 \text{ M}^{-1} \text{ cm}^{-1}$ has been found so far for iodo-substituted azidocholestane.^{23b} The very high K_{a2} and $\Delta\varepsilon_{\max(1:1)}$ absolute values for the $\mathbf{5}@(\alpha\text{-CyD})_2$ apparently do not have a physical sense, since the $\Delta\varepsilon_{\max(1:1)}$ exceeds the highest known value of a chiral azide by a factor of 15. Moreover, the Kuhn anisotropy factor of $g = \Delta\varepsilon/\varepsilon$ usually does not exceed the value of 0.0300, whereas a $g = 1.4$ for the $\mathbf{5}@\alpha\text{-CyD}$ complex was found.

The determinations of thermodynamic parameters for multiple equilibria require a covering of a wide range of host's and guest's concentrations.²¹ The low solubility of the $\mathbf{5}@(\alpha\text{-CyD})_2$ complex and its components might have been precluding satisfaction of this condition and thus obtaining unrealistic thermodynamic parameters. Moreover, low intensity of the 280 nm band ($\varepsilon = 25 \text{ M}^{-1} \text{ cm}^{-1}$) in adamantane azides makes any determination by ICD difficult. Despite this complication, the following can be inferred from the curve-fitting procedure with high probability: aside from the extreme high absolute values, the small K_{a1} and high K_{a2} may signalize cooperative binding as well. For both investigated 1:2 stoichiometric inclusion complexes, the first binding step forming a 1:1 stoichiometric complex contributes by negative values of $\Delta\varepsilon_{\max(1:1)}$ (Table 4). The second binding step affording the 1:2 stoichiometric $\mathbf{5}@(\alpha\text{-CyD})_2$ complex generates a negative contribution to the overall ICD spectrum (Figure 9), whereas a positive value of

²¹ Connors, K. A. *Binding Constants: The Measurement of Molecular Complex Stability*, Wiley: New York, **1987**.

²² Gelb, R. I.; Schwartz, L. M.; Murray, C. T.; Laufer, D. A. *J. Am. Chem. Soc.* **1978**, *100*, 3553.

²³ (a) Levene, P. A.; Rothen, A. *J. Chem. Phys.* **1937**, *5*, 985. (b) Djerassi, C.; Moscowitz, A.; Ponsold, K.; Steiner, G. *J. Am. Chem. Soc.* **1967**, *89*, 347. (c) Paulsen, H. *Chem. Ber.* **1968**, *101*, 1571. (d) Dunstan, D. R.; Mose, W. P.; Scopes, P. M. *J. Chem. Soc. Perkin Trans. 1*, **1973**, *22*, 2749. (e) Paulsen, H.; Györgydeák, Z.; Friedmann, M. *Chem. Ber.* **1974**, *107*, 1568. (f) Fisher, A.; Morse, E.; Romer, B.; You, T-P.; Mosher, C. W.; Mosher, H. S. *Tetrahedron* **1992**, *48*, 2993. (g) Praly, J-P.; Stefèfano, C. D.; Somsák, L.; Hollósi, M.; Majer, Z.; Voelter, W. *Tetrahedron: Asymmetry* **1999**, *10*, 901.

$\Delta\varepsilon_{\max(1:2)}$ has been found for the $1@(\alpha\text{-CyD})_2$ complex. Apparently, the geometrical pathway of the stepwise inclusion processes of both studied complexes differs.

5.4.5 2D ROESY Spectra of the Adamantane Azide – Cyclodextrin Complexes

2D ROESY spectra of adamantane azides showed cross-peaks with the inner β -CyD protons H3 and H5 (Figure 10 and Figure 11) indicating a real inclusion phenomena. The technique allowed a straightforward suggestion of the $1@ \beta$ -CyD complex geometry (Figure 12).

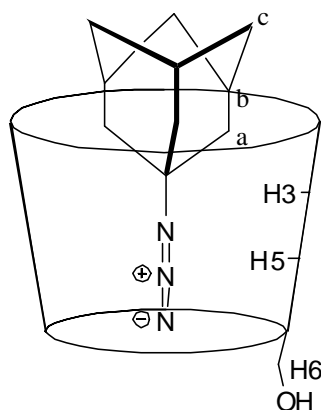


Figure 12. Proposed geometry of the $1@ \beta$ -CyD complex in D_2O based on 2D ROESY measurements.

The adamantane scaffold is located above the host cavity and the azide group penetrates deeply into the β -CyD cavity. *Harata's* rule predicts a negative ICD when the transition dipole moment of the guest chromophore is aligned perpendicular to the principal axis of the CyD cavity.²⁴ This rule was developed on the base of aromatic π - π^* transitions and was later validated for the d-d transitions of ferrocenes,²⁵ n- π^* transition of: diazine chromophore,¹⁴ azoalkanes,²⁶ conjugated alkyl ketones,²⁷ π - π^* transitions of the azo-group in azodyes,²⁸ and here it is being applied on the azide π_z – π_y^* transition.²⁰ Thus, based on the geometry depicted in Figure 12, the azide chromophore should produce a negative ICD band, since the transition dipole moment vector of its 285 nm band is perpendicularly oriented to the C-N-N bond of the azide group (Table 2). Negative ICD bands with the minimum at 285 nm were really observed (Figure 4) and hence, the geometry proposed on the base of the 2D ROESY technique correlates well with the ICD spectra signs.

²⁴ Harata, K.; Uedaira, H. *Bull. Chem. Soc. Jpn.* **1975**, *48*, 375.

²⁵ (a) Harada, A.; Takahashi, S. *Chem. Lett.* **1984**, 2089. (b) Harada, A.; Hu, Y.; Yamamoto, S.; Takahashi, S. *J. Chem. Soc. Dalton Trans.* **1988**, 729. (c) Sokolov, V. I.; Bondareva, V. L.; Golovaneva, I. F. *J. Organomet. Chem.* **1988**, *358*, 401. (d) idem. *Metalloorganicheskaya Khimiya* **1988**, *1*, 716. (English Translation in: *Organomet. Chem. USSR.* **1988**, *1*, 400.). (e) Kobayashi, N.; Opallo, M. *J. Chem. Soc., Chem. Commun.* **1990**, 477.

²⁶ Bakirci, H.; Zhang, X.; Nau, W. *M. J. Org. Chem.* **2005**, *70*, 39 and citations therein.

²⁷ Bonora, G. M.; Fornansier, R.; Scrimin, P.; Tonellato, U. *Carbohydr. Res.* **1986**, *147*, 205.

²⁸ (a) Suzuki, M.; Kajtar, M.; Szejtli, J.; Vikmon, M.; Fenyvesi, E.; Szente, L. *Carbohydr. Res.* **1991**, *214*, 25. (b) Liu, Y.; Zhao, Y-L.; Zhang, H-Y.; Fan, Z.; Wen, G-D.; Ding, F. *J. Phys. Chem. B* **2004**, *108*, 8836.

Interpretation of the 2D ROESY spectra (Figure 11) of **5**@ β -CyD did not lead to the proposal of a single geometry of the complex. Two possible orientations (Figure 13) of the guest molecule would account for the observed cross-signals in the 2D ROESY spectrum (Figure 11).

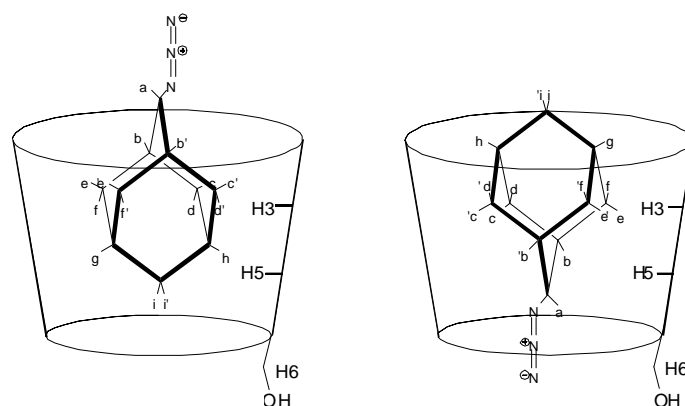


Figure 13. Proposed geometries of **5**@ β -CyD in D₂O based on 2D ROESY measurements.

Due to this bimodal inclusion mode,²⁹ the interpretation of the negative ICD peaks of the **5**@ β -CyD complex would be a complex task.³⁰

5.5 Conclusion

The product distribution from the photolysis of **1** and **5** included in a CyD cavity was investigated with the aim to gain insight into the influence of supramolecular encapsulation on the reaction pathway of reactive species such as adamantyl nitrene. Upon photolysis of the **1**@CyD complexes, only **3** was formed as a sole product. This altering of the reaction pathway is ascribed to classical solution chemistry, that is, to the addition of a water molecule to the formed bridge-head imine **2**, which takes place inside the CyD cavity. The supramolecular encapsulation of **5**, on the other hand, did not alter the reaction pathway of the concomitant nitrene at all.

For the first time, the ICD of the azide group chromophore has been described here. This ICD was utilized for the determination of association constants of inclusion complexes and for the interpretation of their geometry, in connection with the 2D ROESY NMR studies. In H₂O/ EtOH = 8/2, **1** is bound stronger to β -CyD than **5**. The first binding step to form a 1:1 stoichiometric **1**@ α -CyD complex is negligible and due to the cooperative binding only the 1:2 complex is present in a H₂O/EtOH = 9/1 solvent system. Theoretical calculations afforded the orientation of the transition dipole moment vector of the π_z - π_y^* transition of the azide group chromophore. Subsequently, Harata's rule was applied on the geometry of the **1**@ β -CyD complex proposed by the 2D ROESY technique and a good matching of experimental and predicted ICD sign was found. A generalization of this symmetry rule applicability on

²⁹ Dodziuk, H. Ed., *Cyclodextrins and Their Complexes: Chemistry, Analytical Methods, Applications*. Wiley: New York, **2006**.

³⁰ For calculations of ICD spectra and subsequent correlations with ICD see for example: (a) Marconi, G.; Mayer, B. *Pure Appl. Chem.* **1997**, *69*, 779. (b) Mayer, B.; Zhang, X.; Nau, W. M.; Marconi, G. *J. Am. Chem. Soc.* **2001**, *123*, 5240.

the transitions of the azide group chromophore would however require further extensive and complex analyses. Finally, the investigation of the **5**@ β -CyD complex structure showed that **5** experiences a bimodal disposition within the cavity of β -CyD, as determined by 2D ROESY and X-ray single crystal analysis.

5.6 Experimental Section

(Supporting Information)

General Remarks

Cyclodextrins, (+)-Camphor, and adamantanone (**8**) were purchased from commercial sources. Other substances were prepared according to literature: 1-adamantane azide (**1**)³¹, 4-azahomoadamantan-3-ol (**3**)³¹, 4-azahomoadamant-3-ene dimer (**4**)³², 2-adamantane azide (**5**)³³, 4-azahomoadamant-4-ene (**6**).³⁴ Water was highly purified using a Milli-Q system (Millipore®). Methanol p.a. for HPLC analyses was used. Spectral grade ethanol was used for ICD studies.

NMR spectra were recorded on either a Bruker Avance DPX 250, 400 MHz or 600 MHz spectrometers. The attributions of the shifted protons in the 2D ROESY spectra was secured by the consecutive recording of COSY, HMQC, and HMBC spectra.

ESI-MS Spectra were recorded in positive mode on a Bruker Daltonics HTC Plus, ESI-ion trap. The concentration of the CyD samples were ca. 0.1 mg/ mL. With the solvent system consisting of H₂O/isopropanol/CH₃CN = 1.6/1/0.4, a reproducible and stable measurement was achieved.

Analytical RP-HPLC analysis was performed using a HP1090 instrument equipped with RI-detector HP1047 and interface 35900E (Agilent). The instrument was equipped with an auto-injector and was run with the HP ChemStation (Rev. A.08.03; 2000) software.

LC-MS was performed using a HP1100 System (Agilent) on a Zorbax Eclipse XDB-C8 column (150 x 4.6 mm, 5 μ m) at 25°C with 0.8 mL/min flow of isocratic elution with H₂O/CH₃OH =9/1 (v/v). The MS detector was a MDS Sciex API 365 triple-quadrupole MS (Applied Biosystems) with electrospray ionization (flowing rate 5 mL/min; passive split).

GC-MS qualitative analyses were conducted using a Hewlett-Packard 6890 series GC outfitted with a 30 m poly(methylphenylsiloxane) capillary column (Hewlett-Packard, HP-5MS {95% diMe and 5% diPh}, 0.25 mm i.d., and 0.25 μ m film-thickness) and a Hewlett-Packard 5973 MSD; a Hewlett-Packard 59864B ionization gauge controller was used for chemical ionization studies.

GC-FID quantitative analyses were performed on a GC 8160 instrument (Fisons) using a PE-1 column (Perkin Elmer, 30 m, i.d. 0.32 mm, 0.25 μ m dimethylpolysiloxane film), "Chrom-Card" software (Fisons), and a flame-ionization detector. The flow rate of helium was held constant at 2.1 mL/min; oven program: 1

³¹ Sasaki, T.; Eguchi, S.; Katada, T. and Hiroaki, O. *J. Org. Chem.* **1977**, *42*, 3741.

³² Quast, H.; Eckert, P. *Liebigs Ann. Chem.* **1974**, 1727.

³³ Prakash, G. K. S.; Stephenson, M. A.; Shih, J. G.; Olah, G. A. *J. Org. Chem.* **1986**, *51*, 3215.

³⁴ Radziszewski, J. G.; Downing, J. W.; Jawdosiuk, M.; Kovacic, P.; Michl, J. *J. Am. Chem. Soc.* **1985**, *107*, 594.

min stand-by time, 5 min isothermal at 90°C, 8 °C / min to 250°C and 10 min isothermal at 250°C. Injector temperature 200 °C, split ratio of injector 1:14, injection volume 5 µL. Temperature of detector was 270 °C.

Determination of Association Constants by ICD titration

UV-VIS and CD spectra were recorded with a Perkin-Elmer Lambda 7 spectrometer and a CD6 circular dichrograph (I.S.A. Jobin-Yvon), respectively, in thermostated quartz cuvettes (10 cm path length). The ICD titration was done by the dilution technique and subsequently, an iterative Scatchard plot for the K_a determinations of 1:1 stoichiometric complexes of adamantane azides with β -CyD was used.³⁵ For the 1:2 stoichiometric complexes with α -CyD, four parameter curve fitting procedure was applied for the K_a determinations. Microsoft Excel was utilized for the evaluation of the data obtained from ICD measurements and for the determination of association constants. LINEST function was used for the assessing standard deviation of the linear Scatchard plot. For the non-linear regression, the standard deviation was calculated with the help of Excel Add-In “solvstat.xls”.³⁶ Table S 1 - Table S 4 show ICD titration data.

c(1) [M]	c(β -CyD) [M]	$\Delta\varepsilon$ at 285 nm [M ⁻¹ cm ⁻¹]
0.002	0.004	-0.00871
0.0001	0.00012	-0.00519
0.0005	0.00075	-0.00799
0.0005	0.0006	-0.00727
0.0005	0.0015	-0.00884
0.0008	0.0016	-0.00889
0.001	0.012	-0.00908

Table S 1. ICD titration data for K_a determination of the **1** – β -CyD complex.

³⁵ Krois, D.; Brinker, U.H. *J. Am. Chem. Soc.* **1998**, *120*, 11627.

³⁶ Billo, E. J. *Excel for Scientists and Engineers: Numerical Methods*. Wiley: New Jersey, 2007.

$c(\mathbf{5})$ [M]	$c(\beta\text{-CyD})$ [M]	$\Delta\varepsilon$ at 286 nm [$\text{M}^{-1}\text{cm}^{-1}$]
0.001	0.0015	-0.00678
0.0002	0.00024	-0.004
0.0001	0.00012	-0.00311
0.0005	0.00075	-0.00625
0.0005	0.003	-0.00742
0.0005	0.009	-0.00794
0.001	0.0075	-0.00798

Table S 2. ICD titration data for K_a determination of the $\mathbf{5} - \beta\text{-CyD}$ complex.

$c(\mathbf{1})$ [M]	$c(\alpha\text{-CyD})$ [M]	$\Delta\varepsilon$ at 290 nm [$\text{M}^{-1}\text{cm}^{-1}$]
1.00E-03	0.022	0.00728
1.00E-03	0.012	0.00493
5.00E-04	0.008	0.00334
5.00E-04	0.004	0.000784
5.00E-04	0.006	0.00205
2.00E-03	0.022	0.00684
2.00E-03	0.018	0.00654
2.00E-03	0.016	0.00602

Table S 3. ICD titration data for K_a determination of $\mathbf{1} - \alpha\text{-CyD}$ complex.

$c(\mathbf{5})$ [M]	$c(\alpha\text{-CyD})$ [M]	$\Delta\varepsilon$ at 290 nm [$\text{M}^{-1}\text{cm}^{-1}$]
5.00E-04	0.002	-0.0359
3.00E-04	0.003	-0.0417
3.00E-04	0.0015	-0.0284
3.00E-04	0.0009	-0.0177
3.00E-04	0.0012	-0.0266
5.00E-04	0.015	-0.045
5.00E-04	0.008	-0.045
5.00E-04	0.006	-0.044
5.00E-04	0.004	-0.0428

Table S 4. ICD titration data for K_a determination of the $\mathbf{5} - \alpha\text{-CyD}$ complex.

General Procedure for Preparation of Cyclodextrin Complexes

A saturated cyclodextrin solution (5 mol. equiv.) was placed into a high-walled beaker and adamantane azide in a small amounts of ether was added. The content of the beaker was magnetically stirred and simultaneously argon was bubbled via a needle for 8 h. In between the beaker was sonicated to disperse the organic azide and to protect against azide clumps formation. The procedure was done in a dark and the beaker was wrapped in aluminium foil. The white suspension was filtered via a synther filter of porosity # 4. The complex was dried at RT in a desiccator over CaCl₂ for 1 d at 0.5 mm Hg. The approximate stoichiometry was inferred from integrals of ¹H NMR spectra of complexes recorded in *d*₆-DMSO.³⁷ The exact stoichiometry was determined by elemental analysis based on a nitrogen content and are summarized in Table S 5.

Adamantane azide	CyD	Stoichiometry Azide/CyD	Yield (%)
1	α	1 / 2.27	90
	β	1 / 1.05	63
4	α	1 / 2.17	93
	β	1 / 1.04	76

Table S 5. Stoichiometries and yields of prepared solid adamantane azide - cyclodextrin complexes.

Photolyses of solid cyclodextrin complexes

100 to 300 mg of the solid complexes were weighted into a 250 mL round-bottomed Pyrex flask and dispersed over the whole inner surface. Utilizing manifold, the flask was evacuated and argon was let to flow through in three cycles. The flask was closed quickly with a septum pierced with two needles (one inlet for argon and one outlet). After a short flow of argon, the needles were removed and the septa wrapped with parafilm, then alufoil, and parafilm again to protect the septa against corrosion by ultraviolet light. The flask was clutched into clamp and the clamp fixed into a KPG – stirrer. The flask was immersed into a large ultrasonic bath with circulating tap water (16-24 °C). The photolyses of the complexes were conducted by placing a medium pressure mercury lamp (Heraeus TQ718-Z4, 700 W, doped with FeI₂, Duran® glass jacket) over the flask in a 10-20 cm distance. The photolyses took 1 – 2 d depending on the amount of complex used. During the photolysis, once and then, a short sonication was applied to redistribute the solid complex over the walls of the flask and so exposing a fresh surface of the complex towards the UV light. Consequently, full conversion was achieved within 1 to 2 d of irradiation.

Separation of low molecular weight adamantane derivatives from the cyclodextrins was performed by dissolving the solid in water (100 mL) and dichloromethane (50 mL) followed by continuous extraction with the appropriate apparatus (apparatus for extraction of liquids of higher density). After 24 h the dichloromethane was replaced by a new portion, thus giving a first fraction, and after

³⁷ In diluted DMSO solutions, the complex is totally dissociated and the proton spectrum can be seen as a sum of proton spectra of neat components.

48 h a second dichloromethane extract was collected. In this way one could account for the possible evaporation of some quite volatile products. These dichloromethane solutions were analyzed by GC-MS and the components were quantified by GC-FID calibrated by reference substances. (+)-Camphor was used as a internal standard.

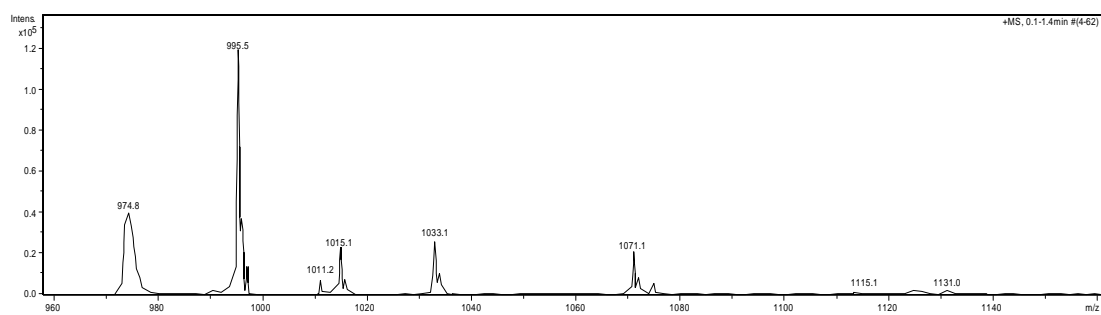
Table S 6 summarizes the GC-FID analytical data:

Compound	Retention time / min
(+)-Camphor	4.66
1	7.33
4	10.66
3	24.13
5	8.98
6	8.44
7	11.17

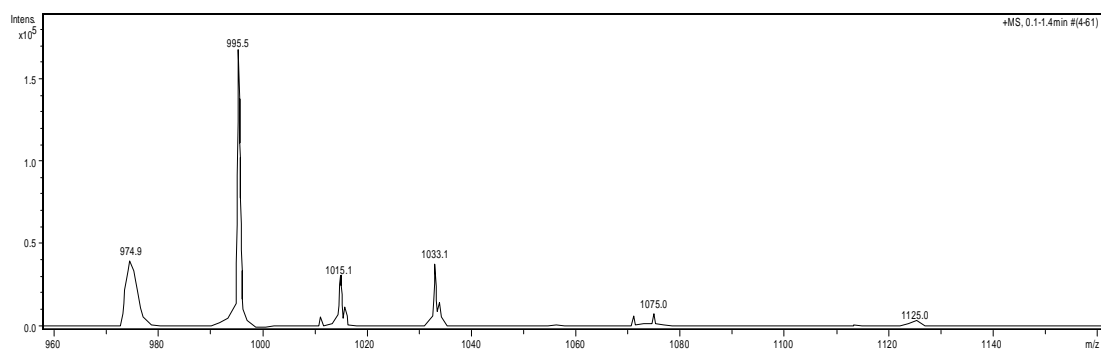
Table S 6. GC-FID retention times of **1**, **5**, and its photodecomposition products.

After continual extraction, water from the water phase was evaporated and analyzed for the presence of possible insertion or modification products formed by the reaction with adamantyl nitrene. All CyD fractions, exhibited identical ESI-MS spectra and proved to be pure α - or β -CyD (Figure S 1).

α -CyD (2):



hv of **1**@(α -CyD)₂:



hv of **5**@(α -CyD)₂:

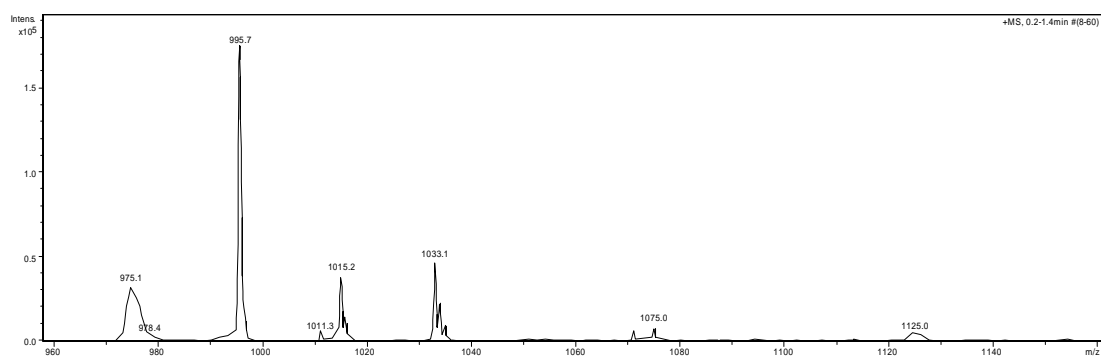
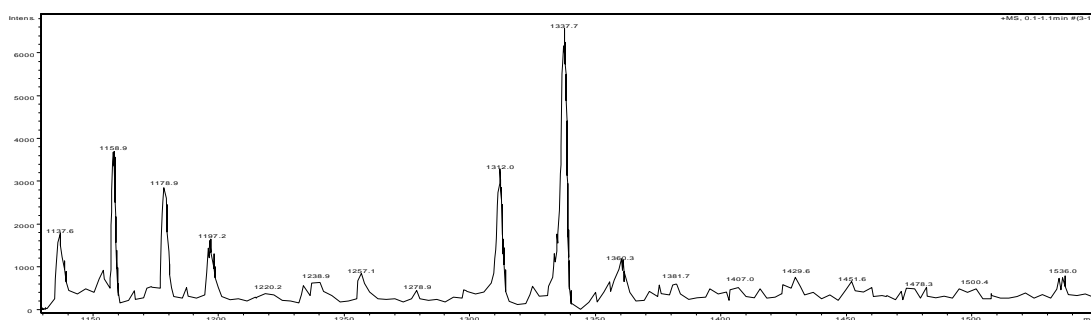
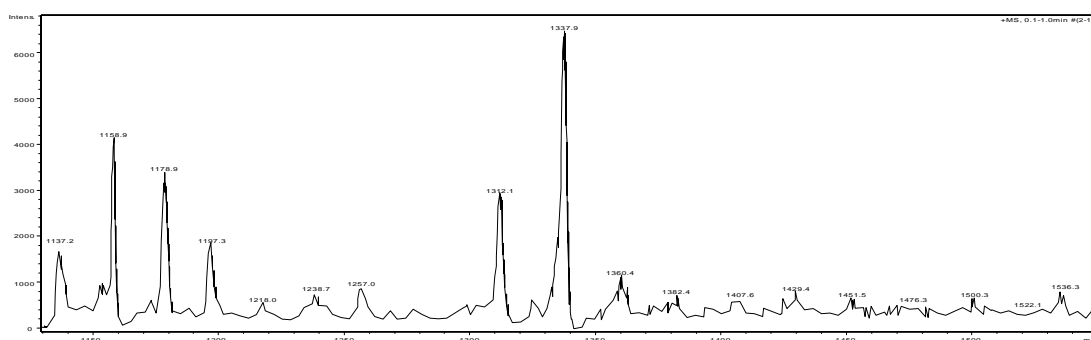


Figure S 1. ESI-MS spectra of α -, β -CyD, and the CyD fraction upon photolysis of their inclusion complexes with **1** and **5**.

β -CyD (2):



hv of **1**@ β -CyD:



hv of **5**@ β -CyD:

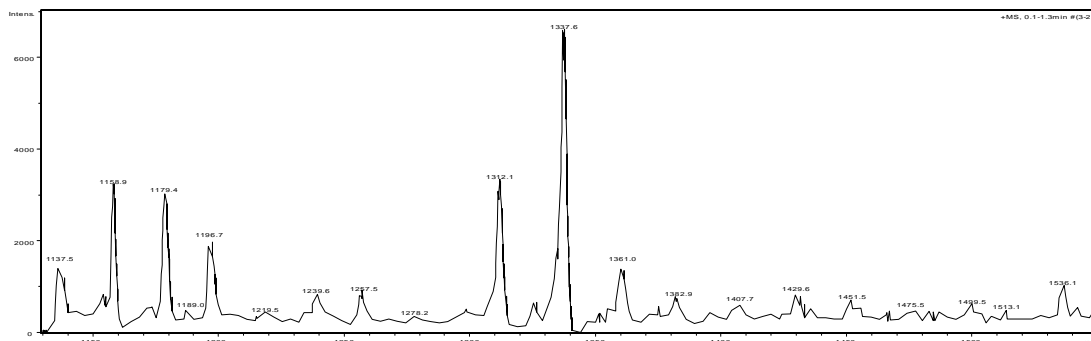


Figure S 1 (Continuation). ESI-MS spectra of α -, β -CyD, and the CyD fraction upon photolysis of their inclusion complexes with **1** and **5**.

The CyD fraction from the photolysis of adamantane azide - α -CyD complexes was analyzed by RP-HPLC as well as by LC-MS. From the latter analysis, no mass corresponding to sum of adamantyl nitrene and α -CyD masses or masses nearby were found.

According to the RP-HPLC-RI analysis, the CyD fractions from the photolysis of the adamantane azide - β -CyD complexes were found to be intact native β -CyD. The RP-HPLC retention characteristics of the CyD's we already described elsewhere.³⁸

X-Ray crystallographic analysis

X-ray diffraction measurements were performed on a Bruker X8 APEXII CCD diffractometer with graphite monochromated MoK α radiation, $\lambda = 0.71073 \text{ \AA}$ at 100(2) K. A single crystal was positioned at 50 mm from the detector and 1996 frames were measured, each for 30 s over 1° scan width. The data were processed using SAINT software.³⁹ The structure was solved by direct methods and refined by full-matrix least-squares techniques. Non-hydrogen atoms were refined with anisotropic displacement parameters, except those of partially populated 2-adamantane azide molecules, one component of the disordered hydroxyl group (O63X) and oxygen atoms of lattice water molecules, which are also partially populated and/or disordered. H atoms of β -cyclodextrin molecules were placed in geometrically calculated positions and refined as riding atoms in the subsequent least squares model refinements. The isotropic thermal parameters of located H atoms were estimated to be 1.2 times the values of the equivalent isotropic thermal parameters to which hydrogens were bound. Attempts to locate hydrogen atoms at water oxygen atoms O10, O11, O12 and O13 with s.o.f. 1.0 from a difference map failed. The positions of the hydrogen atoms of lattice water molecules have not been calculated. The location of 2-adamantane azide inside the first crystallographically independent molecule of β -cyclodextrin (occupancy 0.5 disordered over two positions) and inside the second β -cyclodextrin host molecule (occupancy 0.25) was possible by using restraints (DFIX at 1.50 \AA and SADI) for C-C and C-N bonds (within a standard deviation of 0.01 \AA). The following computer programs were used: structure solution, SHELXS-97,⁴⁰ refinement, SHELXS-97,⁴¹ molecular diagrams;⁴² Computer: Pentium IV; scattering factors were taken from the literature.⁴³ Details of crystal data, data collection and refinement are as follows:

Crystal data: C_{91.5}H_{194.25}N_{2.25}O_{91.5}, $M_r = 2790.24$, triclinic, $P1$, $a = 15.168(1)$, $b = 15.495(1)$, $c = 15.637(1) \text{ \AA}$, $\alpha = 87.555(3)$, $\beta = 81.938(2)$, $\gamma = 76.855(2)^\circ$, $V = 3543.2(5) \text{ \AA}^3$, $Z = 1$, $\mu(\text{MoK}\alpha) = 0.170 \text{ mm}^{-1}$, 89092 measured reflections, 16243 independent, $R_{\text{int}} = 0.056$, $R(F) = 0.0694$, $wR(F^2) = 0.2008$, Flack parameter 0(10).

³⁸ Walla, P.; Brecker, L.; Arion, V. B.; Brinker, U. H. in "Structure - Chemistry Relationship in Ferrocenyl Azide - Cyclodextrin Complexes", *manuscript in preparation*.

³⁹ Bruker Programs SAINT-NT, version 6.0; SAINT, version 7.12A; Bruker AXS: Madison, WI, USA, 2003.

⁴⁰ Sheldrick, G.M. SHELXS-97: *Program for Crystal Structure Solution*, University of Göttingen, Germany, 1997.

⁴¹ Sheldrick, G.M. SHELXL-97: *Program for Crystal Structure Refinement*, University of Göttingen, Germany, 1997.

⁴² Mercury, http://www.ccdc.cam.ac.uk/free_services/mercury.

⁴³ *International Tables for X-ray Crystallography*; Kluwer Academic Press, Dordrecht, The Netherlands, 1992, Vol. C, Tables 4.2.6.8 and 6.1.1.4.

Calculations

The calculations were done with Gaussian 03.⁴⁴ Becke's⁴⁵ three-parameter hybrid method and the exchange functional of Lee, Yang, and Parr (B3LYP)⁴⁶ with the 6-31G(d) basic set were used for the geometry optimizations and for the TD⁴⁷ vertical excitation calculations. Six singlet states were computed by the CIS⁴⁸ and TD methods.

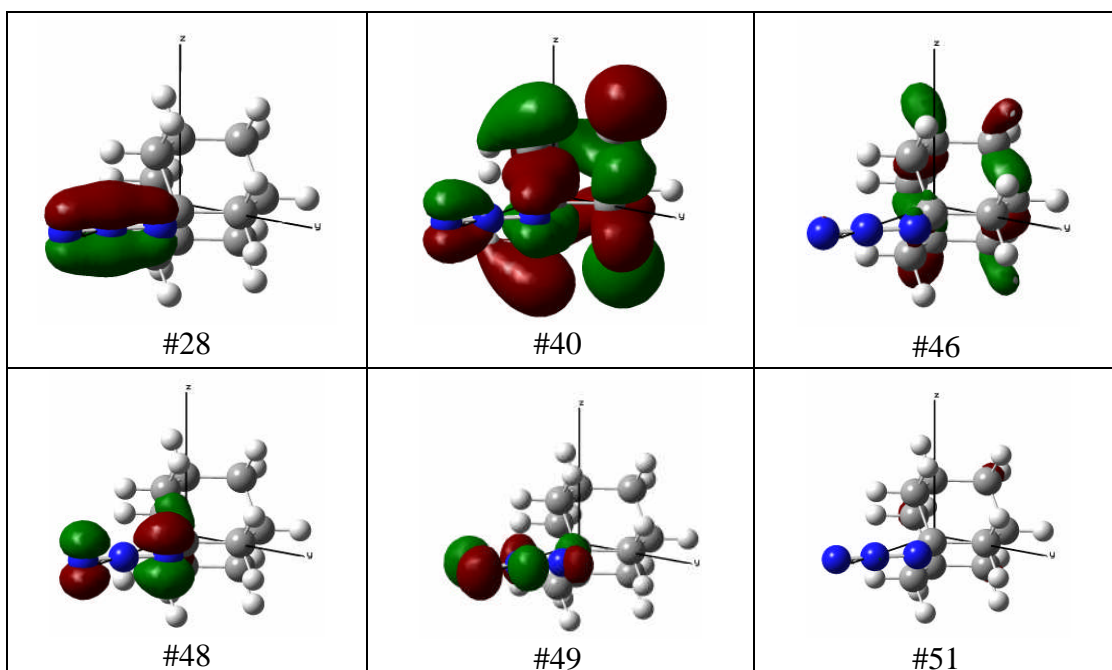


Figure S 2. Orbitals involved in the CIS/6-31G(d) calculated transition at 281 nm based on B3LYP/6-31G(d) optimized geometry of **1** (isosurface value = 0.07).

⁴⁴ Frisch, M. J.; Trucks, G. W.; Schlegel, H. B.; Scuseria, G. E.; Robb, M. A.; Cheeseman, J. R.; Montgomery, J. A., Jr.; Vreven, T.; Kudin, K. N.; Burant, J. C.; Millam, J. M.; Iyengar, S. S.; Tomasi, J.; Barone, V.; Mennucci, B.; Cossi, M.; Scalmani, G.; Rega, N.; Petersson, G. A.; Nakatsuji, H.; Hada, M.; Ehara, M.; Toyota, K.; Fukuda, R.; Hasegawa, J.; Ishida, M.; Nakajima, T.; Honda, Y.; Kitao, O.; Nakai, H.; Klene, M.; Li, X.; Knox, J. E.; Hratchian, H. P.; Cross, J. B.; Bakken, V.; Adamo, C.; Jaramillo, J.; Gomperts, R.; Stratmann, R. E.; Yazyev, O.; Austin, A. J.; Cammi, R.; Pomelli, C.; Ochterski, J. W.; Ayala, P. Y.; Morokuma, K.; Voth, G. A.; Salvador, P.; Dannenberg, J. J.; Zakrzewski, V. G.; Dapprich, S.; Daniels, A. D.; Strain, M. C.; Farkas, O.; Malick, D. K.; Rabuck, A. D.; Raghavachari, K.; Foresman, J. B.; Ortiz, J. V.; Cui, Q.; Baboul, A. G.; Clifford, S.; Cioslowski, J.; Stefanov, B. B.; Liu, G.; Liashenko, A.; Piskorz, P.; Komaromi, I.; Martin, R. L.; Fox, D. J.; Keith, T.; Al-Laham, M. A.; Peng, C. Y.; Nanayakkara, A.; Challacombe, M.; Gill, P. M. W.; Johnson, B.; Chen, W.; Wong, M. W.; Gonzalez, C.; Pople, J. A. *Gaussian 03, revision C.02*; Gaussian, Inc.: Wallingford, CT, 2004.

⁴⁵ Becke, A. D. *J. Chem. Phys.* **1993**, *98*, 5648.

⁴⁶ Lee, C.; Yang, W.; Parr, R. G. *Phys. Rev. B* **1988**, *37*, 785.

⁴⁷ Casida, M. E.; Jamorski, C.; Casida, K. C.; Salahub, D. R. *J. Chem. Phys.* **1998**, *108*, 4439.

⁴⁸ Foresman, J. B.; Head-Gordon, M.; Pople, J. A.; Frisch, M. J. *J. Phys. Chem.* **1992**, *96*, 135.

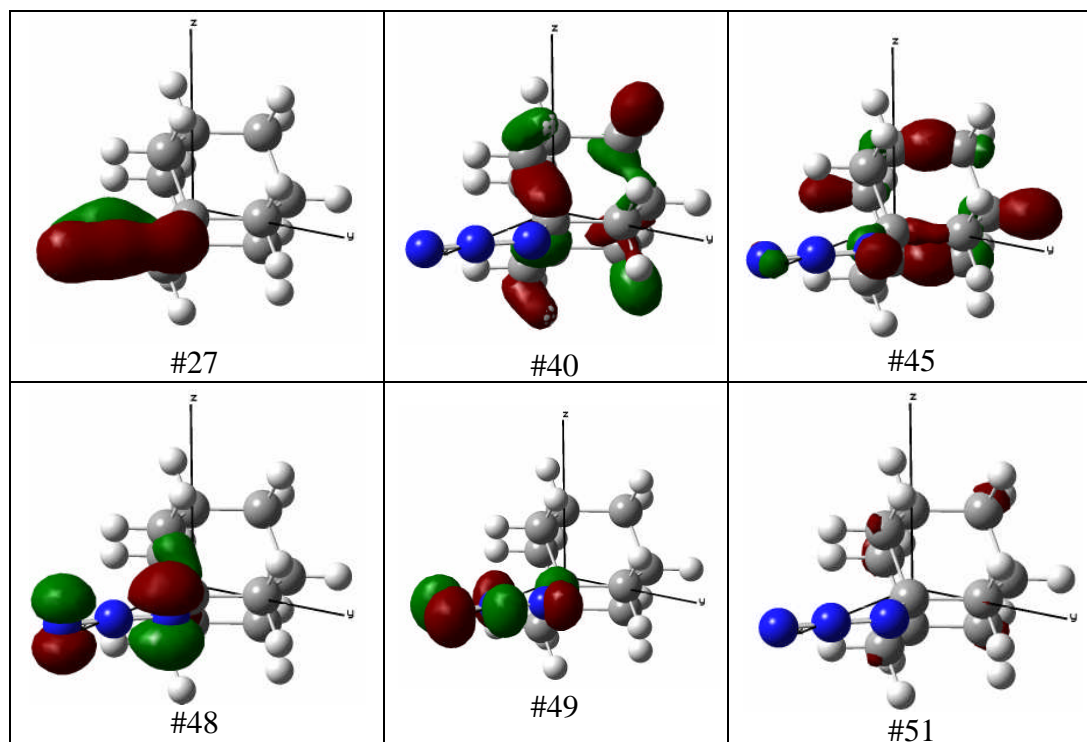
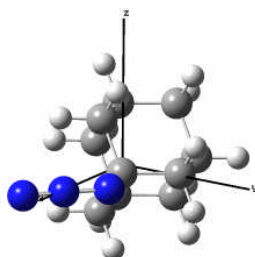


Figure S 3. Orbitals involved in the CIS/6-31G(d) calculated transition at 280 nm based on B3LYP/6-31G(d) optimized Cs symmetric geometry of **5** (isosurface value = 0.07).

Cartesian coordinates of 1 optimized at the B3LYP/6-31G(d) level of theory:

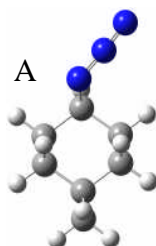


N	2.08034400	0.93501600	-0.00100800
N	2.97762400	0.08843500	0.00015700
N	3.89531700	-0.59524600	0.00062000
C	-2.00322100	0.39001900	1.24720600
C	-1.71370500	1.21497600	-0.02461500
C	-0.23482800	1.65678400	-0.02478500
C	0.67536900	0.41669300	-0.00041100
C	0.38451800	-0.40677700	1.27292200
C	-1.09336300	-0.85525000	1.27301000
C	-1.36704300	-1.72079900	0.02507500
C	-1.99136000	0.34844000	-1.27147300
C	-1.08142900	-0.89667500	-1.24780400
C	0.39628800	-0.44787300	-1.24894300
H	-3.05842100	0.08565300	1.26722400
H	-1.83041100	1.00198500	2.14299200
H	-2.35394200	2.10615700	-0.04224300
H	-0.01564300	2.28335100	0.84894000
H	-0.00738300	2.25536800	-0.91583900
H	0.60322900	0.20483700	2.15750300
H	1.04714500	-1.28252100	1.31125500
H	-1.29071200	-1.44029000	2.18051300
H	-2.41113500	-2.06175600	0.02562400
H	-0.73749700	-2.62111200	0.04264100
H	-1.81023800	0.93095500	-2.18509500
H	-3.04642400	0.04353700	-1.29129200
H	-1.27048900	-1.51103100	-2.13750900
H	0.62273700	0.13465100	-2.15105900
H	1.05883400	-1.32445000	-1.25312300

Number of imaginary frequencies: 0

Sum of electronic and zero-point energies=	-554.065451
Sum of electronic and thermal energies=	-554.055701
Sum of electronic and thermal enthalpies=	-554.054757
Sum of electronic and thermal free energies=	-554.100577

Cartesian coordinates of 5 (the most stable conformation) optimized at the B3LYP/6-31G(d) level of theory:

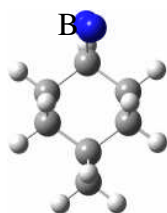


C	2.49587400	0.10613100	0.61148900
C	2.00995000	0.69362100	-0.73099000
C	0.90876700	1.74112900	-0.46344900
C	-0.27406300	1.07680800	0.27420400
C	0.21465000	0.48572700	1.61314400
C	1.31506900	-0.56256900	1.34590700
C	0.73308000	-1.69181600	0.46910400
C	1.42889500	-0.43727900	-1.60609500
C	0.24731500	-1.10985900	-0.87526500
C	-0.83898200	-0.04512900	-0.63055700
N	-2.02514200	-0.72251500	-0.02743600
N	-3.07080900	-0.06912200	-0.02263000
N	-4.09690200	0.43390800	0.03122900
H	2.92645400	0.90128300	1.23589700
H	3.29434400	-0.62741600	0.43369200
H	2.84987400	1.16948000	-1.25377100
H	0.56796200	2.18393900	-1.40977300
H	1.30507800	2.56346300	0.14706100
H	-1.06152900	1.82083000	0.45702900
H	-0.62286100	0.02670500	2.15180700
H	0.60389000	1.29314700	2.24799300
H	1.66271500	-0.98058100	2.29963600
H	-0.09840900	-2.18608800	0.98503600
H	1.49703600	-2.45786200	0.27885100
H	2.20175300	-1.18792000	-1.81840800
H	1.10075500	-0.03641800	-2.57538400
H	-0.17603200	-1.90739400	-1.49807600
H	-1.14438200	0.38835100	-1.59468300

Number of imaginary frequencies: 0

Sum of electronic and zero-point energies=	-554.061806
Sum of electronic and thermal energies=	-554.052049
Sum of electronic and thermal enthalpies=	-554.051105
Sum of electronic and thermal free energies=	-554.097433

Cartesian coordinates of **5** (less stable conformation) optimized at the B3LYP/6-31G(d) level of theory:

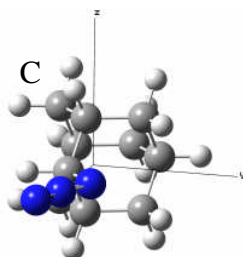


C	-2.12934000	1.15163600	-0.07022000
C	-2.22603500	-0.38036000	0.08576100
C	-1.48918200	-0.81312000	1.37213100
C	-0.00053100	-0.39978000	1.29083500
C	0.08117700	1.13541300	1.13508500
C	-0.64659100	1.57090500	-0.15427900
C	0.01414700	0.88534000	-1.36962800
C	-1.57027100	-1.05803800	-1.13620300
C	-0.08198700	-0.64905100	-1.22499300
C	0.61140000	-1.13478400	0.07214900
N	2.09482400	-1.13604300	0.00246400
N	2.74605300	-0.09174700	0.00124200
N	3.50401500	0.76768700	-0.00490100
H	-2.61398500	1.64907100	0.78118900
H	-2.66500900	1.47248400	-0.97428300
H	-3.28003200	-0.68061300	0.14973900
H	-1.57478600	-1.89939700	1.51225700
H	-1.95254700	-0.34198000	2.24925500
H	0.52618000	-0.71824000	2.19892500
H	1.12054600	1.48047900	1.12168100
H	-0.38741500	1.60706200	2.00950600
H	-0.57573500	2.66055800	-0.26456100
H	1.05799400	1.20654500	-1.46851100
H	-0.49116700	1.19113100	-2.29575100
H	-2.08929800	-0.76069400	-2.05722100
H	-1.65888800	-2.15046900	-1.05986600
H	0.39214800	-1.14081600	-2.08299600
H	0.40103300	-2.20337400	0.18516700

Number of imaginary frequencies: 0

Sum of electronic and zero-point energies=	-554.056709
Sum of electronic and thermal energies=	-554.047007
Sum of electronic and thermal enthalpies=	-554.046063
Sum of electronic and thermal free energies=	-554.092023

Cartesian coordinates of 5 (transition state Cs symmetric conformer) optimized at the B3LYP/6-31G(d) level of theory:



N	-0.98156700	1.86255000	0.00000000
N	-2.11006400	2.35397800	0.00000000
N	-3.10333100	2.92263600	0.00000000
C	-0.16771400	-1.66634200	1.25645400
C	0.56397700	-2.18281100	0.00000000
C	2.01720500	-1.66153000	0.00000000
C	2.01740000	-0.11847100	0.00000000
C	1.28552500	0.39706000	1.25710000
C	-0.16771400	-0.12190200	1.26271800
C	-0.91072200	0.36948900	0.00000000
C	-0.16771400	-1.66634200	-1.25645400
C	-0.16771400	-0.12190200	-1.26271800
C	1.28552500	0.39706000	-1.25710000
H	0.32809300	-2.03470400	2.16442700
H	-1.19808300	-2.04820400	1.27921400
H	0.56358300	-3.28062500	0.00000000
H	2.55179200	-2.03974500	-0.88246600
H	2.55179200	-2.03974500	0.88246600
H	3.05130900	0.25046400	0.00000000
H	1.29149200	1.49306100	1.27856800
H	1.79905000	0.05170000	2.16466700
H	-0.69517500	0.25020900	2.15011300
H	-1.93282800	-0.03448000	0.00000000
H	-1.19808300	-2.04820400	-1.27921400
H	0.32809300	-2.03470400	-2.16442700
H	1.29149200	1.49306100	-1.27856800
H	1.79905000	0.05170000	-2.16466700
H	-0.69517500	0.25020900	-2.15011300

Number of imaginary frequencies: 1 (-30.5953 cm⁻¹)

Sum of electronic and zero-point energies=	-554.061515
Sum of electronic and thermal energies=	-554.052624
Sum of electronic and thermal enthalpies=	-554.051680
Sum of electronic and thermal free energies=	-554.095323

6. Summary

In this PhD thesis, structure assessments of supramolecular host – guest inclusion complexes in solution as well as in the solid state were investigated. Organic azides – ferrocenyl azide (FcN_3) and 1- and 2-adamantane azides (**1**) and (**5**), respectively, served as a guest molecules; native and permethylated cyclodextrins (CyDs) were used as hosts. Association constants of these assemblies were determined to gain knowledge about the thermodynamic affinities of the guests towards the cyclodextrins. Finally, the solid inclusion complexes were decomposed and attention was paid to the analysis of the products formed with the aim to find new reaction pathways of the involved nitrenes.

Ferrocenyl azide forms a 1:1 stoichiometric complex with β -cyclodextrin and with its permethylated analogue TRIMEB. Also, mainly a 1:1 stoichiometry was detected for the binding of ferrocenyl azide towards permethylated α -CyD (TRIMEA), whereas with native α -CyD, a 1:2 inclusion complex was isolated. Moderate binding of ferrocenyl azide to β -CyD in ethylene glycol ($K_a = 180 \pm 5 \text{ M}^{-1}$) and to TRIMEB in CD_3OD ($K_a = 37 \pm 3 \text{ M}^{-1}$) was found. In DMSO, the $\text{FcN}_3@ \beta$ -CyD complex is practically dissociated ($K_a < 5 \text{ M}^{-1}$). Generally, the substitution of ferrocene by the azide group leads to a lowering of the association constants. The ROESY techniques allowed a straightforward suggestion of the disposition of ferrocenyl azide inside the β -CyD cavity in two solvents – d_6 -DMSO/ $\text{D}_2\text{O} = 40/60$ and d_6 -DMSO (Figure 1 and Figure 2, respectively).

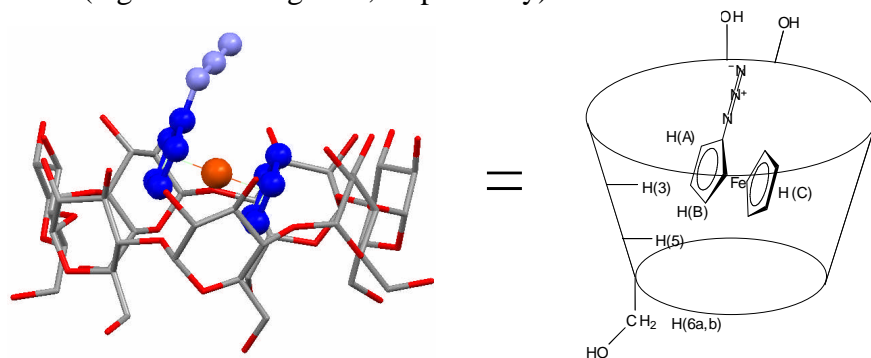


Figure 1. Proposed disposition of FcN_3 within the β -CyD cavity in $\text{DMSO}/\text{H}_2\text{O} = 40/60$ (v/v) according to 2D ROESY. The hydrogen atoms are omitted for clarity.

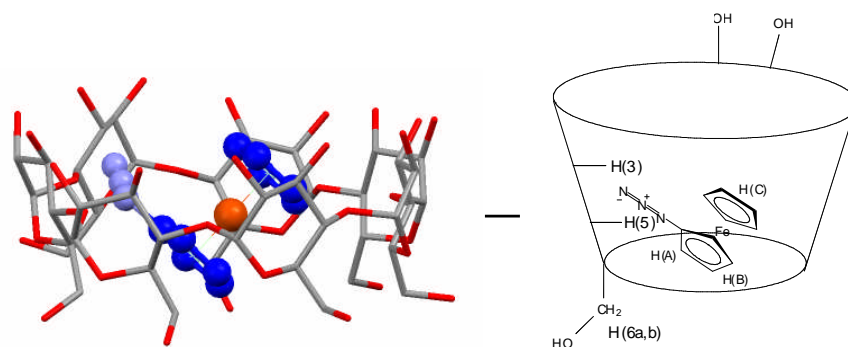


Figure 2. Proposed disposition of FcN_3 within the β -CyD cavity in d_6 -DMSO according to 2D ROESY. The hydrogen atoms are omitted for clarity.

In d_6 -DMSO/D₂O = 40/60, ferrocenyl azide adopts an equatorial alignment in β -CyD whereas an axial orientation in d_6 -DMSO is found. In addition, in d_6 -DMSO ferrocenyl azide is immersed more deeply in the β -CyD cavity than in d_6 -DMSO/D₂O = 40/60. The structure of this complex is tuned by the solvent, as corroborated by an Induced Circular Dichroism (ICD) study as well. Beside the solvent, also the temperature controls the orientation of ferrocenyl azide inside β -CyD. In contrast to the axial orientation of ferrocene in native β -CyD, inside the TRIMEB cavity an equatorial alignment was determined (Figure 3).

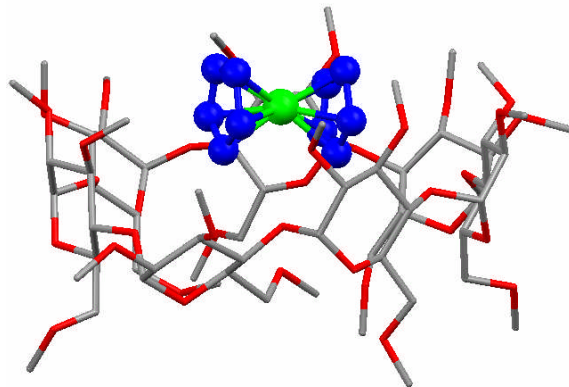


Figure 3. X-ray single crystal structure of the FcH@TRIMEB complex.

Ferrocenyl azide adopts a bimodal disposition within the cavity of TRIMEB (Figure 4).

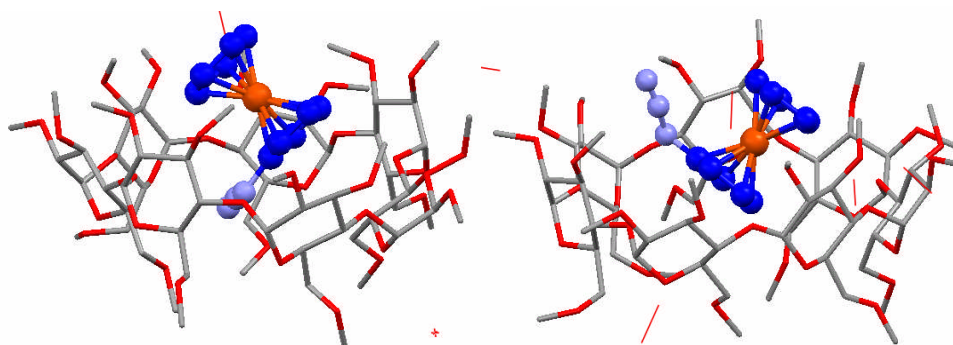


Figure 4. X-ray single crystal structure of the FcN₃@TRIMEB complex.

The solution structures of the FcH and FcN₃ – TRIMEB complexes seem to be consistent with those in the solid state, as inferred from ICD and 2D ROESY measurements.

As a ¹H NMR study demonstrated, the AA'B₅CC' spin system pattern of FcN₃ changes to an ABC₅DD' pattern upon addition of TRIMEB, due to the hindering of the rotation of the azide group (Figure 5).

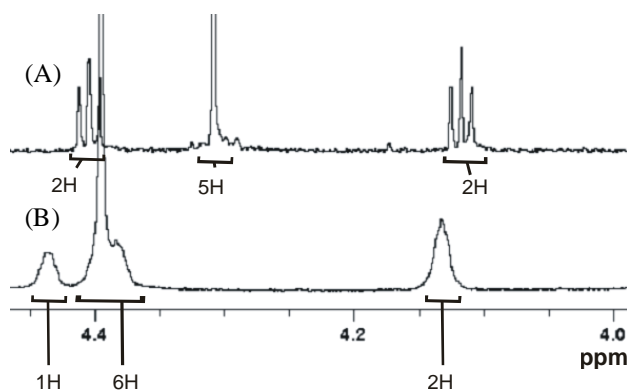


Figure 5. ^1H NMR spectra of (A) FcN_3 in $\text{DMSO-}d_6$, 250 MHz (B) $\text{FcN}_3@$ TRIMEB complex in D_2O . 400 MHz, $c(\text{FcN}_3) = 3.7 \text{ mM}$, $c(\text{TRIMEB}) = 14.4 \text{ mM}$, $[\text{H}]/[\text{G}] = 3.9$, $27 \text{ }^\circ\text{C}$.

Finally, a new unusual reaction pathway of ferrocenyl nitrene generated within the cavity of α -CyD was revealed. Instead of an expected nitrene C-H bond insertion, a pyranose – furanose conversion took place and a product with a complex structure was isolated (Figure 6).

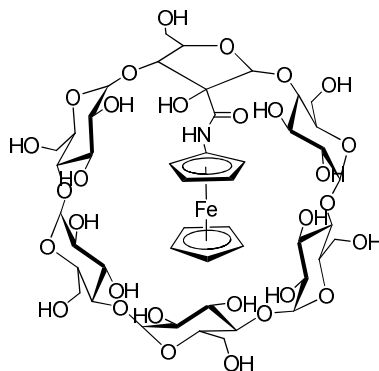
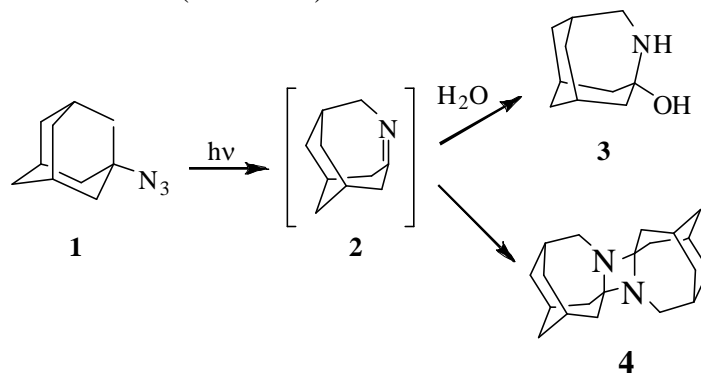


Figure 6. Structure of the product formed upon decomposition of the solid $\text{FcN}_3@(\alpha\text{-CyD})_2$ complex.

In addition, a typical nitrene reaction, i.e., a dimerization to the corresponding azo compound was prohibited.

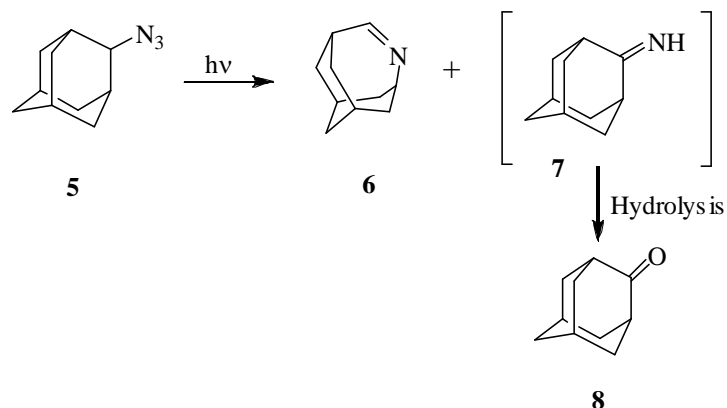
Analogously, the dimerisation reaction of **1** to **4** upon photolysis of the **1**@CyD complexes was not observed (Scheme 1).



Scheme 1. Photolyses reactions of **1**.

Instead, like in classical solution chemistry, the addition of a water molecule to the intermediate bridge-head imine **2** took place inside the α - and β -CyD cavities.

From the literature it is known that the photolysis of **5** affords 4-azahomoadamant-4-ene (**6**) and labile imine **7**, which upon work-up hydrolyzes to adamantanone (**8**) (Scheme 2).



Scheme 2. Photolyses products of **5**.

In our hands, the supramolecular encapsulation of **5** by α - and β -CyD did not dramatically alter the reaction pathway of the intermediate nitrene.

The ICD was utilized for the determination of association constants of **1** and **5** – CyD inclusion complexes and in connection with 2D ROESY NMR studies for the interpretation of their geometries. Thus, **1** forms a stronger inclusion complex with β -CyD in $\text{H}_2\text{O}/\text{EtOH} = 8/2$ at 293 K ($K_a = 20240 \pm 1000 \text{ M}^{-1}$) than **5** does ($K_a = 7450 \pm 400 \text{ M}^{-1}$). **1** and **5** form a 1:2 stoichiometric complexes with α -CyD. The first binding step to give a 1:1 stoichiometric **1**@ α -CyD complex is negligible and due to the cooperative binding only the 1:2 complex is present in the $\text{H}_2\text{O}/\text{EtOH} = 90/10$ (v/v) solvent system. Theoretical calculations of vertical electronic transitions of the azide group chromophore made a correlation between the 2D ROESY proposed **1**@ β -CyD complex geometry and the ICD spectra possible. In deuterium oxide, **1** takes on an apical orientation within the cavity of β -CyD, as inferred from 2D ROESY measurement (Figure 7).

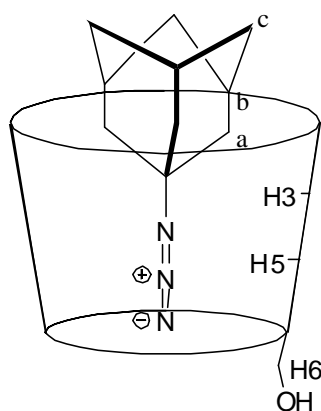


Figure 7. Proposed geometry of the **1**@ β -CyD complex in D_2O based on 2D ROESY measurements.

Investigation of the **5**@ β -CyD complex structure has shown that **5** experiences a bimodal disposition within the cavity of β -CyD, as confirmed by 2D ROESY (Figure 8) and X-ray single crystal analysis (Figure 9).

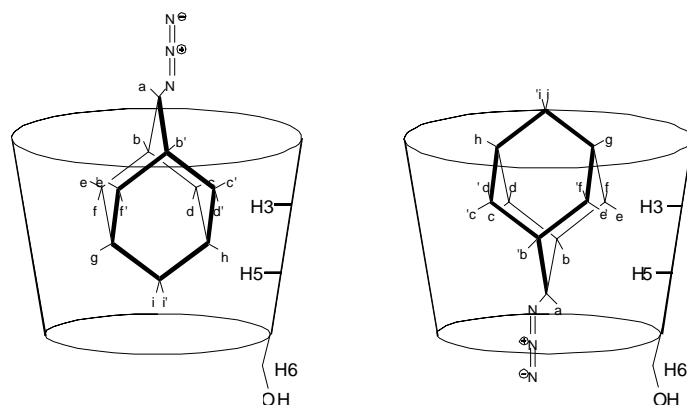


Figure 8. Proposed geometries of **5**@ β -CyD in D₂O based on 2D ROESY measurements.

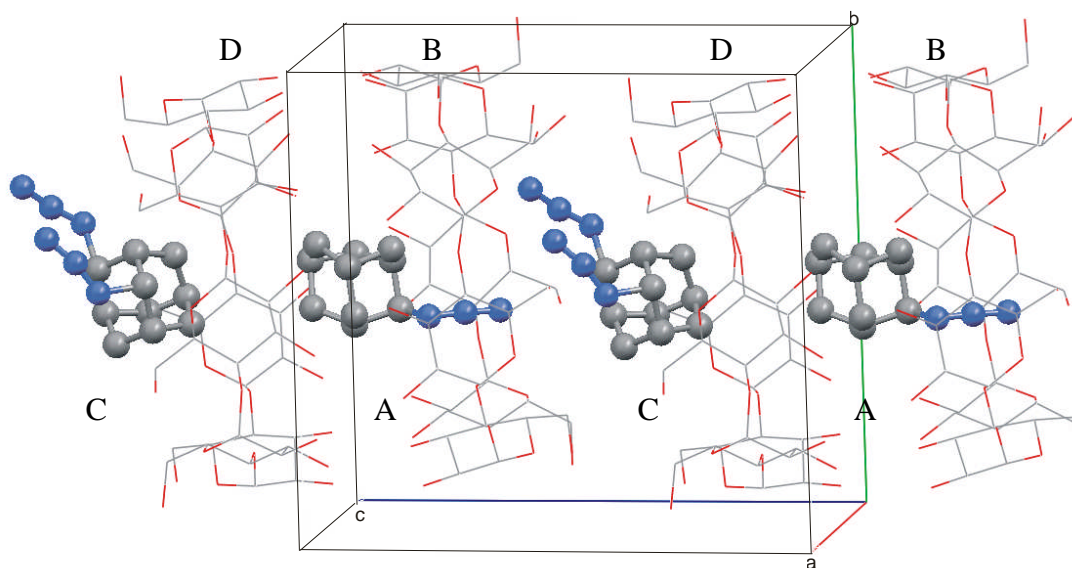


Figure 9. X-ray single crystal structure of the **5**@ β -CyD complex. Hydrogen and water molecules were removed for clarity. Two crystallographically independent β -CyD molecules B and D are present in the unit cell. The guest molecule C is disordered over two positions.

Curriculum Vitae

PERSONAL DATA

Name Peter Walla
Birth date 5. December 1978
Birthplace Nové Zámky, Slovakia
Citizenship Slovakia
Family Status married, one son (*2003)



EDUCATION

1985-1993 Elementary School, Nové Zámky, Slovakia
1993-1997 Grammar School, Nové Zámky, Slovakia
1997-2002 MSc. in Chemistry, Specialization in Organic Chemistry, Department of Organic Chemistry, Faculty of Natural Sciences, Comenius University, Bratislava, Slovakia
2002 Polymer Institute, Slovak Academy of Sciences, Bratislava, Slovakia
2002 – 2003 Institute of Chemistry, Karl-Franzens University Graz, Austria
2003 – 2007 Performing a practical work for this PhD thesis at the Institute of Organic Chemistry, University of Vienna, Austria
2008 Product development chemist at Dynea Austria, Krems
2008 Service technician at Shimadzu Austria, Korneuburg